Establishment of Fluorescence Assays for the Characterization of Site-Specific Proteases in E. coli

Ranglack, Jan

(2020)

TECHNISCHE UNIVERSITÄT DARMSTADT

Establishment of Fluorescence Assays for the Characterization of Site-Specific Proteases in *E. coli*

at the Department of Biology of the Technische Universität Darmstadt

submitted in fulfilment of the requirements for the

degree of Doctor rerum naturalium

(Dr. rer. nat.)

Doctoral thesis

By Jan Ranglack

First assessor: Prof. Dr. Viktor Stein

Second assessor: Prof. Dr. Harald Kolmar

Darmstadt 2020 (year of the viva voce)

Ehrenwörtliche Erklärung:

Ich erkläre hiermit ehrenwörtlich, dass ich die vorliegende Arbeit entsprechend den Regeln guter wissenschaftlicher Praxis selbstständig und ohne unzulässige Hilfe Dritter angefertigt habe.

Sämtliche aus fremden Quellen direkt oder indirekt übernommenen Gedanken sowie sämtliche von Anderen direkt oder indirekt übernommenen Daten, Techniken und Materialien sind als solche kenntlich gemacht. Die Arbeit wurde bisher bei keiner anderen Hochschule zu Prüfungszwecken eingereicht.

Darmstadt, den 10.10.2020

Table of contents

Acknowledgements

First and foremost, I wish to thank Prof. Dr. Viktor Stein for the opportunity to be part of his newly founded working group and the chance to conduct the research for my PhD thesis in this inspiring and creative environment. Moreover, I thank the department of biology for accepting me as a PhD candidate.

Heartful thanks to my fellow PhD candidate Wadim Weber for his honest feed-back and exceedingly helpful input to my research. Additional thanks to him for saving me at a crucial time point during the project by providing me with his excellent pCtrl2 expression vector. I would like to express my exceptional gratitude to all the bachelor and master students that contributed to my thesis. In particular I am grateful to Tim Maier and Isabelle Marquardt for helping me to get the project running. Likewise, I am grateful to Ciaran Rühmkorff for assisting me in rounding up the project. To close the academic segment, I wish to show gratitude for our fruitful cooperation to Julia Weigand and Stephen Peter.

Furthermore, I express my sincere appreciation to all current and former members of the WG Stein for the great time I had with them during the last three and a half years. The same appreciation is due to the whole WG Thiel and WG Meckel as well as every member of the iNAPO project for all the nice memories of retreats, barbecues and PhD celebrations.

My deep gratitude and utmost appreciations to my caring wife and all my family and friends. Without their constant support and never-ending encouragement, I would not have made it through these stressful years.

Lastly, I thank the federal state of Hesse, the LOEWE project iNAPO and Pioneer ACTIVATOR for founding.

1. Abstract

Recent years have seen the increasing development and application of protease-based sensors and switches in the construction of artificial signaling functions in synthetic biology. Even though they were extensively characterized *in vitro*, robust and quantitative assays to characterize them *in vivo* remains elusive. This particularly concerns assays that can provide real-time kinetic data on the apparent activity of proteases and protease-based sensors and switches in the genetically-tractable *E. coli* and are compatible with high-throughput screening formats.

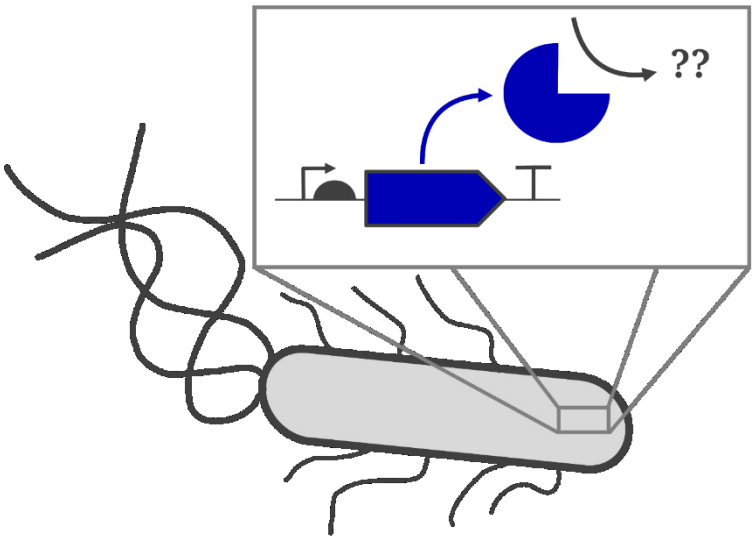

Scheme 1 Graphical abstract. A protease (blue circular section) is functionally expressed in *E. coli* and the question arises how to transform its catalytic activity into a quantitative, measurable read-out with the mid-term goal to engineer and characterize protease switches, sensors and circuits in high-throughput.

Addressing these limitations, several different protease sensor designs featuring different types of fluorescent protein reporters were developed and tested over the course of the project. Protease-cleavable degradation tags (degrons) were identified as the best way to directly modulate the fluorescent output signal through proteolytic activity in *E. coli*. To this end, two different assay modes were successfully established: The first assay mode is based on a conventional positive read-out where the fluorescent signal scales proportionately with the protease activity while the second mode provides enhanced quantitative data based on a ratiometric two color assay. The assay was validated with the nuclear inclusion protein a (NIa) of tobacco vein mottling virus (TVMV) while the general utility of the assay was additionally validated with the NIa protease of tobacco etch virus (TEV) and the NS3 protein of hepatitis C virus (HCV). Finally, the assay was utilized for the preliminary screening of a library of opto-switchable auto-inhibited TVMV candidates.

2. Motivation and aim of this project

“We, the Stein Lab, aim to transform protein switches into generally applicable tools for synthetic biology. In particular we are interested in the characterization of these switches within their cellular context in various *in vivo* scenarios.” *V. Stein 2019*

The quote above summarizes the overall goal of our group. To achieve the goal of characterizing novel protein switches within living cells a set of easy to adapt assays is required to evaluate the performance and consistence of behavior in *in vivo* scenarios. Therefore, the project was conceived to create necessary assays to characterize and engineer protease-based switches, signal transducers and actuators in living cells [1-3]. Furthermore theses assays could be employed by the SynBio community for the characterization of various other protease-based modules for post-translational circuits which we previously summarized [4]. With these assays we thought to provide a solid foundation for the development of post-translational circuits and the future the creation of tailor-made auto-regulated cell lines for synthetic biology or green chemistry approaches.

3. Introduction

3.1. Synthetic biology - from basic parts to auto-regulating cells

The main goal of synthetic biology is to devise systematic approaches to engineer biological functions to specification. The construction of tailored biological functions occurs through iterative design-build-and-test cycles. This comprises both the development of enabling technologies to facilitate the construction of biological systems with tailored properties and functions and their development into distinct biotechnological applications.

One area of interest concerns the construction of sensors, switches and complex signaling functions to detect, compute and translate input signals into tailored output signals. This comprises the construction of individual sensors and switches that are composed of a receptor and an actuator that are capable of receiving a range of inputs such as light [5], small molecules [6, 7] or ions [8] and translate them either into a physical or physiological signal such as fluorescence or proteolytic activity. Based on individual protein sensors and switches, more complex sensory functions can subsequently be engineered in the form of logic gates, complex response functions or cell-cell-communication devices [9-20]. Of particular interest are circuits that mediate biomolecular signals entirely by post-translational means independent of time-consuming transcription or translation. In this regard, the previously established switches and signal transducers based on auto-inhibited proteases are to mention[1, 3]. As well other protease-based devices such as Boolean Gates [21-23] or metabolic flux control by regulating the abundance of enzymes [24, 25].

Normally, these outputs either trigger a reporter signal or a phenotypic response. In this regard, reporter signals are extensively used in the development and characterization of individual sensors, switches and circuits. Phenotypic responses are frequently developed as tools to regulate cell fate, morphology or the metabolic profile of the host cell. Therefore, they are often used in medical applications [26] or for bioecological production [27]. In case of reporters, there are different types of output signals available such as fluorescent proteins[28]. Alternatively, reporters can also be based on light-emitting luciferases. Luciferases carry the advantage that they can generate an optical signal directly from within the host cell independent of a fluorescent irradiation step [29]. The last class of reporters comprises of enzymes like β-galactosidase that turn over a colorless substrate into an optically active product and thus generate a colorimetric signal that is cost-effective and easy to detect [30]. Phenotypic actuators on the other hand change the viability, morphology or behavior of the host cell. Cell fate actuators include amongst others apoptosis inducers [31], morphology comprises amongst other of motility [32] or biofilm formation [33] regulators and lastly a metabolic actuator in

most cases is an enzyme that is activated through the synthetic device [34]. The often times overlooked yet crucially important class of parts are adaptors which interconnect the multiple parts of a synthetic device either on genetic or on protein level or direct it to its desired location. The first form of adapters are linkers which exist in two variants static linkers or spacers that keep two parts at the necessary distance from one another. Close enough for direct interaction or co-activity but far enough apart to avoid steric clashes or hindrances. Spacers for DNA, RNA or proteins are available in all sorts of lengths or mechanical stiffness [11-13]. The other form of linkers are anchors that tether proteins or nucleic acids to membranes or other cellular structures.

Intrinsically, proteases offer a promising building platform for all parts required for all forms of synthetic devices. By expressing them in a non-active state (e.g. auto-inhibited) that is activated through an input signal a sensor module is realized. Input could be ligand binding [1] or a physical parameter like light (see **Chapter 4.6**). By introducing a different cleavage site in the peptide linker interconnecting the protease and the disactivating domain protease can act as signal transducers and or signal amplifiers. Lastly proteases can act as actuators by modulating protein stability. This modulation can be positive by cleaving off degradation tags (see **Chapter 4.2**) or negative by unmasking cryptic N-degrons (see **Chapter 4.3**). The following chapter describes the requirements and design principles of turning protease into synthetic sensors, signal transducers and actuators in further details.

3.2. Proteases as promising building blocks for sensors, signal transducers and actuators

Proteases are a subclass of hydrolases that have evolved to cleave peptide bonds within fully maturated proteins or even polyproteins. A large natural repertoire of proteases exist that comprise a range of functional and structural properties. This includes proteases with low substrate specificities, like trypsin or pepsin. On the other hand, there are sequence specific proteases like the viral proteases used in this work (see **Chapter 4**). These sequence specific proteases recognize short sequence motives and subsequently cleave at one specific position within their recognition sequence. Therefore, this recognition sequences are often called cleavage sites.

3.2.1. Potyvirus proteases

In recent years, proteases originating of various potyviruses (EC: 3.4.22.44) have emerged as promising tools in synthetic biology. The most prominent one being the Nuclear Inclusion Protein Ia of tobacco etch virus (TEV). Two other commonly used potyvirus protease originate from tobacco vein mottling virus (TVMV) and sunflower mild mosaic virus (SuMMV) [21]. For both TEV protease (TEV) and TVMV protease (TVMV), the crystal structures were solved through efforts made by the Waugh Lab [35, 36]. Both adopt a chymotrypsin-like fold with a catalytic triad comprised of a histidine, an aspartic acid and the actual nucleophile a cysteine [37, 38]. A structural alignment of both structures is shown in **Figure 1**. SuMMV has not been characterized as well as its two close relatives. But the Voigt Lab has proven that SuMMV shares the typical high substrate specificity of potyvirus proteases with TEV and TVMV respectively. Hence all three may be used orthogonal to one another even though their recognition sequences appear quite similar (see **Table 1**, [21]).

Table 1 Commonly used virus proteases and their respective cleavage sites [1, 21, 39]

Protease	Cleavage site
TEV	ENLYFQ|notP
TVMV	ETVRFQ|notP
SuMMV	EEIHLQ|notP
consensus	EX_4Q|notP
HCV	DDVTPCSM|S
SARS-CoV-2 ^{M}Pro	SAVLQ|SGFRK

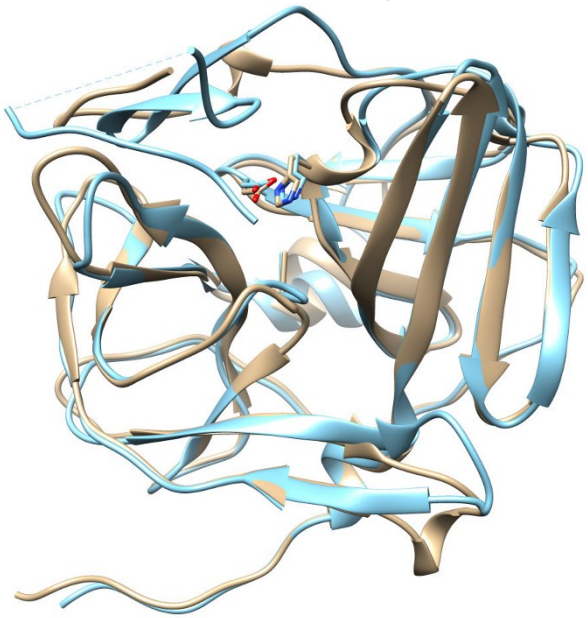

Figure 1 Structural alignment of TEV and TVMV. Structures are depicted as ribbons, catalytic triad (H46, D81, C151) as sticks (catalytic cysteine mutated to alanine in both structures), TEV (PDB: 1Q31) in cyan, TVMV (PDB: 3MMG) in tan, catalytic triad colored by heteroatom; structural alignment was performed with UCSF Chimera 1.11.2 (MatchMaker tool).

All three potyvirus proteases can be functionally expressed in *E. coli* and readily purified from lysates [21]. To increase yield, these proteases are frequently fused to maltose binding protein (MBP) especially for the purpose of purification. MBP greatly increases the solubility of the fused viral protease and thereby acts as a pseudo-chaperone. The increased solubility increases the chances of the protease domain to adopt its proper fold. The poor solubility of viral protease as well as their slow folding rates originate from the fact there are neither expressed in their natural environment, cytosol of their original host cells, nor part of the viral polyprotein, in which they were evolved to properly fold. By incorporating the respective cleavage sites into the linker between MBP and the protease, MBP is cleaved of *in situ* if desired [40, 41]. Alternatively, chaperones may be co-expressed to increase the yield of fully functional protease [42].

Over the last six years, V. Stein demonstrated that proteases with specific recognition sequences can be turned into tailored molecular switches by covalently linking them with an autoinhibitory (AI) domain. These AI domains are derived from the actual cleavage site and act as competitive inhibitors. They bind to the active site of the proteases with reasonable high affinities but are not cleaved by it. By introduction of sensory domains into the peptide linker connecting the AI domain with the protease, a switch can be created. Upon input detection (e.g. ligand binding) the sensory domain undergoes a conformational change. Following this change the AI domain is removed from the active site due mechanical tension within the peptide backbone of the fusion protein. Hence the protease is activated, meaning it is enabled to act on its cleavage site. By removing the molecular input signal, the sensory domain adopts its default conformation once again. Subsequently the AI domain binds to active site of the protease rendering it inactive [1, 3, 4].

3.2.2. Flavivirus proteases

Alternatively, proteases from flaviviruses (EC 3.4.21.98) like hepatitis C virus can be used in synthetic biology. These proteases offer similar sequence specificities and processivities compared to potyviral proteases. In contrast to potyviral proteases, flavivirus proteases are serine proteases[43, 44]. Like for TVMV as representative of potyvirus proteases, V. Stein demonstrated the general utility of this design principle for protein switches based on auto-inhibited protease switches with HCV NS3 protease (HCV) as a representative of flavivirus proteases[1, 3].

3.2.3. From site-specific proteases to synthetic devices

Naturally, those intricate designs require extensive linker optimization to ensure proper folding and stability of such large multi-domain fusion proteins and to enable the proper behavior in the presence and absence of the input signal. Addressing these limitations, we developed a new cloning strategy to facilitate the laborious and time-consuming endeavor of linker optimization. The method is particularly amenable to the co-optimization of multiple linkers in a multi-domain fusion protein.

This new strategy was termed iterative Functional Linker Cloning (iFLinkC) and was published this year in Nucleic Acid Research[45]. iFLinkC is based on the usage of TypeIIS restriction endonucleases which recognize and cleave short non-palindromic sequence motifs that can be used to assemble DNA fragments in a direction manner. In addition, the four chosen enzymes (BbsI, BtsI, BsrDI and BsaI) cleave directly adjacent to their recognition sequence which renders them particularly amenable to the in-frame assembly of fusion proteins. The two key enzymes BtsI and BsrDI create essential two nucleotide long overhangs. These two nucleotide overhangs that are directly adjacent to the recognition sequence allow the cloning of linkers as short as a single glycine residue (single triple guanosine codon) between any two functional domains. For further details on iFLinkC refer to **Chapter 6.2.9** of this thesis or the corresponding publication [45].

3.2.4. Excurse: Coronavirus proteases

During the last months another family of RNA virus rose to utmost relevance. Corona viruses share a similar replication mechanism to the above mentioned flavivirus and potyvirus. Likewise, a site-specific protease exists in their viral polyprotein. Coronavirus share the usage of serine proteases with the flaviviruses. But unlike the flavivirus proteases coronavirus proteases are always monomeric[46]. In terms of inherent handling properties, this puts them somewhere in-between potyvirus and flaviviruses. The lack of a catalytic cysteine renders them less vulnerable to oxidation but offers a weaker nucleophile compared to potyviruses. The monomeric state increases changes of proper folding when heterologous expressed in e.g. *E. coli*. With the crystal structure from the main protease form corona virus strain SARS-CoV-2 recently solved, the basis was set to develop potential inhibitors as precursors for drug development [47].

3.3. Challenges in the construction of *in vivo* proteases assays - *E. coli* a preferable host

The aim of this work was to develop a platform assay to assay the activity of protease switches in the cytosol of live *E. coli* cells and apply it to engineer the function of protease switches in high-throughput.

E. coli has been one of the most pre-dominant host organisms in molecular biology for the last three decades. This stands true for modern synthetic biology as well. The advantages of *E. coli* range from fast and easy cultivation to a large repertoire of regulatory elements that can be readily used to express proteins in recombinant form. In terms of expressing and functionally assaying proteases, direct quantification of peptide bond hydrolysis *in vivo* is challenging and prone to high background noise through the general protein turn-over during cell growth. Therefore, most *in vivo* assays rely on sensors that alter their signaling behavior upon proteolytic processing. In addition to diffusion-based effects, cryptic signal sequences that are unmasked trough proteolytic cleavage can be utilized as well. In this regard, fluorescent read-outs are the most straight forward approach. In particular, fluorescence-based assay methods carry the advantage that the output signal can be measured non-invasively without disrupting the cell. The latter is only true when extensive and frequent irradiation with short wavelength light is omitted.

Even though *E. coli* is a widely used host for recombinant protein expression and prototyping of synthetic genetic circuits, this can lead to a variety of negative effects [48]. This particularly applies to a reduction in growth rates and the capacity of a cell to express proteins. In addition, cell viability can be reduced as key components of the transcriptional and translational machinery, in particular RNA polymerases and ribosomes, becoming limiting upon recombinant overexpression of proteins and circuits [49]. In addition, the intrinsic degradation machinery might be overloaded by overexpression of certain circuit proteins. This overload may further compromise cell viability or interfere the performance of the circuit (see **Chapter 4.2.1**). In addition, the number of expression vectors is strictly limited to three at a time. This limitation is based on the three distinct classes of replication origins (oris) in *E. coli* (A – ColE1/pMB1, B - p15A, C - pSC101). If two plasmids with oris from the same class are present, stable propagation is not guaranteed even though two different selection markers are used [50].

3.4. *In vivo* read-outs for protease activity in *E. coli*

3.4.1. Fluorescent Read-outs

In terms of suitable protease assay, extensive efforts were made to visualize proteolytic activity in live (mammalian) cells especially in the context of cell biology. This particularly applies to caspases and other proteases that have been linked with cell proliferation or oncogenesis. In general terms, a positive read-out in a protease assay is preferred over negative one. This means, upon detection of proteolytic activity a fluorescent signal should be generated instead of one being reduced or lost.

Direct sensors

One way of achieving this was elaborated by the Hardy group. They created a quenching peptide that promoted the controlled aggregation and formation of non-fluorescent conglomerates of the green fluorescent protein (GFP) when it was fused to its C-terminus. Through introduction of a protease cleavage site into the linker interconnecting the quenching peptide and the GFP proteolytic dequenching of GFP fluorescence was achieved (**Scheme 2**) [51-53].

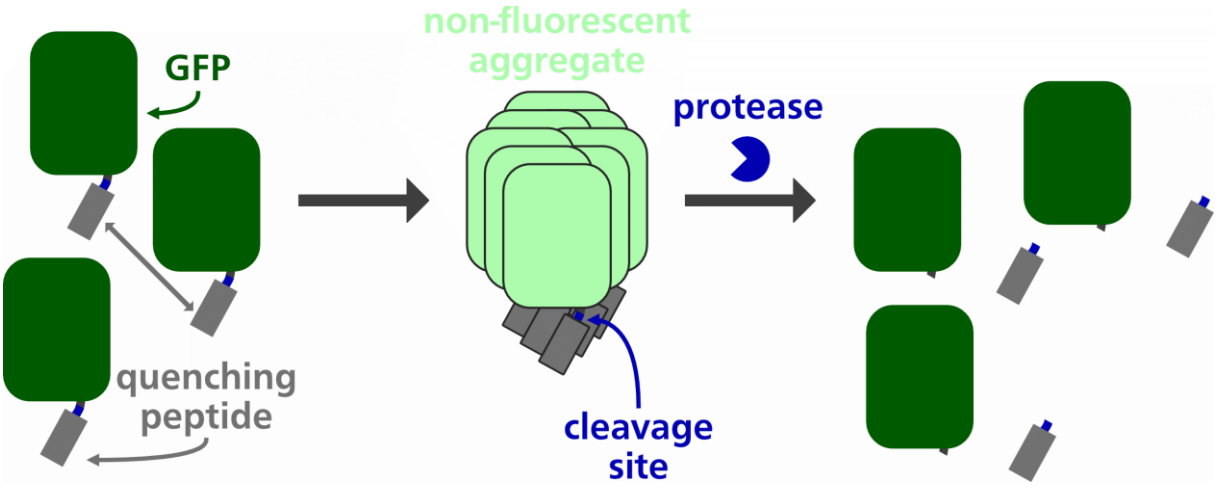

Scheme 2 An *in vivo* gain-of-function protease assay based on the principle of fluorescence dequenching. GFP is fused to an aggregation inducing peptide which leads to over-aggregation and self-quenching to abolish detectable fluorescence. The self-quenching is terminated by proteolytic removal of the aggregation inducing peptide and fluorescence is restored.

In 2013 Do and Boxer reported a protease sensor based on split-GFP. $GFP_{11\text{-}1}$ was expressed fused to two different GFP_{10} β-strands. At the N-terminus, the native GFP_{10} β-strand was located while at the C-terminus the YFP_{10} β-strand introduced. Both β-strands are identical except for position 203. The native GFP possesses a threonine at this position in contrast to YFP which features a tyrosine here. Depending on which of the two β-strands folds into the β-barrel a

different interaction partner for the central fluorophore is provided. Threonine 203 induces green fluorescence while tyrosine 203 induces yellow fluorescence (**Scheme 3**) [54, 55].

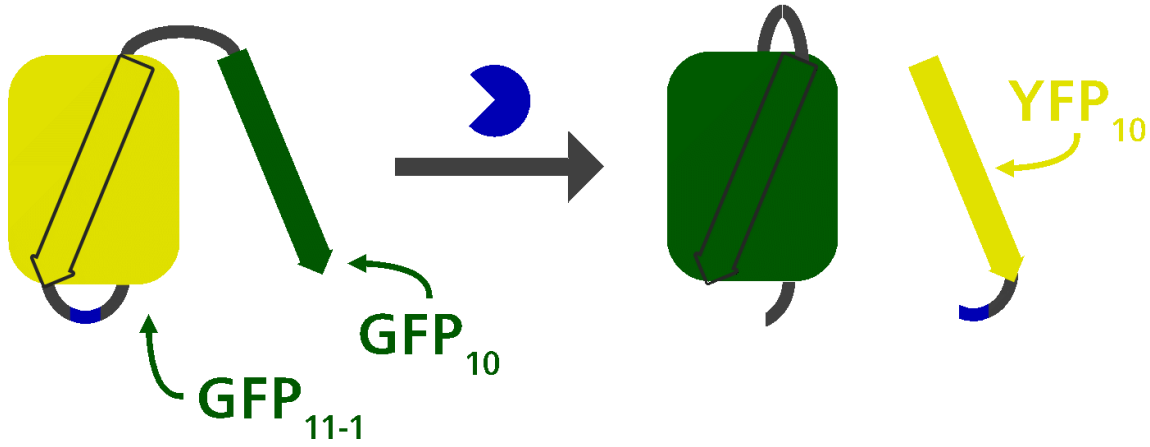

Scheme 3 A color changing split-GFP variant as a ratiometric *in vivo* protease sensor. GFP_{11-1} is fused with alternative GFP_{10} β-strands that facilitate a switching from yellow to green fluorescence. In the default state the Y203 containing YFP_{10} β-strand closes the β-barrel fold, hence a yellow fluorescence is emitted, through proteolytic activity YFP_{10} is cleaved off, allowing GFP_{10} to fold into the β-barrel, through this rearrangement T203 now interacts with the internal fluorophore changing the fluorescence from yellow to green.

After linker optimization, a sensor was created carrying a protease cleavage site between GFP_1 and YFP_{10}. In the default state, no green fluorescent signal could be observed. Following proteolytic cleavage, a switch from yellow to green fluorescence occurred. The dissociation of the YFP_{10} could be accelerated through irradiation with excitation light for green fluorescence (blue light, ~485 nm). This led to a ratiometric yellow-to-green sensor [55]. However, the general utility of this design is hampered through linker optimization. This is because one has to ensure that after altering the cleavage site the non-cleaved population remains in the yellow fluorescing state exclusively. Otherwise, the dynamic range of the sensor is significantly reduced.

Other protease sensor designs exploited Förster resonance energy transfer (FRET, [56]) or bioluminescence resonance energy transfer (BRET, [57-59]). FRET occurs when two fluorophores with overlapping spectra are in close proximity and correct angular orientation to one another. In this case, overlapping refers to the emission peak of the donor and the excitation peak of the acceptor. If all three criteria (overlapping spectra, close proximity and correct angular orientation) are met, excitation energy from the donor fluorophore is transmitted emission less to the acceptor fluorophore. In other words, when the donor fluorophore absorbs

a photon, the resulting excitation energy is directly transferred to the acceptor fluorophore. The now excited acceptor fluorophore then emits a photon to reach its ground state again. Under ideal circumstances this leads to a scenario where upon donor excitation acceptor emission is exclusively detected. Through this effect, unnaturally high stokes shifts are observed (**Scheme 4**) [56].

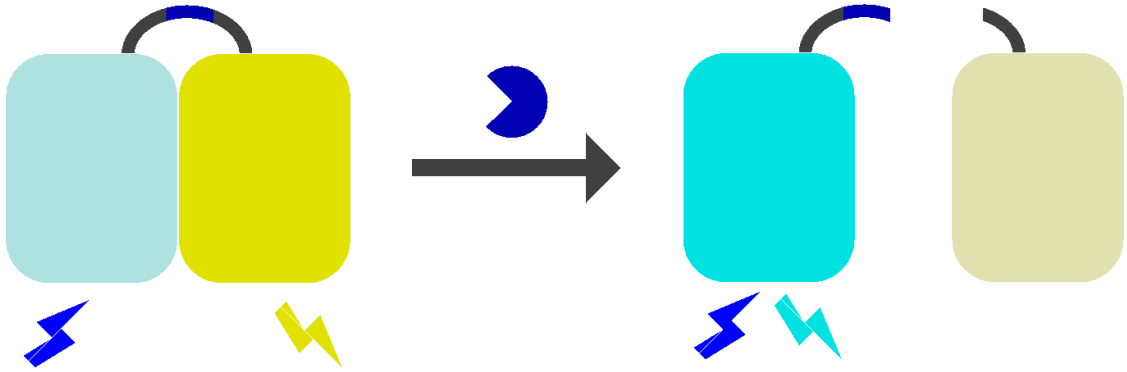

Scheme 4 Förster Resonance Energy Transfer (FRET) based protease sensors. As long as both fluorescent proteins remain in close proximity emission less energy transfer from the donor fluorophore (CYP in this example) to the acceptor fluorophore (YFP in this example) can occur, hence upon exiting the donor fluorophore mostly acceptor emission is observed, once a protease cleaves the interconnection linker both fluorescent proteins are separated through diffusion and upon donor excitation only donor emission is observed.

BRET is a variation of FRET where a luciferase acts as the energy donor (**Scheme 5**) [57-59].

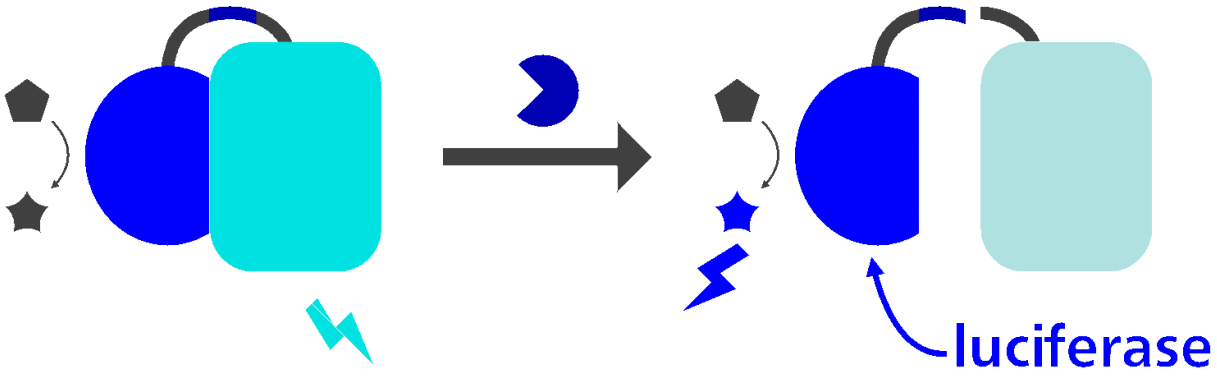

Scheme 5 Bioluminescence Resonance Energy Transfer (BRET) based protease sensors. As long as both the luciferase and the fluorescent proteins remain in close proximity, a transfer of energy from the donor (a blue light emitting luciferase in this example) to the acceptor fluorophore (CFP in this example) can occur. In the uncleaved state, mostly acceptor emission is observed, but once a protease cleaves the linker the luciferase and the fluorescent protein are physically separated so that mostly direct luciferase emission is observed

Therefore, irradiation with potentially harmful high-intensity light is omitted, but instead is generated *in situ* through a light-emitting enzymatic reaction. However, the substrate of the luciferase has to be administered externally or has to be produced *in situ* by the cells themselves. The first can drastically increase the cost of the experiment or is not applicable at all if the substrate is not cell permeable or internalized by the cells through phagocytosis [60]. The latter alternative of internal production increases the metabolic burden an assay circuit imposes on the host cell. This in turn can reduce robustness or performance of the BRET assay. Therefore, BRET assays are mostly used with eukaryotic host which easily take up externally administered luciferase substrates through phagocytosis. In conclusion, neither FRET nor BRET is superior over the other [61].

Fluorescent proteins optimized for FRET are often referred to as "FRET pairs". For *E. coli*, one such FRET pair is currently available and comprises a cyan fluorescent protein (CyPet) and a yellow fluorescent protein (YPet)[62]. When used as protease sensors, FRET/BRET pairs are typically connected with a linker that features the cleavage site of a protease. Hence, through proteolytic processing the efficiency of the FRET/BRET should decrease. This translates into a time-dependent loss of acceptor fluorescence and, in theory, a rise of the donor fluorescence/luminescence [63]. Recently, a FRET sensor was used to screen for protease inhibitors *in vivo* [64]. Based on the smallest available luciferase NanoLuc, the Merkx lab presented a new set of protease sensors in 2017 [65].

Finally, the Campbell lab created a new class of fluorescent protein sensors based on dimerization-dependent fluorescent proteins. The principle was termed Fluorescent Protein eXchange (FPX; **Scheme 6**).

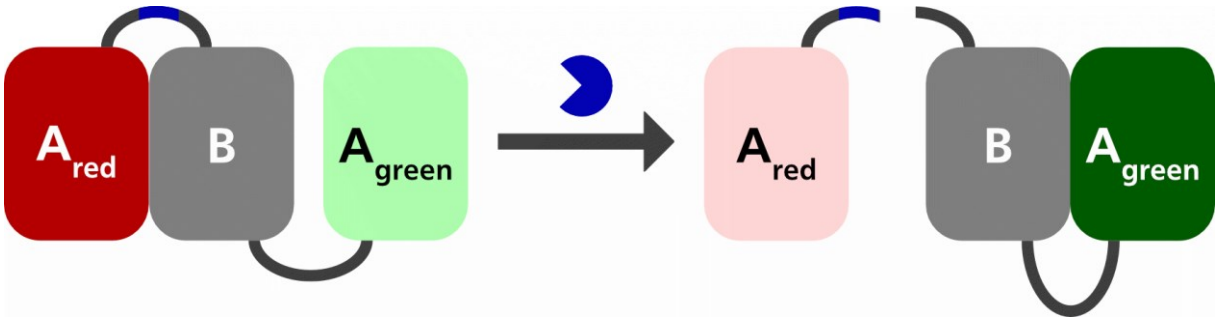

Scheme 6 Fluorescence Protein eXchange (FPX) based protease sensors. FPX biosensors rely on dimerization-dependent fluorescent proteins. The non-fluorescent enhancer – referred to as the "B domain" (grey) – lacks the fluorophore-forming amino acids but provides the essential dimerization partner for the other two fluorescent protein – referred to as "A domains" (red and green respectively). In the default state, all three domains are part of the same polypeptide chain and the thermodynamically favored dimer of Ared and B is formed; Upon proteolytic cleavage, the Ared domain is separate from the polypeptide chain which in turn drastically increases the local concentration of Agreen and results in the formation of a green fluorescent dimer

The sensor is comprised of three different fluorescent protein domains. Two so called “A domains” containing one fluorophore each. The third domain called “B domain” lacks the amino acids necessary for fluorophore formation. Upon dimerization with the “B domain”, one “A domain” emits green light while the other “A domain” emits red light. Given both domains compete for the dimerization interface of the single “B domain”, an equilibrium of three different dimerization states is achieved upon expression of the sensor. In the first state Ared and B dimerize, in the second state Agreen dimerizes with B and in the third state - the transition state - no dimer is formed. In this way, the overall fluorescence of the population depends on the distribution of all three states within the thermodynamic equilibrium. In order to create a ratiometric sensor, the Campbell lab employed “A domains” with unequal affinities towards the B domain. Therefore, in the default state the equilibrium is shifted towards one of the two dimers. Hence, the overall fluorescence of the sensor population is shifted accordingly.

Finally, a protease cleavage site was introduced into the linker between the favored “A domain” and the “B domain”. Thus, upon cleavage, the favored “A domain” is separated from the “B domain” which drastically increases the local concentration of the disfavored “A domain”. As a result, the thermodynamic equilibrium of mutually exclusive binding interaction is shifted along with the overall fluorescent signal. In this way, a ratiometric caspase sensor was created [66]. Unfortunately, the soluble expression of the full-length sensor in *E. coli* did not turn out feasible (unpublished data, Bachelor thesis T. Maier, see **Chapter 4.1**).

Indirect or coupled sensors

Instead of directly measuring the cleavage through the modulation of a fluorescent sensor protein, protease activity can be coupled to key cellular functions such as transcription or translocation analogous to naturally protease-regulated processes.

In 2017 Hahlbrock *et al*. published a general design principle for proteolytic translocation assays. The sensor comprised of a fluorescent protein (e.g. GFP) that was fused to a N-terminal nuclear localization sequence (NLS) and a C-terminal nuclear export sequence (NES). The recognition sequence for the protease of interest is cloned into the linker between the reporter protein and the NES. As long as both localization sequences are present, the fluorescent signal associated with the sensor is dispersed over the cytoplasm. Once proteolytic cleavage occurs, the nuclear export sequence is removed and the reporter accumulates in the nucleus resulting in a concentration of the fluorescent signal within the nucleus (**Scheme 7**) [67].

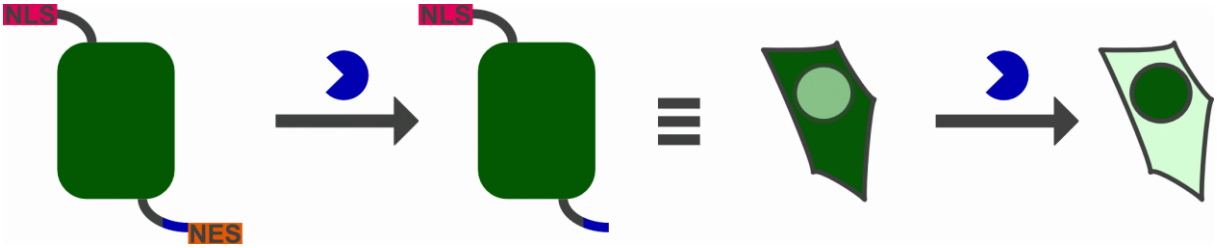

Scheme 7 Proteolytic translocation assay. A fluorescent reporter protein is expressed with both a nuclear localization sequence (NLS) and a nuclear export sequence (NES). As long as both targeting sequences are present, the fluorescence is dispersed over the whole cytoplasm. But once the NES is removed through proteolytic activity, the NLS causes accumulation of the fluorescent reporter in the nucleus.

Translocation assays are however limited to organisms with multiple organelles which does not apply to most prokaryotes. In addition, protein localization sequences must be known for any given host. Lastly, the throughput of translocation assays is limited as the distribution of the fluorescent signal needs to be tracked with subcellular resolution which is technically challenging to achieve by means of fluorescence microscopy. Therefore, methods like fluorescence activated cell sorting (FACS) or droplet microfluidics-based cell sorting are preferable which quantify fluorescence at a similar single cell resolution, provide high through put platforms and are commercially available as automated devices.

Alternatively, proteolytic activity can be coupled to transcription instead of translocation which is generally compatible with greater throughput. In this case, the expression of a fluorescent reporter protein is modulated by the protease of interest. Different modes of regulating transcription through proteolysis have been published. In one example, Pu and colleagues engineered a protease-responsive version of T7 RNA polymerases (**Scheme 8**). In the default state, T7 RNA polymerase was fused to inactive T7 lysozyme which rendered T7 RNA polymerase unable to bind its promoter. Crucially, the flexible linker connecting T7 RNA polymerase and inactive T7 lysozyme featured a cleavage site for the protease of interest. This means, upon proteolytic cleavage the inactive T7 lysozyme is separated from the T7 RNA polymerase enabling it to bind its promoter and drive the expression of a fluorescent reporter protein [68].

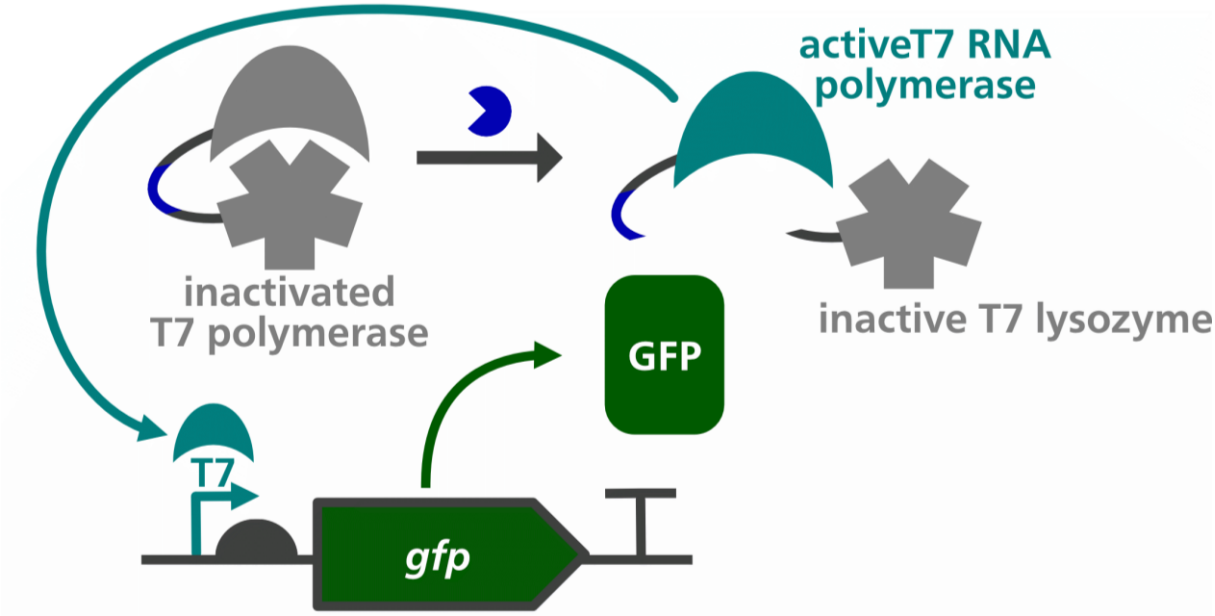

Scheme 8 Protease responsive RNA polymerases (RNA pols). In the default state, an T7 RNA polymerase is expressed fused to inactive T7 lysozyme that masks the promotor binding site of T7 RNA polymerase. Upon cleavage by a protease, the T7 lysozyme is cleaved off the RNA polymerase which in turn renders its capable to recognize its respective promoter and thus drives reporter gene expression (*gfp* in this example).

Alternatively, transcription can be regulated by protease-responsive repressors (**Scheme 9**). An elegant way of building protease sensitive repressors utilizes transcription activator like effectors (TALEs) as programmable repressors. TALEs comprise a class of modular-organized DNA binding proteins that naturally occur in bacterial plant pathogens [69]. Notably, the DNA binding specificity can be readily programmed as individual modules selectively recognize single base independent of sequence context. In addition, the affinity of TALEs to their binding sequences correlates with number of repeat units of the TALE contributing to binding. TALEs can therefore be rendered protease-responsive by introducing cleavage sites for a protein of interest between individual modules. In this way, the repressor loses its affinity for its operator as multiple DNA binding sites are physically separated from each. Given the binding specificity of TALEs can be readily programmed, no specific operator sequence is required. This is especially beneficial for scenarios in which multiple orthogonal proteases are tested within the same cell or with the same reporter gene.

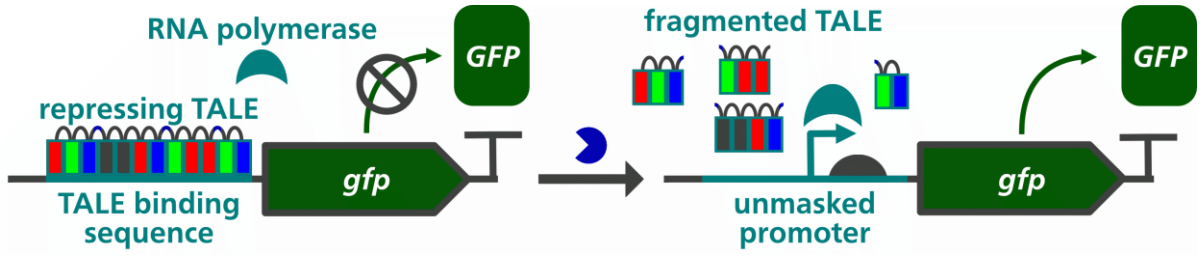

Scheme 9 Protease sensitive transcriptional repressors. Through proteolytic activity, the multiple DNA binding sites of a transcriptional repressor (here, exemplified with a TALE) are separated from one another rendering the repressor unable to suppress reporter gene expression.

In 2016, the Pfleger lab demonstrated that a 19 repeat TALE could completely suppress expression driven by a constitutive variant of the lac promoter. Three TEV cleavage sites were introduced to the TALE repressor. This resulted in cleavage fragments with four to five repeat units each. This reduced the affinity of the TALE sufficiently after proteolytic processing to recover around 50% of the fluoresce without TALE expression [70].

Finally, transcription factors can be rendered protease-responsive by caging (**Scheme 10**).

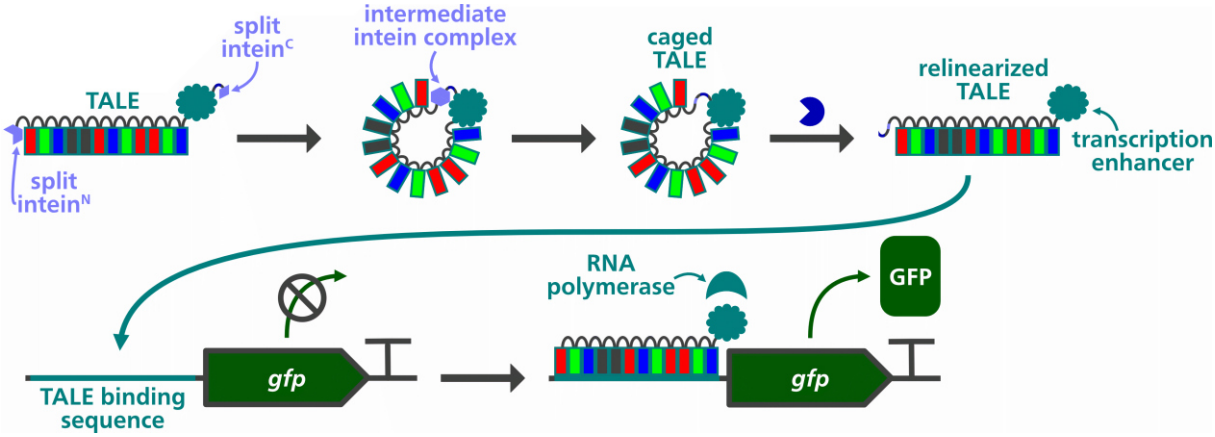

Scheme 10 Caged transcription factors. A transcription factor is expressed flanked by two split-intein fragments which immediately induce cyclization once the C-terminus exits the ribosome tunnel. Cyclized transcription factors cannot adopt their proper fold and are in turn not capable of binding their cognate repressor. Upon proteolytic cleavage, the transcription factor is re-linearized and thus able to adopt its proper fold in order to drive reporter gene expression.

Caging is achieved by expressing any given transcription factor as a fusion protein that is flanked by two fragments of a split intein. This results in cyclization of the transcription factor following ribosomal exit and renders it unable to bind its operator. De-caging is achieved through a cleavage site for the protease of interest that is incorporated into one of the linkers connecting the transcription factor and one the split intein fragments. Thus, protease activity leads to re-linearization of the transcription factor and subsequently refolding into its active

conformation. The now active transcription factor can bind to its operator and drive expression of the reporter gene. Once again generalization of this system was achieved by employing TALEs as programmable transcription factors [71].

3.4.2. Non-fluorescent read-outs

Beyond non-fluorescent read-outs, the activity of a protease can be associated with cell growth, for instance, by coupling cleavage to the function of an essential gene protein. In one example, Köhler and colleagues demonstrated this approach by using a yeast strain with a thermo-labile mutant of CDC25. At 30 °C normal growth occurred but by elevating the temperature to 37 °C CDC25 was inactivated and in turn it lost the ability to bind and activate endogenous RAS (yRAS) and essential membrane anchored protein. In the strain created by the authors yRAS was complemented by CDC25 independent human RAS (hRAS). To turn this strain into a protease sensor Köhler and coworkers incorporated a TEV cleavage site into the membrane anchor of hRAS (**Scheme 11**). Consequently, cell growth was abolished at the selection temperature of 37 °C as long active TEV was present in the cytosol. With this simply assay, the authors could screen TEV inhibitors *in vivo* with a simple colony formation assay on agar plates. In addition, optical density measurements of overnight cultures were performed to validate the colony formation assay. Even though growth-based proteolytic assays can be established relatively easy – provided a suitable target protein can be identified within the given host – the lack of real-time data and the diverse molecular factors influences on growth rates, such assays primarily yield qualitative data. For instance, in this particular case, it was possible to differentiate active from inactive protease variants and potent from mild inhibitors. In contrast, apparent protease kinetics or subtle differences between individual candidates typically remain beyond the resolution of growth assays [72].

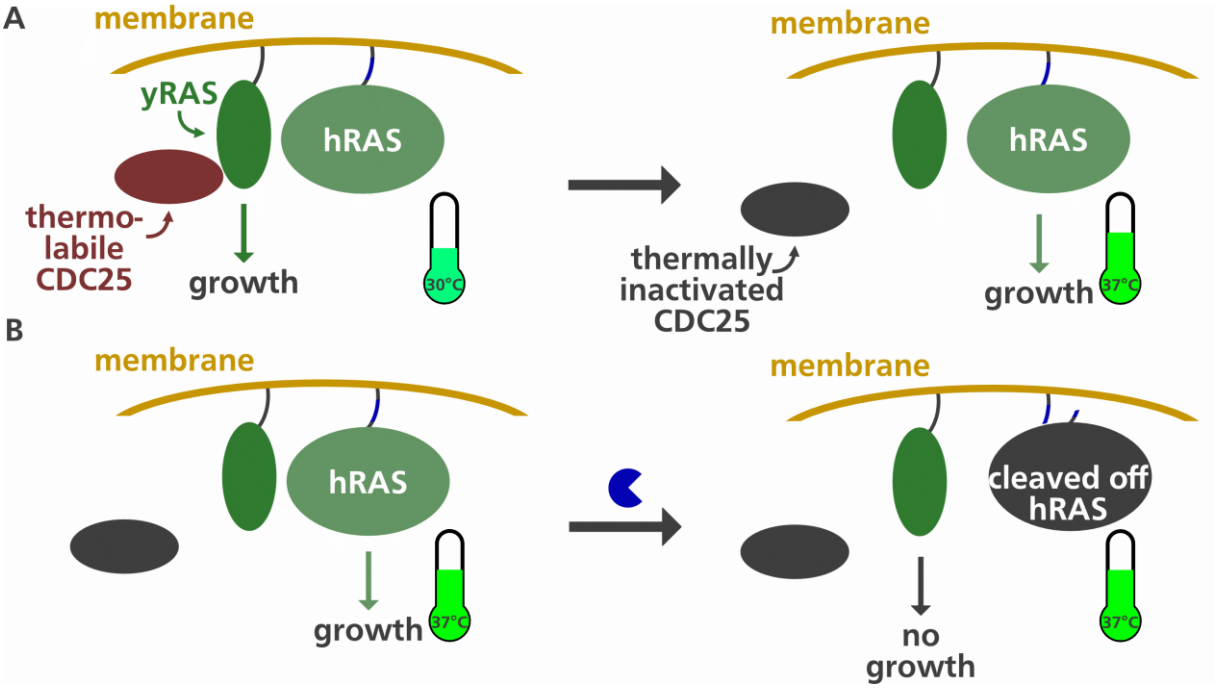

Scheme 11 Proteolytic assay based on growth. **A:** A thermo-labile CDC25 mutants binds to the yeast RAS (yRAS) protein and thereby enables cell growth, when the growth temperature is elevated from 30 °C to 37 °C CDC25 is inactivated and yRAS uses its activator, constitutively active human RAS (hRAS) complements the lost yRAS function and growth is still possible; **B:** the protease of interest cleaves the membrane anchor of hRAS at the selection temperature; non-membrane-associated hRAS is now unable to complement the lost yRAS activity and growth is prohibited.

3.5. Degradation tags as easy-to-adapt tools to generate protease responsive parts for synthetic biology

Beyond transcription, translocation or growth, protease-based activities can also be coupled to protein degradation. One mechanism of cellular protein degradation is mediated by the N-End rule which was postulated by Alexander Varshavsky as a universal mechanism to modulate the half-live of proteins [73-75]. The N-End rule states that the first one to three amino acids at the N-terminus of a protein determine its degradation rates – hence, the name N-end rule. The exact half-lives underlying the N-end rule vary across individual organisms, but in general terms small, hydrophilic and non-charged amino acids increase half-lives. In contrast, bulky, hydrophobic or positively charged amino acids decrease half-lives [73-75].

In eukaryotes the N-end rule is expanded trough several ubiquitinoylation pathways that contribute to increased degradation or fragmentation rates [76]. In prokaryotes however, ubiquitinylation does not occur. Here, the caseinolytic protease P (ClpP) complex as well as the soluble lon protease recognize and degrade proteins according to the N End rule. Analogous to the N-End rule, the C-End rule was discovered by A. Varshavsky stating that cysteine residues

found within unstructured C-termini of proteins drastically reduce their half-lives [77]. From this naturally occurring sequences, certain degradation signal sequences (degrons) were derived. These degrons can be fused to proteins to reduce their half-life even below the detection limits of expression assays or Western blots [78, 79].

In recent years, optimized degrons for the use in *E. coli* were published among others by the Keith and Voigt groups. The Keith group published the Ntag N-degron while the Voigt group published the XLFVQ N-degron and several C-degrons based on the naturally occurring ssrA C-degron [21, 80]. In both studies, the utility of the degrons was demonstrated in the form of cryptic degrons. A cryptic degron is a degron that is not directly located at the appropriate terminus of the protein, but unmasked through a proteolytic cleavage event and in this way renders the degron active.

In 2019 the Liu group from Jiagnan University (China) beautifully demonstrated the combination of potyvirus proteases with strong degrons to create fast switching synthetic circuits for flux optimization [24]. In another recent example, the potyvirus proteases were used to create Boolean Gates - the simplest logic gates - required for computing multi input information [23].

4. Results

4.1. Initial sensor designs – FRET and FPX

The utility of FRET or FPX sensors to probe potyvirus protease activities in *E. coli* was elaborated in the Bachelor dissertations of Tim Oliver Maier and Isabelle Marquardt. Both dissertations were conceptually designed and supervised by myself.

4.1.1. Bachelor thesis Tim Oliver Maier

Tim Oliver Maier's Bachelor thesis was entitled "Development and Characterization of Genomically Integrated, Synthetic Protease Switches in *E. coli*". A key goal was to validate the FPX sensor in *E. coli*. To facilitate the propagation of expression constructs in *E.coli*, Tim Maier integrated three different variants of TVMV protease (TVMV, TVMV-FKBP and MBP-^{TEV}AI-FKBP-FRB-TVMV) into the chromosome of *E. coli* BL21(DE3) cells using the modified clonetegration protocol [47] described in the Supplementary Methods (**see Chapter 13.3.1**). Constructs were integrated under control of different mutants of the T7 promoter with varying transcription activities [81]. For the majority of the integrated constructs, expression could be detected *via* Western Blotting as confirmed in **Figure 2** and **Figure 3**.

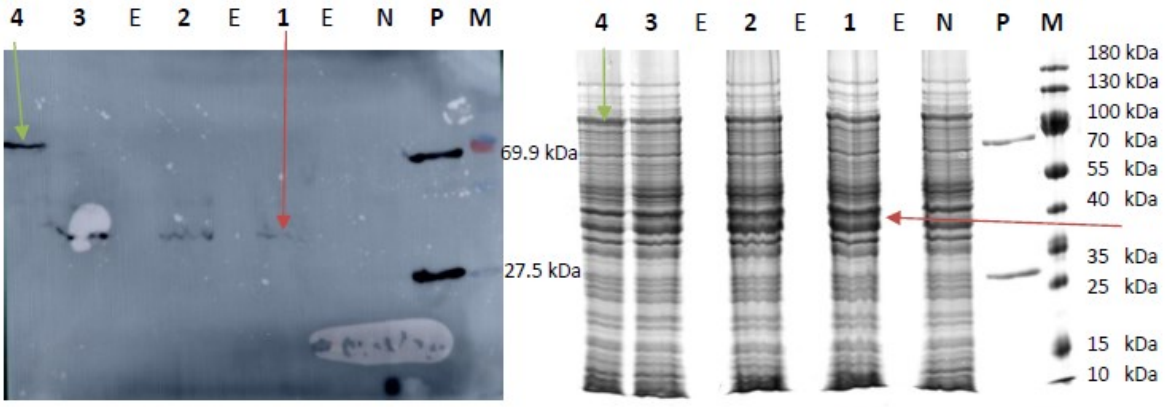

Lane	4	3	2	1	N	P	M
Load	$T7_{11}$ 29MBP^{TEV}-AI-FKBP-FRB-$TVMV_p$ (96.3 kDa)	$T7_{11}$ 29MBP^{TVMV}-$TVMV_p$-FKBP (80.5 kDa /38.8 kDa)	$T7_3$ 29MBP^{TVMV}-$TVMV_p$-FKBP (80.5 kDa /38.8 kDa)	$T7_n$ 29MBP^{TVMV}-$TVMV_p$-FKBP (80.5 kDa /38.8 kDa)	BL21 DE3	MBP^{TVMV}-sfGFP (69.9 kDa) $TVMV_p$ (27.5 kDa) (purified proteins)	PageRuler™ Prestained Protein Ladder (#26616)

Figure 2 Western Blot and SDS-PAGE of TVMV protease variants expressed in *E. coli* BL21(DE3) after clonetegration. Samples were taken 3 hours after induction of protease expression with 500 µM IPTG. All protease constructs carried a C-terminal His_6-tag for detection. Western Blot (left) was performed with a murine anti-His_6-mAB and rat anti-mouse mAB HRP-conjugate 0.44 µM PVDF membranes. Bands were visualized with chemiluminescence. Lane index of western blot and SDS-PAGE (right) refers to table below the images. Index "E" represents an empty lane. As positive control in the Western blot purified His-tagged MBP-^{TVMV}sfGFP-His_6 (69.9 kDa) and TVMV-His_6 (27.5 kDa)

were used. A 12 % polyacrylamide gel with Tris/Glycin buffer system was used. As protein size standard PageRuler™ Prestained Protein Ladder (#26616) (ThermoFisher) was used. Western blot is positive for $T7_n$_RBS29_MBP-^{TVMV}TVMV-FKBP (lane **1**), $T7_3$_RBS29_MBP^{TVMV}TVMV-FKBP (lane **2**), $T7_{11}$_RBS29_MBP^{TVMV}TVMV-FKBP (lane **3**) (red arrow) and $T7_{11}$_RBS29_MBP-^{TEV}AI-FKBP-FRB-TVMV (lane **4**) (green arrow). Electrophoretic mobility of MBP-^{TVMV}TVMV-FKBP samples (lane **1-3**) correspond to the size of cleaved TVMV-FKBP (without MBP), indicating proteolytic activity of these TVMV variants *in vivo*. Predicted sizes of proteins are given in table below. For MBP-^{TVMV}TVMV-FKBP variants predicted sizes for non-cleaved and cleaved proteins (referring to C-terminal cleavage fragment) are given. Figure and caption were adapted from the bachelor thesis of Tim Maier.

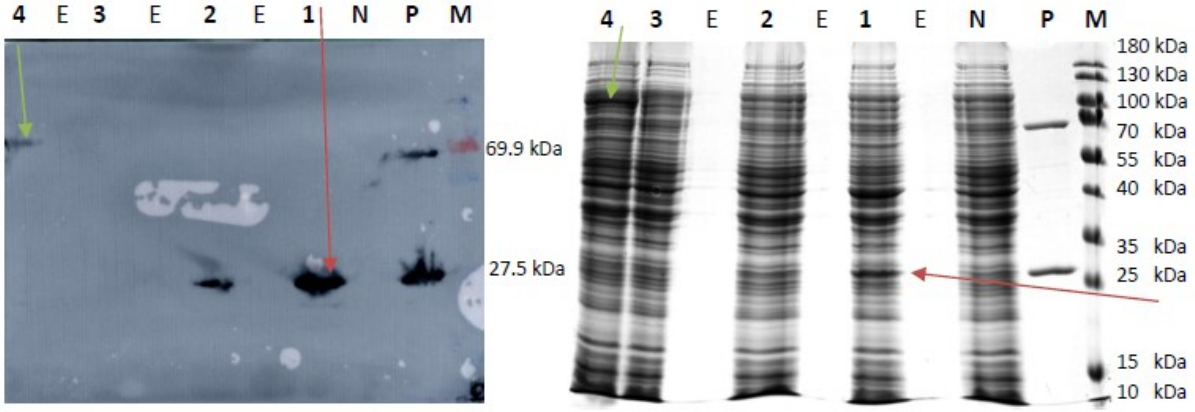

Lane	4	3	2	1	N	P	M
Load	$T7_3$ 29MBP^{TEV}-AI-FKBP-FRB-$TVMV_p$ (96.3 kDa)	$T7_n$ 29MBP^{TEV}-AI-FKBP-FRB-$TVMV_p$ (96.3 kDa)	$T7_{11}$ 29MBP^{TVMV}-$TVMV_p$ (71.8 kDa, 27.6 kDa)	$T7_n$ 29MBP^{TVMV}-$TVMV_p$ (71.8 kDa, 27.6 kDa)	BL21 DE3	MBP^{TVMV}-sfGFP (69.9 kDa) $TVMV_p$ (27.5 kDa) (purified proteins)	PageRuler™ Prestained Protein Ladder (#26616)

Figure 3 Western Blot and SDS-PAGE of TVMV protease variants expressed in *E. coli* BL21(DE3) following integration into the chromosomal DNA of *E.coli* by means of the clonetegration. Samples were taken 3 hours after induction of protease expression with 500 µM IPTG. All protease constructs bore a C-terminal His_6-tag for detection. Western Blot (left) was performed with a murine anti-His_6-mAB and rat anti-mouse mAB HRP-conjugate on 0.44 µM PVDF membranes. Bands were visualized with chemiluminescence. Lane index of western blot and SDS-PAGE (right) refers to table below the images. Index "E" represents an empty lane. As positive control in western blot purified His-tagged MBP-^{TVMV}sfGFP-His_6 (69.9 kDa) and TVMV-His_6 (27.5 kDa) were used. 12 % polyacrylamide gel was with Tris/Glycin buffer system used. As protein marker PageRuler™ Prestained Protein Ladder (#26616) (ThermoFisher) was used. Western blot is positive for $T7_n$_RBS29_MBP-^{TVMV}TVMV-FKBP (lane **1**), $T7_3$_RBS29_MBP^{TVMV}TVMV-FKBP (lane **2**), $T7_{11}$_RBS29_MBP^{TVMV}TVMV-FKBP (lane **3**) (red arrow) and $T7_{11}$_RBS29_MBP-^{TEV}AI-FKBP-FRB-TVMV (lane **4**) (green arrow). Electrophoretic mobility of MBP-^{TVMV}TVMV-FKBP samples (lane **1-3**) correspond to the size of cleaved TVMV-FKBP (without MBP), indicating proteolytic activity of these TVMV variants *in vivo*. Predicted sizes of proteins are given in table below. For MBP-^{TVMV}TVMV-FKBP variants predicted sizes for non-cleaved and cleaved proteins (referring to C-terminal cleavage fragment) are given. Figure and caption were adapted from the bachelor thesis of Tim Maier

To further verify the functional expression of the integrated protease constructs, gel-shift assays were performed with a TVMV-cleavable MBP-GFP fusion protein serving as a substrate. To this end, the BL21(DE3) strains were transformed with pACYCT2_MBP-^{TVMV}sfGFP-His_6. Proteolytic activity was confirmed by a shift of the reporter band from 70 kDa (MBP-^{TVMV}sfGFP) to 28 kDa

(sfGFP) on a semi-denaturing SDS-PAGE via in gel epi-fluorescence. **Figure 4** shows the results of the gel-shift assays. Purified MBP-^{TVMV}sfGFP-His_6 was included as a control as well as non-transformed BL21(DE3) cells and wild-type BL21(DE3) transformed exclusively with the reporter carrying plasmid. The fluorescent bands in **Figure 4** do not match the actual molecular masses of the corresponding cleavage fragments due to incomplete denaturation. Therefore, the hydrodynamic radii of the proteins may vary greatly based on the degree of denaturing.

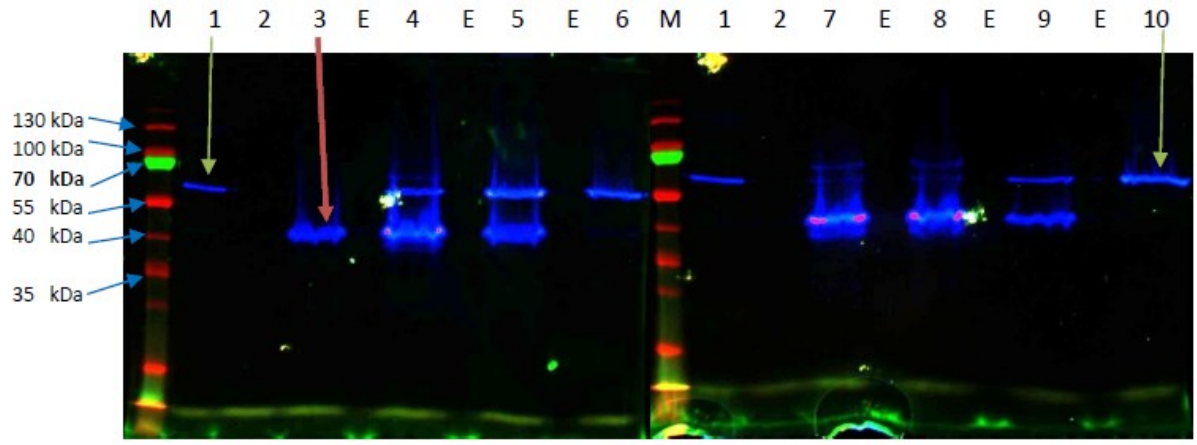

Index	1	2	3	4	5
Load	MBP^{TVMV}sfGFP (purified)	BL21 DE3	MBP^{TVMV}sfGFP + $T7_n$ 29MBP^{TVMV}-$TVMV_p$	MBP^{TVMV}sfGFP + $T7_{11}$ 29MBP^{TVMV}-$TVMV_p$	MBP^{TVMV}sfGFP + $T7_3$ 29MBP^{TEV}-AI-FKBP-FRB-$TVMV_p$
Index	**6**	**7**	**8**	**9**	**10**
Load	MBP^{TVMV}sfGFP + $T7_{11}$ 29MBP^{TEV}-AI-FKBP-FRB-$TVMV_p$	MBP^{TVMV}sfGFP + $T7_n$ 29MBP^{TVMV}-$TVMV_p$-FKBP	MBP^{TVMV}sfGFP + $T7_3$ 29MBP^{TVMV}-$TVMV_p$-FKBP	MBP^{TVMV}sfGFP + $T7_{11}$ 29MBP^{TVMV}-$TVMV_p$-FKBP	MBP^{TVMV}sfGFP (no protease)

Figure 4 Gel shift assay with MBP-^{TVMV}sfGFP-His_6 for detection of proteolytic TVMV activity. Fluorescence of SDS-PAGE gels was imaged with Amersham imager 600 RGB. Images above are overlays of three fluorescence channels (blue: Ex.: 460 nm/Em.:525 nm, green: Ex.:520 nm/Em.:605 nm and red: Ex.:630 nm/Em.:705 nm). GFP fluorescence was detected in the blue channel and is visualized by blue bands in overlay images. The able below the images states the samples on each lane. Empty lanes are marked with a "E". 12% polyacrylamide gels with Tris/Glycine buffer system were used. As a protein size standard marker PageRuler™ Prestained Protein Ladder (#26616) (ThermoFisher) was used. Images were processed with ImageJ. Figure and caption were adapted from the bachelor thesis of Tim Maier.

After Tim Maier verified the proteolytic activity of the non-auto-inhibited variants of the chromosomal integrated TVMV variants, he transformed the strains with pBS1A2 carrying the full-length FPX sensor under regulation of the RBS from the T7 phage gene 10 [82] and the constitutive Anderson-promoter J23101 (BBa_J23101, iGem registry). A schematic depiction of his sensor design is shown in **Scheme 12**. From several tested combination of promoters and

ribosome binding sites, this was the only combination were the GFP emission spectrum that showed any difference from wild-type BL21(DE3). The results of this experiments are summarized in **Figure 5**.

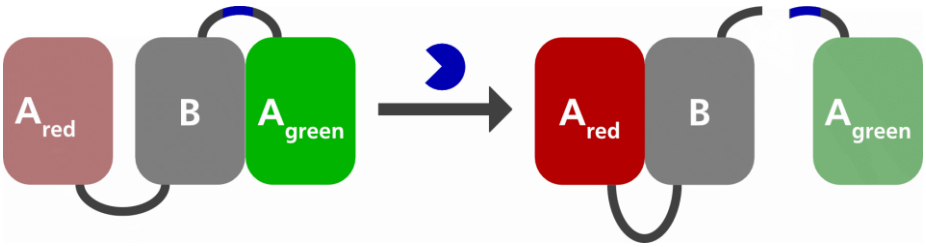

Scheme 12 Schematic depiction of the FPX based sensor design used by T. Maier in his bachelor thesis. The sensor comprised of two dimerization dependent fluorescent protein A_{red} and A_{green} which competed for the dimerization interface of the fluorophore deficient B to reconstitute their fluorescence. In the default state dimerization of A_{green} and B should have been preferred and thereby the overall fluorescence of the population should have been green. Upon TVMV (blue circular section) cleavage within the linker region (blue segment representing the TVMV cleavage site) between B and A_{green}, A_{green} is separated from the fusion protein and thus intramolecular association of A_{red} and B is now preferred over intermolecular dimerization of B and A_{green}. Accordingly, proteolytic activity of TVMV should have shifted the overall fluorescence of the population from green to red.

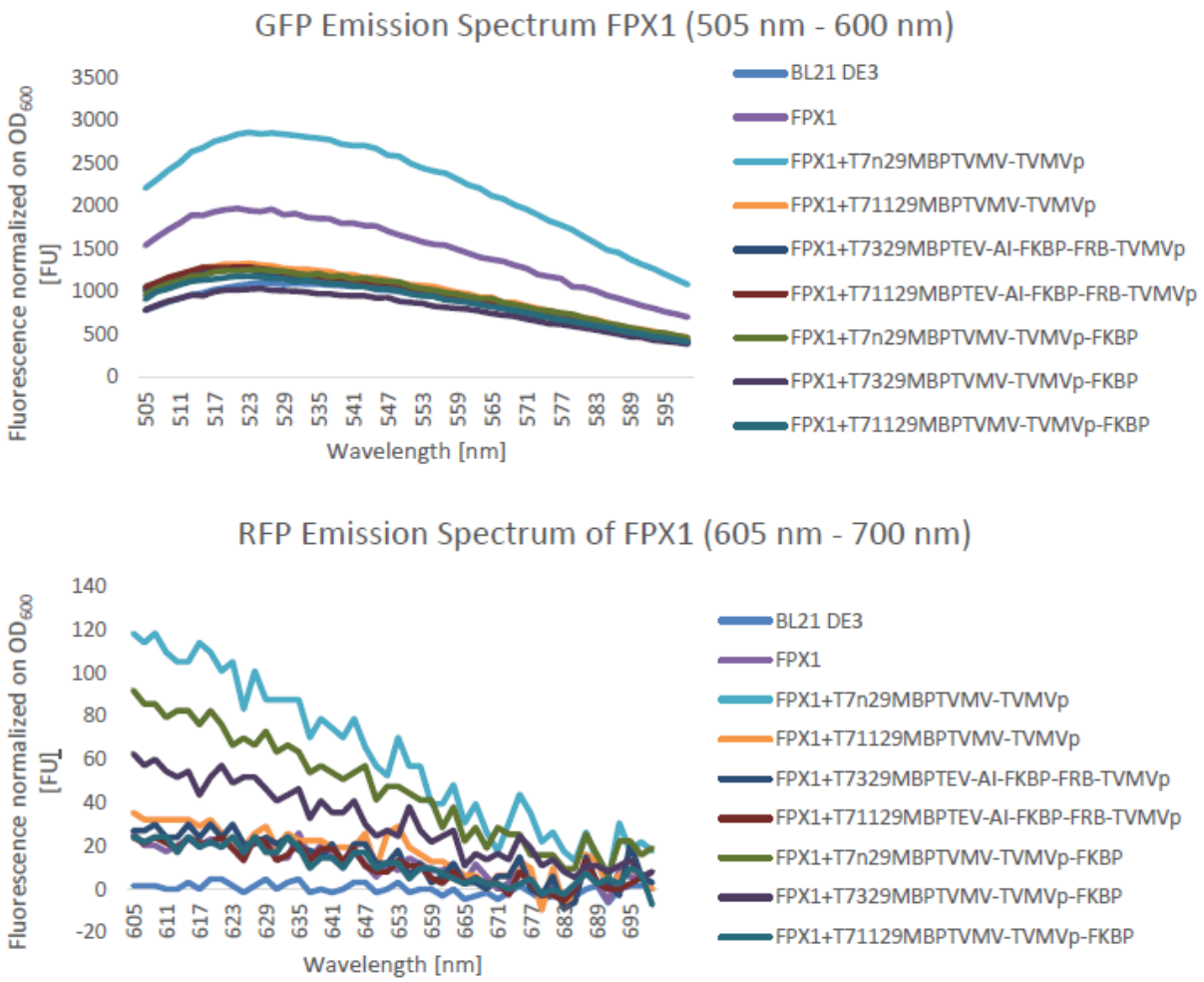

Figure 5 In cell GFP and RFP emission spectra of FPX1. GFP and RFP emission spectra of cells co-expressing the TVMV-FPX-sensor and chromosomal integrated TVMV constructs. *E. coli* BL21 DE3 wildtype cells as negative control. Measurements were performed with TECAN Spark®. Excitation wavelength for GFP emission spectrum (505 nm to 600 nm) was 460 nm with 20 nm bandwidth. Excitation wavelength for RFP emission spectrum (605 nm – 700 nm) was 560 nm with 20 nm bandwidth. Fluorescence values were normalized to the OD_{600} of the samples. Constructs in this figure are the chromosomal integrated TVMV variants from **Figure 2** and **Figure 3** and pBS1A2_J3101_RBS_A_{red}-B-$^{TVMV}A_{green}$-Strep.

As evident in **Figure 5**, distinct emission spectra for GFP or RFP could now be measured after inducing the expression of the full-length FPX either without or with co-expression of one his TVMV protease constructs. Tim Maier also demonstrated that soluble expression of the three domain FPX sensor in *E. coli* was not feasible. Therefore, the focus shifted to FRET-based protease sensors. The rationale behind this was that in contrast to the dimerizing fluorescent proteins of FPX, FRET can be performed with monomeric fluorescent proteins. Therefore, it was though that aggregation of the sensor proteins could be reduced in *E. coli*.

4.1.2. Bachelor thesis and research internship Isabelle Annina Catherine Marquardt

The widely used FKBP-FRB recruitment system where rapamycin induces the heterodimerization of FKBP and FRB was also integrated into the sensor construct with the aim of facilitating and accelerating cleavage by means of induced molecular proximity [1, 83]. This system was incorporated by I. Marquardt into her FRET sensor design.

Building on the work in the dissertation of Tim Maier, Isabelle Marquardt expanded the repertoire of chromosomally integrated TVMV protease constructs under control various T7 promoter variants. In her case, this included a native T7 promoter ($T7_n$) and $T7^{C9A}$ ($T7_9$). The latter was reporter to poses a drastically reduced transcriptional activity [81, 84] . As T. Maier before her, she was following the modified clonetegration protocol established in our group by M. Röder (see **Chapter 13.3.1**). All integrated protease constructs showed proteolytic activity *in vivo*. For the native T7 promoter expression could be proven by Western blot analysis but for all constructs *in vivo* activity was proven *via* gel-shift assays. For this purpose, I. Marquardt cloned a new FRET based TVMV sensor using the widely used FRET pair CyPet/Ypet [62]. She also included the rapamycin-inducible co-localization system of FKBP12/FRB into her design. The sensor design and the basic assay are shown in **Scheme 13**. To verify the *in vivo* activity I. Marquardt performed the same gel-shift assay that T. Maier used in **Chapter 4.1.1. Figure 6** shows the result of this gel-shift assay.

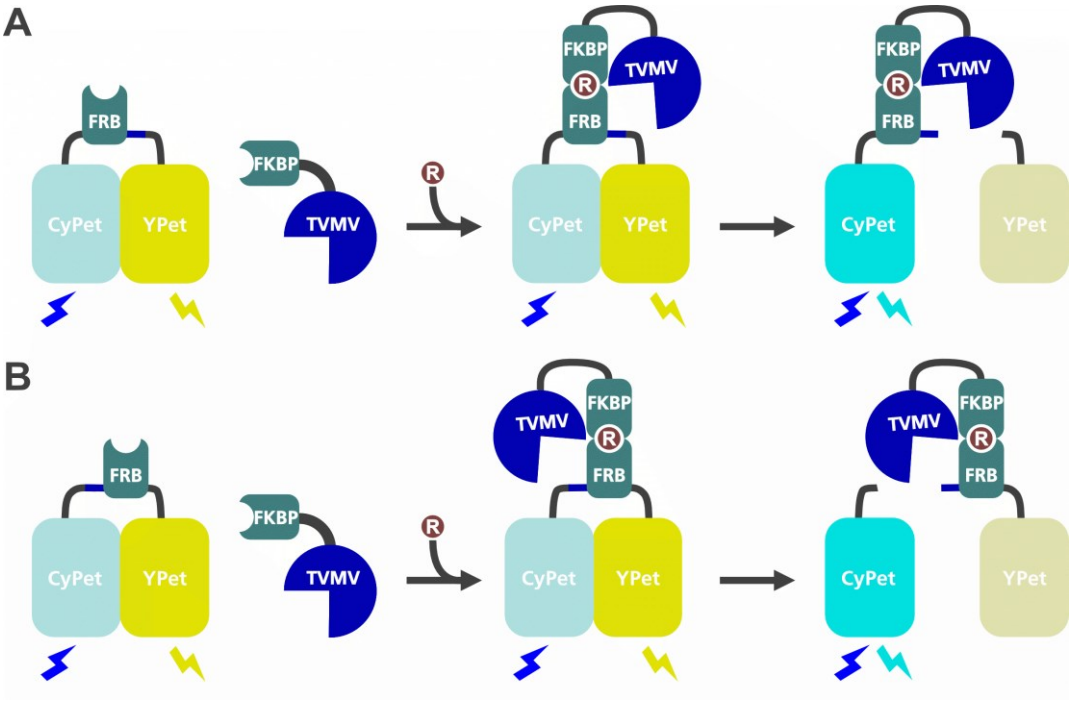

Scheme 13 TVMV FRET sensor design used by I. Marquardt in her bachelor thesis. The sensor comprises of the FRET pair CyPet/Ypet and a TVMV cleavage site (blue bar) within the linker region. Adjacent to TVMV cleavage site FRB was inserted into the sensor to facilitate Rapamycin dependent recruitment of the FKBP12-fused TVMV to the cleavage site. In the default state CyPet and YPet are located in close proximity and FRET occurs, upon rapamycin addition (R labeled brown circle) FRB and FKBP12 form a heterodimer and thereby direct the FKBP-fused TVMV to its cleavage site. Upon cleavage, CyPet and YPet are separated from one another and FRET is no longer possible. **A:** FRB is located N-terminally of the cleavage site and a larger N-terminal cleavage fragment is generated. **B:** FRB is located C-terminally of the cleavage site and a smaller N-terminal cleavage fragment is generated.

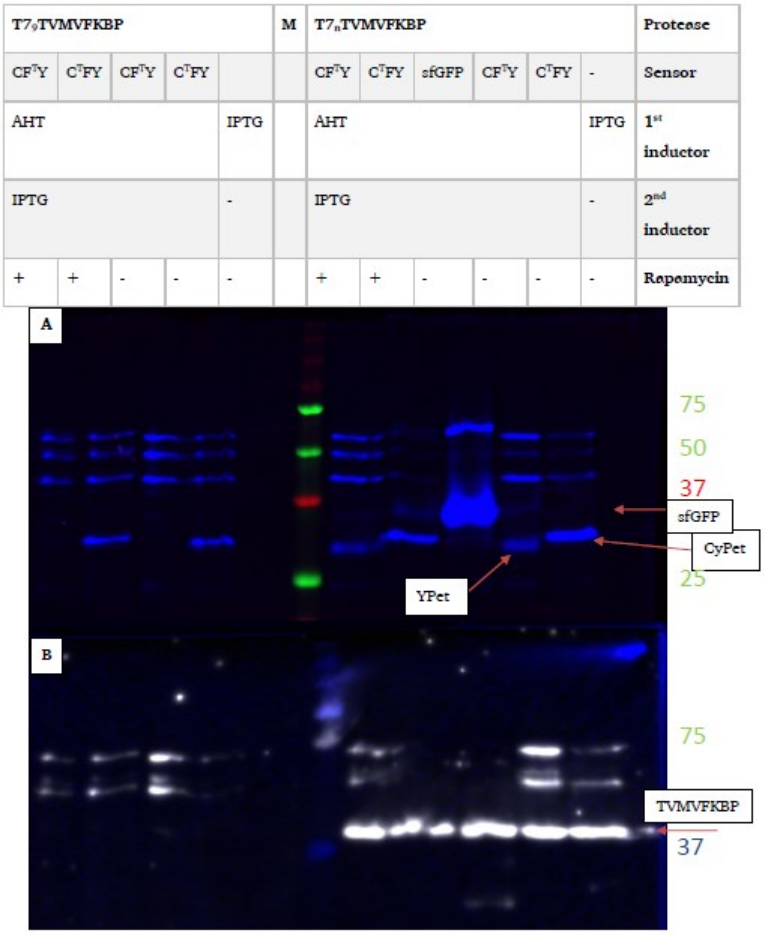

Figure 6 Gel-Shift Assay performed by I. Marquardt to verify the *in vivo* activity of a TVMV-FKBP fusion construct that was chromosomal integrated under the control of either the native T7 promoter ($T7_n$) or the $T7^{C9A}$ mutant ($T7_9$). The two sensor constructs tested (CyPet-FRB-^{TVMV}YPet-His_6 = CF^TY and CyPet-^{TVMV}FRB-YPet-His_6 = C^TFY) were expressed und the control of the tet promoter of pASK-IBA3. TVMV expression was induced with 500 µM IPTG while sensor expression was induced with 200 ng/L AHT, co-localization of protease and sensor was induced by the addition of 25 nM rapamycin. The first inducer (see table above the gels) was added once cultures reached an optical density of approx. 0.3, the second inducer two hours later and rapamycin one hour after the second inducer, finally two hours after rapamycin addition (total expression of expression time of first component 6 hours and 4 hours for the second one) samples equal to 5 ODU in 40 µL were taken. 10 µL of this sample diluted 1:1 with 2x SDS loading were loaded per lane on to 12 % polyacrylamide gels with Tris/Glycine buffer system. Proteins were plotted on 0.44 µM PVDF membranes and bands were detected with a murine anti-His_6-mAB and rat anti-mouse mAB HRP-conjugate. Visualization of bands in semi-denatured SDS-PAGE wit epi-fluorescence in three channels (blue: Ex.: 460 nm/Em.:525 nm, green: Ex.:520 nm/Em.:605 nm and red: Ex.:630 nm/Em.:705 nm) and on Western blot with chemiluminescence. Constructs in this figure *E. coli* BL21(DE3) with $T7_9$_MBP-^{TVMV}TVMV-FKBP-His_6 and T7MBP-^{TVMV}TVMV-FKBP-His_6 integrated into HK022 locus and pASK-IBA3_ CyPet-FRB-^{TVMV}YPet-His_6 or CyPet-^{TVMV}FRB-YPet-His_6.

The low molecular weight of the TVMV-FKBP bands in **Figure 6 B** indicated functional expression of the TVMV fusion construct because the fused N-terminal solubility tag MBP was cleaved off *in situ* (TVMV cleavage included in the linker region between MBP and TVMV-FKBP). Expression of TVMV-FKBP under control of the $T7^{C9A}$ ($T7_9$) could not be detected but the presence of sensor cleavage fragments in left half of **Figure 6 A** indicated TVMV activity.

The appearance of the uncleaved sensor in triple bands in in-gel epi-fluorescence (**Figure 6 A)** or double bands on the Western blot (**Figure 6 B**) is explained through semi-denaturing conditions during sample preparation to enable epi-fluorescence detection of the sensor in the gels. Unfortunately, the fixed channels of the used Amersham imager 600 RGB (blue: Ex 460 nm / Em.:525 nm, green: Ex.:520 nm / Em.:605 nm and red: Ex.:630 nm / Em.:705 nm) did not enable differentiation of CyPet and YPet because both were excited in the blue channel. Therefore the *in vivo* emission spectrum of the sensor was measured by I. Marquardt. If FRET would have occurred a distinct maxim for YPet fluorescence around 530 nm would be expected upon excitation of CyPet fluorescence at 435 nm. The corresponding spectra for all four strains generated by I. Marquardt in her thesis can be found in **Figure 7**.

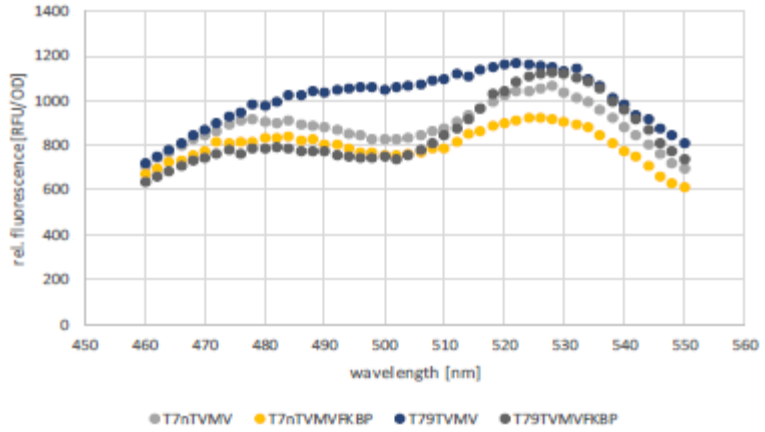

Figure 7 Emission of TVMV strains created by I. Marquardt transform with pASK-IBA3_CyPet-^{TVMV}FRB-YPet-His$_6$ following 3 hours of induction of the sensor with 200 ng/L AHT. The fluorescence was measured with the TECAN Spark plate reader and normalized to the OD_{600} of the wells. CyPet fluorescence was exited with 415 ± 20 nm, emission was quantified from 460 nm to 550 nm with a bandwidth of 20 nm. Two distinct maxima were observed at approx. 480 nm ($\lambda_{max, em}$ CyPet 477 nm, [62]) and approx. 528 nm ($\lambda_{max, em}$ YPet 530 nm, [62]). Spectra for chromosomal integrated: T7$_n$_MBP-^{TVMV}TVMV in light grey, T7$_n$_MBP-^{TVMV}TVMV-FKBP in yellow, T7$_9$_MBP-^{TVMV}TVMV in blue, T7$_9$_MBP-^{TVMV}TVMV-FKBP in dark grey. Strains used in this figure: T7$_n$_MBP-^{TVMV}TVMV-His$_6$, T7$_n$_MBP-^{TVMV}TVMV-FKBP-His$_6$, T7$_9$_MBP-^{TVMV}TVMV-His$_6$, T7$_9$_MBP-^{TVMV}TVMV-FKBP-His$_6$ integrated in HK022 locues of BL21(DE3).

The spectra showed two distinct emission maxima at ~480 nm and ~528 nm which aligned with the emission maxima of CyPet and YPet at 477 nm and 530 nm, respectively [62]. This results clearly indicated that FRET was observable upon expression of the sensor construct. In the subsequent experiments, I. Marquardt tried to co-express both her protease constructs and the sensor and monitor the changes of the fluorescence intensities at the two maxima. In theory upon excitation with 415 ± 20 nm the emission at the CyPet emission maximum at 477 ± 20 nm should have increased through proteolytic processing of the sensor while the emission at the YPet emission maximum at 530 ± 20 nm should have decreased. The modulation in emission intensities should have been the result of FRET abolishment through separation of

CyPet and YPet due to TVMV cleavage in the linker region. The result of this experiment is shown in **Figure 8**. For all strains a rise in YPet fluorescence over time was observed meaning despite the gel-shift assays revealed partial cleavage of the sensor no TVMV mediated loss in YPet fluorescence as a consequence of TVMV-mediated reduction in FRET could be observed by I. Marquardt. A similar increase in fluorescence intensity for CyPet was observed. This led to the assumption that the production rate of new uncleaved sensor overshadowed any TVMV mediated effects. Consequently, the FRET sensor design of I. was discarded.

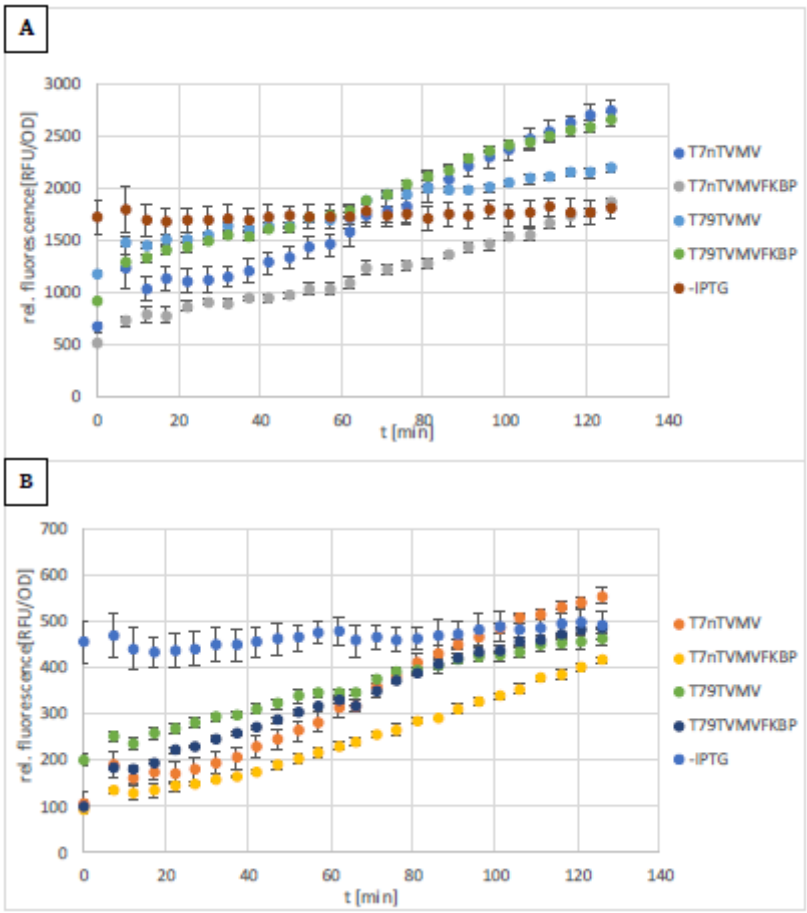

Figure 8 Monitoring of *in vivo* TVMV-mediated modulation of the fluorescent signals generated by CyPet-^{TVMV}FRB-YPet-His$_6$. Data points represent the mean fluorescence intensities of dependent biological triplicates of BL21(DE3) strains with TVMV constructs integrated into the HK022 locus transformed with pASK-IBA3_CyPet-^{TVMV}FRB-YPet-His$_6$ normalized to OD_{600} of the wells. Sensor expression was induced once cultures reach exponential growth phase and protease construct expression was induced one hour later. Measurements were started directly after protease expression induction (t_0). Fluorescence was excited at 415 ± 20 nm and emission was measured at 477 ± 20 nm (CyPet, **B**) and 530 ± 20 nm (YPet, **A**). Color code is stated in the legends on the right, a no induction of protease expression with T7$_n$_MBP-^{TVMV}TVMV (-IPTG) was included as a negative control.

As elucidated above, consistent changes in FRET spectra as a function of protease activity could not be observed by I. Marquardt even though the expression and *in vivo* cleavage of the FRET-based protease sensor could be verified *via* in gel epi-fluorescence measurements and by means of Western blot analysis.

Therefore, in order to increase the chances of success, the system was further simplified to two completely independent fluorescent proteins. In the linker connecting both fluorescent proteins (FPs), a TVMV dependent cryptic N-degron was inserted. This simplification led to the first design of degron-based protease sensors. In addition, a sensor design was conceived based on a single FP fused to a C-terminal degradation tag (C-degron). This most basic design was used to screen for the optimal expression conditions during the assay (see **Chapter 4.2**).

4.2. C-Degron based positive read-out protease assay

4.2.1. Design of a two-plasmid-based *in vivo* assay

For the basic sensor design, a single fluorescent protein – mNeonGreen (mNG) [85] – was fused to a recently discovered C-degron. The degron was identified by the Weigand Lab at our department in the C-terminus of splice isoform E of the human Myc associated factor X (MAX) and termed “E99-134”. This name refers to isoform E of human MAX and amino acid positions 99 to 134 in that isoform. Fusion of this C-terminal part of MAX isoform E to eGFP or firefly luciferase lead to strong downregulation of reporter protein levels without reducing the mRNA abundance in human cells Based on a personal communication of on-going research a truncated version of the degron E118-134 selected selected as the initial model C-degron for this project. The amino acid sequence of E118-134 was FGTWACRVRASHGVCAQ. As expected from C-degron at least one cysteine residue was present in a putative unstructured sequence.

Because previous findings indicated that TVMV fusion proteins might have impaired activities, all possible combinations and relative orientations of domains both in the sensor and the protease constructs were cloned and tested.

Based on previous findings demonstrating that active TVMV recruitment can accelerate cleavage, the FKBP/FRB system was integrated into both the sensor and the protease constructs [1, 3]. The general design principle of the assay is depicted in **Scheme 14** featuring a minimal set of functional domains necessary to conduct the assay.

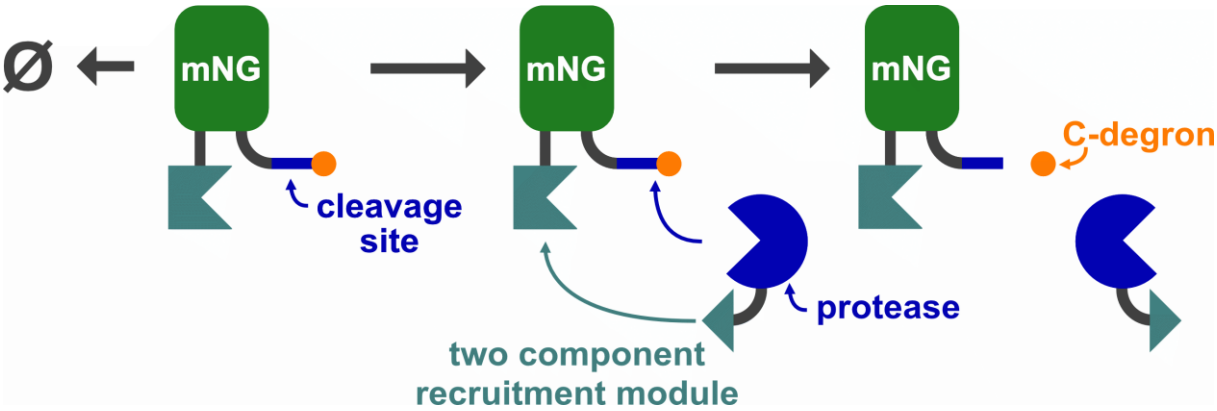

Scheme 14 General design of the single FP C-degron assay for sequence specific proteases. mNeonGreen (mNG) is tagged with a C-degron (orange circle). Left: The sensor is expressed and the degron induces rapid degradation (**Ø**) of the sensor to suppress a fluorescent signal in the cell. Center: The protease of interest (blue circular sector) is co-expressed with the sensor. The two-component recruitment module (teal rectangular section and teal triangle) directs the protease to the sensor and the protease binds to its cleavage site (blue part of the linker). Right: The protease cleaves off the C-degron and the fluorescent sensor can accumulate and generate a fluorescent signal in the cell.

In the first design iteration, the rapamycin-dependent FKBP-FRB recruitment module was tested. Recruitment was included to accelerate the rate of proteolytic cleavage through the rapamycin induced colocalization of the TVMV and its substrate. In addition, a recently established protein co-expression system (unpublished results by W. Weber) was employed to facilitate the stable co-expression of both the protease and the sensor. This co-expression system is based on the well-established pPRO24 vector originally created by the Keasling group [87] and the pCtrl2 vector that was created in the AG Stein and derived from pACYCT2 [88].

pCtrl2 possesses pACYCT2's class B p15A ori and its chloramphenicol resistance. The key difference is the expression cassette: While pACYCT2 features a leaky dual expression cassette, pCtrl2 is an extremely tight single expression vector. In addition, protein expression in *E. coli* BL21(DE3) cells was controlled by a lacI/lacO system and driven by the T7 promotor. Furthermore, the multiple cloning site (MCS) was flanked by three transcriptional terminators on each side to prevent any form of leaky expression. The dual expression system is summarized in **Scheme 15** while a detailed view of the expression cassette is shown in **Figure 9**.

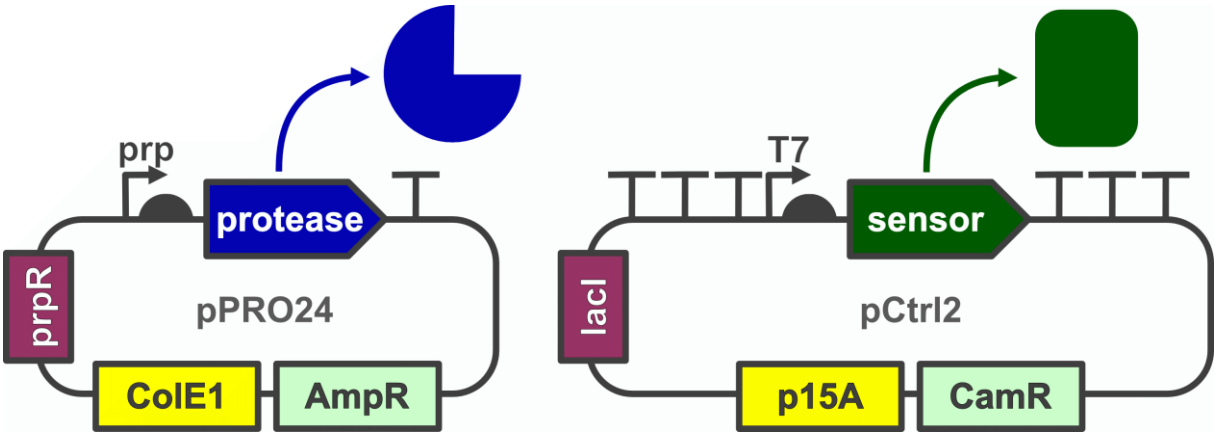

Scheme 15 Dual expression system for the stable, independent co-expression of a protease and its substrate in *E. coli* BL21(DE3) cells. Origins of replication (oris) in yellow, selection markers in mint green, repressors in purple, genetic elements in grey and coding sequences in colors matching their gene product. Left: pPRO24 (Pprp/prpR, class A ColE1 ori, AmpR) for propionate inducible expression of protease constructs. Right: pCtrl2 (PT7-lacO/lacI, class B p15A ori, CamR) for IPTG/lactose inducible expression of sensor/substrate constructs.

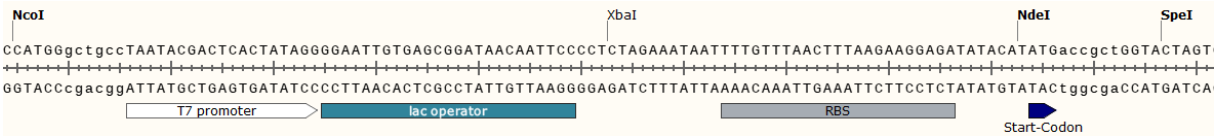

Figure 9 Expression cassette of the newly constructed pCtrl2 (pCtrl2 was generated by W. Weber, unpublished results). The expression cassette was cloned between a NcoI and a NdeI restriction site, a XbaI site is located between the operator and ribozyme binding site (RBS). T7 promoter in white, lac operator in cyan, RBS in grey and Start-Codon in blue, restriction sites are annotated above the DNA double strand. pCtrl2 was created on the basis of pACYCT2 by W. Weber. Figure was created with SnapGene (GSL Biotech LLC).

4.2.2. Effect of Rapamycin-Dependent Recruitment based on the FKBP-FRB module

In order to differentiate fluorescence generated from prematurely terminated translation of the sensor or cleavage of the degron through unspecific proteases, a mock control was included for every protease construct tested. In case of TVMV, the mock was the catalytically inactive C151A variant. This single amino acid substitution stripped the protease of its catalytic nucleophile and thereby rendered it inactive without negatively impacting its capacity to fold [36]. In this way, an identical metabolic burden could be imposed as the exact same proteins were translated except that the catalytic cysteine residue was replaced by a catalytically inactive alanine residue.

In the first set of experiments, three parameters were subsequently tested: **(i)** the influence of the relative orientations of domains on the performance of TVMV was examine, **(ii)** the effect of adding rapamycin and, in this way, induce co-localization of the protease with its substrate, and **(iii)** whether it made any difference if FKBP was fused the protease and FRB to the sensor or *vice versa*.

As a positive control for each individual sensor construct, a version without the E118-134 C-degron was included. The results for one of the tested relative orientations are exemplarily shown in **Figure 10**. Furthermore, experiments concerning the relative orientation of domains and the effect of rapamycin-dependent effects are summarized in **Table 2**. The data for all measured orientations can be found in the supplementary figures (**Figure S1** to **Figure S6**). Even though rapamycin was added at a concentration of up to 250 nM – while the K_D for complex formation is in the low nanomolar range [83] – no significant effect of induced colocalization was detected. Accordingly, rapamycin was omitted from this point onward in order to keep the cost per assay within reasonable limits.

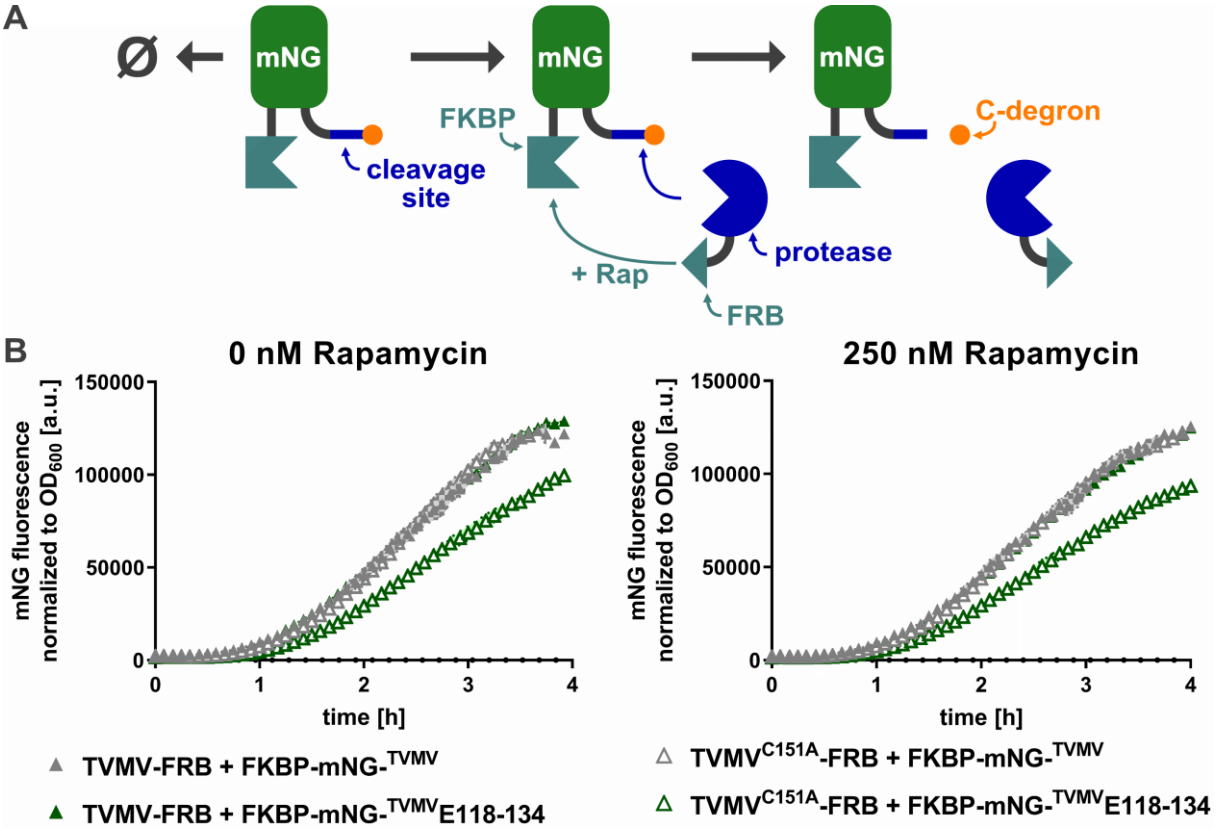

Figure 10 Effect of induced co-localization based on the rapamycin-dependent FKBP-FRB protein-protein interaction module. **A:** Schematic depiction of the assay, elements as in **Scheme 14**, except constitutive recruitment is replaced through rapamycin dependent heterodimerization of FKBP and FRB. **B:** Exemplary data for the relative orientation of TVMV-FRB in conjunction with FKBP-mNG-^{TVMV}E118-134. Active TVMV depicted as filled triangles; inactive TVMV^{C151A} (mock controls) as empty triangles; positive controls without E118 134 C-degron in grey; actual sensor constructs with E118-134 C-degron cloned to the C-terminus in green; all data points represent the mean values of three dependent biological replicates measured; the error areas depict the standard error of the mean (SEM) in colors matching the corresponding data points, dark checkered areas belong to data sets of active TVMV constructs, plain areas belong to data sets of inactive TVMV^{C151A} constructs, rapamycin concentration used stated above the corresponding graph, legend at the bottom refers to all graphs. Constructs used: pPRO24_MBP-^{TVMV}TVMV-FRB,

pPRO24_MBP-^{TVMV}TVMV^{C151A}-FRB, pCtrl2_FKBP-mNG-^{TVMV}, pCtrl2_FKBP-mNG-^{TVMV}-E118-134, pCtrl2_mKO$_{\kappa}$ Protein Sequences are stated in the supplement (see **13.4.1**).

Table 2 FKBP/FRB orientation screening and effect of rapamycin on the protease performance. Rapamycin: positive effect (+), negative effect (-) no effect (o). Promising results marked with grey-shading.

Protease construct	Sensor construct	Performance	Rapamycin
FRB-TVMV	FKBP-mNG-^{TVMV}E118-134	Fluorescence independent of protease activity	o
	mNG-^{TVMV}FKBP-E118-134	Fluorescence independent of protease activity	o
	mNG-FKBP-^{TVMV}E118-134	No expression with degron	o
TVMV-FRB	FKBP-mNG-^{TVMV}E118-134	Protease slightly increases fluorescence compared to mock	o
	mNG-^{TVMV}FKBP-E118-134	Fluorescence independent of protease activity	o
	mNG-FKBP-^{TVMV}E118-134	No expression with degron	o
FKBP-TVMV	FRB-mNG-^{TVMV}E118-134	Fluorescence independent of protease activity	o
	mNG-^{TVMV}FRB-E118-134	Fluorescence independent of protease activity	o
	mNG-FRB-^{TVMV}E118-134	Fluorescence independent of protease activity	o
TVMV-FKBP	FRB-mNG-^{TVMV}E118-134	Protease slightly increases fluorescence Compared to mock when Rapamycin is present	+
	mNG-^{TVMV}FRB-E118-134	Fluorescence independent of protease activity	o
	mNG-FRB-^{TVMV}E118-134	Fluorescence independent of protease activity	o

In order to assess whether low degradation rates or high background fluorescence of free riboflavin in the LB medium were the cause of the high fluorescence intensities measured for the mock control, the culture medium during the assay was switch to riboflavin free M9 minimal medium. In order to omit catabolite repression, switching to a minimal medium also required the selection of a carbon source that is compatible with the underlying expression system. In 2014 Aidelberg *et al*. unveiled the hierarchy of non-glucose sugar uptake and utilization. This hierarchy manifests itself in a characteristic repression cascade that forms part of catabolite repression. As long as a higher order sugar is present, all genes for uptake and utilization of sugars lower in the hierarchy are repressed [89]. Catabolite repression plays a key role in heterologous gene expression in *E. coli* when promoters of sugar operons, like the widely used lac promoter, are driving gene expression. The latter always applies to vectors harboring the T7 promoter – as is the case for pCtrl2 – because the chromosomal integrated T7 RNA polymerase is generally under the control of the T7 promoter in *E. coli* BL21(DE3). The effect of the sugar hierarchy is amplified during cultivation of *E. coli* in minimal media like the M9 medium selected for all further experiments.

Based on the findings of Aidelberg and colleagues as wells as tests within our group (research Internship I. Marquardt) arabinose was chosen as the carbon source for all experiments in M9 medium in this work [89]. Additionally, the effect of the genetic background was estimated by changing the host strain from BL21(DE3), a *lonp*$^{-}$ B-strain, to a *lonp*$^{+}$ K-strain.

4.2.3. Effect of *lonp*$^{+}$ Genetic Background

KRX was chosen as a BL21(DE3) replacement because it also harbored a chromosomal integrated T7 RNA polymerase with the only difference was that in case of KRX, the T7 RNA polymerase expression was under control of a rhamnose-inducible promoter.

The rationale behind this decision was the thought that the strong over-expression driven by the T7 promoter could have overloaded the crippled degradation machinery of BL21(DE3). Based on the findings summarized in **Table 2**, the combination of TVMV-FRB and FKBP-mNeonGreen-^{TVMV}E118-134 was chosen as the most promising candidate for further improvements. Therefore, these relative orientations were tested in minimal media and with cells of the *lonp*$^{+}$ *E. coli* strain KRX.

In addition, an auto-fluorescence control was devised in order to estimate to what extent endogenous riboflavin affected the fluorescent signal in the assay. For this control, cells were co-transformed with a protease construct in pPRO24 and with pCtrl2 containing mKOκ a non-green fluorescent protein. This control should impose a similar metabolic burden on the cells and provide an estimate of any background fluorescence that would arise independent of the expression of a fluorescent protein.

Figure 11 shows the increase in mNG fluorescence over time under the conditions tested. In LB medium both strains performed similar: This means, BL21(DE3) displayed higher overall expression levels compared to KRX even higher than the detection limit of the plate reader which is why some data points in the left graph of **Figure 11 A** are missing. **Figure 11 B** shows the same data but in M9 minimal medium. The lack of data for KRX in M9 minimal medium was caused by a lack of thiamine in the medium which is non-essential for BL21(DE3) but essential for KRX. But the results in LB medium indicate that the Lon protease present in KRX has no significant impact on the dynamics of the assay.

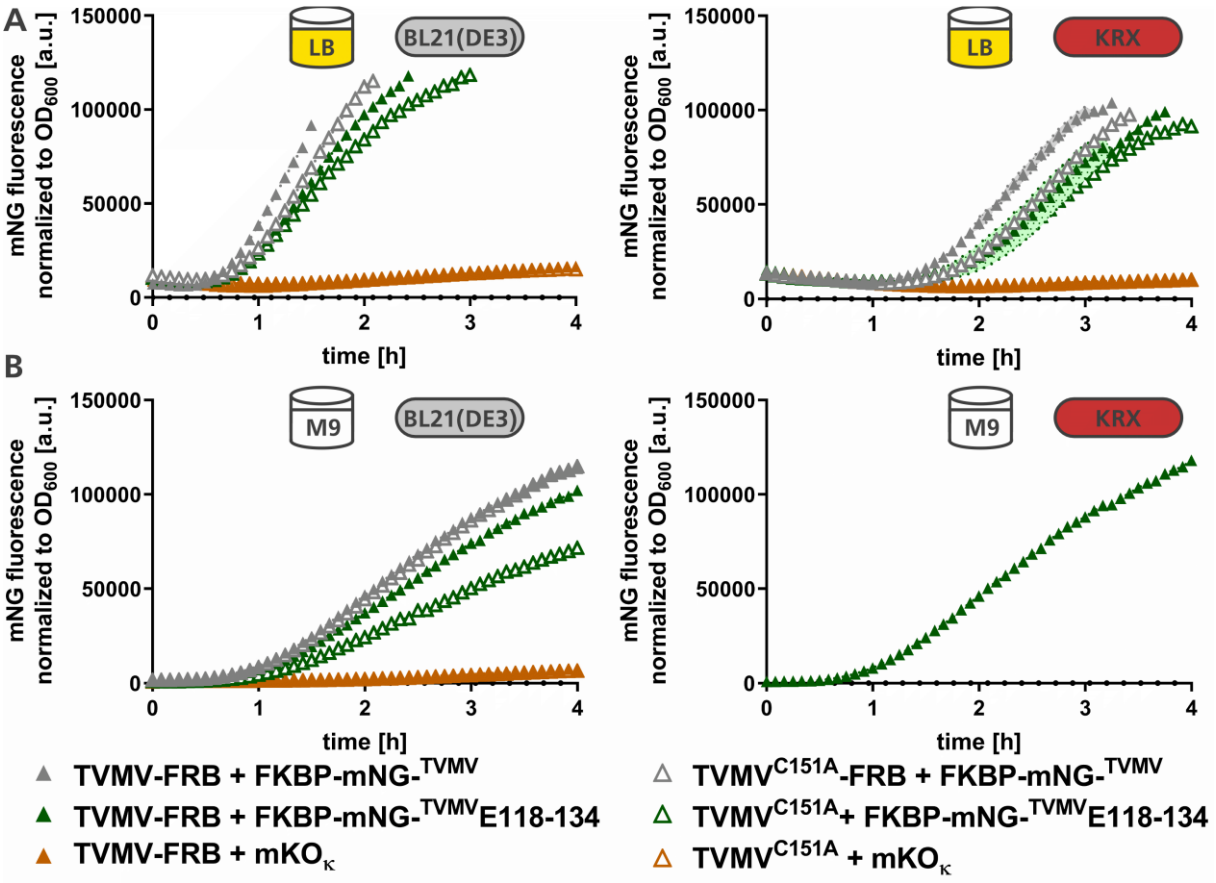

Figure 11 Effect of genetic background and media composition on assay dynamics. Constructs, colors and symbol as in **Figure 10** except orange triangles depict results for *E. coli* auto fluorescence control mKO_{κ} as non-green fluorescent mNG substitute; tested conditions riboflavin containing LB medium (yellow) vs riboflavin free M9 minimal medium (transparent), additional *lon*⁻ B-strain BL21(DE3) (grey rods) vs *lonp*⁺ K-strain KRX (red rods). **A:** Comparison of *lonp*⁻ BL21(DE3) and *lonp*⁺ KRX in LB complex medium. **B:** Comparison of *lonp*⁻ BL21(DE3) and *lonp*⁺ KRX in M9 minimal medium. Data points represent the mean values of dependent biological triplicates measured, the error areas depict the SEM, strain and cultured medium used stated above the corresponding graph, legend at the bottom refers to all four graphs. Constructs used: pPRO24_MBP-^{TVMV}TVMV-FRB, pPRO24_MBP-^{TVMV}TVMV^{C151A}-FRB, pCtrl2_FKBP-mNG-^{TVMV}, pCtrl2_FKBP-mNG-^{TVMV}-E118-134, pCtrl2_mKO_{κ} Protein Sequences are stated in the supplement (see **13.4.1**).

4.2.4. Effect of Temperature

Therefore, another parameter was varied in the following set of experiments, temperature. The reason behind this was the idea thermal stress could increase the effectiveness of the degron and thereby the dynamic range of the sensor. **Figure 12** shows the results for three temperatures tested in addition to the previously used 30 °C. 25 °C was chosen to simulate cold stress while still allowing cell proliferation. 37 °C was chosen because it is the optimal growth temperature for *E. coli*. Lastly, 40 °C was chosen to simulate heat stress while not outright killing the bacteria. The temperature experiments were performed in M9 minimal medium to keep background fluorescence as low as possible.

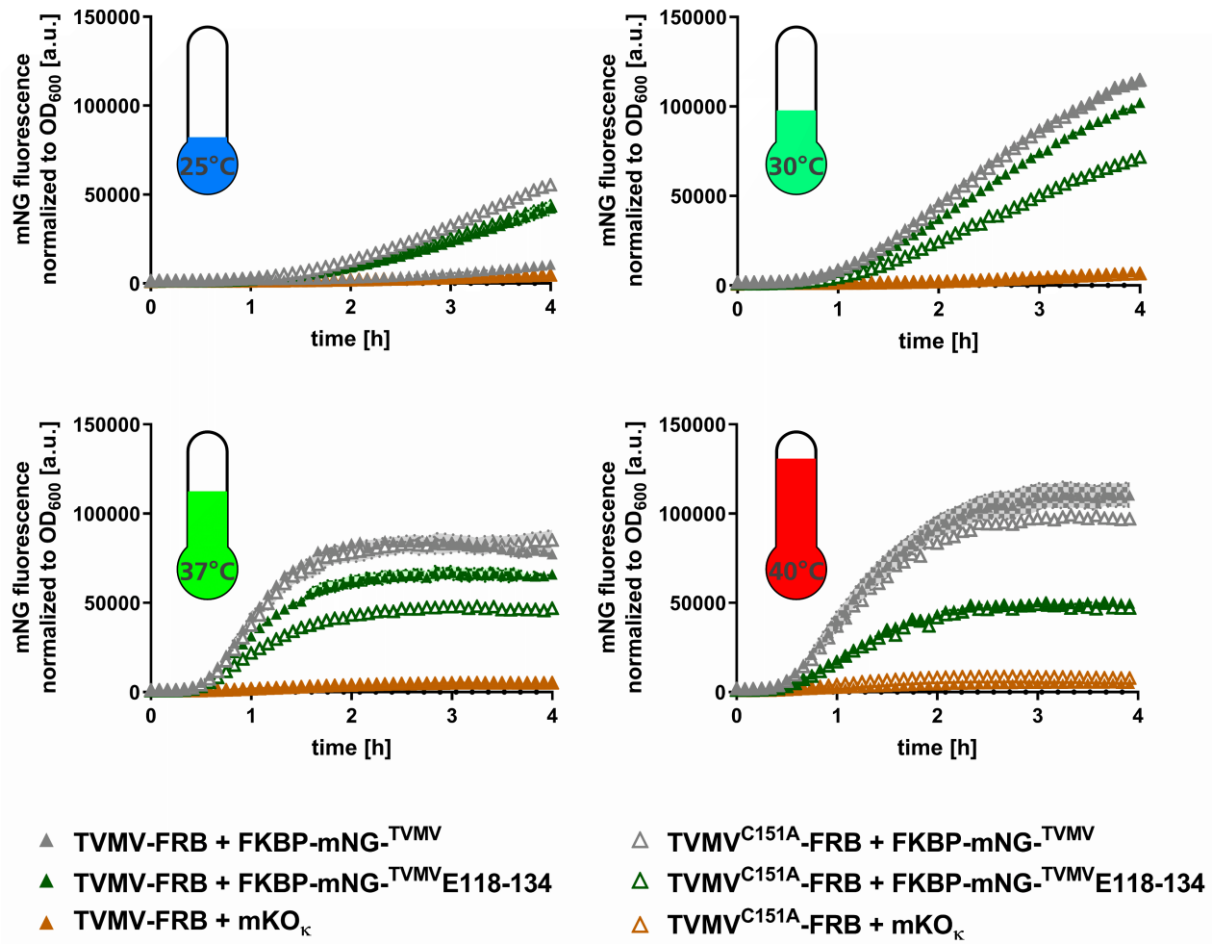

Figure 12 Effect of temperature on assay performance. Constructs, colors and symbols as in **Figure 11**. The analogue rod thermometers symbolize the induced thermal stress levels, color code: blueish color for cold stress, green color for optimal growth temperature and red color for heat stress. Experimental results for the four different temperatures (25, 30, 37 and 40 °C) tested. Data points represent the mean values of dependent biological triplicates measured, the error areas depict the SEM, incubation temperatures during assay stated inside the thermometers, legend at the bottom refers to all four graphs. Constructs used: pPRO24_MBP-^{TVMV}TVMV-FRB, pPRO24_MBP-^{TVMV}TVMV^{C151A}-FRB pCtrl2_FKBP-mNG-^{TVMV}, pCtrl2_FKBP-mNG-^{TVMV}-E118-134, pCtrl2_mKO$_κ$ Protein Sequences are stated in the supplement (see **13.4.1**)

At 25 °C, very low growth rates were observed which led to rather high normalized fluorescence values. Compared to 30 °C however, the dynamic range was substantially reduced as both green curves aligned nearly perfectly. At 37 °C, the assay already reached saturation after two hours. The degron seemed to actively reduce expression and the protease was able to recover some of the lost fluorescence. Overall however, no significant improvement was achieved compared to 30 °C. At 40 °C, the E118-134 degron exerted the highest effect on the normalized fluorescence – in this case, the greatest difference between the no-degron-controls (grey curves in **Figure 12**) and the actual sensor with the degron fused to the C-terminus (green curves in **Figure 12**) was achieved. However, TVMV seemed to be completely inactivated at this point, which is seen by both green curves near to completely align.

In summary, alteration in incubation temperature proved not to be an expedient strategy to increase the dynamic range of the assay. Therefore, the focus was shifted towards the production rate of the sensor. It seemed plausible that by reducing the expression rate of the sensor the dynamic range of the assay should have increased by reducing the abundance levels of degron tagged sensor in presence of the inactive TVMV^{C151A}.

4.2.5. Effect of sensor production rate through IPTG Titrations

Until now, an isopropyl β-D-1-thiogalactopyranoside (IPTG) concentration of 500 μM was used to express proteins in BL21(DE3) under control of the T7-promoter-lacO system. To examine how variable expression of the sensor affects the dynamics of the assay, a serial dilution of IPTG was performed. This resulted in a final concentration of IPTG in culture medium that ranged from 500 μM down to 0.03 μM. **Figure 13** shows the results for the four highest IPTG concentrations for which a mNG fluorescent signal could be detected. In contrast, in the lowest four concentration, the normalized mNG fluorescence values showed no increase in the fluorescent signal even decreased overtime as cell density rose without any fluorescence signal rising (see **Figure S7**).

As expected, the overall fluorescence values decreased with decreasing inducer concentration. The negative control (TVMV^{C151A}-FRB + E118-134, empty green triangles) consistently showed the lowest normalized fluorescence values. The two positive controls – TVMV and TVMV^{C151A} FRB – with no degron attached (grey filled and empty triangles) showed the highest standard error of the mean between the triplicates measured. In addition, in all cases the TVMV^{C151A} positive control (empty grey triangles) surprisingly deviated from the TVMV positive control (filled grey triangles). Overall, this indicated that titration of the IPTG inducer seemed to be too error prone to yield quantitative results. But the general idea to reduce expression of the sensor in order to increase the dynamic range appeared to be a promising route for optimization.

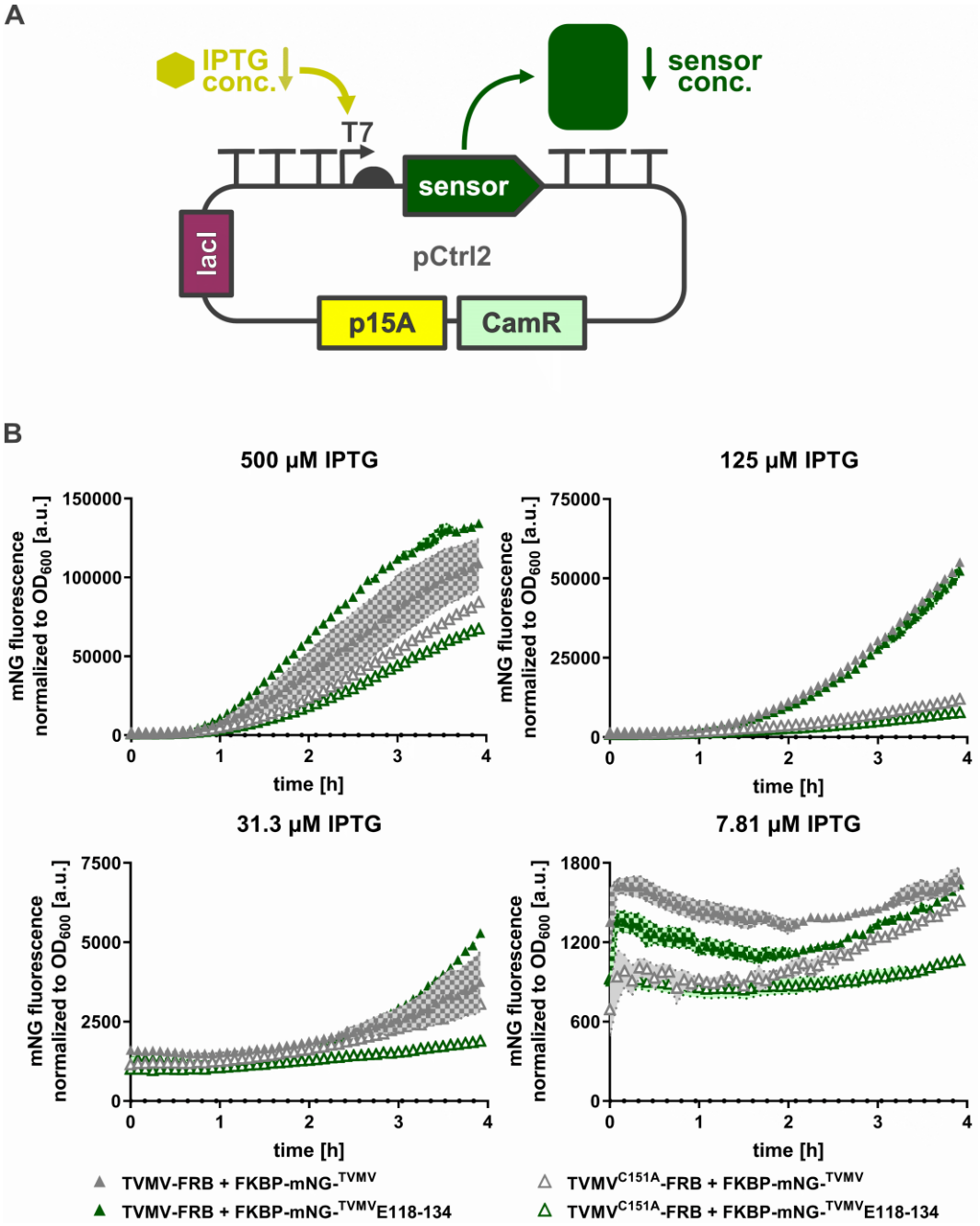

Figure 13 Summary of titrating the sensor with IPTG from 500 µM to 7.8 µM in the culture medium during measurements in 1:4 dilution steps. Concentrations from 1.95 to 0.03 µM are found in **Figure S7**. Constructs, colors and symbols as in **Figure 12**. **A:** Schematic depiction of the experiment, by reducing the IPTG concentration the amount of T7 RNA polymerase was reduced that should in turn decrease the expression rate of the sensor. **B:** Experimental results on the effect of lowered IPTG concentration on the dynamics of the assay. Data points represent the mean values of independent biological triplicates, the error areas depict the SEM, the final IPTG concentration in the medium stated above the corresponding graph, legend at the bottom refers to all four graphs. Constructs used: pPRO24_MBP-^{TVMV}TVMV-FRB pPRO24_MBP-^{TVMV}TVMV^{C151A}-FRB, pCtrl2_FKBP-mNG-^{TVMV}, pCtrl2_FKBP-mNG-^{TVMV}-E118-134, pCtrl2_mKO$_{\kappa}$ Protein Sequences are stated in the supplement (see **13.4.1**).

4.2.6. Effect of DMSO on the Bio-availability of Rapamycin in *E. coli*

Based on an article on FRB/FKBP filament formation in live *E. coli* cells, the DMSO concentration in the assay was elevated from 0.5 %(v/v) to 2 %(v/v) to match the values in this publication [90]. The authors demonstrated rapamycin dependent association of FKBP and FRB in live *E. coli* cells. Which was elusive with the assay to that point in time. The only difference between their experiments and the assay was that their lower concentrated rapamycin stock solution led to 2 %(v/v) DMSO in the medium when 8 μM rapamycin were administrated while our stock solution led to only 0.5 %(v/v) DMSO in the culture medium. **Figure 14** shows the results with and without 8 μM rapamycin administered with 2 %(v/v) DMSO present in the medium regardless of rapamycin was added or not.

As visible in **Figure 14**, there was no significant difference in the development of the fluorescent signal in the presence or absence of rapamycin. But without a suitable Rapamycin biosensor available the question whether the recruitment made no difference or rapamycin could not accumulate in sufficient amounts within the cytoplasm could not be conclusively answered at this stage.

Following changes in the genetic background, temperature and concentrations of the inducer had no substantial effect on the dynamic range, a literature search was performed to identify more potent degrons that previously proved effective in *E. coli*. To this end, the LVA C-degron (Sequence: AANDENYA**LVA** [21]) which was derived from the naturally occurring ssrA degron (Sequence: AANDENYA**LAA** [91, 92]) by the Voigt Lab was chosen as the lead candidate. In the first try, its effect on the dynamics of the assay was compared relative to the newly discovered E118-134 C-degron.

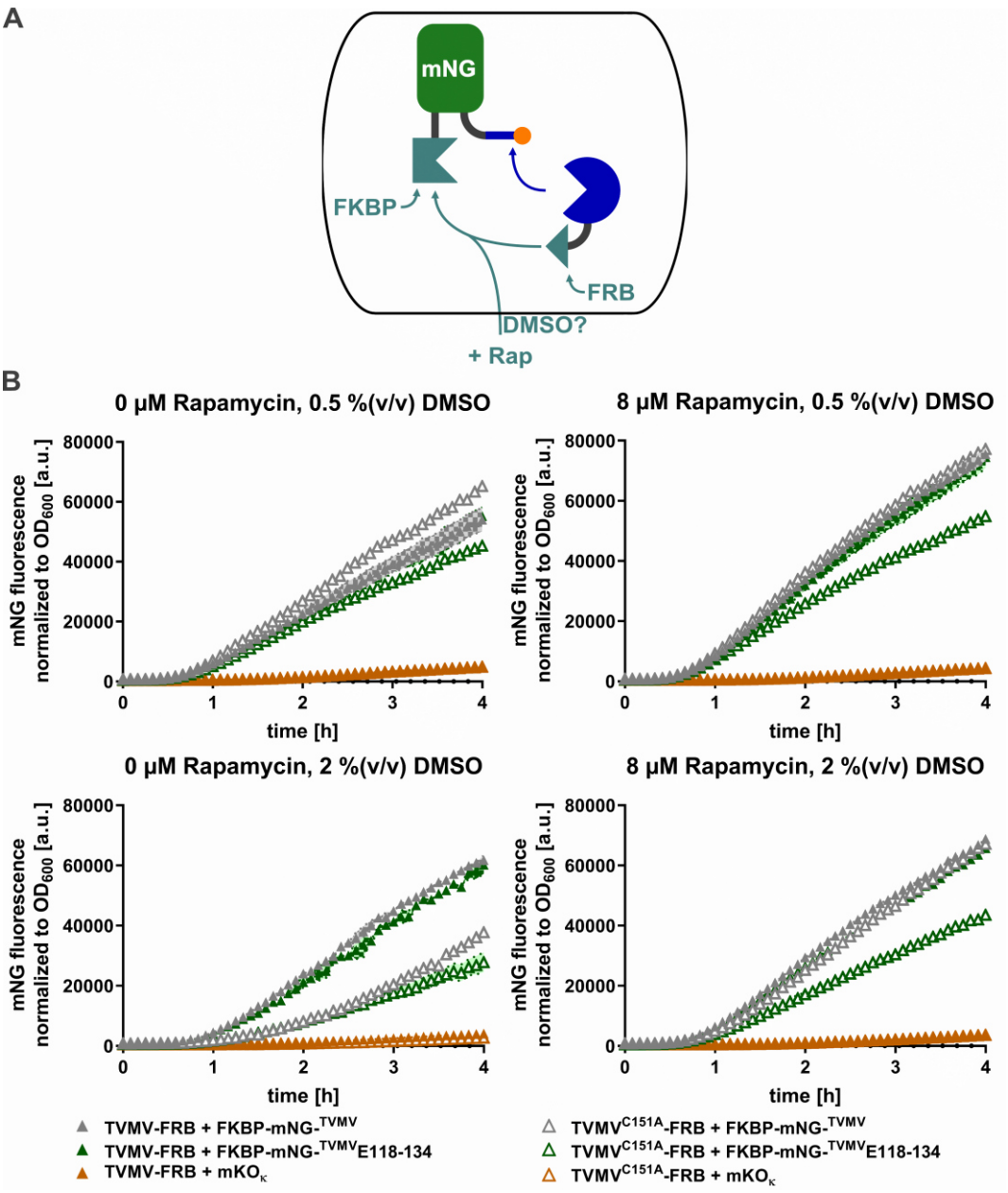

Figure 14 Effect of increased DMSO concentration on rapamycin-induced colocalization of the protease and the sensor. Constructs, colors and symbols as in **Figure 11**. **A:** Schematic depiction of the experiment, identical assay conditions as in **Figure 10** except DMSO concentration was increased from 0.5 %(v/v) to 2 %(v/v) with the aim of increasing the bio-availability of rapamycin in *E. coli* cells (dark grey rounded rod-shaped border). **B:** Experimental results for the effect of DMSO in the culture medium during measurements. Data points represent the mean values of dependent biological triplicates measured, the error areas depict the SEM, rapamycin and DMSO concentrations stated above the corresponding graphs, legends at the bottom refers to all graphs. Constructs used: pPRO24_MBP-^{TVMV}TVMV-FRB, pPRO24_MBP-^{TVMV}TVMV^{C151A}-FRB, pCtrl2_FKBP-mNG-^{TVMV}, pCtrl2_FKBP-mNG-^{TVMV}-E118-134, pCtrl2_mKO$_κ$ Protein Sequences are stated in the supplement (see **13.4.1**).

4.2.7. New C-Degron LVA

After altering the assay conditions did not seem a promising route to success, the E118-134 was replaced by a putative stronger one in the form of the LVA C-degron that has been derived from the naturally occurring ssrA degradation tag [21]. To allow for an accurate comparison, all constructs remained unchanged except that the E118-134 degron was replaced with the LVA degron. **Figure 15** shows the direct comparison of both degrons in M9 minimal medium and at 30 °C. As apparent in **Figure 15**, both degrons performed nearly identical. Therefore, it was concluded that the T7 promoter-based expression rate greatly exceeded the degron induced degradation rates. Derivates of the original pCtrl2 with mutations in either the T7 promoter or in the ribosome binding site (RBS) or both were tested. These mutations should reduce sensor production in a more uniform and less error-prone manner compared to the previous IPTG titrations (see **Chapter 4.2.5**).

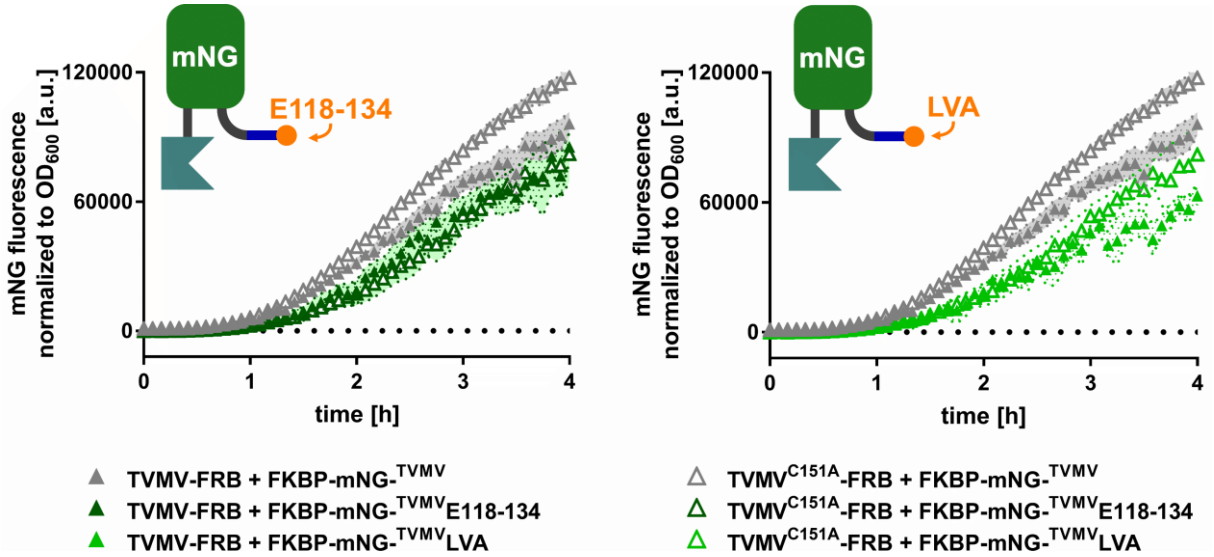

Figure 15 Direct comparison of the C-degrons E118-134 and LVA. Constructs, colors and symbols as in **Figure 14**, except LVA C-degron was introduced (light green triangles). **B:** direct comparison of both degrons in M9 medium at 30 °C, Data points represent the mean values of dependent biological triplicates measured, the error areas depict the SEM, degron used stated in the respective pictograms. Constructs used: pPRO24_MBP-^{TVMV}TVMV-FRB, pPRO24_MBP-^{TVMV}TVMV^{C151A}-FRB, pCtrl2_FKBP-mNG-^{TVMV}, pCtrl2_FKBP-mNG-^{TVMV}-E118-134, pCtrl2_FKBP-mNG-^{TVMV}-LVA, pCtrl2_mKO$_{\kappa}$ Protein Sequences are stated in the supplement (see **13.4.2**).

4.2.8. Optimizing Expression of the Protease Sensor

Based on findings shown **Figure 16** and the other pCtrl2 derivatives tested (data can be found in the supplement in **Chapter 13.2.5** in **Figure S15** to **Figure S17**), pCtrl2_T7.03_U9 was chosen as the standard expression vector for all sensor constructs throughout this project. It is comprised of a T7 promoter mutant with 3% transcription activity compared to the wild type T7 promoter [84] and an RNA thermometer which reduces the translation activity to 5% compared to the unmasked RBS [93] (see **Table 9**). In total, this should have led in theory to 99.8% reduction in total protein production rate.

As evident in **Figure 16**, the sensor production rate of pCtrl2_T7.03_U9 was sufficiently low that proteolytic activity of TVMV triggered a substantial increase in mNG fluorescence (filled green triangles in **Figure 16**) relative to the corresponding mock controls TVMV^{C151A} constructs (empty green triangles in **Figure 16**). However, the LVA induced degradation rates seemed to exceed the proteolysis rates of TVMV. As visible in the right graph of **Figure 16 B**, TVMV was unable to fully restore the mNG fluorescence compared to the corresponding positive control (filled grey triangles). The achieved fold changes and actual normalized fluorescence values were nevertheless considered sufficiently high to keep pCtrl2_T7.03_U9 as the expression vector for all future sensor constructs. The updated version of the standard dual expression system is depicted in **Scheme 16** and **Figure 17** shows a detailed view of the updated expression cassette of pCtrl2.

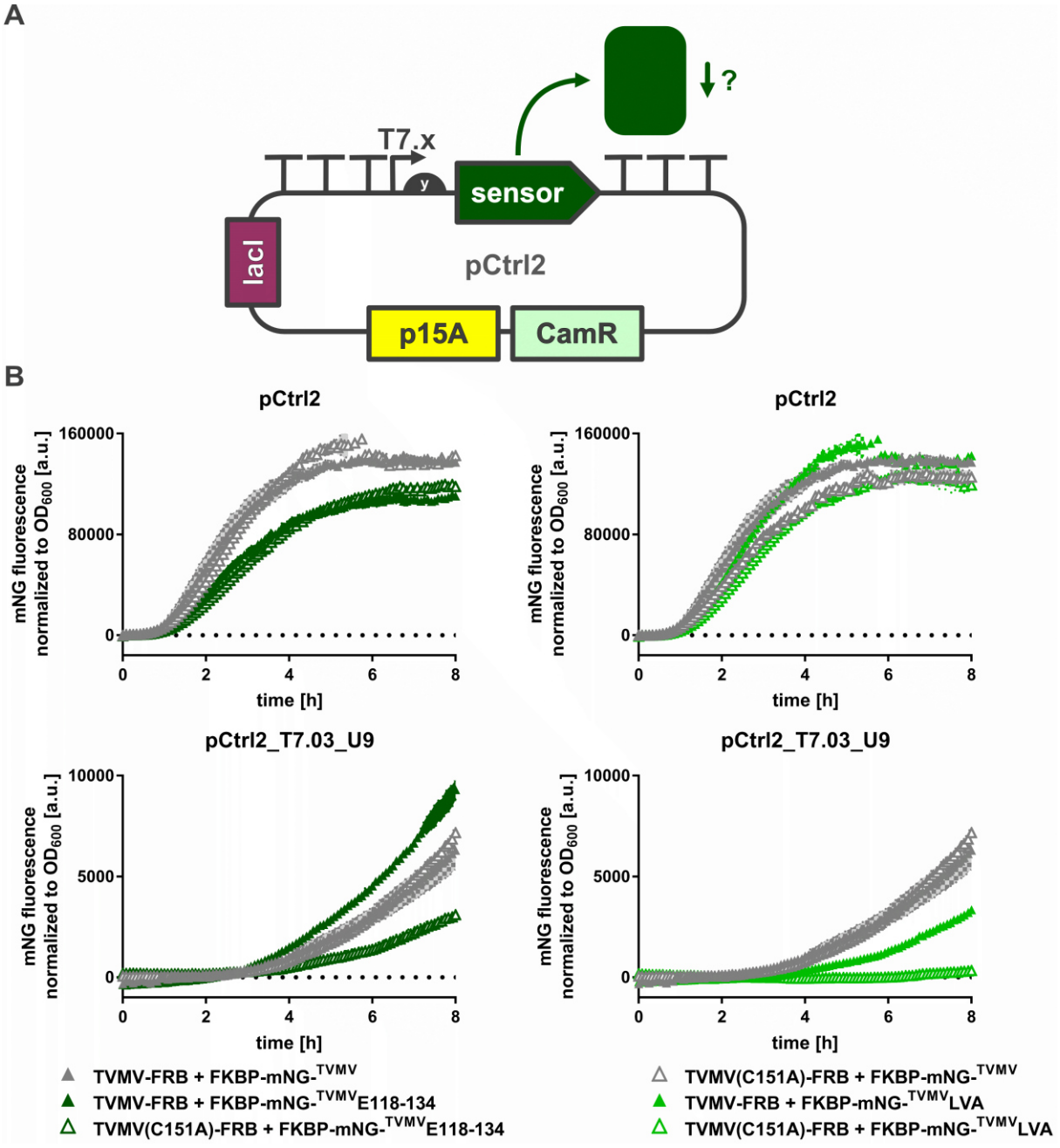

Figure 16 Effect of reduced transcription and translation rates for the sensor on the assay dynamics. Constructs, colors and symbols as in **Figure 15**. **A:** Schematic depiction of the experiment, several different variants of pCtrl2 with different mutation in either the T7 promoter of the ribosome binding site (RBS) or an RNA thermometer partial masking the RBS at 30 °C were tested (data not shown). **B:** Experimental results for the original pCtrl2 vector and the best performing derivative pCtrl2_T7.03_U9. pCtrl2_T7.03 bore a mutation in the T7 promoter that reduced transcription to approx. 3 % compared to the wild type [84], additional the previously used RBS was replaced with U9 RNA thermometer that possessed a approx. 5 % probability to adopt the open conformation at 30 °C [93]; Data points represent the mean values of dependent biological triplicates measured, the error areas depict the SEM, pCtrl2 derivate used stated above the corresponding graph, legend at the bottom refers to all graphs. . Constructs used: pPRO24_MBP-^{TVMV}TVMV-FRB, MBP-^{TVMV}TVMV^{C151A}-FRB, pCtrl2_FKBP-mNG-^{TVMV}, pCtrl2_FKBP-mNG-^{TVMV}-E118-134, pCtrl2_FKBP-mNG-LVA, pCtrl2_mKO$_{\kappa}$, pCtrl2_T7.03_U9_FKBP-mNG-^{TVMV}, pCtrl2_T7.03_U9_FKBP-mNG-^{TVMV}E118-134, pCtl2_T7.03_U9_FKBP-mNG-^{TVMV}LVA, pCtrl2_T7.03_U9_mKO$_{\kappa}$ Protein Sequences are stated in supplement (see **13.4.3**).

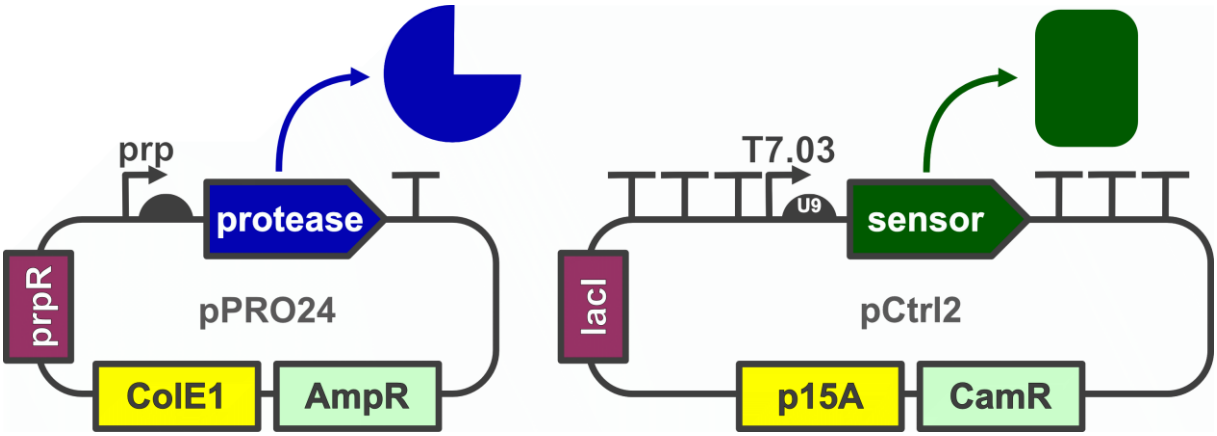

Scheme 16 Dual expression system for the stable, independent co-expression of proteases and their substrates in *E. coli* BL21(DE3) cells version 2. Origins of replication (oris) in yellow, selection markers in mint green, repressors in purple, genetic elements in grey and coding sequences in colors matching their respective gene products. Left: pPRO24 (Pprp/prpR, class A ColE1 ori, AmpR) for propionate inducible expression of protease constructs. Right: pCtrl2_T7.03_U9 (PT7-lacO-U9/lacI, class B p15A ori, CamR) for IPTG/lactose inducible expression of sensor/substrate constructs.

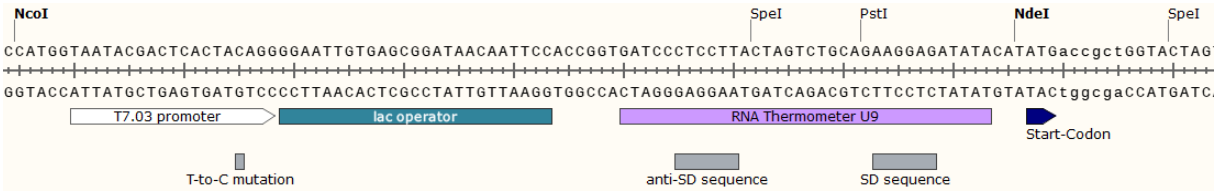

Figure 17 Expression cassette of the selected pCtrl2 variant pCtrl2_T7.03_U9. The wild type T7 promoter was replaced with a mutant with a single T-to-C mutation [84] and the ribozyme binding site (RBS) was replaced with the synthetic U9 RNA thermometer [93]. The expression cassette was cloned between a NcoI and a NdeI restriction site, the XbaI site was lost during insertion of the RNA thermometer. T7 promoter mutant in white (T-to-C mutation marked with a grey rectangle), lac operator in cyan, synthetic U9 RNA thermometer in violet (Shine-Dalgarno (SD) sequence as a grey bar and anti-SD sequence as a grey bar) and Start-Codon in blue, restriction sites above the DNA double strand. pCtrl2_T7.03_U9 was created on basis of pCtrl2 by W. Weber, Figure was created with SnapGene (GSL Biotech LLC).

4.2.9. Effect of induction regime on assay dynamics

The new expression system enabled a clear differentiation between catalytically-inactive and catalytically-active protease variants. But as visible in **Figure 16**, there was an approximately three-hour lag phase between the initiation of protein expression at 0 h and the first time point where the signals for the positive controls, the active protease and the inactive, mock protease (negative control) started to diverge.

In order to reduce this delay, an additional incubation step at 30 °C was therefore introduced after protease induction but before sensor induction. The incubation times were 0 h (i.e. no change to previous approach) 2 h, 4 h and 6 h. The results from this four sets of measurement

are shown in **Figure 18**. The inverted induction order had been tested already during a research internship in our group and led to complete abolishment of protease production if propionate was added after IPTG (see Bachelor dissertation of Isabelle Marquardt).

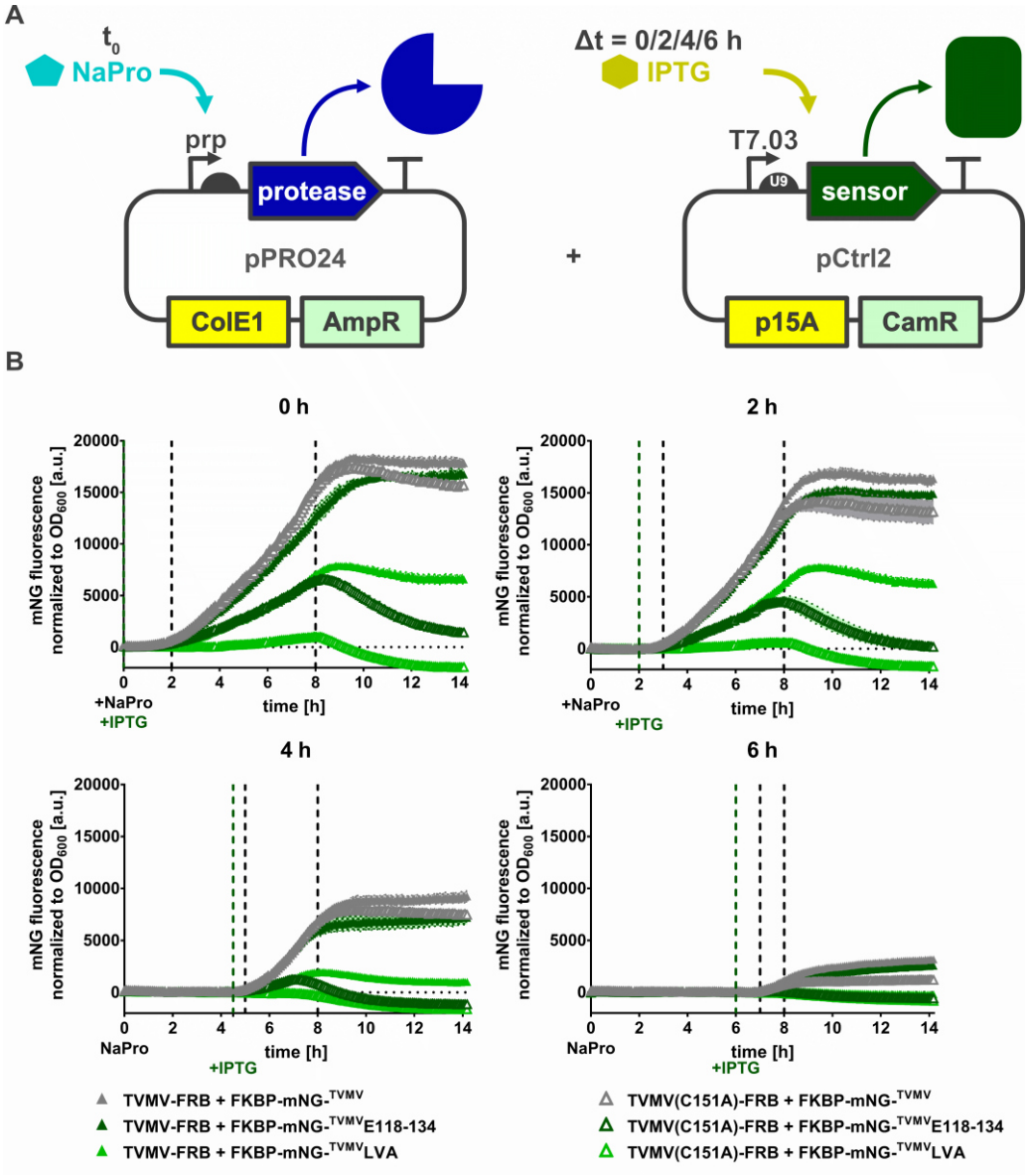

Figure 18 Effect of delaying the expression of the sensor relative to the protease. Constructs, colors and symbols as in **Figure 16**. **A:** Sodium propionate was added at t_0 to induce expression of the protease constructs. IPTG was added after 0, 2, 4 or 6 h (vertical dashed green line in the graphs in **B**). **B:** Experimental results for the postponed sensor induction; the dotted horizontal line shows the corrected baseline (autofluorescence subtracted from normalized fluorescence values), vertical dashed black lines depict the range in which the slope of linear increase in fluorescence was calculated by linear regression. Data points represent the mean values of dependent biological triplicates measured, the error areas depict the SEM, time interval between protease expression induction at t_0 and sensor expression induction stated above the corresponding graph, legend at the bottom refers to all graphs. Constructs used: pPRO24_MBP-^{TVMV}TVMV-FRB, MBP-^{TVMV}TVMV^{C151A}-FRB, pCtrl2_T7.03_U9_FKBP-mNG-^{TVMV}, pCtrl2_T7.03_U9_FKBP-mNG-^{TVMV}E118-134, pCtl2_T7.03_U9_FKBP-mNG-^{TVMV}LVA, pCtrl2_T7.03_U9_mKO$_κ$ Protein Sequences are stated in supplement (see **13.4.3**)

Based on the developing the normalized mNG fluorescence, over time the slope of the linear increase in fluorescence was calculated *via* a linear regression. The dashed black lines indicate the time intervals in which a sufficient linear correlation ($R^2 \geq 0.9$) was observed.

The slope of the curves in those intervals was used to estimate and compare the apparent protease activities depending on the degron used. **Figure 19** shows the calculated slopes ordered by duration of the sensor induction postponement for three of the tested time intervals.

The results for the six-hour postponement were omitted because the low overall expression levels did not allow any reliable interpretation of the data. Based on the calculated slopes, the apparent protease activity *in vivo* quantified in terms of the fold-change difference between active and inactive protease construct.

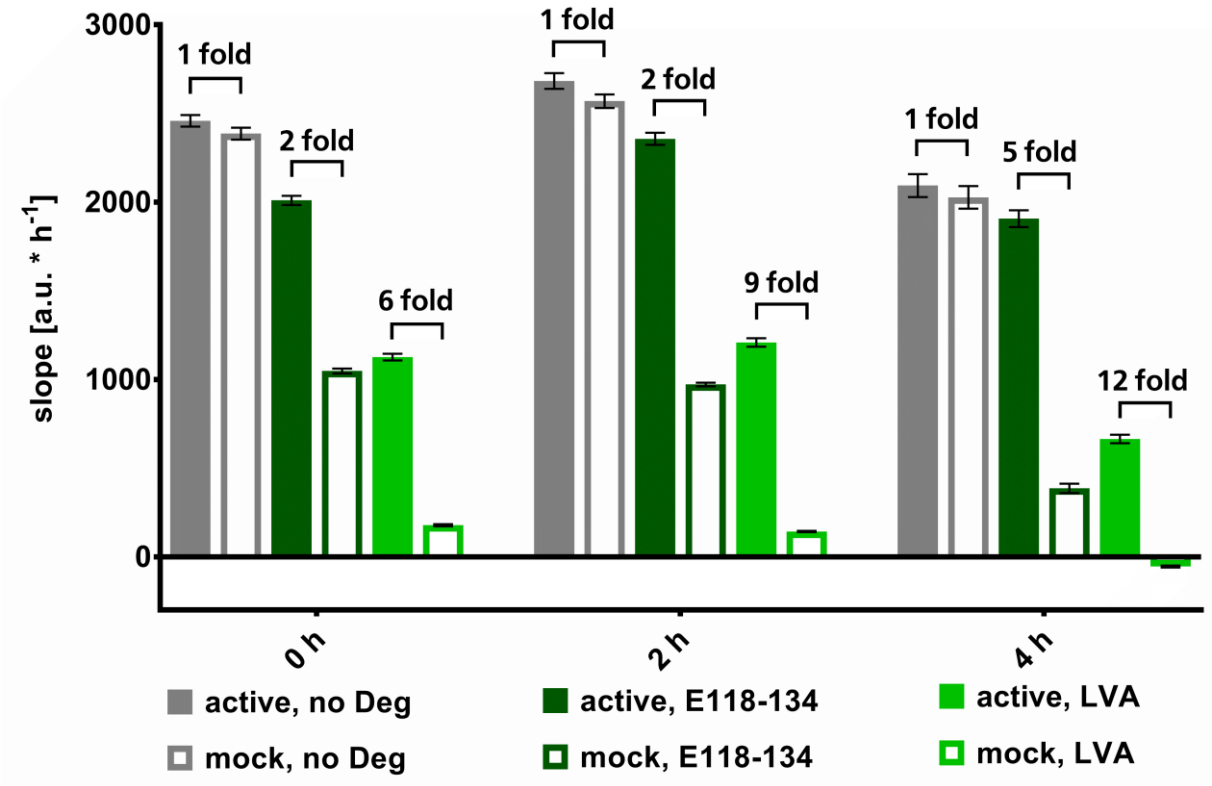

Figure 19 Slopes of the linear increase in normalized mNG fluorescence depending on the time interval between protease and sensor expression induction. Values for the six-hour interval were omitted. Bars represent the mean slope the dependent biological triplicates measured, error bars show the standard error of the mean (SEM). Grey: no degron present, dark green: E118-134 C-degron present, light green: LVA C-degron present; filled bars TVMV-FRB (active protease), empty bars: TVMV(C151A)-FRB (inactive protease, mock control). Constructs used: pPRO24_MBP-^{TVMV}TVMV-FRB, MBP-^{TVMV}TVMV^{C151A}-FRB, pCtrl2_T7.03_U9_FKBP-mNG-^{TVMV}, pCtrl2_T7.03_U9_FKBP-mNG-^{TVMV}E118-134, pCtl2_T7.03_U9_FKBP-mNG-^{TVMV}LVA, pCtrl2_T7.03_U9_mKO$_\kappa$ Protein Sequences are stated in supplement (see **13.4.3**)

As expected, a 1-fold change in slope was observed for the positive controls – i.e. without any degron fused to the sensor (gray bars in **Figure 19**). As in previous experiments, TVMV was not able to fully restore mNG fluorescence when the LVA degron was employed (light green curves in **Figure 18**, light green bars in **Figure 19**). Consistent with previous experiments, fluorescence was fully restored when the weaker E118-134 degron was used (dark green curves in **Figure 18**, dark green bars in **Figure 19**). Furthermore, significant mNG fluorescence was detected for the mock control TVMV^{C151A} only when the E118-134 degron was used. This further confirmed that the E118-134 degron was weaker compared to LVA. But apparent protease activities received for both degrons showed increased fold changes with increasing time intervals between the induction of the protease and the expression of the sensor respectively.

Even though a 4 h delay displayed the highest fold-changes (paired bars in **Figure 19**) and the shortest delay between the initiation of sensor expression and the subsequent rise in the fluorescent signal (**Figure 18**), a 2 h delay was ultimately chosen for the following reasons: First of all, the duration of individual experiments was reduced. Secondly, the absolute fluorescent signal values were not significantly reduced compared to when the sensor and the protease were expressed simultaneously that in terms of autofluorescence provided better signal-to-ratios. In addition, all subsequent measurements were started upon induction of the sensor rather than the protease to reduce occupation of the plate reader. Finally, the assay times were reduced to 6 h (which corresponds to the 8 h time point in **Figure 18**) as fluorescent signals either became stable or started to decline as cells entered the later growth phases.

Furthermore, the next set of experiments was conducted with the mNG-based C-degron sensors, but this time the rapamycin-dependent FKBP12-FRB module was replaced with a constitutive Src Homology 3 (SH3) protein-peptide interaction module. This change enabled constitutive recruitment independent of an external stimulus. In addition, the SH3 recruitment was previously used in combination with TVMV based switches [1, 3].

4.2.10. SH3 Recruitment Effect of Relative Orientation on Assay Dynamics

Src Homology 3 (SH3) domains bind are commonly found in many proteins and mediated protein-protein-interaction by binding to proline rich peptide motive. The binding affinities are dependent on the number of proline residues with the peptide motive. Additional positively charged residues within the proline-rich motive can further enhance binding affinities [94]. Based on previous results two different ligands for the SH3 domain were tested. One with a high affinity (K_D = 96 nM, sSH3L) and one with a low affinity (K_D =2 μM, wSH3L) [3, 94]. To reduce steric hindrance the small SH3 peptide ligands were fused to the protease while the larger SH3 domain was incorporated into the sensor.

All constructs were cloned analogues to the FKBP-FRB constructs listed in **Table 2**. In contrast to **Chapter 4.2.2** where the orientation was screen with a single degron, this time it was performed with the E118-134 and LVA degrons and both SH3 peptide ligands. The results for the best performing orientation are shown in **Figure 20** in full detail while **Table 3** summarizes the results for all other orientations tested. For clarity, the results from **Figure 20** are highlighted with grey-shading in **Table 3**. From the two sets with the highest fold changes for both degrons (sSH3L- TVMV with SH3-mNG-^{TVMV}degron or mNG-^{TVMV}SH3-degron). The combination of sSH3L-protease and SH3-mNG-^{TVMV}degron was selected for further analysis because the SH3-mNG-^{TVMV}degron sensor design displayed the highest overall fluorescence values.

Table 3 SH3 based recruitment - relative orientation screening. All tested relative orientation sorted after the respective protease construct. The first column lists the protease constructs, the second the sensor constructs, the third column states the fold change in mean slope of the normalized mNG fluorescence averaged over the measured dependent biological duplicates of two independent experiments. Relative orientation chosen for further experiments as well as featured in **Figure 20** is highlighted with grey-shading

Protease construct	Sensor construct	Fold Change	Protease construct	Sensor construct	Fold Change
sSH3L-TVMV	SH3-mNG-^{TVMV}E118-134	2	TVMV-sSH3L	SH3-mNG-^{TVMV}E118-134	1
	SH3-mNG-^{TVMV}LVA	4		SH3-mNG-^{TVMV}LVA	5
	mNG-^{TVMV}SH3-E118-134	2		mNG-^{TVMV}SH3-E118-134	1
	mNG-^{TVMV}SH3-LVA	4		mNG-^{TVMV}SH3-LVA	3
	mNG-SH3-^{TVMV}E118-134	1		mNG-SH3-^{TVMV}E118-134	1
	mNG-SH3-^{TVMV}LVA	2		mNG-SH3-^{TVMV}LVA	1
wSH3L-TVMV	SH3-mNG-^{TVMV}E118-134	2	TVMV-wSH3L	SH3-mNG-^{TVMV}E118-134	1
	SH3-mNG-^{TVMV}LVA	1		SH3-mNG-^{TVMV}LVA	1
	mNG-^{TVMV}SH3-E118-134	1		mNG-^{TVMV}SH3-E118-134	1
	mNG-^{TVMV}SH3-LVA	1		mNG-^{TVMV}SH3-LVA	1
	mNG-SH3-^{TVMV}E118-134	0		mNG-SH3-^{TVMV}E118-134	1
	mNG-SH3-^{TVMV}LVA	-2		mNG-SH3-^{TVMV}LVA	-2

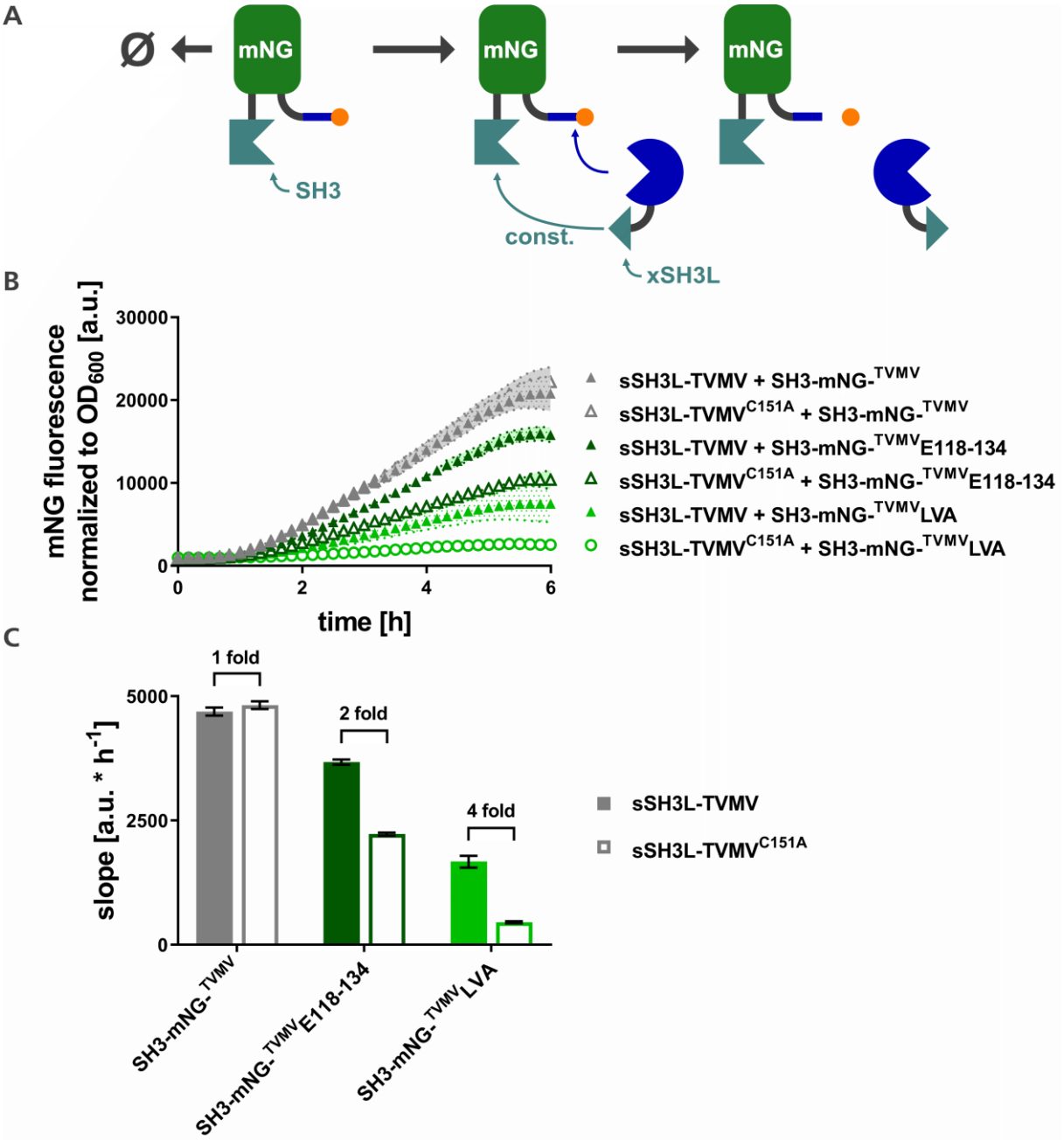

Figure 20 Summary of SH3-dependent recruitment with both C-degrons E118-134 and LVA. **A:** Schematic depiction of the assay design, components as in **Figure 10**, except the rapamycin-dependent FRKBP-FRB module was replaced with the constitutively active SH3 protein-peptide interaction module. **B:** Experimental comparison of the two previously tested degrons based on the best performing combination of sSH3L-TVMV and SH3-mNG-^{TVMV} sensor; continuous assay with the parameters established in **Chapter 4.2.9**, constructs as listed in the legend, colors and symbols as in **Figure 18**. Data points represent the mean values of dependent biological triplicates measured, the error areas depict the SEM. **C:** slopes for protease and corresponding mock constructs TVMV^{C151A} as pairwise columns. Bars represent the average of the two dependent biological replicates measured in two independent experiments, error bars represent the standard error of the mean; filled bars for protease constructs, empty bars for mock constructs, brackets above the paired bars denote the corresponding fold change in slope. Constructs used: pPRO24_MBP-^{TVMV}sSH3L-TVMV-Strep, pPRO24_MBP-^{TVMV}sSH3L-TVMV^{C151A}-Strep pCtrl2_T7.03_U9_myc-SH3-mNG-^{TVMV}, pCtrl2_T7.03_U9_myc-SH3-mNG-^{TVMV}E118-134, pCtrl2_T7.03_U9_myc-SH3-mNG-^{TVMV}LVA, pCtrl2_mKO$_κ$. Protein Sequences are stated in the supplement (see **13.4.4**)

With the best performing orientation identified, the effect of constitutive SH3-based recruitment was estimated by repeating the experiments with protease variants that were devoid of the SH3 peptide ligand (a respective mock control was also included). Due to the reduced number of individual combinations the number of repeats was increased from duplicates to quadruplicates in order to increase the accuracy of the assay. The results of this experiment are shown in **Figure 21**.

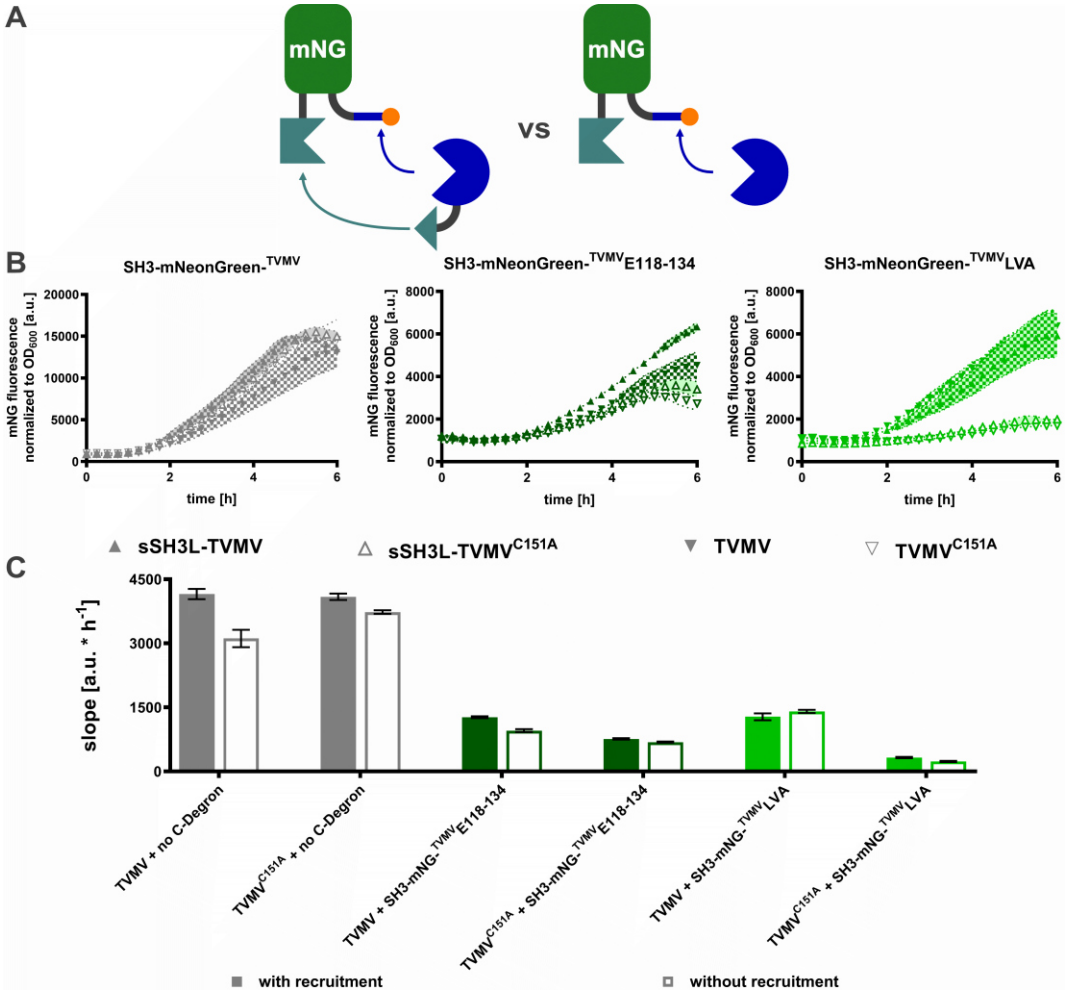

Figure 21 Effectiveness of SH3-based recruitment on assay dynamics. Constructs, colors and symbols as in **Figure 20**. **A:** The activity of protease constructs with and without SH3 ligand (green triangles) were compared. **B:** Realtime data of the protease activity dependent alteration in sensor fluorescence over time, sensor constructs are noted above the corresponding graph, data points represent the mean values of dependent biological quadruplicates measured, error areas depict the SEM in colors matching the corresponding data set, dark checked areas belong to data sets of active proteases, plain areas belong to inactive proteases. **C:** comparison of the slopes the increase in normalized mNG fluorescence, bars represent the mean slope of the dependent biological quadruplicates measured over the time interval between 2 h and 5 h, error bars depict the SEM, filled bars show slopes for protease constructs with the strong SH3 ligand fused to the N-terminus of the protease, empty bars show the slops for the corresponding protease constructs without any SH3 ligand fused. Constructs used: pPRO24_MBP-^{TVMV}sSH3L-TVMV-Strep, pPRO24_MBP-^{TVMV}sSH3L-TVMV^{C151A}-Strep, pPRO24_MBP-^{TVMV}TVMV-Strep, pPRO24_MBP-^{TVMV}TVMV^{C151A}-Strep, pCtrl2_T7.03_U9_myc-SH3-mNG-^{TVMV}, pCtrl2_T7.03_U9_myc-SH3-mNG-^{TVMV}E118.134, pCtrl2_T7.03_U9_myc-SH3-mNG-^{TVMV}LVA, pCtrl2_mKO$_K$. Protein Sequences are stated in the supplement (see **13.4.4** and **13.4.5**)

As evident in **Figure 21**, the presence of the SH3 ligand had little to no impact on the slopes of the protease-activity-dependent increase in sensor fluorescence. In case of the weaker E118-134 degron, the recruitment delayed the time needed to reach the equilibrium between protease processing of the sensor and the increased degron efficacy due to stationary growth phase.

In general, the apparent catalytic activity of the protease turned out to be the rate-limiting factor of the assay. This becomes particularly obvious when comparing the scales of the graph for the positive controls (left graph in **Figure 21 B**) with two other graphs in **Figure 21 B**. Irrespective whether a degron was fused or not, TVMV was able to restore about half of the maximum fluorescence. This could mean that for future experiments, the amount of IPTG could be reduced in accordance to the findings in **Chapter 4.2.5** to enable full processing of all sensor molecules through the available protease molecules.

4.2.11. Minimal E118-134 Variant

The Weigand group previously performed truncation studies with the E118-134 C-degron which led to minimal version of the degron. In further experiments, they also demonstrated that three repeats of degron yielded in the highest degradation rates (personal communication on unpublished results).

Therefore, the performance of this triple minimal C-degron was once again benchmarked against the LVA degron. In order to obtain comparable results, two sets of constructs were cloned. The first comprised an α-helical $(EAAAK)_2$ linker and the respective C-degron. The second incorporated the flexible SG_4 linker that was previously used by the Weigand group. Because iFLinkC introduces a single glycine scar between a functional domain and a linker, the SG_4 linker was realized with the cloning of pL2_SG_3. Therefore, the final constructs were SH3-mNG-^{TVMV}G(SG_3)G-(C-degron). This was the closest to SG_4-(C-degron) sequence used by the Weigand Lab that could be achieved with the iFLinkC assembly process [45].

After all combinations of linkers and degrons were cloned, they were added to the best performing sensor construct (SH3-mNG-^{TVMV}degron). **Figure 22** shows the results for this triple comparison while the corresponding raw data can be found in **Figure S18**.

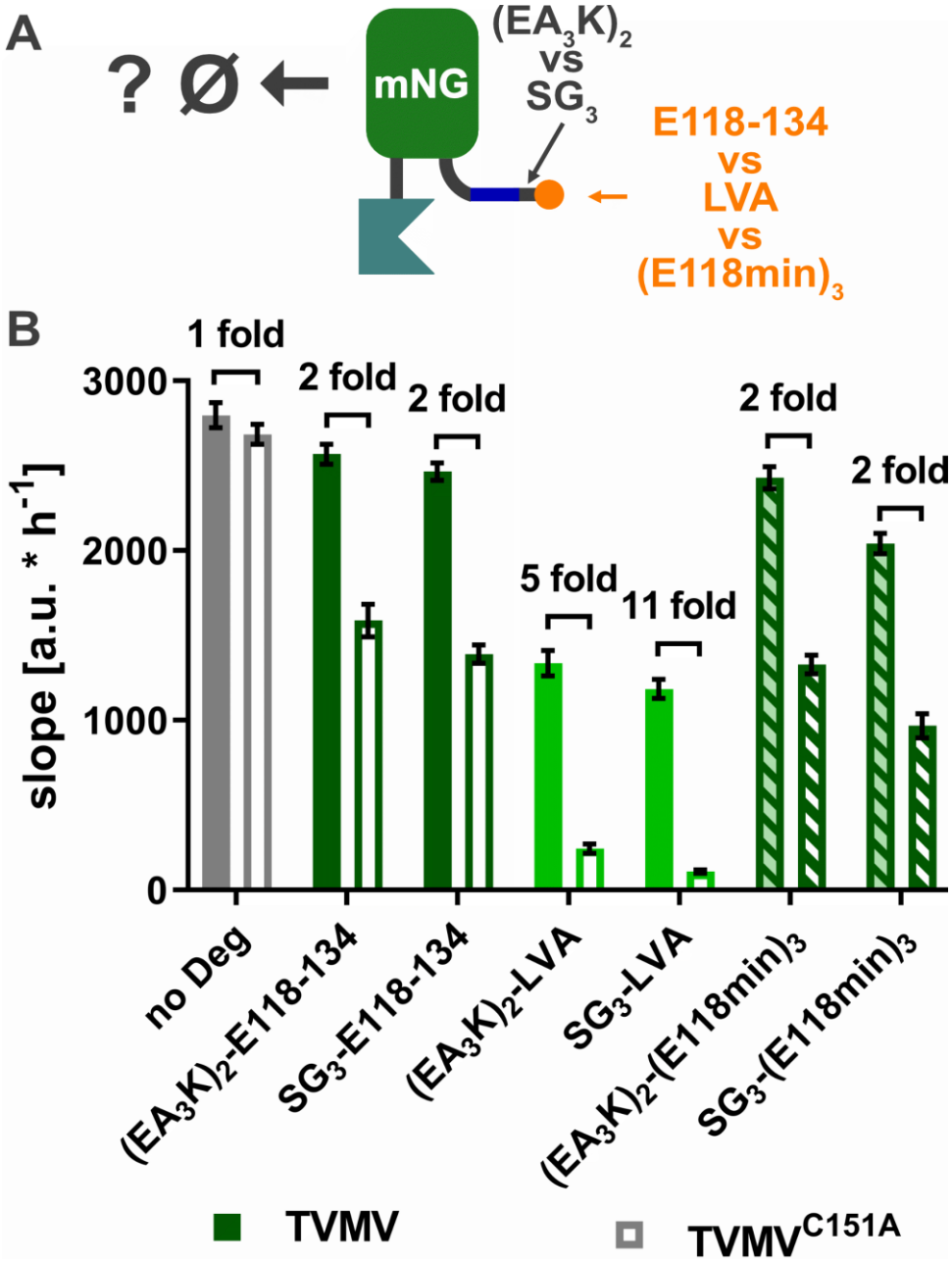

Figure 22 Comparison of the E118-134 C-degron with its triple minimal version and the LVA C-degron. Constructs, colors and symbols as in **Figure 20**, except triple minimal E118-134 C-degron $(E118min)_3$ (striped dark green bars). **A:** Schematic depiction of the experiment, three different degrons and two different linkers connecting the cleavage site and the degron were tested. **B:** Fold changes in slope of the increase in protease dependent mNG fluorescence ordered by linker degron combination tested, bars represent the mean slope of dependent biological quadruplicates measured; error bars represent the SEM (original curves from which the slopes were calculated can be found in **Figure S18**). Constructs used: pPRO24_MBP-^{TVMV}sSH3L-TVMV-Strep, pPRO24_MBP-^{TVMV}sSH3L-TVMV^{C151A}-Strep, pCtrl2_T7.03_U9_myc-SH3-mNG-^{TVMV}, pCtrl2_T7.03_U9_myc-SH3-mNG-^{TVMV}E118.134, pCtrl2_T7.03_U9_myc-SH3-mNG-^{TVMV}LVA, pCtrl2_T7.03_U9_myc-SH3-mNG-TVMV$(E118min)_3$, pCtrl2_T7.03_U9_mKO$_\kappa$. Protein Sequences are stated in the supplement (see **12.4.5**)

As is in **Figure 22**, the triple minimal version performed comparable to its precursor. Both degrons were clearly outperformed by the LVA C-degron. This further confirms that E118-134 is not a strong C-degron when used in *lonp⁻ E. coli* strains. In addition, the flexible SG_3 linker (iFLinkC annotation, actual sequence GSG_4) turned out to enhance C-degron activity relative to the rigid, α-helical EAAAK linker that was used previous experiments.

4.3. N-Degron based Ratiometric Protease Assays

With a suitable co-expression system for the protease and the sensor established (see **Chapter 4.2**), the C-degron assay was adapted to establish a ratiometric *in vivo* protease assay. To this end, a second fluorescent protein was incorporated in order to enable ratiometric measurements. The resulting sensor enabled a more accurate normalization of the fluorescent signal. This means, rather than normalizing the fluorescent signal to the optical density, it was normalized to the fluorescence of the second FP that was part of the same polypeptide chain and therefore should be present in equimolar ratios. The basic principle of the assay is depicted in **Scheme 17**. Both fluorescent proteins are fused together into one fusion protein. The linker region comprised the cleavage site and a cryptic N-degron in the P1' position that was activated upon cleavage. This way no additional amino acids remained N-terminally of the N-degron after cleavage. Two different N-degrons were tested: FLFVQ and YLFVQ[21] which resulted in the corresponding cryptic degrons: ETVRFQ|FLFVQ and ETVRFQ|FLFVQ.

Scheme 17 depicts the final design of the ratiometric *in vivo* protease sensor based on cryptic N-degrons.

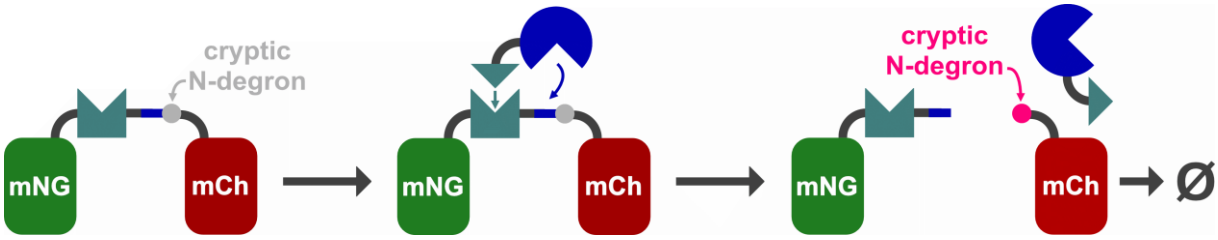

Scheme 17 General design of a ratiometric, two FP cryptic N-degron *in vivo* assay for site-specific proteases. mNeonGreen (mNG) and mCherry (mCh) are connected with a polypeptide linker (grey); the linker features the cryptic N-degron (light grey circle) which is comprised of the cleavage site (blue part of the linker), the N-degron and the recruitment domain (teal rectangular section). Left: The sensor is expressed and the cryptic N-degron is not recognized and therefore both fluorescent signals are detected. Center: the protease (blue circular section) is co-expressed with the sensor and directed to the sensor through interaction of the two-component recruitment module (teal rectangular section and teal triangle); once in close proximity the protease recognizes its cleavage site. Right: the protease cleaves off mNG and thereby unmasks the N-degron. Thus, the now freed and thereby activated N-degron (pink circle) induces rapid degradation (**Ø**) of mCh while mNG remains in the cell. In conclusion the red fluorescent signal is drastically reduced compared to the green signal.

Given the rapamycin-dependent recruitment of the protease and the sensor *via* a FKBP12-FRB dimerization module previously proved non-functional in *E. coli* (see **Chapter 4.2.2**), the new set of ratiometric sensors was exclusively cloned with the SH3 domain in both N- and C-terminal orientations relative to the cryptic N-degron. Insertion sites were chosen to direct the protease as close as possible to its cleavage site. The two SH3 ligand presented in **Chapter 4.2.10** were incorporated only into the protease constructs to reduce steric hindrance. Even though SH3 based recruitment did not improve apparent protease activities on the single FP sensors (see **Chapter 4.2.10**), it could still have benefited cleavage of the two FP sensor based on the *in vitro* data from **Chapter 4.3.1**. **Table 4** lists all orientations tested, as before promising orientations are high-lighted by grey-shading.

Table 4 SH3/xSHL orientation screening for protease assay performance. Best performing combinations of relative orientations high-lighted by grey-shading.

Protease construct	Sensor construct
sSH3L-TVMV	mNG-^{TVMV}FLFVQ-SH3-mCh
	mNG-^{TVMV}YLFVQ-SH3-mCh
	mNG-SH3-^{TVMV}FLFVQ–mCh
	mNG-SH3-^{TVMV}YLFVQ–mCh
wSH3L-TVMV	mNG-^{TVMV}FLFVQ-SH3-mCh
	mNG-^{TVMV}YLFVQ-SH3-mCh
	mNG-SH3-^{TVMV}FLFVQ–mCh
	mNG-SH3-^{TVMV}YLFVQ–mCh
TVMV-sSH3L	mNG-^{TVMV}FLFVQ-SH3-mCh
	mNG-^{TVMV}YLFVQ-SH3-mCh
	mNG-SH3-^{TVMV}FLFVQ–mCh
	mNG-SH3-^{TVMV}YLFVQ–mCh
TVMV-wSH3L	mNG-^{TVMV}FLFVQ-SH3-mCh
	mNG-^{TVMV}YLFVQ-SH3-mCh
	mNG-SH3-^{TVMV}FLFVQ–mCh
	mNG-SH3-^{TVMV}YLFVQ–mCh

The results for the best performing combination of sSH3L-TVMV and mNG-SH3-^{TVMV}FLFVQ-mCh are explanatorily discussed here where all remaining combination can be found in **Figure 24**. As visible in **Figure 23**, the measured arbitrary units for the mNG fluorescence were three orders of magnitudes higher compared to the mCh fluorescence – despite the fact, that the gain for mNG was set to 70 while the mCh fluorescence was recorded with a gain of 100. In turn, the normalized data found in the third graph **Figure 23 B** are within the range of ten to the power of minus two. Nevertheless, it is clearly visible that active TVMV prevents a significant rise in mCherry fluorescence which is slightly more pronounced when the values are normalized relative to the mNG fluorescence.

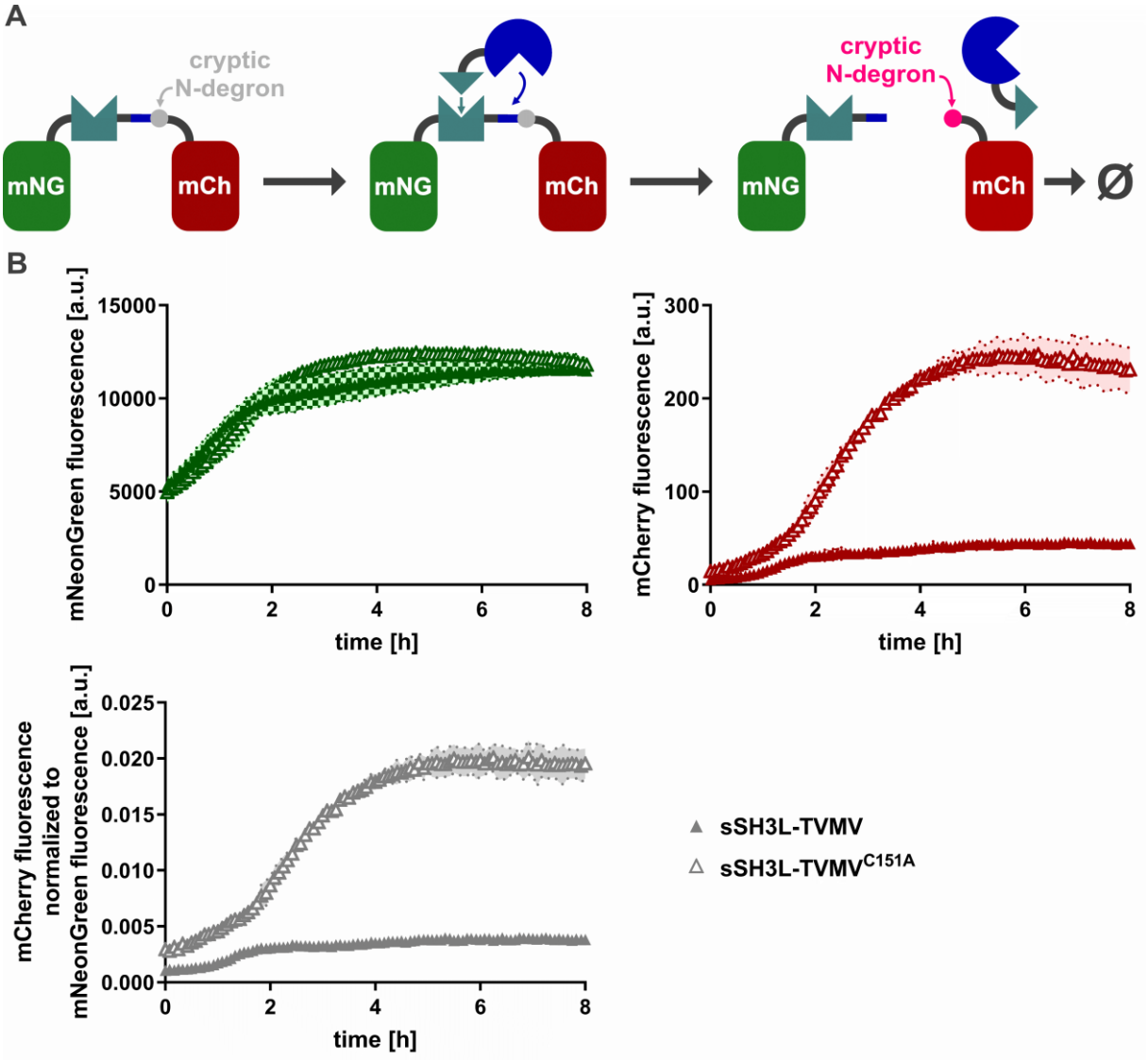

Figure 23 Ratiometric *in vivo* protease assay based on a cryptic N-degron. **A:** Schematic depiction of the experiments. **B:** Results for the best performing combination of sSH3L-TVMV and mNG-SH3-^{TVMV}FLFVQ-mCh. Data points represent the mean of dependent biological triplicates, error bars as colored area represents the SEM, dark checkered areas belong to active protease constructs, plain areas belong to inactive protease constructs. Constructs used: pPRO24_MBP-^{TVMV}sSH3L-TVMV-Strep, pPRO24_MBP-^{TVMV}sSH3L-TVMV^{C151A}-Strep pCtrl2_T7.03_U9_myc-mNG-SH3-^{TVMV}FLFVQ-mCh-Strep. Protein sequences are stated in the supplement (see **13.4.7**)

For all combinations of relative orientations, the slope of the linear increase in normalized fluorescence (between two and four hours) was calculated and compared to identify the best performing combinations. The results of this analysis are plotted in **Figure 24**.

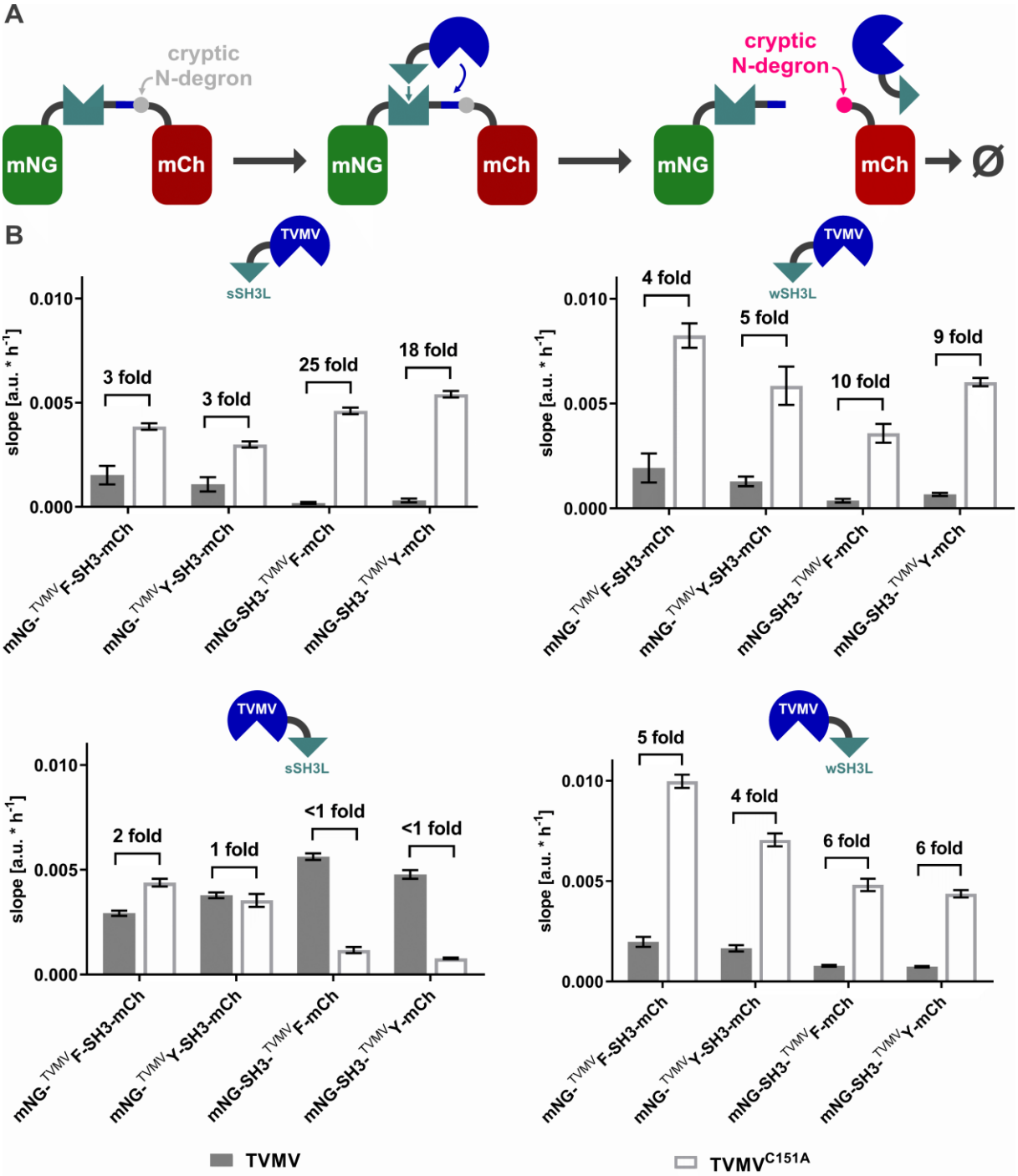

Figure 24 Orientation screen for the ratiometric *in vivo* protease assay based on cryptic N-degrons. **A:** Schematic depiction of the experiment. **B:** Comparison of the slopes of the linear increase in normalized mCh fluorescence for the orientation screen. The protease constructs used are stated above the corresponding graph, while the sensors are listed on the X-axis, bars represent the mean slopes for the dependent biological triplicates measured; error bars depict the SEM, filled bars for the active TVMV, empty bars for the mock controls TVMV^{C151A}, brackets above the paired bars state the fold change in slope between a protease and its corresponding mock construct. Constructs used: pPRO24_MBP-^{TVMV}sSH3L-TVMV-Strep, pPRO24_MBP-^{TVMV}sSH3L-TVMV^{C151A}-Strep, pPRO24_MBP-^{TVMV}wSH3L-TVMV-Strep, pPRO24_MBP-^{TVMV}wSH3L-TVMV^{C151A}-Strep, pPRO24_MBP-^{TVMV}TVMV-sSH3L-Strep, pPRO24_MBP-^{TVMV}TVMV^{C151A}-sSH3L-Strep, pPRO24_MBP-^{TVMV}TVMV-wSH3L-Strep, pPRO24_MBP-^{TVMV}TVMV^{C151A}-wSH3L-Strep, pCtrl2_T7.03_U9_myc-mNG-SH3-^{TVMV}FLFVQ-mCh-Strep, pCtrl2_T7.03_U9_myc-mNG-SH3-^{TVMV}YLFVQ-mCh-Strep. Protein Sequences are stated in the supplement (see **12.4.7**)

As visible in **Figure 24**, the best fold changes were achieved when the SH3 domain was located N-terminal of the cleavage site. A similar observation was made for the protease constructs where an N-terminal SH3 ligand seemed to benefit the most. This orientation corresponds to a localization of the active site of TVMV close to its C-terminus [36]. In contrast, no significant difference between phenylalanine (F) or tyrosine (Y) at the P1' position was observed. Therefore, it was concluded that TVMV tolerates both amino acid residues at the P1' site in a comparable fashion. In case of a C-terminal localization of the strong SH3 peptide ligand apparent protease activity led to reduced mCh degradation. This finding seemed counter-intuitive and inconsistent with the other orientations tested. A reasonable explanation could a mishap at the picking step. Colonies were picked from quartered plates. Because plates were labelled on the bottom in clock-wise manner picking order was counter-clockwise (plates were flipped for easier picking). So maybe for this plate the picking order was accidently inverted.

4.3.1. Effect of SH3 based Recruitment on Ratiometric Assay Dynamics

After the best relative orientation for incorporation the SH3 domain/SH3 ligands were identified for the ratiometric assay, the effect of the recruitment was quantified analogous to the C-degron based sensors (see **Chapter 4.2.10**). **Figure 25** shows the result of the recruitment test. Consistent to the approach for the C-degron sensor protease constructs devoid of the SH3 peptide ligand were included. In contrast to the previous experiments where the strong SH3 ligand seemed to be superior compared to the weak one, no pronounced effect was observed. Indicating that yet again proteolytic activity of the proteases was the limiting factor.

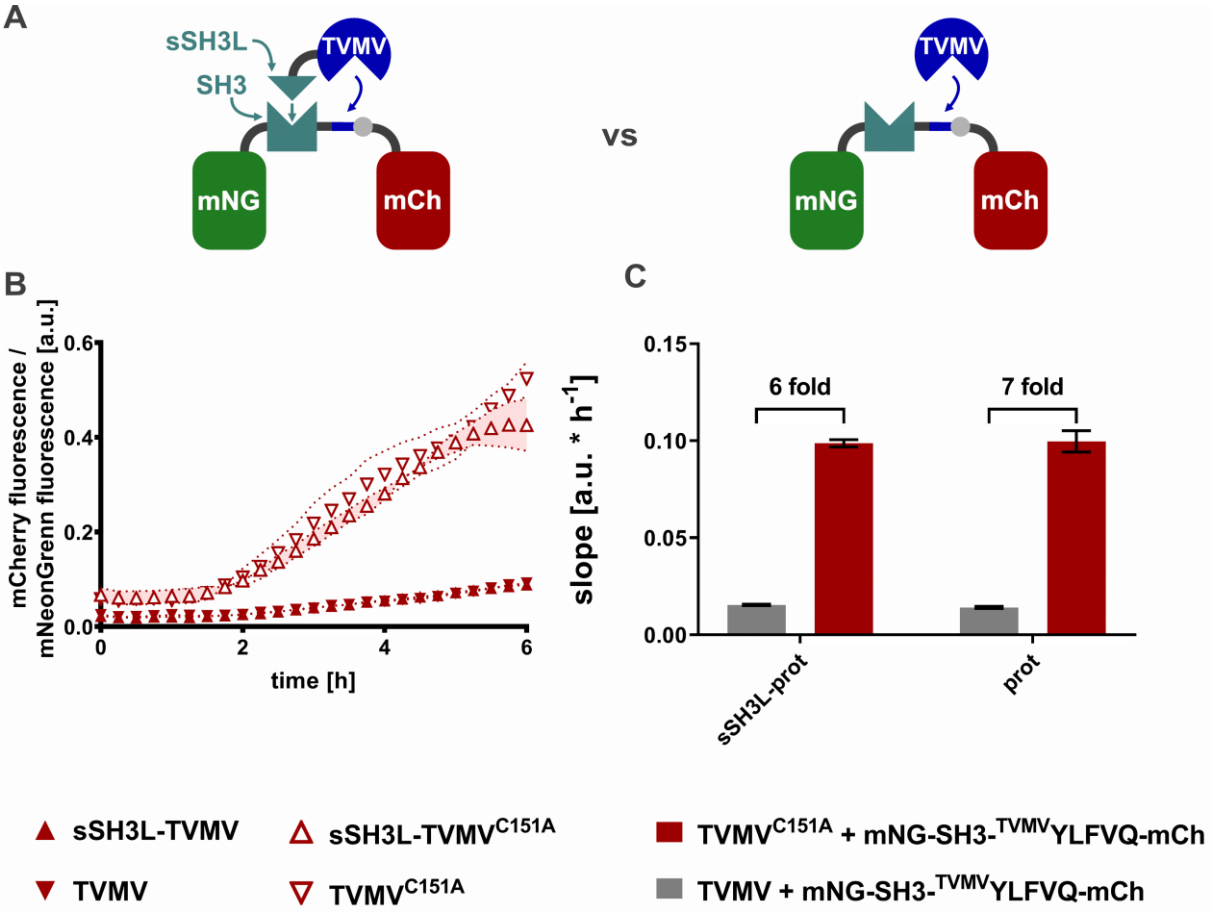

Figure 25 Effectiveness of SH3-based recruitment on ratiometric assay dynamics. Constructs, colors and symbols as in **Figure 24**, except no SH3 ligands protease constructs were included as well (upside down triangles) and grey coloration for normalized mCh fluorescence replaced with red. **A:** Schematic depiction of the experiment. The effect of the sSH3L ligand on the dynamics of the assay was tested **B:** Real-time kinetic data of the protease-dependent development in the fluorescent signal over time, sensor construct is indicated above the graph, data points represent the mean values of dependent biological quadruplicates measured, error areas depict the SEM. **C:** bars represent the mean slope in normalized mCh fluorescence of the dependent biological quadruplicates measured over the time interval between 2 h and 5 h, error bars depict the SEM, grey bars show slopes for protease constructs (mCh/red fluorescence is lost through proteolytic activity), red bars show the slopes for the corresponding mock constructs (mCh/red fluorescence is retained without proteolytic activity), brackets over the paired bars state the fold change in protease dependent reduction in slope of the increasing normalized mCh fluorescence compared to the respective mock construct TVMV^{C151A}. Constructs used: pPRO24_MBP-^{TVMV}sSH3L-TVMV-Strep, pPRO24_MBP-^{TVMV}sSH3L-TVMV^{C151A}-Strep, pPRO24_MBP-^{TVMV}TVMV-Strep, pPRO24_MBP-^{TVMV}TVMV^{C151A}-Strep, pCtrl2_T7.03_U9_myc-mNG-SH3-^{TVMV}YLFVQ-mCh-Strep. Protein sequences are stated in the supplement (see **12.4.7**).

4.4. Effect of *lonp*$^{+}$ Genetic Background

In the subsequent experiment, two commercially available lonp+ *E. coli* K-strains were tested. The first was Shuffle T7 from New England Biolabs and the second was KRX from Promega. Both featured a chromosomal integrated T7 RNA polymerase: under control of an IPTG inducible lac promoter (Shuffle T7) and a rhamnose inducible derivative of the araBAD promoter (KRX). The latter required switching from M9 minimal medium to LB medium because only ribose was lower in hierarchy than rhamnose which however turned out to be such poor carbon source that experiments were impossible. This meant switching from a mNeonGreen based sensor to a mCherry based sensor to avoid background fluorescence of the LB medium. In addition, both strains required consecutive single transformation of the protease and sensor carrying constructs instead of the usual double transformation of BL21(DE3). Otherwise, insufficient transformation efficiencies were observed. The results of this test are shown in **Figure 26**.

In general, both strains performed poorly compared to BL21(DE3). Possibly because the lon protease present in the cytoplasm might have reduced the amount of TVMV below an effective detection limit. For this reason, as well as ease of handling, BL21(DE3) remained the preferred expression host for the remainder of this work. Because of the suboptimal performance of the newly clone mCh sensor in the two K strains, a control measurement in BL21 was performed to validate the function of the mCh sensor. The results of this experiment are found in **Figure 27**.

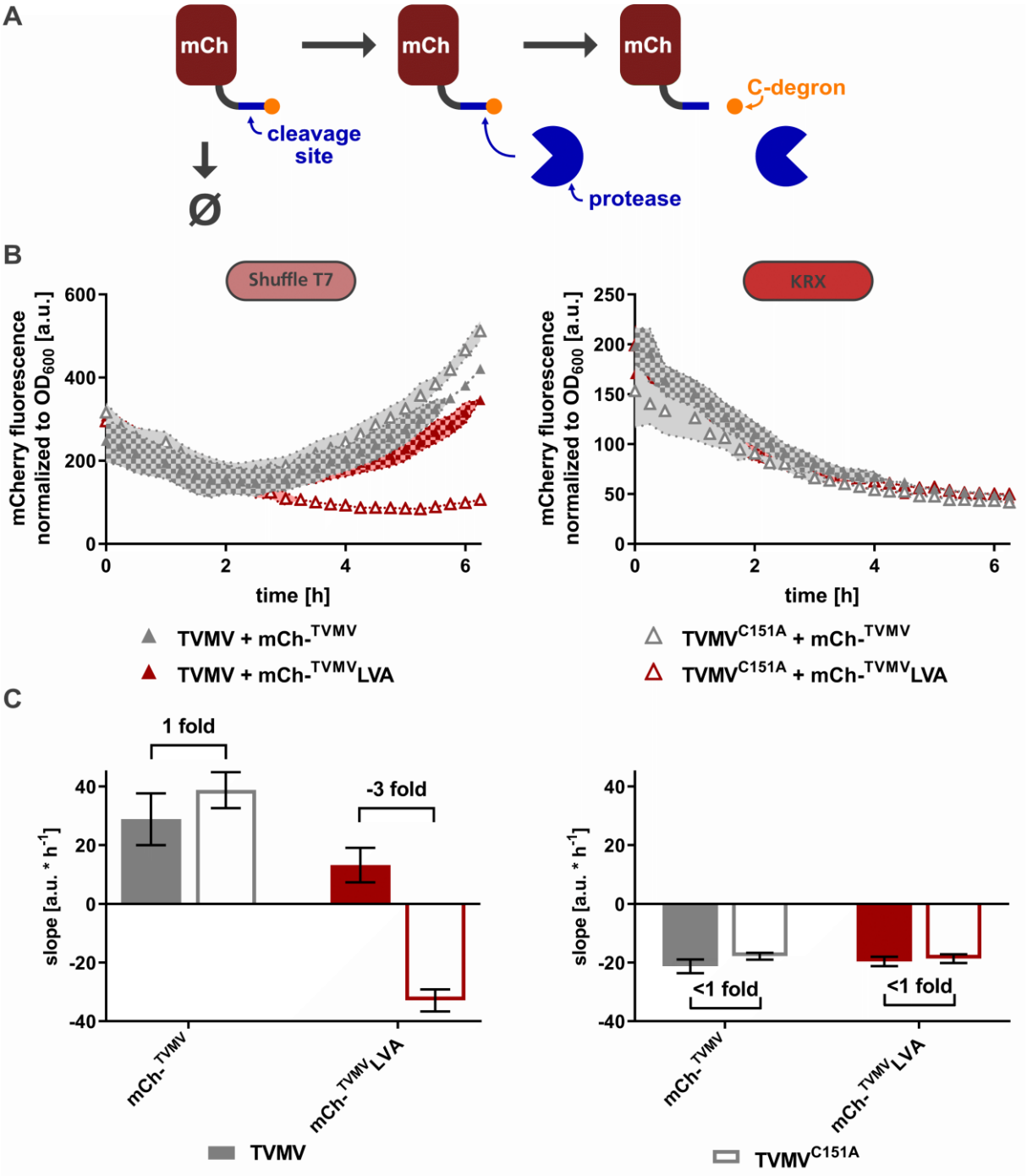

Figure 26 Comparison of the *lonp*$^{+}$ K-strains Shuffle T7 and KRX. **A:** Schematic depiction of the experiment, the assay design was based on the C-degron based assay presented in **Chapter 4.2** except for the following changes: **(i)** the non-beneficial recruitment domains were omitted, **(ii)** mNG was replaced with mCh to reduce any background fluorescence associated with riboflavin. **B:** mCh fluorescence normalized to OD_{600} over time, strain used stated above the corresponding graph, data points represent the mean of the dependent biological quadruplicates measured, error areas depict the SEM. **C:** Bars represent the average of dependent biological quadruplicates measured; error bars represent the SEM, pairwise bars for TVMV and corresponding mock construct showing the slope of the linear increase in normalized mCh fluorescence, brackets denoted the fold change in slope between paired bars. Constructs used: pPRO24_MBP-^{TVMV}TVMV-Strep, pPRO24_MBP-^{TVMV}TVMV^{C151A}-Strep, pCtrl2_T7.03_U9_myc-mCh-^{TVMV}, pCtrl2_T7.03_U9_myc-mCh-^{TVMV}LVA. Protein Sequences are stated in the supplement (see **13.4.8**).

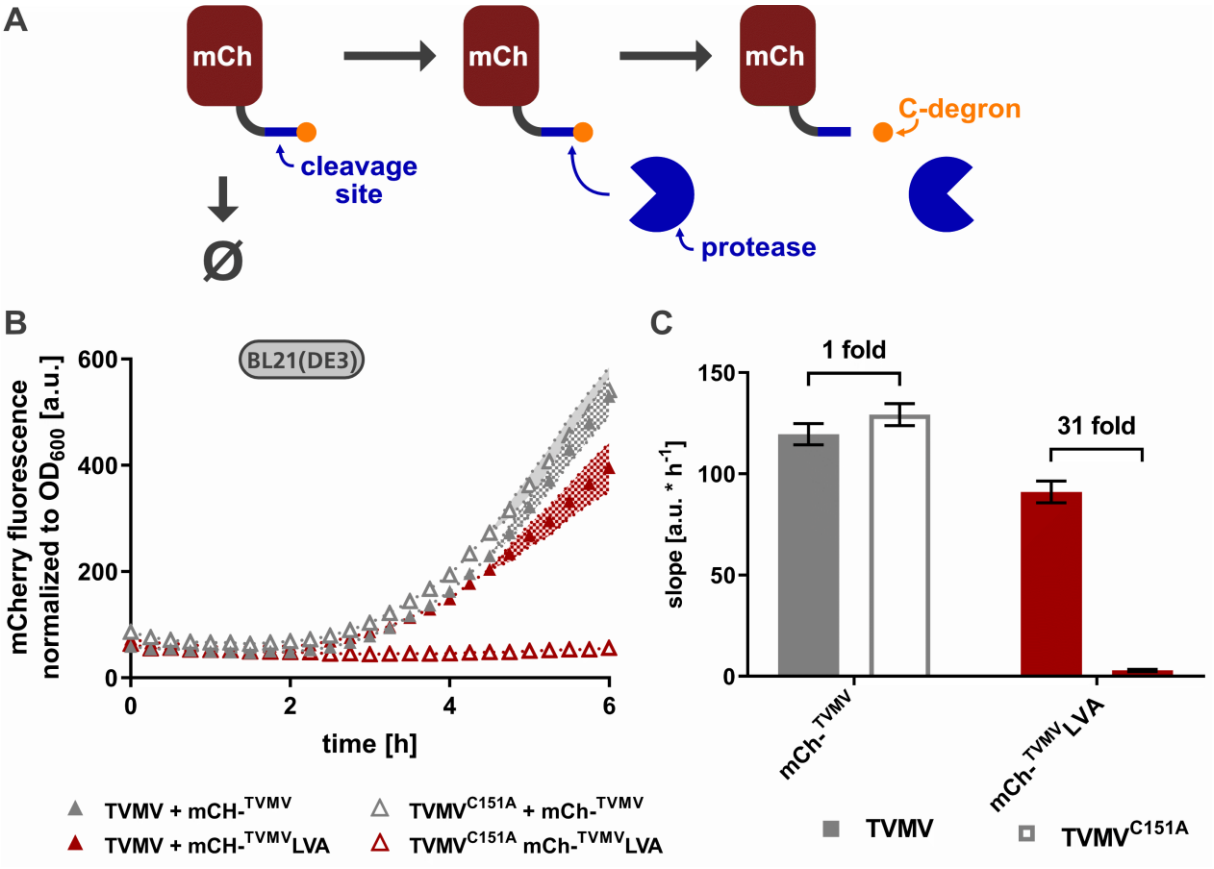

Figure 27 Validation of the mCh sensor in a BL21(DE3) genetic background. Constructs, colors, symbols as in **Figure 26**. **A:** schematic depiction of the experiment. **B:** Real-time normalized mCh fluorescence over six hours after induction of the mCh sensor following a two hour pre-induction of the protease; Data points represent the mean values for the dependent biological quadruplicates measured, error areas depict the SEM; **C:** Slope of the linear increase in mCh fluorescence between 3 and 5 hours, bars represent the mean slope of the dependent biological quadruplicates measured, filled bars: active protease, empty bars: inactive protease TVMV^{C151A} (mock control), error bars depicted the SEM, brackets above the paired bars depict the fold change in slope between a protease construct and its corresponding mock control. Constructs used: pPRO24_MBP-^{TVMV}TVMV-Strep, pPRO24_MBP-^{TVMV}TVMV^{C151A}-Strep, pCtrl2_T7.03_U9_myc-mCh-^{TVMV}, pCtrl2_T7.03_U9_myc-mCh-^{TVMV}LVA. Protein Sequences are stated in the supplement (see **13.4.8**).

In BL21, the shape of the curves perfectly matched those obtained with the mNG sensors. This indicates the assay functions independently of the identity of the underlying fluorescent protein. The extremely high fold change between active and inactive TVMV is particularly striking (**Figure 27 B**). The high fold change is mainly based on the very slow rise in the mCh fluorescent signal when catalytically inactive TVMV is used in conjunction with degron-tagged sensor. The most plausible explanation for this phenomenon is the slower maturation rate of mCherry – 15 min [95] – compared to mNG – 10 min [85] – which gives the ClpP degradation machinery more time to degrade the fluorescent reporter before the fluorophore matures.

4.5. General Assay Utility with TEV and HCV (Master Thesis C. Rühmkorff)

After the elementary assay was established for TVMV in **Chapter 4.2**, the general utility of the assay was demonstrated for additional site-specific proteases. To this end, TEV and HCV proteases were selected as candidates that have been subject to substantial engineering efforts before [1, 3, 45]. The assay could be readily adapted by replacing the appropriate protease and the protease cleavage site in the sensor construct by means of the iFLinkC assembly process. Considering iFLinkC constitutes a scarless assembly process, constructs were generally assembled from elementary parts. The assembly and characterization of all TEV and HCV constructs was the subject of the master thesis of C. Rühmkorff. Therefore, all data below were generated by him. **Figure 28** shows a direct comparison of all three proteases in the same measurement using the LVA C-degron assay (**Chapter 4.2.7**).

As is evident in **Figure 28**, the closely related TVMV and TEV proteases perform similarly while HCV is only able to manifest a two-fold change. This might be based on the weaker serine nucleophile in case of HCV compared to cysteine in case of TVMV and TEV. In addition, the difference could be explained by lower expression levels. Nevertheless, discrimination of active from inactive variant was possible in all three cases.

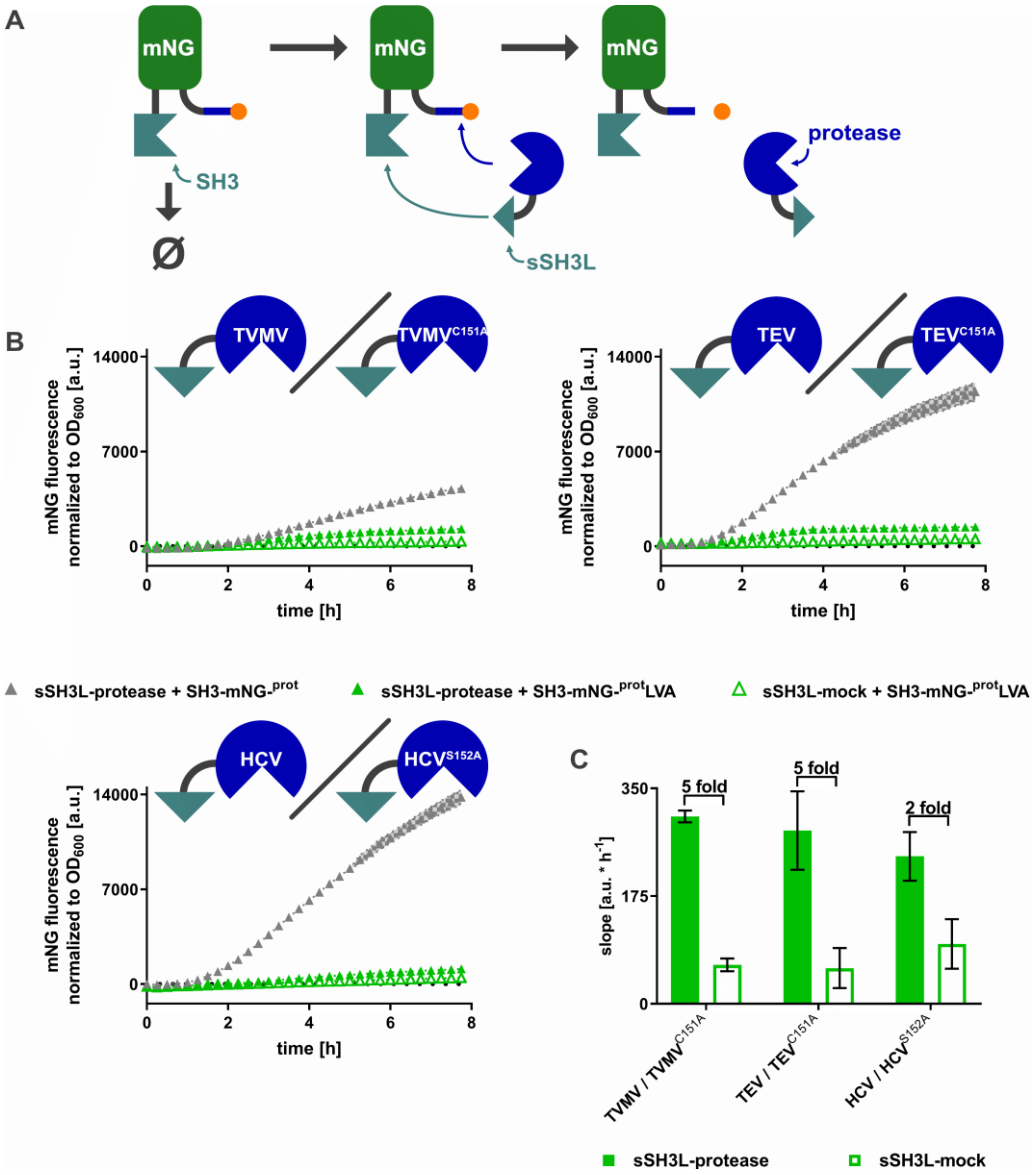

Figure 28 Direct comparison of three different proteases with the LVA C-degron based assay. **A:** Schematic depiction of the experiment: The basic C-degron assay was performed as explained in **Chapter 4.2** with three site-specific proteases TEV, TVMV and HCV in direct comparison. **B:** Real-time kinetic data of *in vivo* protease activity measured over the course of 8 hours; Colors and symbols as in **Figure 15,** proteases and corresponding inactive variants are listed above the corresponding graphs, sensors are listed in the central legend, data points represent the mean values of dependent biological quadruplicates measured, error areas depict the SEM. **C:** Fold changes between active and inactive protease variant, bars represent the mean slopes of the protease dependent increase in mNeonGreen fluorescence, error bars depict the SEM, filled bars for active proteases, empty bars for inactive proteases, brackets above the paired bars state the corresponding fold changes in slope. Constructs used: pPRO24_MBP-^{TVMV}sSH3L-TVMV-Strep, pPRO24_MBP-^{TVMV}sSH3L-TVMV^{C151A}-Strep, pPRO24_MBP-^{TVMV}sSH3L-TEV-Strep, pPRO24_MBP-^{TVMV}sSH3LTEV^{C151A}-Strep, pPRO24_MBP-^{TVMV}sSH3L-HCV-Strep, pPRO24_MBP-^{TVMV}sSH3L-HCV^{S152A}-Strep, pCtrl2_T7.03_U9_myc-SH3-mNG-^{TVMV}, pCtrl2_T7.03_U9_myc-SH3-mNG-^{TVMV}LVA, pCtrl2_T7.03_U9_myc-SH3-mNG-^{TEV}, pCtrl2_T7.03_U9_myc-SH3-mNG-^{TEV}LVA, pCtrl2_T7.03_U9_myc-SH3-mNG-^{HCV}, pCtrl2_T7.03_U9_myc-SH3-mNG-^{HCV}LVA, pCtrl2_mKO$_\kappa$. Protein Sequences are stated in the supplement (see **13.4.9**). TEV and HCV related constructs were cloned by C. Rühmkorff; all data shown in this figure were generated by C. Rühmkorff under my supervision.

To confirm the functional expression of all three tested proteases, C. Rühmkorff detected the C-terminally Strep-tagged protease constructs by means of Western blotting. To this end, Strep-tagged proteases were resolved by means of a Strep-tactin-HRP conjugate (BioRad) using enhanced chemiluminescence substrate (BioRad). The obtained blots are shown in **Figure 29** and further demonstrate the general utility of the assay for different proteases.

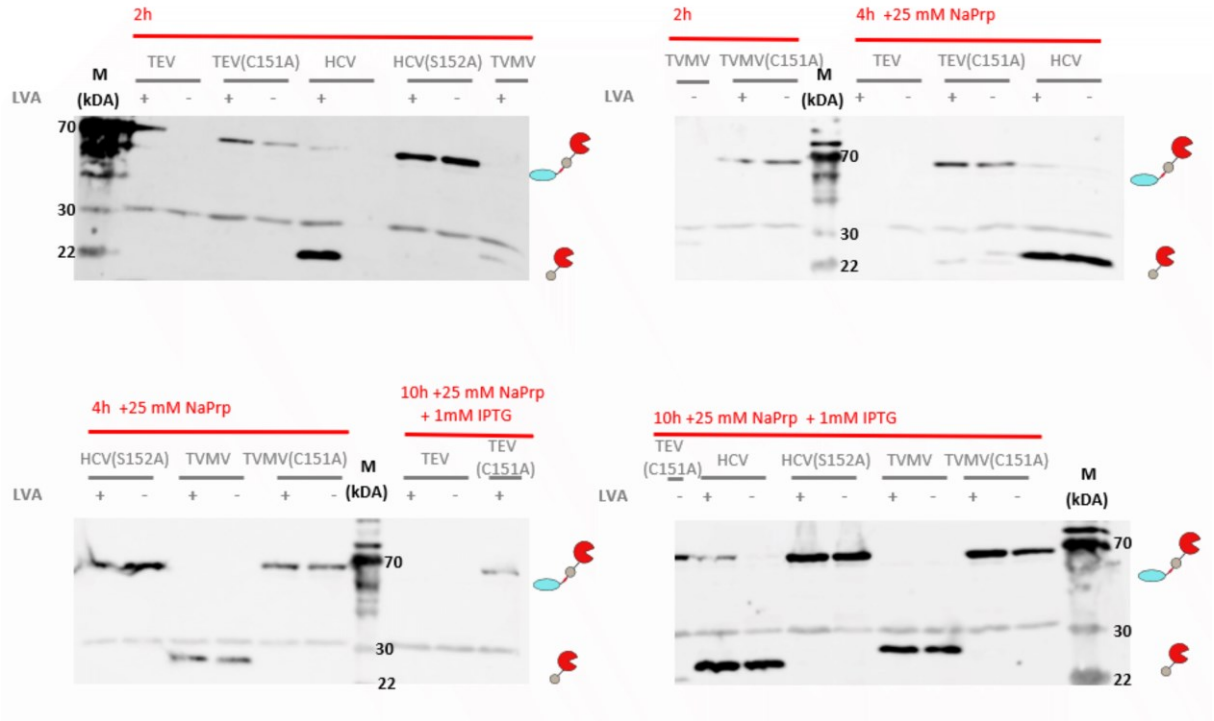

Figure 29 Western blot analysis of protease expression under assay conditions. Double transformed *E. coli* BL21(DE3) cultures were grown in M9 at 37 °C for 2 h. Subsequently, protease expression was induced with 25 mM sodium propionate and cultures were incubated at 30 °C. Another two hours later, the expression of the sensor was induced with 1 mM IPTG. Samples were taken before protease induction (2h timepoint), before sensor induction (4h timepoint) and 6 h after sensor induction (10 h timepoint, the usually endpoint of the *in vivo* assays). Then 20 µL cell suspension with an OD_{600} = 5 were loaded per lane. The pictograms to the right of the individual Western blots show the expected protease bands, the upper band around 68 kDa when the MBP solubility tag is not cleaved off and the lower band around 28 kDa for the autocatalytically processed protease construct. The weak band at 35 kDa belongs to BirA which corresponds to the the biotin ligase of *E. coli* and is always detected through Strep-Tactin. The +/- refers to the presence of the LVA C-Degron in the co-expressed sensor constructs. The expression of the sensor was generally included to fully mimic the assay conditions during expression tests. Constructs used: pPRO24_MBP-^{TVMV}sSH3L-TVMV-Strep, pPRO24_MBP-^{TVMV}sSH3L-TVMV^{C151A}-Strep, pPRO24_MBP-^{TVMV}sSH3L-TEV/-Strep, pPRO24_MBP-^{TVMV}sSH3L-TEV^{C151A}-Strep, pPRO24_MBP-^{TVMV}sSH3L-HCV-Strep, pPRO24_MBP-^{TVMV}sSH3L-HCV^{S152A}-Strep, pCtrl2_T7.03_U9_myc-SH3-mNG-^{TVMV}, pCtrl2_T7.03_U9_myc-SH3-mNG-^{TVMV}LVA, pCtrl2_T7.03_U9_myc-SH3-mNG-^{TEV}, pCtrl2_T7.03_U9_myc-SH3-mNG-^{TEV}LVA, pCtrl2_T7.03_U9_myc-SH3-mNG-^{HCV}, pCtrl2_T7.03_U9_myc-SH3-mNG-^{HCV}LVA. Protein Sequences are stated in supplement (see 13.4.9). TEV and HCV related constructs were cloned by C. Rühmkorff; all data shown in this figure were generated by C. Rühmkorff under my supervision.

Figure 29 reveals substantial leakage of the propionate-inducible promoter when cells are grown in M9 minimal media with arabinose as the sole carbon source. This could point towards an insufficient level of catabolite repression of the prp operon through arabinose. Otherwise, the bands of individual proteases became more intense compared to biotinylated BirA (which serves as an internal loading control), the longer overexpression was induced with sodium propionate. As expected for the catalytically-inactive variants $TVMV^{C151A}$, TEV^{C151A} and HCV^{S152A}, only bands with a high molecular mass could be detected as individual proteases remained fused to MBP. In contrast, for catalytically-active proteases, only processed bands were detected which further confirms *in vivo* activity of the protease. The only exception was native TEV protease for which no bands were detected at all. One explanation of this observation could be that TEV protease recognizes the C-terminal Strep-Tag as a substrate (TEV-site: ENLYQS vs Step-TagII: WSHPQFEK) even though there is little sequence similarity between them except that both sequences feature a glutamine residue.

4.6. Design of Light-switchable TVMV Switches

Finally, the newly developed protease assay was applied to engineer a light-responsive variant of TVMV protease. Recently, fungal VIVID domains which are highly similar to plant derived light-, oxygen-, and voltage-sensitive domains 1 (LOV1 domains) were engineered from homodimerizing photo-receptors into strictly heterodimerizing photo-receptors. These novel semi synthetic photoreceptors were called magnets. This name was chosen because upon irradiation with blue light at 450 nm, the positive magnet and the negative magnets dimerize in an anti-parallel orientation just like real bipolar magnets would do [96, 97].

The magnet heterodimers spontaneously dissociate in the dark. The creators around Akihiro Furuya and Moritoshi Sato from the University of Tokyo provided a whole set of different magnets. The negative magnets (nMags) were optimized in regards to their binding affinity to accelerate the dimer formation upon irradiation down to the scale of seconds. The positive magnets (pMags) were selected to provide different dissociation rates in the dark. The rates ranged from hours (original pMag) to a couple of seconds (pMagFast2)[96].

In 2017, the Khammash group from ETH Zürich demonstrated that the magnet system can be used in *E. coli* without any further adaptation [98]. With a proof of principle in *E. coli* reported and the magnet co-factor flavin adenine dinucleotide (FAD) being a natural metabolite of *E. coli*, an opto-switch based on the general auto-inhibited TVMV module was designed.

The autoinhibited TVMV module features an auto-inhibition domain (AI) which acts as a competitive peptide inhibitor that is derived from the natural cleavage site of TVMV. The AI domain was developed in previous studies by V. Stein the supervisor of this project and published in PNAS in 2014 [1]. The basic idea was to identify peptide sequences that bind to the cleavage site with reasonable affinities without being actually cleaved by the protease. By covalently linking this peptide inhibitors to the protease *via* a peptide linker a fully genetically encodable synthetic zymogen was created. By introducing an allosteric receptor domain into the linker between the AI domain and the protease, synthetic protein switches could be engineered in previous studies [99]. The basic design principle of these switches and signal transducers is shown in **Scheme 18**.

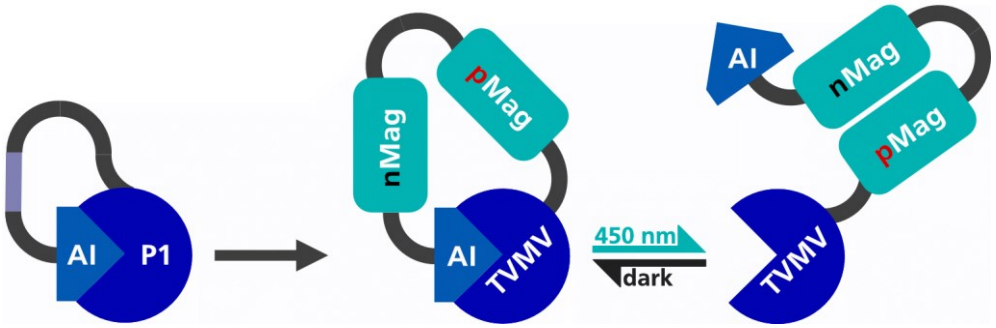

Scheme 18 Design of the new blue-light responsive TVMV switched based on V. Stein's design for allosteric switches based on auto-inhibited proteases.

Table 5 Blue light switchable TVMV with focused linker libraries. Construct is shown from N- to C-terminus.

AI	Short linkers: G_1 G(GS)G G(SPA)G G(GASPAG)G G(P)G $G(P_3)G$	**nMagHigh1**	Long linkers: $G(L(G_3S)_3ET)G$ $G(GS)(G_2S)_7G$ $G(NS_3N_{10})G$ $G(((TP)_4TGSG)_2(TP)_4T)G$ $G(P_{19})G$ $G(A(EA_3K)_8AG)G$	**pMagFast2**	Short linkers: G_1 G(GS)G G(SPA)G G(GASPAG)G G(P)G $G(P_3)G$	**TVMV**

To engineer light-responsive protease switches, a combination of nMagHigh1 and pMagFast2 was chosen in preliminary studies. According to the Khammash publication, these displayed the fasted switching behavior in *E. coli*. To account for the critical role of linkers, a focused linker library was devised featuring a mix of short, long, flexible and rigid linker (**Table 5**). After visual inspection of the crystal structures, short linkers were chosen to connect an AI domain and the TVMV protease with the photoreceptor. In contrast, long linkers were chosen to connect the nMag and pMag modules. In theory, this arrangement (see **Scheme 18**) should confer enough intrinsic flexibility for the AI domain to bind to the active site of the protease. Upon irradiation and subsequent dimerization of the two magnets, the short linkers between the

photoreceptor domains and the AI domain would disfavor simultaneous dimerization of the photoreceptor domain and binding of AI to the active site of TVMV. **Table 5** shows the focused library in an N- to C-terminal orientation.

4.7. Combinatorial Assembly of Light-Regulated TVMV Switches with iFLinkC

The library was assembled in four hierarchic steps by means of a new DNA assembly method termed 'iterative Functional Linker Cloning' or in short iFLinkC. iFLinkC provides a general route to the assembly of complex multi-domain fusion proteins [45] and was specifically applied to construct a combinatorial library of light-regulated TVMV switches.

Briefly, iFLinkC is based on the use of Type IIS restriction enzymes with three distinct feature **(i)** they recognize non-palindromic and thereby directional DNA sequences, **(ii)** they cut directly adjacent of their recognition sequences and **(iii)** they generate two nucleotide long single stranded overhangs. Based on these criteria the two restriction enzymes BtsI and BsrDI, both commercially available from *New England Biolabs*, were selected for iFLinkC.

The recognition sequences for these two enzymes were cloned flanking the cloning site of the two iFLinkC deposit/entry vectors termed pFD and pL2. pFD is the deposit/entry vector for Functional Domains which is any part of a fusion protein that is not a linker. Accordingly, pL2 is the deposit/entry vector for Linkers. Aside from one nucleotide spacers between the coding sequence of the deposited part and the flanking restriction sites pFD and pL2 are identical. The spacers in pL2 are crucial to ensure that the two nucleotide overhangs generated by BtsI and BsrDI are reconstituted into a single in-frame glycine codon. Otherwise, the two nucleotide overhangs would result in frame shifts during the iterative assembly steps of iFLinkC. The direct consequence of this assembly method is that a one glycine scar between a functional domain and a linker is always created. Therefore, all linkers introduced with iFLinkC are G[actual linker sequence]G. The only exceptions are the specifically modified plasmid pL2_G_1 and pL2_G_2 which introduce a single or two glycine codons into the coding sequence. All other pL2 plasmids introduce linkers of at least three amino acids in length.

Both vectors include the same class A origin of replication and a kanamycin resistance cassette separated by an EcoRI restriction site, however both vectors lack an expression cassette. pFD and pL2 are explicit deposit vector. Therefore, it is crucial that all protein coding sequences stored in either vector are deficient of start or stop codons.

In the initial assembly step, a linker or linkers mix is cloned up- or downstream a functional domain. Therefore, one deposit vector is digested with BsrDI (the upstream CDS) while the other is digested with BtsI (the downstream CDS). It is noteworthy that both enzymes prefer elevated temperatures during restriction and in the case of BsrDI may require a specific buffer. After the restriction steps at elevated temperature, EcoRI is added to the reaction mixes and restriction is continued at 37 °C. After restriction the generated fragments are separated through electrophoresis and the desired restriction fragments are recovered und subsequently ligated with one another. Due the fact that pFD and pL2 are nearly identical all restriction sites are regenerated during ligation. The most upstream part defines the identity of the newly assembled construct. In case of a functional domain, the construct is treated as a pFD for further assembly steps. In the opposite case, it is treated as linker instead. **Scheme 19** depicts the initial iFlinkC assembly reaction. After ligation, the newly generated plasmid or plasmid library – depending if a single linker or a linker mix was used – can be used to transform *E. coli* cells for plasmid propagation or long-term storage as a glycerol cryo-stock.

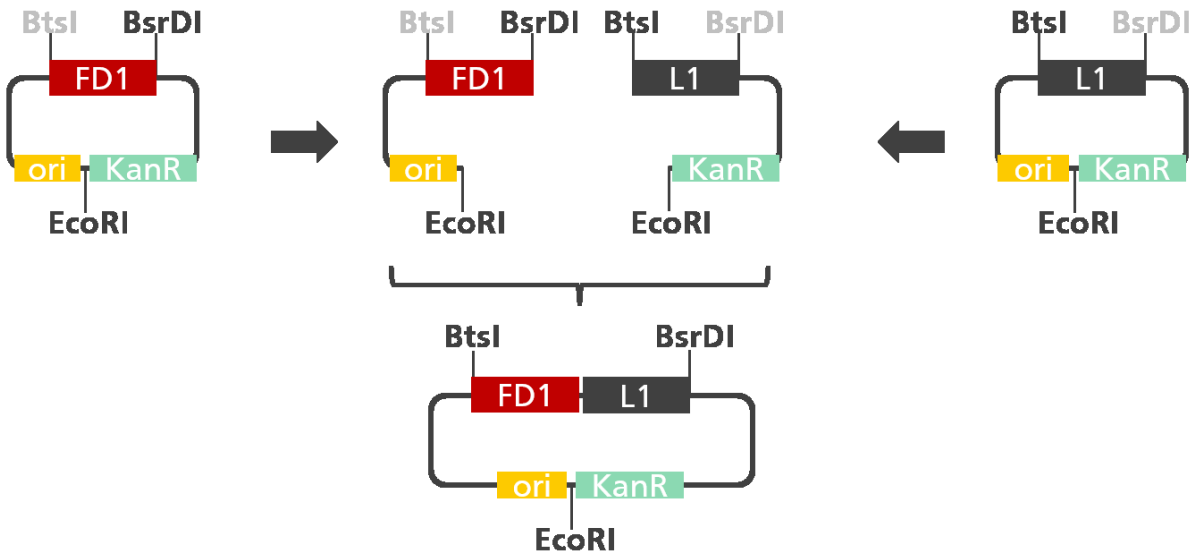

Scheme 19 Initial iFLinkC assembly step. In the initial assembly a linker cloned up or down stream of a functional domain (downstream in this example). Arrows indicate restriction steps while brackets depict the ligation step. All necessary purification steps are omitted, origin of replication (ori) as a yellow rectangle, kanamycin resistance cassette (KanR) as a mint green rectangle, functional domain coding sequence (FD) as a red rectangle, linker/linker mix (L) as a grey rectangle, restriction side indicated with annotated lines.

For more complex constructs time and effort may be saved by following a hierarchical assembly order than a sequential. In this case, the desired fusion protein coding sequences is split into sets one domain one linker/linker mix pairs which are assembled simultaneously. By repeating

these pairwise assembly steps complex constructs or libraries are assembled in an efficient and straight-forward manner. This process is exemplarily depicted in **Scheme 20** for a 4-domain-3-linker/linker mix multi-domain fusion protein.

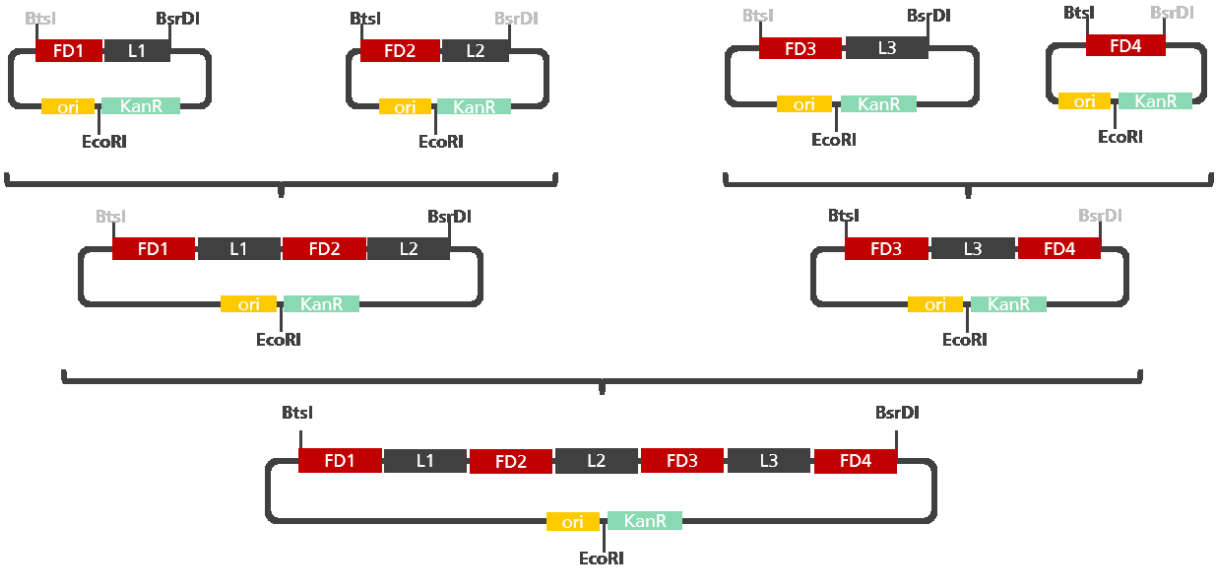

Scheme 20 Iterative assembly of 4-domain-3-linker multi-domain fusion protein with iFLinkC. In the initial step three pairs one functional domain (FD, red rectangles) and one linker/linker mix were assembled. In the following two steps the pairwise assembly is continued until the full-length CDS for a 4-domain-3-linker fusion protein is assembled.

Once the multi-domain fusion protein coding sequence is assembled, it can be cloned into an expression vector of choice. This can either be one the iFLinkC expression vectors termed iFLinkC_XE or in the case of this work pPRO24 and pCtrl2, respectively (see **Chapter 4.2.1**). Because iFLinkC assembled coding sequences lack a start-codon, the expression vector of choice has to provide it. Alternatively, cloning into the final expression vector can be performed with PCR based methods that introduce the missing start-codon through primer overhangs. This alternative should be considered with caution because many linker coding sequences are GC-rich, highly repetitive or if linker mixes were used internal homology within the library could occur. In this case, PCR based cloning could become quite challenging. For these reasons, we recommend classical restriction ligation cloning of iFLinkC assembled constructs or libraries into expression vectors.

Cloning into iFLinkC_XE vectors with BtsI and SpeI automatically provides in frame start and stop codons. The start codon is provided through the iFLinkC expression vector while a stop codon is included in all iFLinkC assembled coding sequences when they are restricted with SpeI instead of the more upstream BsrDI. For this work, I chose adapter cloning to clone BtsI…SpeI restriction fragments of my iFLinkC assembled constructs into pPRO24 and pCtrl2. Used adapter oligos were phosphorylated and hybridized before used as additional ligation

fragments. The sequences of hybridized oligos are listed in **Table 6** For better visualization, the aptamer cloning step is exemplarily shown in **Scheme 21**.

Table 6 Adapter oligos for cloning of iFLinkC assembled constructs and libraries into pPRO24 or pCtrl2. Start-codons highlighted in bold.

Name	Sequence	Usage
BtsI-to-NdeI	5′-T**ATG**AGCTCAGGATCTAGTGGG-3′ 3′-ACTCGAGTCCTAGATCAC-5′	Cloning of iFLinkC assembled constructs to pCtrl2
SpeI-to-KpnI	5′CTAGTGATACGGGACAGATGGGGTAC-3′ 3′-ACTATGCCCTGTCTACCC-5′	Cloning of iFLinkC assembled constructs to pCtrl2
BtsI-to-EcoRI	5′-AATTC**ATG**GGATCTGGCTCGATCGGG-3′ 3′-GTACCCTAGACCGAGCTAGC-5′	Cloning of iFLinkC assembled constructs to pPRO24
SpeI-to-SalI	5′-CTAGGGATACGCAGATGGG-3′ 3′-CCTATGCGTCTACCCAGCT-5′	Cloning of iFLinkC assembled constructs to pPRO24

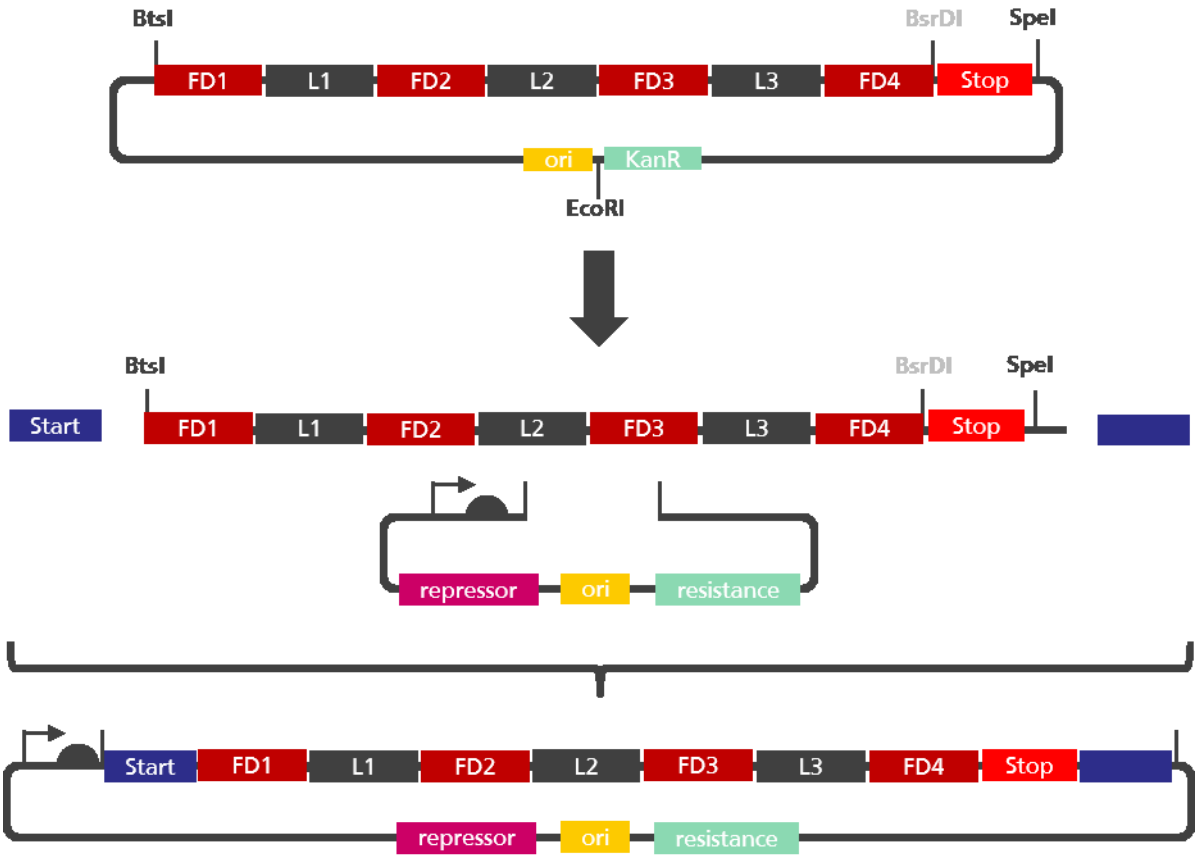

Scheme 21 Final cloning step into a suitable expression vector. Double stranded adapter oligos in blue, restriction step symbolized by the arrow, ligation step by the bracket, oris in yellow, antibiotic resistance cassettes in mint green and the repressor in purple.

In the context of the optically-regulated protease switches, the linker mixes were cloned downstream of the prepended domains. Afterwards, the N-terminal and C-terminal halves were assembled. Subsequently, the final library was assembled by joining both halves. Finally, a solubility tag was added to the N-terminus in the form of maltose binding protein. In summary, the final library comprised of MBP-^{TVMV}AI-[shLinkers]-nMagHigh1-[lgLinkers]-pMagFast2-[shLinkers]-TVMV-Strep. The C-terminal Strep-Tag was included for subsequent purification of potential switches – i.e. a Strep-tagged TVMV was already available as an iFLinkC part. The additional TVMV cleavage site between MBP and the AI domain was added to allow activated TVMV to cleave off the solubility tag as well as to prevent the selection of switches that required MBP for proper switching behavior.

4.8. Screening Light-Regulated TVMV Switches – Preliminary Results

Figure 30 shows the results of the first library screening. To avoid undesired simultaneous excitation of the fluorescent sensor and the photoreceptor domain, the mCh C-degron sensor was used. As previously established, the expression of the protease was induced during exponential growth phase. After two hours of protease pre-production at 30 °C and exposure to ambient light, the sensor production was induced and the 12 cycles of the 5 min irradiation and 30 min incubation in the dark were performed. Irradiation was performed by placing a black 96 well plate with transparent bottoms onto a custom-made blue light emitting diode (LED) panel at 30 °C (see **Figure S20** for a photograph of the device). After 5 min of irradiation, the plate was incubated in a TECAN Spark spectrophotometer and continuously shaken at 30 °C. mCh fluorescence was quantified at 0, 15 and 30 mins of incubation per cycle.

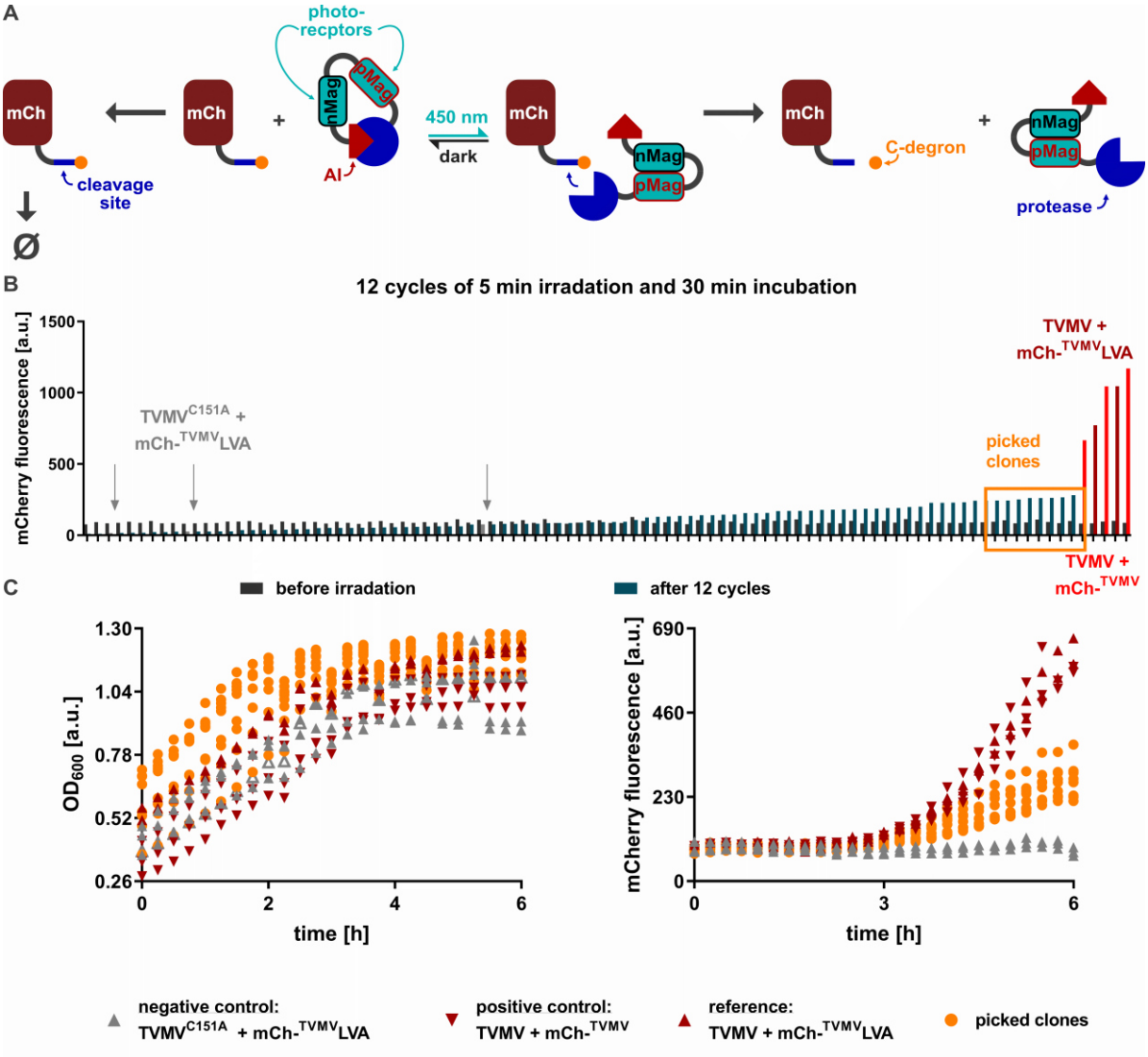

Figure 30 Engineering a blue light switchable TVMV. **A:** A blue light activated photoreceptor (nMag/pMag) is inserted between TVMV and the corresponding auto-inhibitor domain (AI); The three linkers interconnecting the photoreceptors, the AI domain and TVMV were recombined through a focused library (see **Table 5**); Upon irradiation with blue light at approx. 460 nm, the two opposite magnet domains form a heterodimer and, in this way, dislodge the AI domain from the TVMV active site; Active TVMV cleaves off the C-degron from the mCh sensor (see **Chapter 4.4**). **B:** results of the initial screening of 87 clones in 96 well plate format, dark grey bars show mCh fluorescence prior to irritation, light blue bar shown mCh fluorescence after 12 cycles of 5 min irradiation with blue light (approx. 460 nm, custom made device) and subsequent 30 min incubation in the dark (inside TECAN Spark reader) mCh fluorescence was quantified at 0, 15 and 30 min of incubation in the dark; 3 dependent biological triplicates of TVMV^{C151A} and mCh-^{TVMV}LVA served as negative controls (grey arrows), 3 dependent biological replicates of TVMV and mCh-^{TVMV} served as positive control (light red bars instead of light blue bars), and 3 dependent biological triplicates of TVMV and mCh-^{TVMV}LVA served as reference for full TVMV activity (dark red bars instead of light blue bars, 1 replicate did not display any fluorescence and is excluded), orange box shows the clones picked for a retest on the following day. **C:** results of the control measurement with no irradiation during measurements, datapoint represent individual clones, legend at the bottom refers to both graphs. Constructs used: pPRO24_MBP-^{TVMV}TVMV-Strep, pPRO24_MBP-^{TVMV}TVMV^{C151A}-Strep, pCtrl2_T7.03_U9_myc-mCh-^{TVMV}, pCtrl2_T7.03_U9_myc-mCh-^{TVMV}LVA., pDESTara2_MBP-^{TVMV}AI-L_1-nMagHigh1-L_2-pMagFast2-L_3-TVMV-Strep. Protein Sequences are stated in supplement (see **13.4.10**).

As evident in **Figure 30 C**, the picked clones showed the same activity as during the primary screen even though in the re-test the plates were not irradiated with blue light. To reduce the number of false positives, the library was transformed a second time. This time, a pre-measurement in the dark for 6 hours was performed and variants with slightly higher activity than the mock control were selected to be re-tested. **Figure 31** shows the results for this inverted screening.

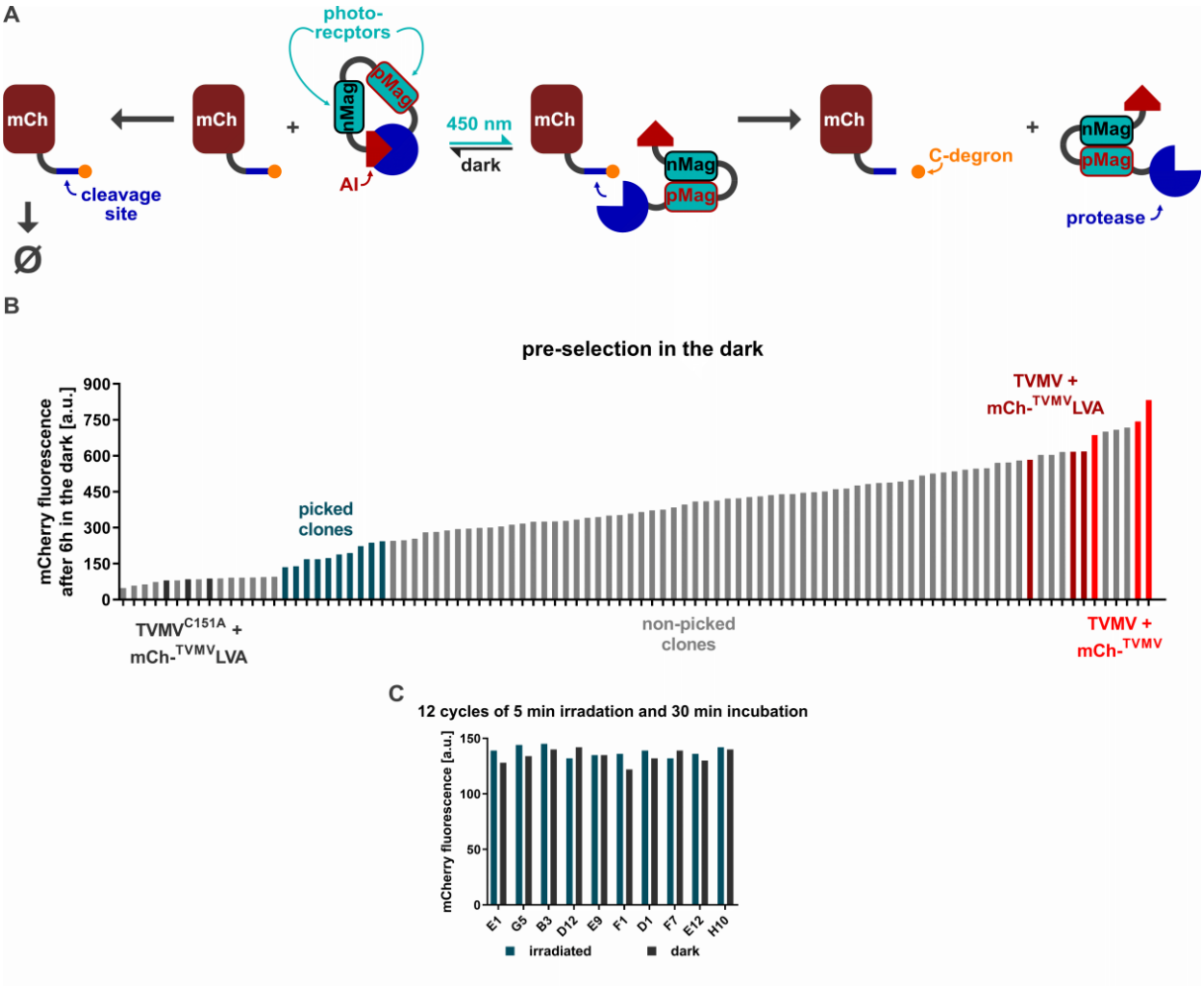

Figure 31 Second screening of the blue light switch library wit pre-incubation in the dark to filter out constitutive active variants. **A:** Schematic depiction of the experiment, same as in **Figure 30**. **B:** mCh fluorescence after six-hour incubation in the dark of 87 randomly picked clones, controls as in **Figure 30**, except exclusively final fluorescence values plotted and light blue bars show picked clones. **C:** Results of the control measurement with the 9 picked clones, blue bars 12 cycles of 5 min irradiation and 30 min incubation in the dark, dark grey bars constantly in the dark. Constructs used: pPRO24_MBP-^{TVMV}TVMV-Strep, pPRO24_MBP-^{TVMV}TVMV^{C151A}-Strep, pCtrl2_T7.03_U9_myc-mCh-^{TVMV}, pCtrl2_T7.03_U9_myc-mCh-^{TVMV}LVA., pDESTara2_MBP-^{TVMV}AI-L_1-nMagHigh1-L_2-pMagFast2-L_3-TVMV-Strep. Protein Sequences are stated in the supplement (see **13.4.10**).

Yet again, no blue-light responsive clones could be selected due to a lack of a suitable positive control to compared the picked clones to. The degron based assay seems not to be the most promising route towards an opto-switch. At the very least, the assay was able to differentiate between highly active and largely inactive variants.

5. Conclusion and Outlook

5.1. Conclusion

The primary aim of this project was to develop an *in vivo* assay for the real-time characterization of protein switches based on auto-inhibited proteases in *E. coli*. To this end, the assay was required to **(i)** exclusively comprise fully genetically encodable components that can be produced in standard *E. coli* lab strains, **(ii)** the output signal has to be quantifiable with standard lab equipment, and **(iii)** the assay should be scalable up to ultra-high throughput formats like FACS or droplet-based microfluidics. For this aim, a constitutive active protease from tobacco vein mottling virus was chosen as a model protease. The reason for this were **(i)** site-specific proteolytic activity, **(ii)** ease of soluble expression in *E. coli* and **(iii)** small monomeric protease without any cofactors. In addition, a fluorescent output signal should directly depend on the proteolytic activity within the cell.

After unsuccessful attempts to construct distance and dimerization dependent fluorescent protein sensors based on FRET and FPX, the system was simplified. The simpler design comprised of a single bright fluorescent protein (mNG) and a C-terminal degradation-tag (C-degron). In the linker between reporter and C-degron, a cleavage site for TVMV cleavage was introduced. In contrast to other working groups which published similar system since the beginning of this project, a unique negative control was established. This negative control was the most accurate mock control possible. Instead of co-expressing the sensor and some random protein or an orthogonal protease, a single point mutation was introduced to TVMV to replace the catalytic cysteine nucleophile with an alanine. This control was crucial during the adjustment of the co-expression system. Furthermore, it was used as the lower limit of the dynamic range of the sensor. Over the course of this work, the co-expression system for the protease and sensor was optimized to enhance the dynamic range of the assay. A key effort focused on improving the performance of the protease assay through active recruitment based on the rapamycin-dependent FKBP-FRB and constitutive SH3 protein-peptide interaction module. In initial tests, the relative orientation of said recruitment domains did influence the apparent proteolytic activities. Unfortunately, the best performing variants showed no significant improvement in apparent activity compared to native TVMV with no additional recruiting domains. Conversely, these results proved that the assay can resolve even minor relatively minor changes in the apparent proteolytic activities.

Furthermore, three different C-degrons were tested overall which lead to different dynamic ranges of the assay. This led to first downside of the assay. The assay is prone to the intricate network of kinetic rates revolving around the assay components. To be precise, the production

rate of both sensor and the protease, degradation rates of both protease and cleavage rate of the protease itself. Meaning extensive optimization would be necessary to adjust the assay to any given switch if exact *in vivo* kinetics should be determined. However, for the general discrimination of active and inactive states/variants, the assay could be quickly adapted by exchanging the cleavage site within the sensors. The general applicability of the assay was proven with TEV, another potyvirus protease, as well as HCV, a flavivirus protease with clinical relevance. In addition to the protease, the fluorescent protein reporter was also exchanged. Precisely, mNeonGreen was exchanged with mCherry. This led to reduced fluorescence intensities due to mCherry's inferior optical properties [85, 95] but in turn led to much higher fold changes between active and inactive TVMV variants. These findings prove that the assay should be functional irrespective of the fluorescent protein utilized.

The second design iteration of the assay aimed to increase the quality of the normalization condition of the generated fluorescent signals from optical density of the culture to another fluorescent signal. Therefore, a sensor with two fluorescent proteins within the same polypeptide chain was designed. To this end, a cryptic N-degron was inserted into the linker separating the two fluorescent proteins. The cryptic degron comprised of a TVMV cleavage site and a strong, semi-synthetic N-degron that overlapped with the P1' position of the TVMV cleavage site. Accordingly, proteolytic activity did not just separate the two fluorescent proteins, but also the rapid degradation of the C-terminal fluorescent protein while the N-terminal fluorescent protein accumulated in the cell. This sensor design was functional without any changes to the previously established co-expression system. While the relative orientation of the functional domains influenced the apparent activities, constitutive recruitment by means of SH3 domains did not significantly improve the assays dynamics.

Finally, the first protein switch based on auto-inhibited TVMV was to be characterized. Unfortunately, the previously established input signals [1, 3, 45] – i.e. rapamycin – did not turn out to be bio available in *E. coli* hence a new input signal had to be found. Light was selected as the first input signal candidate. Based on a semi-synthetic blue light receptor system called Magnets. A prototype library for a blue light switchable TVMV was cloned and screened in *E. coli*. The assay proved able to resolve different proteolytic activities within the library that ranged from mock-like to native TVMV activities. However, no blue light dependent activity could be identified within a total of 194 clones screened. In any case, the results demonstrate that the assay can be used to screen that library if better equipment would be available in the future. This could facilitate continuous incubation and irradiation alongside online measurement combined in one device or automated platform.

5.2. Outlook

Currently, three different follow-up projects for this PhD project are either in planning or in early lab stage. The first is a Bachelors Thesis conducted currently adapting the assay to the main protease form SARS-CoV-2 corona virus, the second is an opto-switch based on Phytochrome B and the third is the establishment of a two-protease signal transducer which in itself is not a protein switch but would at least proved that the assay can be employed to characterized simple logic gates in live *E. coli* cells.

5.2.1. Preliminary results with SARS-CoV-2 ^{M}Pro (Bachelor Thesis L. Chalwatzis)

The synthetic DNA coding for the SARS-CoV-2 main protease (SARS-CoV2 ^{M}Pro) and its corresponding cleavage site were ordered and deposited in the iFLinkC storage vector for functional domains (pFD). At the time this thesis was written, the assembly process of the protease expression constructs as well as its inactive variant SARS-CoV2 MPro^{C145A} [47] and the corresponding sensor constructs were nearly finished.

5.2.2. Alternative photo-receptor

In addition, a second opto-switchable TVMV protease exists in early concept stage. This one is based on a second photo-receptor established in *E. coli* among others by the Weber group at the Albert Ludwigs Universität Freiburg. It is based on Phytochrome B (PhyB) which binds to phytochrome interacting factor 6 (PIF6) [100, 101]. The advantages of PhyB would be that it can be actively switch between heterodimer and monomers by alternating between red light and near infrared light, respectively [100, 101]. This is in strict contrast to the magnets-based design which relies on spontaneous dissociation in the dark [96-98]. In addition, the PhyB dimerization can be suppressed by illumination with green light to avoid undesired reactions due to ambient light. The two drawbacks which lead to the current postponement of the design are the following. First of all, discussions with the Weber group indicated that PhyB cannot simply be cloned into the linker region of the basic auto-inhibited TVMV design because its prone to misfolding unless it is in the most N-terminal position. The second more challenging aspect concerns its cofactor dependency. While the magnets require FAD which is a natural metabolite of *E. coli*, Phytochrome B requires phycocyanobilin (PCB) for which's biosynthesis pathway *E. coli* lacks the two final enzymes [96, 97, 100]. Accordingly, a co-expression of two additional enzymes would be necessary for the switch's functionality. Therefore, this opto-switch should be constructed after a PCB producing operon is integrated into the genome of an *E. coli* strain without negatively impacting its endogenous heme metabolism.

5.2.3. Preliminary results for a two-protease signal transducer (Master thesis C. Rühmkorff)

During a practical course conducted throughout this project, several BL21(DE3) strains with chromosomal integrated TVMV variants had been generated. All integrations were performed as single copy integration using the HK022 phage integrase following the Clonetegration protocol [102] modified by M. Röder (see **Chapter 13.3.1**). Previously, TVMV activity within these strains could not be detected with the C-degron based *in vivo* assay (data not shown). By using plasmid-based expression of AI-TVMVHCV, as TVMV signal transducer and amplifier, TVMV activity within these strains might have been detectable. **Figure 32** shows the results for the first test of the signal amplifier using the BL21(DE3)[HK022 attB::T7.03_MBP-TVMVTVMV-His6] as the first test strain.

As visible in **Figure 32** both AI-^{TVMV}HCV and AI-^{TVMV}HCV^{S152A} behaved like HCV^{S152A} meaning no HCV activity and in turn no TVMV activity was detected. One reason could be insufficient production of TVMV due a shared promoter with sensor construct. In future experiments, this could be circumvented by using three different promoters for all three components.

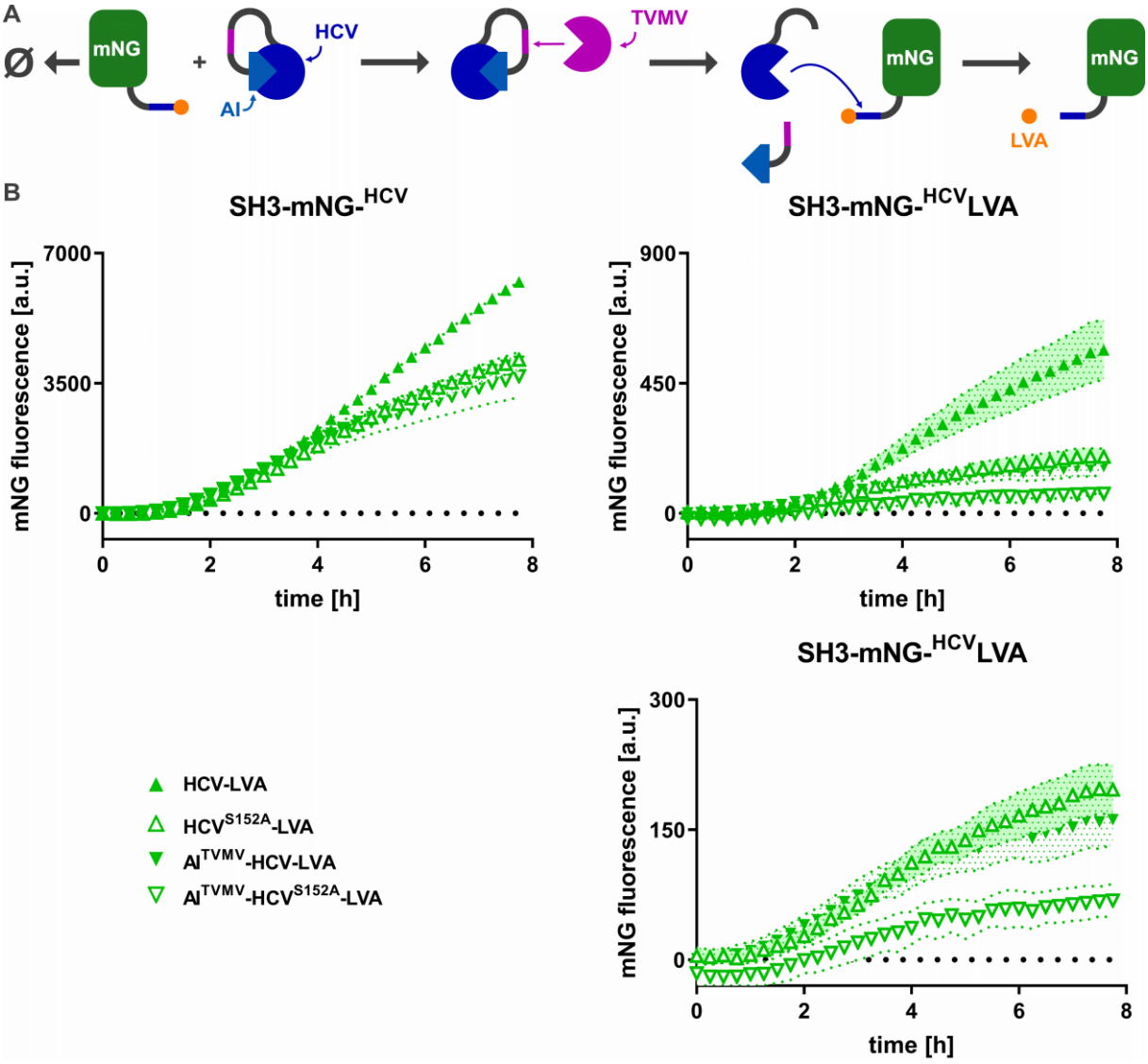

Figure 32 Preliminary results for the two-protease signal transducer. **A:** Schematic depiction of the design principle of the signal transducer: In the default state, the C-degron tagged HCV sensor is co-expressed with auto-inhibited HCV; Accordingly, no fluorescent signal is generated; In presence of TVMV, the AI domain is cleaved off and active HCV can now remove the C-degron which leads to increase in the mNG-dependent fluorescent signal. **B:** The three graphs show the protease dependent mNG fluorescence over the course of 8 hours. HCV constructs were pre-produced from pPRO24 for 2 hours (25 mM sodium propionate) before the sensor and a chromosomal-integrated variant of TVMV was induced with 500 µM IPTG (both T7.03 promoter, sensor additional U9 RNA thermometer); data points represent the mean values for the dependent biological quadruplicates measured, error areas depict the SEM, sensor constructs stated above the corresponding graph, bottom left legend refers to all graphs. Left: positive controls without any degron attached. Right: actual data with LVA C-degron present, the lower right graph shows the same data as the upper right one except the active HCV reference was removed to better visualize the differences between HCV^{S152A} and $AI\text{-}^{TVMV}HCV$ / $AI\text{-}^{TVMV}HCV^{S152A}$. Constructs used: pPRO24_MBP-^{HCV}HCV-Strep, pPRO24_MBP-$^{HCV}HCV^{S152A}$-Strep, pPRO24_MBP-^{HCV}AI(HCV)-^{TVMV}HCV-Strep, pPRO24_MBP-^{HCV}AI(HCV)-$^{TVMV}HCV^{S152A}$-Strep, pCtrl2_T7.03_U9_myc-SH3-mNG-^{HCV}, pCtrl2_T7.03_U9_myc-SH3-mNG-^{HCV}LVA. Protein Sequences are stated in the supplement (see **13.4.11**).

5.3. Closing remarks

A suitable and robust *in vivo* assay for the characterization of protease-based switches in live *E. coli* was finally established. Due to a lack of bioavailable input signals, a fully operational switch could not be identified or characterized.

6. Materials and Methods

6.1. Materials

6.1.1. Strains

Table 7 Strains used in this work

Strain	Geneotype	Usage	Originator
E. coli DH10β	*Δ*(ara-leu) 7697 araD139 fhuA *Δ*lacX74 galK16 galE15 e14- *ϕ*80*d*lacZ*Δ*M15 recA1 relA1 endA1 nupG rpsL *(StrR)* rph spoT1 *Δ*(mrr-hsdRMS-mcrBC)	Cloning and plasmid propagation	NEB
E. coli BL21(DE3)	*fhuA2 [lon] ompT gal (λ DE3) [dcm] ΔhsdS λ DE3 = λ sBamHIo ΔEcoRI-B int::(lacI::PlacUV5::T7 gene1) i21 Δnin5*	expression of recombinant proteins; *in vivo* assays	NEB
E. coli Shuffle T7	*F´ lac, pro, lacIq / Δ(ara-leu)7697 araD139 fhuA2 lacZ::T7 gene1 Δ(phoA)PvuII phoR ahpC* galE (or U) galK λatt::pNEB3-r1-cDsbC (SpecR, lacIq) ΔtrxB rpsL150(StrR) Δgor Δ(malF)3*	*lon*⁺ *E. coli* K strain for *in vivo* assays	NEB
KRx	[F´, traD36, ΔompP, proA+B+, lacIq, Δ(lacZ)M15] ΔompT, endA1, recA1, gyrA96 (Nalr), thi-1, hsdR17 (rk–, mk+), e14– (McrA–), relA1, supE44, Δ(lac-proAB), Δ(rhaBAD)::T7 RNA polymerase	*lon*⁺ *E. coli* K strain for *in vivo* assays	Promega
EcJR1	BL21(DE3)::HK022[$PT7_9$_MBP-tvmv-TVMV-FKBP-His6]	Stable, IPTG inducible, low level expression of a Rapamycin recruitable TVMV	I. Marquardt
EcJR2	BL21(DE3)::HK022[$PT7_n$_MBP-tvmv-TVMV-His6]	Stable, IPTG inducible, expression of TVMV	I. Marquardt
EcJR3	BL21(DE3)::HK022[$PT7_n$_MBP-tvmv-TVMV-FKBP-His6]	Stable, IPTG inducible, expression of a recruitable TVMV	I. Marquardt
EcJR4	BL21(DE3)::HK022[$PT7_9$_MBP-tvmv-TVMV-His6]	Stable, IPTG inducible, low level expression of TVMV	I. Marquardt
EcJR5	BL21(DE3)::HK022[$PT7_n$_MBP-tev-AI-FKBP-FRB-TVMV-His6]	Stable, IPTG inducible, expression of a rapamycin switchable TVMV	J. Ranglack
EcJR6	BL21(DE3)::HK022[$PT7_3$_MBP-tvmv-TVMV-His6]	Stable, IPTG inducible, medium level expression of a Rapamycin recruitable TVMV	J. Ranglack
EcJR7	BL21(DE3)::HK022[$PT7_3$_MBP-tev-AI-FKBP-FRB-TVMV-His6]	Stable, IPTG inducible, medium level expression of a rapamycin switchable TVMV	J. Ranglack
EcJR8	BL21(DE3)::HK022[$PT7_{11}$_MBP-TVMV-TVMV-FKBP-His6]	Stable, IPTG inducible, low level expression of a Rapamycin recruitable TVMV	J. Ranglack
EcJR9	BL21(DE3)::HK022[$PT7_n$_MBP-tvmv-TVMV-His6]	Same as EcJR2	J. Ranglack
EcJR10	BL21(DE3)::HK022[$PT7_{11}$_MBP-TEV-AI-FKBP-FRB-TVMV-His6]	Stable, IPTG inducible, low level expression of a rapamycin switchable TVMV	J. Ranglack
EcJR11	BL21(DE3)::HK022[$PT7_9$_MBP-tev-AI-FKBP-FRB-TVMV-His6]	Stable, IPTG inducible, low level expression of	J. Ranglack

		a rapamycin switchable TVMV	
EcJR12	BL21(DE3)::HK022[PT7$_9$_MBP-tvmv-TVMV-His6]	Same as EcJR4	J. Ranglack
EcJR13	BL21(DE3)::HK022[Pprp_RBS_MBP-L(G3S)3ET-tvmvs-NS3N10-sSH3L-(GGS)8-TVMV(C151A)-(GGS)2-Strep]	Stable, propionate inducible expression of a recruitable TVMV mock	J. Ranglack
EcJR14	BL21(DE3)::HK022[Pprp_RBS_MBP-L(G3S)3ET-tvmvs-NS3N10-wSH3L-(GGS)8-TVMV(elong.)-(GGS)2-Strep]	Stable, propionate inducible expression of a recruitable TVMV	J. Ranglack
EcJR15	BL21(DE3)::HK022[Pprp_RBS_MBP-L(G3S)3ET-tvmvs-NS3N10-TVMV(C151A)-(GGS)8-sSH3L-(GGS)2-Strep]	Stable, propionate inducible expression of a recruitable TVMV mock	J. Ranglack
EcJR16	BL21(DE3)::HK022[Pprp_RBS_MBP-L(G3S)3ET-tvmvs-NS3N10-TVMV(C151A)-(GGS)8-wSH3L-(GGS)2-Strep]	Stable, propionate inducible expression of a recruitable TVMV mock	J. Ranglack
EcJR17	BL21(DE3)::HK022[Pprp_RBS_MBP-L(G3S)3ET-tvmvs-NS3N10-TVMV(elong.)-(GGS)8-sSH3L-(GGS)2-Strep]	Stable, propionate inducible expression of a recruitable TVMV	J. Ranglack
EcJR18	BL21(DE3)::HK022[Pprp_RBS_MBP-L(G3S)3ET-tvmvs-NS3N10-TVMV(elong.)-(GGS)8-wSH3L-(GGS)2-Strep]	Stable, propionate inducible expression of a recruitable TVMV	J. Ranglack
EcJR19	BL21(DE3)::HK022[Pprp_RBS_MBP-L(G3S)3ET-tvmvs-NS3N10-TVMV(elong.)-(GGS)8-wSH3L-(GGS)2-Strep]	Stable, propionate inducible expression of a recruitable TVMV mock	J. Ranglack
EcJR20	BL21(DE3)::HK022[Pprp_RBS_MBP-L(G3S)ET-tvmvs-NS3N10-sSH3L-(GGS)8-TVMV(elong.)-(GGS)2-Strep]	Stable, propionate inducible expression of a recruitable TVMV	J. Ranglack
EcJR21	BL21(DE3)::HK022[Pprp_RBS_MBP-L(G3S)3ET-tvmv-NS3N10-TVMV(elong.)-(G2S)2-Strep]	Stable, propionate inducible expression of a recruitable TVMV	J. Ranglack
EcJR22	BL21(DE3)::HK022[Pprp_RBS_MBP-L(G3S)3ET-tvmv-NS3N10-TVMV(C151A)-(G2S)2-Strep]	Stable, propionate inducible expression of a recruitable TVMV mock	J. Ranglack

6.1.2. Vectors

Table 8 Vectors used in this work.

Name	Promotor - repressor (inducer)	Ori (Class)	Selection marker	Usage	Originator
pPRO24	*prp* - PrpR (propionate)	ColE1 + F1 (A)	AmpR	Expression of protease constructs	Addgene 17805, [87]
pACYCT2	*pT7* in tandem with tac – both LacI (IPTG)	p15A (B)	CamR	Basis for creation of pCrtl2	Addgene 45799, [88]
p-ET24(+)	*pT7* – LacI (IPTG)	f1 ori (A)	KanR	Intimal expression vector for protease construcs	Novagen
pASK-iba3	*ptet*-TetR (AHT)	pBR332 (A)	AmpR	Initial expression vector for sensor constructs	iba
pCtrl2	*T7* – LacI (IPTG)	p15A (B)	CamR	Overexpression of sensor constructs	W. Weber
pCtrl2_T7.03_U9	*T7.03* – LacI (IPTG); U9 RNA thermometer	p15A (B)	CamR	Low level expression of sensor constructs	J. Ranglack, T7.03: [84]; U9: [93]
pFD	none	ColE1 (A)	KanR	Deposition of functional domains as parts for iFLinkC	Addgene 137108
pL2	none	ColE1 (A)	KanR	Deposition of linkers as parts for iFLinkC	Addgene 137090
pDESTara2	*Araba* – AraC (arabinose)	ColE1 (A)	AmpR	Expression of iFLinC libraries	A. Gräwe
pDESTprp	*prp* – PrpR (propionate)	ColE1 (A)	AmpR	Expression of protease constructs cloned with iFLinkC	J. Ranglack
pOSIP-CH	has to cloned alongside the insert	R6KY (C)	CamR	Integration of expression cassette into genome of *E. coli* using HK022 integrase (is coded on the vector as well)	Addgene #45980 [102]
pE-FLP	pE (constitutive)	pSC101 (C)	AmpR (50 µg/mL Amp !)	Excission of the integration module of pOSIP vectors following successfully integration	Addgene #45978 [102]

Vector map of pPRO24

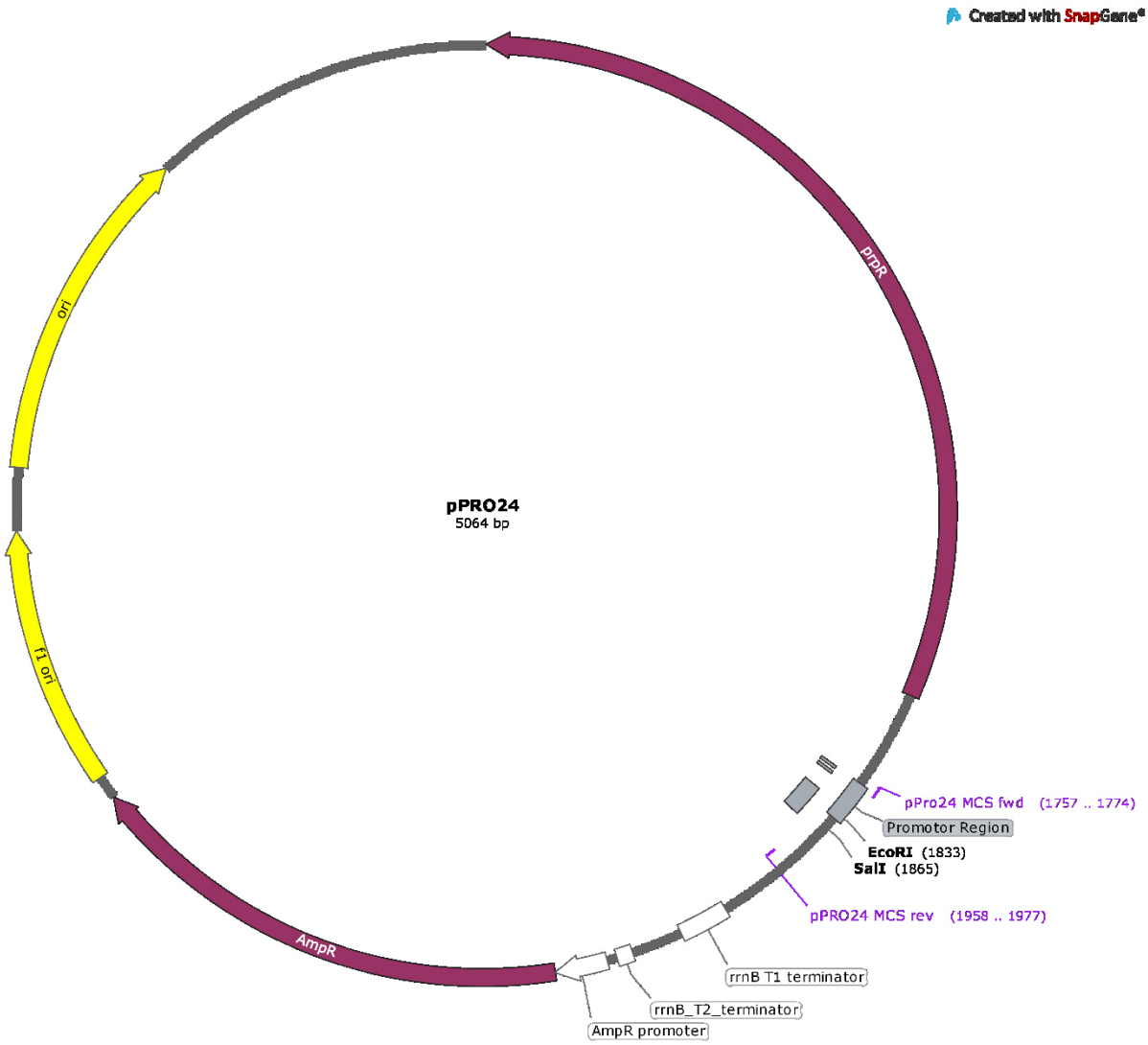

Figure 33 Vector map of pPRO24 (Addgene 17805, [87]). The vector comprises of two class A origins of replication, an ampicillin resistance cassette and a propionate inducible expression cassette. The expression cassette includes the promoter region of the propionate operon (*prpBCDE*) of *E. coli* and the repressor gene of the propionate operon *prpR*. Figure generated with SnapGene (GSL Biotech LLC).

Complete nucleotide sequence of pPRO24

EcoRI and **SalI** sites used for cloning into pPRO24 highlighted in **bold**.

ATCGATTCAGCTTTTCAGCCGCCGCCAGAACGTCGTCCGGCTGATGCCTAAATAATTCGCCGCTGCTGTTTTATCGCCATTAAATTTCTCCAGTGCCTGTTGTGGTG
TCAGTAAGCGTGGAGCGGGAGTTTTCGCCGACTCGCGCGCCAGTTCCGGCAGTAGCAGCTGCAAAAATTGCGGCGTTAAATCCGGCGTCGGTTCCACACTTAAAAAT
AGCGCCAGTCGCTCCATCATATTGCGCAGTTCACGAATATTGCCCGGCCAGTCGTAGTGCACCAGCACGGTTTCGCTTGCCTGTAATCCCTGGCGTAATGCGGCAGA
AAACGGGGTGGAGAGCGCCGCCAGAGACACTTTCAAAAAGCTTTCCGCCAGTGGCAGAATATCCGCCACCCGCTCGCGCAGTGGTGGCAATTGCAGACGCAAAATAC
TCAGCCGATAAAACAGGTCACGGCGAAACTGCCCTTGCCGCATATCTTCTTCCAGATTGCAGTGAGTGGCGCTAATGACCCGCACATCCACCGGAACAGGCTGATGC
CCGCCGACGCGGGTGACCTCTTTTTCTTCCAGCACCCGCAGCAGCCGGGTCTGCAACGGCAGCGGCATTTCGCCAATCTCATCGAGAAACAGCGTACCTCCGTGGGC
GATTTCAAACAGCCCGGCGCGACCGCCGCGTCGCGAGCCGGTAAACGCCCCTTCCTCATAGCCAAACAGTTCTGCTTCCAGCAGCGATTCGGCAATCGCCCCGCAGT
TGACTGCAACAAACGGATGCGACTTTTTGCCCTGTCGCGCATCGTGGCGGGCAAAATATTCCCGATGAATCGCCTGGGCCGCCAGCTCTTTGCCCGTCCCCGTTTCC
CCCTCAATCAACACCGCTGCACTGGAGCGGGCATACAGCAAAATAGTCTGCCGTACTTGTTCCATCTGTGGTGATTGACCGAGCATATCGCCCAGCACGTAACGAGT
TCTCAGGGCGTTGCGGGTGGCATCGTGAGTGTTATGGCGTAACGACATGCGCGTCATATCCAGCGCATCGCTGAACGCCTGGCGCACGGTGGCGGCGGAATAGATAA
AAATTCCGGTCATTCCGGCTTCTTCTGCCAGATCGGTAATCAGCCCCGCGCCGACCACCGCTTCGGTGCCGTTAGCTTTTAGCTCGTTAATCTGCCCGCGTGCGTCT
TCTTCGGTAATGTAGCTACGTTGATCGAGGCGCAAATTAAAGGTTTTTTGAAACGCCACCAGTGCCGGAATAGTTTCCTGATAAGTGACAACGCCGATAGAAGAGGT
GAGTTTTCCGGCTTTTGCCAGTGCCTGTAACACATCGTAGCCGCTCGGTTTAATCAAAATAACTGGCACTGACAGGCGGCTTTTCAGGTACGCGCCGTTAGATCCAG
CGGCGATGATGGCGTCACAGCGTTCGTTTGCCAGTTTCTTGTGGATGTAGGTCACCGCTTTTTCAAAGCCAAGCTGGATAGGGGTAATGTTCGCCAGGTGATCAAAC
TCGAGGCTGATATCGCGAAACAGCTCGAACAGGCGCGTTACAGATACCGTCCAGATAACCGGTTTGTCGTCATTAAGCCGTGGTGGATGTGCCATAGCGCACCGCAA
AGTTAAGAAACCGAATATTGGGTTTAGTCTTGTTTCATAATTGTTGCAATGAAACGCGGTGAAACATTGCCTGAAACGTTAACTGAAACGCATATTTGCGGATTAGT
TCATGACTTTATCTCTAACAAATTGAAATTAAACATTTAATTTTATTAAGGCAATTGTGGCACACCCCTTGCTTTGTCTTTATCAACGCAAATAACAAGTTGATAAC
AAGCTAGCAGGAG**GAATTC**ACCATGGTACCCGGGGATCCTCTAGA**GTCGAC**CTGCAGGCATGCAAGCTTGGCTGTTTTGGCGGATGAGAGAAGATTTTCAGCCTGAT
ACAGATTAAATCAGAACGCAGAAGCGGTCTGATAAAACAGAATTTGCCTGGCGGCAGTAGCGCGGTGGTCCCACCTGACCCCATGCCGAACTCAGAAGTGAAACGCC
GTAGCGCCGATGGTAGTGTGGGGTCTCCCCATGCGAGAGTAGGGAACTGCCAGGCATCAAATAAAACGAAAGGCTCAGTCGAAAGACTGGGCCTTTCGTTTTATCTG
TTGTTTGTCGGTGAACGCTCTCCTGAGTAGGACAAATCCGCCGGGAGCGGATTTGAACGTTGCGAAGCAACGGCCCGGAGGGTGGCGGGCAGGACGCCCGCCATAAA
CTGCCAGGCATCAAATTAAGCAGAAGGCCATCCTGACGGATGGCCTTTTTGCGTTTCTACAAACTCTTTTGTTTATTTTTCTAAATACATTCAAATATGTATCCGCT
CATGAGACAATAACCCTGATAAATGCTTCAATAATATTGAAAAAGGAAGAGTATGAGTATTCAACATTTCCGTGTCGCCCTTATTCCCTTTTTTGCGGCATTTTGCC
TTCCTGTTTTTGCTCACCCAGAAACGCTGGTGAAAGTAAAAGATGCTGAAGATCAGTTGGGTGCACGAGTGGGTTACATCGAACTGGATCTCAACAGCGGTAAGATC
CTTGAGAGTTTTCGCCCCGAAGAACGTTTTCCAATGATGAGCACTTTTAAAGTTCTGCTATGTGGCGCGGTATTATCCCGTGTTGACGCCGGGCAAGAGCAACTCGG
TCGCCGCATACACTATTCTCAGAATGACTTGGTTGAGTACTCACCAGTCACAGAAAAGCATCTTACGGATGGCATGACAGTAAGAGAATTATGCAGTGCTGCCATAA
CCATGAGTGATAACACTGCGGCCAACTTACTTCTGACAACGATCGGAGGACCGAAGGAGCTAACCGCTTTTTTGCACAACATGGGGGATCATGTAACTCGCCTTGAT
CGTTGGGAACCGGAGCTGAATGAAGCCATACCAAACGACGAGCGTGACACCACGATGCCTGTAGCAATGGCAACAACGTTGCGCAAACTATTAACTGGCGAACTACT
TACTCTAGCTTCCCGGCAACAATTAATAGACTGGATGGAGGCGGATAAAGTTGCAGGACCACTTCTGCGCTCGGCCCTTCCGGCTGGCTGGTTTATTGCTGATAAAT
CTGGAGCCGGTGAGCGTGGGTCTCGCGGTATCATTGCAGCACTGGGGCCAGATGGTAAGCCCTCCCGTATCGTAGTTATCTACACGACGGGGAGTCAGGCAACTATG
GATGAACGAAATAGACAGATCGCTGAGATAGGTGCCTCACTGATTAAGCATTGGTAACTGTCAGACCAAGTTTACTCATATATACTTTAGATTGATTTACGCGCCCT
GTAGCGGCGCATTAAGCGCGGCGGGTGTGGTGGTTACGCGCAGCGTGACCGCTACACTTGCCAGCGCCCTAGCGCCCGCTCCTTTCGCTTTCTTCCCTTCCTTTCTC
GCCACGTTCGCCGGCTTTCCCCGTCAAGCTCTAAATCGGGGGCTCCCTTTAGGGTTCCGATTTAGTGCTTTACGGCACCTCGACCCCAAAAAACTTGATTTGGGTGA
TGGTTCACGTAGTGGGCCATCGCCCTGATAGACGGTTTTTCGCCCTTTGACGTTGGAGTCCACGTTCTTTAATAGTGGACTCTTGTTCCAAACTTGAACAACACTCA
ACCCTATCTCGGGCTATTCTTTTGATTTATAAGGGATTTTGCCGATTTCGGCCTATTGGTTAAAAAATGAGCTGATTTAACAAAAATTTAACGCGAATTTTAACAAA
ATATTAACGTTTACAATTTAAAAGGATCTAGGTGAAGATCCTTTTTGATAATCTCATGACCAAAATCCCTTAACGTGAGTTTTCGTTCCACTGAGCGTCAGACCCCG
TAGAAAAGATCAAAGGATCTTCTTGAGATCCTTTTTTTCTGCGCGTAATCTGCTGCTTGCAAACAAAAAAACCACCGCTACCAGCGGTGGTTTGTTTGCCGGATCAA
GAGCTACCAACTCTTTTTCCGAAGGTAACTGGCTTCAGCAGAGCGCAGATACCAAATACTGTCCTTCTAGTGTAGCCGTAGTTAGGCCACCACTTCAAGAACTCTGT
AGCACCGCCTACATACCTCGCTCTGCTAATCCTGTTACCAGTGGCTGCTGCCAGTGGCGATAAGTCGTGTCTTACCGGGTTGGACTCAAGACGATAGTTACCGGATA
AGGCGCAGCGGTCGGGCTGAACGGGGGGTTCGTGCACACAGCCCAGCTTGGAGCGAACGACCTACACCGAACTGAGATACCTACAGCGTGAGCTATGAGAAAGCGCC
ACGCTTCCCGAAGGGAGAAAGGCGGACAGGTATCCGGTAAGCGGCAGGGTCGGAACAGGAGAGCGCACGAGGGAGCTTCCAGGGGGAAACGCCTGGTATCTTTATAG
TCCTGTCGGGTTTCGCCACCTCTGACTTGAGCGTCGATTTTTGTGATGCTCGTCAGGGGGGCGGAGCCTATGGAAAAACGCCAGCAACGCGGCCTTTTTACGGTTCC
TGGCCTTTTGCTGGCCTTTTGCTCACATGTTCTTTCCTGCGTTATCCCCTGATTCTGTGGATAACCGTATTACCGCCTTTGAGTGAGCTGATACCGCTCGCCGCAGC
CGAACGACCGAGCGCAGCGAGTCAGTGAGCGAGGAAGCGGAAGAGCGCCTGATGCGGTATTTTCTCCTTACGCATCTGTGCGGTATTTCACACCGCATAGGGTCATG
GCTGCGCCCCGACACCCGCCAACACCCGCTGACGCGCCCTGACGGGCTTGTCTGCTCCCGGCATCCGCTTACAGACAAGCTGTGACCGTCTCCGGGAGCTGCATGTG
TCAGAGGTTTTCACCGTCATCACCGAAACGCGCGAGGCAGCAAGGAGATGGCGCCCAACAGTCCCCCGGCCACGGGGCCTGCCACCATACCCACGCCGAAACAAGCG
CTCATGAGCCCGAAGTGGCGAGCCCGATCTTCCCCATCGGTGATGTCGGCGATATAGGCGCCAGCAACCGCACCTGTGGCGCCGGTGATGCCGGCCACGATGCGTCC
GGCGTAGAGGATCTGCTCATGTTTGACAGCTTATC

Vector map of pCtrl2

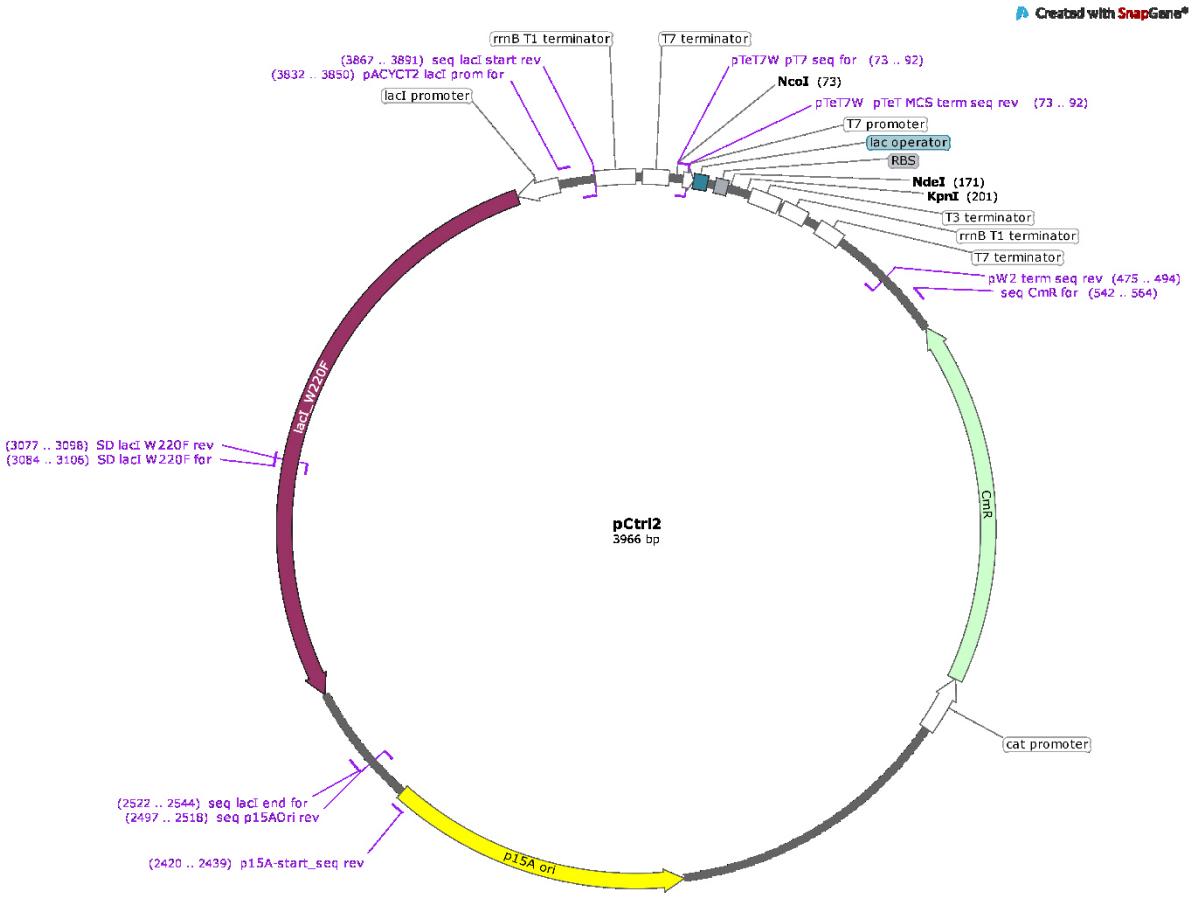

Figure 34 Vector map of pCtrl2 (W. Weber unpublished results). The vector comprises of the class B origin of replication p15A, a chloramphenicol resistance cassette and a lactose/IPTG inducible expression cassette. The expression cassette includes the promoter of the T7 phage and the operator of the *E. coli* lac operon (l*acZYA*) and the repressor gene of the lac operon *lacI* (*lacI* includes W220F mutation for reduced leaky expression). Figure generated with SnapGene (GSL Biotech LLC).

Vector map pDESTara2

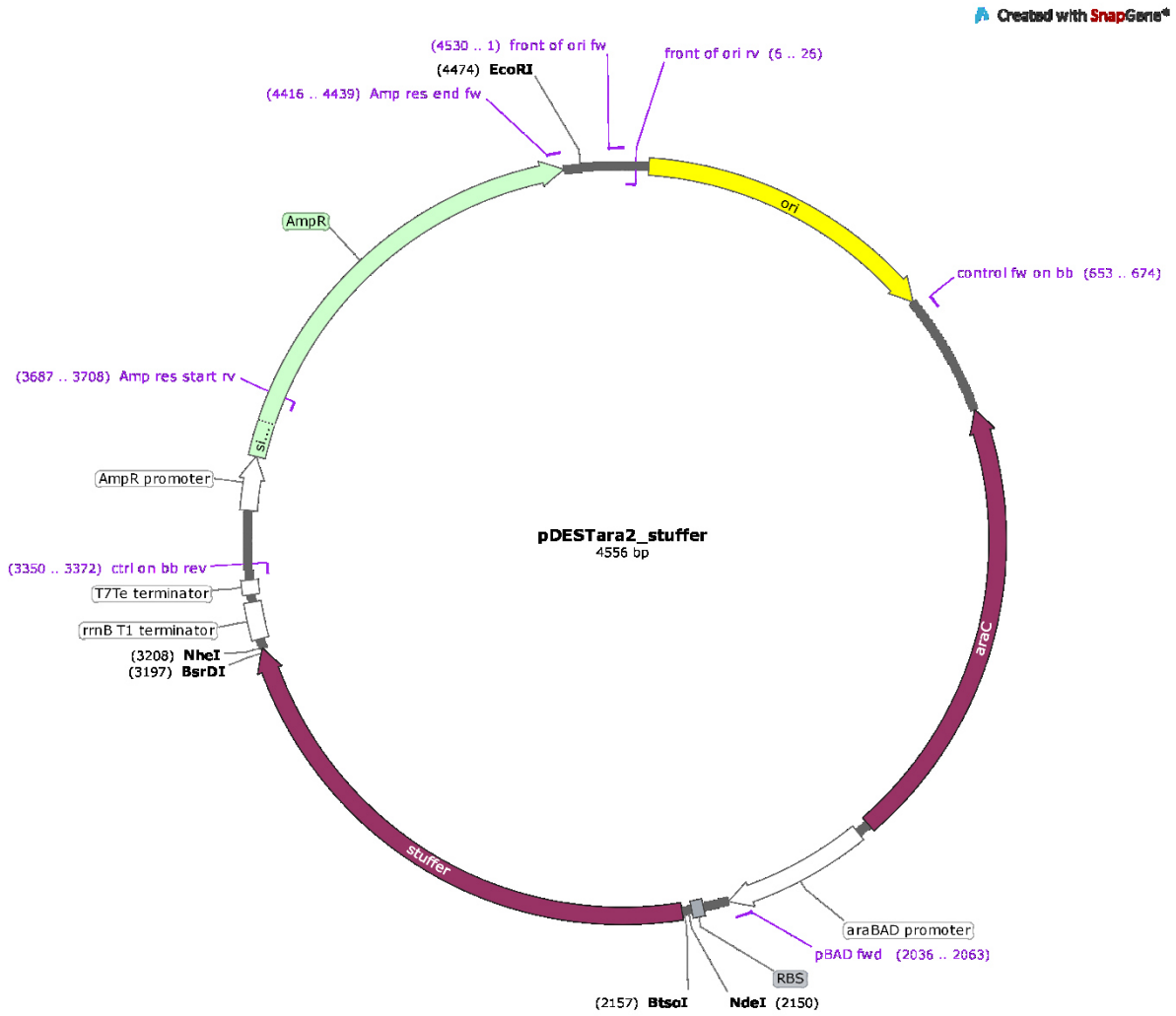

Figure 35 Vector map of pDESTara2 (A. Gräwe, unpublished results). The vector comprises of a class A origin of replication, an ampicillin resistance cassette and an arabinose inducible expression cassette. The expression cassette includes the promoter of the arabinose operon of *E. coli* (*araBAD*) and the repressor gene of the arabinose operon *araC*. The MCS includes a stuffer sequence for better differentiation of NheI...BtsI restriction fragment from unrestricted vector during electrophoresis. Figure generated with SnapGene (GSL Biotech LLC).

Complete nucleotide sequence of pDESTara2

BtsI and **NheI** sites used for cloning of optical regulated TVMV switch candidate library into pDESTara2 highlighted in **bold**.

GTTTTCGTTCCACTGAGCGTCAGACCCCGTAGAAAAGATCAAAGGATCTTCTTGAGATCCTTTTTTTCTGCGCGTAATCTGCTGCTTGCAAACAAAAAAACCACCGC
TACCAGCGGTGGTTTGTTTGCCGGATCAAGAGCTACCAACTCTTTTTCCGAAGGTAACTGGCTTCAGCAGAGCGCAGATACCAAATACTGTTCTTCTAGTGTAGCCG
TAGTTAGGCCACCACTTCAAGAACTCTGTAGCACCGCCTACATACCTCGCTCTGCTAATCCTGTTACCAGTGGCTGCTGCCAGTGGCGATAAGTCGTGTCTTACCGG
GTTGGACTCAAGACGATAGTTACCGGATAAGGCGCAGCGGTCGGGCTGAACGGGGGGTTCGTGCACACAGCCCAGCTTGGAGCGAACGACCTACACCGAACTGAGAT
ACCTACAGCGTGAGCTATGAGAAAGCGCCACGCTTCCCGAAGGGAGAAAGGCGGACAGGTATCCGGTAAGCGGCAGGGTCGGAACAGGAGAGCGCACGAGGGAGCTT
CCAGGGGGAAACGCCTGGTATCTTTATAGTCCTGTCGGGTTTCGCCACCTCTGACTTGAGCGTCGATTTTTGTGATGCTCGTCAGGGGGGCGGAGCCTATGGAAAAA
CGCCAGCAACGCGGCCTTTTTACGGTTCCTGGCCTTTTGCTGGCCTTTTGCTCACATGTTCTTTCCTGCGTTATCCCCTGATTCTGTGGATAACCGTATTACCGCCA
ATTCCGTAGAGGATCTGCTCATGTTTGACAGCTTATCATCGATGCATAATGTGCCTGTCAAATGGACGAAGCAGGGATTCTGCAAACCCTATGCTACTCCGTCAAGC
CGTAAATTGTCTGATTCGTTACCAATTATGACAACTTGACGGCTACATCATTCACTTTTTCTTCACAACCGGCACGGAACTCGCTCGGGCTGGCCCCGGTGCATTTT
TTAAATACCCGCGAGAAATAGAGTTGATCGTCAAAACCAACGTTGCGACCGACGGTGGCGATAGGCATCCGGGTGGTGCTCAAAAGCAGCTTCGCCTGGCTGATACG
TTGGTCCTCGCGCCAGCTTAAGACGCTAATCCCTAACTGCTGGCGGAAAAGATGTGACAGACGCGACGGCGACAAGCAAACATGCTGTGCGACGCTGGCGATGTCAA
AATTGCTGTCTGCCAGGTGATCGCTGATGTACTGACAAGCCTCGCGTACCCGATTATCCATCGGTGGATGGAGCGACTCGTTAATCGCTTCCATGCGCCGCAGTAAC
AACTGCTCAAGCAGATTTATCGCCAGCAGCTCCGAATAGCGCCCTTCCCCTTGCCCGGCGTTAATGATTTGCCCAAACAGGTCGCTGAAATGCGGCTGGTGCGCTTC
ATCCGGGCGAAAGAACCCCGTATTGGCAAATATTGACGGCCAGTTAAGCCATTCATGCCAGTAGGCGCGCGGGCGAAAGTAAACCCACTGGTGATACCATTCGCGAG
CCTCCGGATGACGACCGTAGTGATGAATCTCTCCTGGCGGGAACAGCAAAATATCACCCGGTCGGCAAACAAATTCTCGTCCCTGATTTTTCACCACCCCCTGACCG
CGAATGGTGAGATTGAGAATATAACCTTTCATTCCCAGCGGTCGGTCGATAAAAAAAATCGAGATAACCGTTGGCCTCAATCGGCGTTAAACCCGCCACCAGATGGGC
ATTAAACGAGTATCCCGGCAGCAGGGGATCATTTTGCGCCTCAGCCATACTTTTCATACTCCCGCCATTCAGAGAAGAAACCAATTGTCCATATTGCATCAGACATT
GTCGTCACTGAGTCTTTTACTGGCTCTTCTCGCTAACCAAACCGGTAACCCCGCTTATTAAAAGCATTCTGTAACAAAGCGGGACCAAAGCCATGACAAAAACGCGT
AACAAAAGTGTCTATAATCACGGCAGAAAAGTCCACATTGATTATTTGCACGGCGTCACACTTTGCTATGCCATAGCATTTTTATCCATAAGATTAGCGGATCCTAC
CTGACGCTTTTTATCGCAACTCTCTACTGTTTCTCCATACCCGTTTTTTTGGTCTAGCAAATTCGAGCTTAAATTCTCTAGAAATAATTTTGTTTAACTTTAAGAAG
GAGATATACATATGGGG**CACTGC**ATGGGGGTGTCCAAGGGAGAGGAGGATAATATGGCTTCCCTGCCGGCGACCCATGAACTTCATATCTTTGGTTCGATCAACGGA
GTGGACTTTGATATGGTTGGTCAAGGCACGGGAAACCCGAACGATGGGTATGAAGAGTTGAATCTTAAATCGACAAAAGGGGATCTTCAATTCAGCCCTTGGATTCT
GGTCCCGCATATCGGGTATGGCTTCCACCAGTATTTACCATACCCGGACGGGATGTCTCCATTCCAGGCCGCTATGGTGGATGGCTCTGGTTACCAAGTGCATCGCA
CCATGCAGTTCGAGGACGGAGCATCTCTTACTGTTAACTACCGTTATACCTACGAAGGATCACACATTAAGGGAGAAGCTCAGGTTAAAGGAACGGGATTTCCCGCT
GACGGACCCGTAATGACTAATAGCCTGACAGCTGCCGACTGGTGTCGCAGTAAGAAAACTTATCCTAACGACAAAACGATTATCTCGACGTTCAAATGGTCTTACAC
GACTGGAAATGGGAAGCGCTACCGTAGCACGGCCCGCACGACGTACACCTTTGCCAAACCGATGGCGGCTAACTATCTGAAGAATCAACCCATGTATGTTTTTCGTA
AAACAGAATTGAAACATAGTAAGACTGAACTGAACTTCAAGGAGTGGCAAAAAGCATTTACGGACGTGATGGGGATGGATGAGTTATATAAAGGTGGATCCGGAGGT
AGCTGTCTGAGCTACGACACTGAAATCCTGACGGTAGAATACGGGTTCCTTCCCATCGGTAAGATCGTTGAAGAACGTATCGAGTGTACTGTTTACACTGTGGACAA
AAACGGGTTCGTCTATACGCAGCCGATTGCACAATGGCATAATCGCGGCGAACAAGAGGTTTTTGAGTATTGCCTGGAGGACGGCAGTATCATTCGCGCCACTAAAG
ATCATAAATTTATGACGACCGATGGTCAGATGTTGCCTATTGATGAAATCTTCGAACGTGGGCTTGACTTGAAACAAGTTGATGGCTTACCAGGCATTGCATAA**GCT**
AGCCGATTCCAGGCATCAAATAAAACGAAAGGCTCAGTCGAAAGACTGGGCCTTTCGTTTTATCTGTTGTTTGTCGGTGAACGCTCTCTACTAGAGTCACACTGGCT
CACCTTCGGGTGGGCCTTTCTGCGTTTATACTCCGGGAGCTGCATGTGTCAGAGGTTTAACGAAAGGGCCTCGTGATACGCCTATTTTTATAGGTTAATGTCATGAT
AATAATGGTTTCTTAGACGTCAGGTGGCAGGCTTACTTTTCGGGGAAATGTGCGCGGAACCCCTATTTGTTTATTTTTCTAAATACATTCAAATATGTATCCGCTCA
TGAGACAATAACCCTGATAAATGCTTCAATAATATTGAAAAAGGAAGAGTATGAGTATTCAACATTTCCGTGTCGCCCTTATTCCCTTTTTTGCGGCATTTTGCCTT
CCTGTTTTTGCTCACCCAGAAACGCTGGTGAAAGTAAAAGATGCTGAAGATCAGTTGGGTGCACGAGTGGGTTACATCGAACTGGATCTCAACAGCGGTAAGATCCT
TGAGAGTTTTCGCCCCGAAGAACGTTTTCCAATGATGAGCACTTTTAAAGTTCTGCTATGTGGCGCGGTATTATCCCGTATTGACGCCGGGCAAGAGCAACTCGGTC
GCCGCATACACTATTCTCAGAATGACTTGGTTGAGTACTCACCAGTCACAGAAAAGCATCTTACGGATGGCATGACAGTAAGAGAATTATGTAGTGCTGCCATAACC
ATGAGTGATAACACAGCGGCCAACTTACTTCTGACAACGATCGGAGGACCGAAGGAGCTAACCGCTTTTTTGCACAACATGGGGGATCATGTAACTCGCCTTGATCG
TTGGGAACCGGAGCTGAATGAAGCCATACCAAACGACGAGCGTGACACCACGATGCCTGTAGCGATGGCAACAACGTTGCGCAAACTATTAACTGGCGAACTACTTA
CTCTAGCTTCCCGGCAACAATTAATAGACTGGATGGAGGCGGATAAAGTTGCAGGACCACTTCTTCGCTCAGCACTTCCAGCTGGTTGGTTTATTGCTGATAAATCT
GGAGCCGGTGAGCGTGGATCTCGCGGTATCATAGCAGCACTGGGGCCAGATGGTAAGCCCTCCCGTATCGTAGTTATCTACACGACGGGGAGTCAGGCAACTATGGA
TGAACGAAATAGACAGATCGCTGAGATAGGTGCCTCACTGATTAAGCATTGGTAACTGTCAGACCAAGTTTACTCATATATACTTTGAATTCAAACTTCATTTTTAA
TTTAAAAGGATCTAGGTGAAGATCCTTTTTGATAATCTCATGACCAAAATCCCTTAACGTGA

6.1.3. Genetic elements and protein sequences obtained or adopted from third parties

Table 9 Genetic elements and protein sequences obtained or adopted from third parties

Name	Sequence	Usage	Originator
PT7.03	5′-TAATACGACTCACTA**C**AGG-3′	Reduced gene expression under control of T7 RNA polymerase; mutated base in bold, introduced to pCtrl2 *via NcoI* and NdeI sites	[84]
U9 RNA thermometer	5′-GATCC*CTCCTT*ACTAGTCTGCAGAAGGAGATATA-3′	Reduced gene expression at 30 °C; Shine-Dalgarno sequence in *italic* and anti-Shine-Dalgarno sequence in *underlined and italic*, introduced to pCtrl2 *via NcoI* and NdeI sites	[93]
TVMV	H_2N-SKALLKGVRDFNPISACVCLLENSSDGHSERLFGIGFGPYIIANQHLFRRNNGELTIKTMHGEFKVKNSTQLQMKPVEGRDIIVIKMAKDFPPFPQKLKFRQPTIKDRVCMVSTNFQQKSVSSLVSESSHIVHKEDTSFWQHWITTKDGQCGSPLVSIIDGNILGIHSLTHTTNGSNYFVEFPEKFVATYLDAADGWCKNWKFNADKISWGSFTLVEDAPED-CO_2H	Establishment of *in vivo* protease assay	[41]
TVMV site	H_2N-ETRFQ|S-CO_2H	Construction of TVMV cleavable proteins	[38]
FKBP	H_2N-GVQVETISPGDGRTFPKRGQTCVVHYTGMLEDGKKFDSSRDRNKPFKFMLGKQEVIRGWEEGVAQMSVGQRAKLTISPDYAYGATGHPGIIPPHATLVFDVELLKLE-CO_2H	Rapamycin inducible recruitment	[83]
FRB	H_2N-ILWHEMWHEGLEEASRLYFGERNVKGMFEVLEPLHAMMERGPQTLKETSFNQAYGRDLMEAQEWCRKYMKSGNVKDLTQAWDLYYHVFRRI-CO_2H	Rapamycin inducible recruitment	[83]
mNG	H_2N-VSKGEEDNMASLPATHELHIFGSINGVDFDMVGQGTGNPNDGYEELNLKSTKGDLQFSPWILVPHIGYGFHQYLPYPDGMSPFQAAMVDGSGYQVHRTMQFEDGASLTVNYRYTYEGSHIKGEAQVKGTGFPADGPVMTNSLTAADWCRSKKTYPNDKTIISTFKWSYTTGNGKRYRSTARTTYTFAKPMAANYLKNQPMYVFRKTELKHSKTELNFKEWQKAFTDVMGMDELYK-CO_2H	Fluorescent reporter for *in vivo* assays	[85]
mCherry	H_2N-VSKGEEDNMAIIKEFMRFKVHMEGSVNGHEFEIEGEGEGRPYEGTQTAKLKVTKGGPLPFAWDILSPQFMYGSKAYVKHPADIPDYLKLSFPEGFKWERVMNFEDGGVVTVTQDSSLQDGEFIYKVKLRGTNFPSDGPVMQKKTMGWEASSERMYPEDGALKGEIKQRLKLKDGGHYDAEVKTTYKAKKPVQLPGAYNVNIKLDITSHNEDYTIVEQYERAEGRHSTGGMDELYK-CO_2H	Fluorescent reporter for *in vivo* assays	[95]
mKOκ	H_2N-VSVIKPEMKMRYYMDGSVNGHEFTIEGEGTGRPYEGHQEMTLRVTMAEGGPMPFAFDLVSHVFCYGHRVFTKYPEEIPDYFKQAFPEGLSWERSLEFEDGGSASVSAHISLRGNTFYHKSKFTGVNFPADGPIMQNQSVDWEPSTEKITASDGVLKGDVTMYLKL		[103]

	EGGGNHKCQFKTTYKAAKEILEMPGDHYIGHRL VRKTEGNITEQVEDAVAHS-CO_2H		
His6-tag	H_2N-H_6-CO_2H	Protein purification and detection on Western blots	[104]
MBP	H_2N-KIEEGKLVIWINGDKGYNGLAEVGKKFEKDTGIK VTVEHPDKLEEKFPQVAATGDGPDIIFWAHDRF GGYAQSGLLAEITPDKAFQDKLYPFTWDAVRY NGKLIAYPIAVEALSLIYNKDLLPNPPKTWEEIPA LDKELKAKGKSALMFNLQEPYFTWPLIAADGGY AFKYENGKYDIKDVGVDNAGAKAGLTFLVDLIK NKHMNADTDYSIAEAAFNKGETAMTINGPWA WSNIDTSKVNYGVTVLPTFKGQPSKPFVGVLSA GINAASPNKELAKEFLENYLLTDEGLEAVNKDKP LGAVALKSYEEELVKDPRIAATMENAQKGEIMP NIPQMSAFWYAVRTAVINAASGRQTVDEALKD AQT-CO_2H	Increased solubility of fusion partners	[105]
Strep-TagII	H_2N-WSHPQFEK-CO_2H	Protein purification and detection on Western blots	[106, 107]
myc-tag	H_2N-EQKLISEEDL-CO_2H	detection of proteins on Western blots	[108]
SH3 domain	H_2N-AEYVRALFDFNGNDEEDLPFKKGDILRIRDKPEE QWWNAEDSEGKRGMIPVPYVEKY-CO_2H	Constitutive protein recruitment	[94]
sSH3L	H_2N-PPPPLPPKRRR-CO_2H	Constitutive protein recruitment	[94]
wSH3L	H_2N-PPPALPPKKR-CO_2H	Constitutive protein recruitment	[94]
TEV with enhanced stability	H_2N-GESLFKGPRDYNPISSTICHLTNESDGHTTSLYGIG FGPFIITNKHLFRRNNGTLVVQSLHGVFKVKNTT TLQQHLIDGRDMIIIRMPKDFPPFPQKLKFREPQ REERICLVTTNFQTKSMSSMVSDTSCTFPSGDGIF WKHWIQTKDGQCGSPLVSTRDGFIVGIHSASNF TNTNNYFTSVPKNFMELLTNQEAQQWVSGWR LNADSVLWGGHKVFMVKPEEPFQPVKEATQL MNELVYSQ-CO_2H	Alternative to TVMV	[109]
TEV site	H_2N-ENLYFQ|S-CO_2H	Construction of TEV cleavable constructs	[109]
HCV	H_2N-AKGSVVIVGRINLSGDTAYSQQTRGAAGIAATS ATGRDKNQVDGEVQVLSTATQSFLATCVNGVC WTVYHGAGSKTLAGPKGPITQMYTNVDQDLV GWPAPPGARSMTPCTCGSSDLYLVTRHADVIPV RRRGDSRGSLLSPRPVSYLKGSSGGPLLCPSGHVV GIFRAAVCTRGVAKAVDFIPVESMETTMR-CO_2H	Alternative to TVMV	[110]
HCV site	H_2N-DDVTPCSM|S-CO_2H	Construction HCV cleavable constructs	[110]
E118-134	H_2N-FGTWACRVRASHGVCAQ-CO_2H	Degradation of proteins	Weigand grouop unpublished findings
E118min	H_2N-FGTWACR-CO_2H	Degradation of proteins	Weigand grouop unpublished results
LVA	H_2N-AANDENYALVA-CO_2H	Degradation of proteins	[21]
FLFVQ	H_2N-FLFVQ-CO_2H	Degradation of proteins	[21]
YLFVQ	H_2N-YLFVQ-CO_2H	Degradation of proteins	[21]
AI(TVMV)	H_2N-REYVRFAP-CO_2H	Inhibiting TVMV activity *in vivo*	[1]

6.1.4. DNA and Protein size standards

DNA size standards were purchased from NEB. For the most part Quick-Load® 1 kb Plus DNA Ladder was used. Occasionally Quick-Load® 100 bp DNA Ladder was used for DNA fragments shorter than 300 bp. Likewise for very long fragments (over 5 kb) Quick-Load® 1 kb DNA Ladder was used.

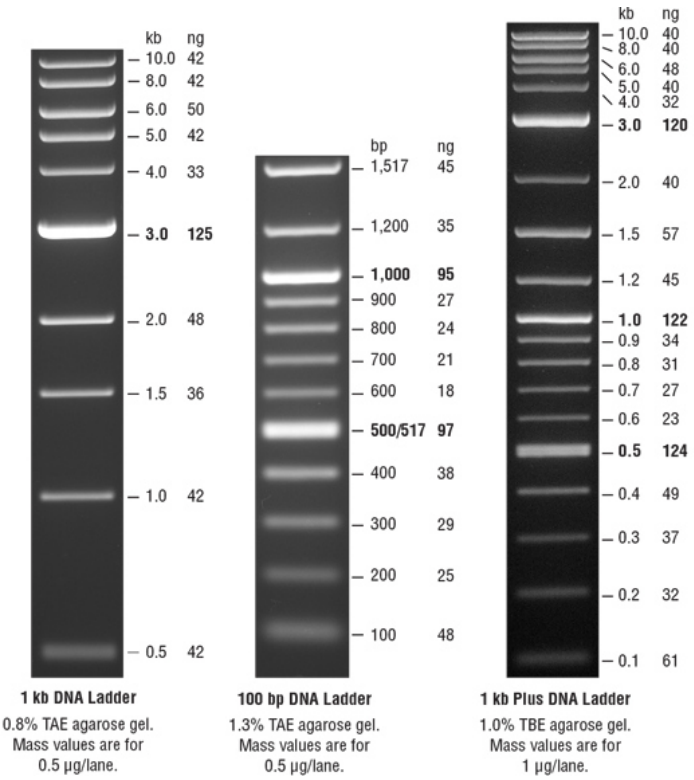

Figure 36 DNA size standards. [Figure gladly adopted from *New England Biolabs; source: https://www.nebiolabs.com.au/-/media/nebus/page-images/newsized-brochure-images/markers-and-ladders/dna_markers.png?la-en&rev-ee28084199b247588a9cfda1292e0b78&hash-02740B22C5139C691D53E1EFF1AD8835AD400D84]*

6.1.5. Synthetic DNA

Short single stranded DNA oligo nucleotides (ssDNA oligos) were ordered from Sigma Alrich (product number: VC00021). All oligos were ordered with 0.025 μg synthesis scale, purified through desalting and shipped in dry format. ssDNA oligos were used directly as primers for PCRs or were pairwise hybridized to assemble short functional domains or linkers as parts for iFLinkC. Additionally, to before mentioned usages, ssoligos were pairwise hybridized to form adaptors in order to ligate ssoverhangs from, by default incompatible, restriction enzymes.

Long double stranded DNA fragments were ordered from Integrated DNA Technologies (IDT) as "gBlock gene fragments™". gBlocks™ were used to constitute new cloning or expression vectors, to code for new functional domains for iFLinkC or in some cases for the cloning of new constructs *via* Gibson Assembly when PCR or restriction enzymes based cloning procedures were not suitable or proofed exceptionally difficult.

6.1.6. Antibodies and western blot reagents

Table 10 Antibodies / reagent used for detection of proteins on western blots.

Antibody / reagent	Host	Clonality and Isotype	Supplier	Product number
Anti-myc Antibody	Sheep	polyclonal, IgG	Invitrogene	PA3-981
Anti-sheep IgG (H+L) Antibody AlexaFluor633 conjugate	Donkey	Polyclonal, IgG	Invitrogene	A-21100
6x-His Tag Antibody	Mouse	Monoconal, IgG2b	Invitrogene	MA1-21315
Anti-mouse IgG (H+L) HRP conjugate	Rat	Monoclonal, IgG1κ	Invitrogene	04-6020
Precision Strep-Tactin HRP conjugate	-	-	BioRad	2-1502-001

If proteins were detected *via* horse radish peroxidase conjugates, HRP reaction was developed using the Clarty™ Western ECL Substrate from Bio Rad (Cat. # 170-5061).

For in gel epifluorescence images as well as western blots shown (see **Chapter 6.2.13**) in this work the BlueStar Prestained Protein Marker (Nippon Genetics) was used as a protein size standard (see **Figure 37**).

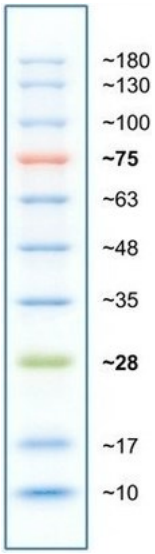

Figure 37 BlueStar Prestained Protein Marker (Nippon Genetics). 4-20% PAA gradient gels with Tris-Glycine buffer system, bands sizes in kDa. Figure gladly adopted from Nippon Genetics; [*source: https://www.nippongenetics.eu/bilder/products/protein-elektrophorese/prestained-protein-marker/blue-star0_500x5200_481x500.jpg*]

6.1.7. Restriction endonucleases, polymerase and additional DNA processing enzymes

All DNA processing enzymes were obtained from New England Biolabs (NEB).

Table 11 DNA processing enzymes

Enzyme	Recognition sequence	Usage	Catalog Number
BamHI-HF®	G|GATCC	Classical restriction ligation cloning	R3136
BbsI-HF®	$GAAGACN_2\|N_4$ $CTTCTGN_6\|$	iFLinkC	R3539
BsaI-HFv2®	$GGTCTCN\|N_5$ $CCAGAGN_5\|N$	iFLinkC	R3733
BsrDI	GCAATGNN| CGTTAC|NN	iFLinkC	R0574
BtsI-v2	GCAGTGNN| CGTCAC|NN	iFlinkC	R0667
EcoRI-HF®	G|AATTC	Classical restriction ligation cloning, iFLinkC	R3101
HindIII-HF®	A|AGCTT	Classical restriction ligation cloning	R3104
KpnI-HF®	GGTAC|C	Classical restriction ligation cloning	R3142
MfeI-HF®	C|AATTG	Classical restriction ligation cloning, iFLinkC	R3589
NcoI-HF®	C|CATGG	Classical restriction ligation cloning	R3193
NdeI	CA|TATG	Classical restriction ligation cloning	R0111
NheI-HF®	G|CTAGC	Classical restriction ligation cloning, iFLinkC	R3131
NotI-HF®	GC|GGCCGC	Classical restriction ligation cloning	R3189
SacI-HF®	GAGCT|C	Classical restriction ligation cloning	R3156
SalI-HF®	G|TCGAC	Classical restriction ligation cloning	R3138
SpeI-HF®	A|CTAGT	Classical restriction ligation cloning, iFLinkC	R3133
XbaI	T|CTAGA	Classical restriction ligation cloning	R0145
XhoI	C|TCGAG	Classical restriction ligation cloning	R0146
T4 DNA Ligase	Sticky or blunt ends	Classical restriction ligation cloning, iFLinkC	M0202
T4 Polynucleotide Kinase	5' hydroxyl groups	Classical restriction ligation cloning, iFLinkC	M0201
Shrimp Alkaline Phosphatase (rSAP)	5' and 3' phosphate groups	Classical restriction ligation cloning, iFLinkC	M0371
Phusion® High-Fidelity DNA Polymerase	Primer-ssDNA-duplexes	DNA amplification, DNA sequence mutagenesis, colony screenings	M0530*
Gibson Assembly® Master Mix	Homologue 35-50 nt dsoverhangs	Gibson Assembly	E2611

*Phusion® High-Fidelity DNA Polymerase was not obtain from NEB but instead produced in-house (see **Chapter 6.2.5**). However, 5x Phusion® GC buffer and 5x Phusion® HF buffer, were obtained from NEB (catalog numbers: B0519, B0518).

6.1.8. Buffers and solutions

Tris-acetate-EDTA (TAE) buffer

- 50x TAE
    - 242 g/L Tris, 57.1 mL glacial acetic acid, 100 mL EDTA (500 mM, pH = 8.0), fill up to 1 L with ddH_2O.

Phosphate buffers

Phosphate buffers were prepared using the appropriate volume equivalents of 1 M NaH_2PO_4 and 1 M Na_2HPO_4 stock solutions to yield the desired pH values and buffer capacities (total phosphate concentrations) according to Cold Spring Harbor Protocols [111].

Phosphate buffered saline

- 1x PBS
    - 4 mM KH_2PO_4, 16 mM Na_2HPO_4, 115 mM NaCl, pH 7.4, prepared as 10x stock, steam sterilized and stored at RT
- PBS blocking buffer
    - 3 %(w/v) BSA, 0.5 %(v/v) Tween20 in 1x PBS, freshly prepared with 10x PBS
- PBS tween buffer
    - 0.1 %(v/v) Tween20 in 1x PBS, freshly prepared with 10x PBS

His-tag buffers

- His binding buffer
    - 20 mM NaH_2PO_4, 500 mM NaCl, 20 mM imidazole, pH 7.4, prepared as 5x stock, steam sterilized and stored at RT, 1x working stock degassed and particle free
- His elution buffer
    - 20 mM NaH_2PO_4, 500 mM NaCl, 300 mM imidazole, pH 7.4, prepared from 5x His binding buffer, degassed and particle free
- Ni solution
    - 100 mM Ni(II)SO_4, degassed and particle free
- Stripping solution
    - 20 mM NaH_2PO_4, 500 mM NaCl, 50 mM EDTA, pH 7.4, degassed and particle free

6.1.9. Chemicals

Table 12 Chemicals used in this work

Chemical	Supplier
Acetone, synthesis grade	Carl Roth
Acetic acid, glacial	Carl Roth
Adenosine triphosphate (ATP)	Sigma Aldrich
Agar-Agar, Kobe	Carl Roth
Agarose	Sigma Aldrich
Ammonium chloride (NH_4Cl)	Merck KGaA
Ammonium heptamolybdate ($(NH_4)_6Mo_7O_{24}$)	Carl Roth
Ammonium persulfate	Carl Roth
Ampicillin sodium salt, BioScience Grade	Carl Roth
Anhydrotetracycline hydrochloride (AHT)	Carl Roth
L(+)-Arabinose	Carl Roth
Boric acid (H_3BO_3)	AppliChem
Bovine serum albumin (BSA)	Carl Roth
Calcium chloride ($CaCl_2$)	Carl Roth
Casein hydrosylate, standard	Carl Roth
Chloramphenicol	Carl Roth
Cobalt(II) chloride ($CoCl_2$)	Merck KGaA
Copper(II) sulfate ($CuSO_4$)	AppliChem
Desthiobiotin	IBA GmbH
Dimethyl sulfoxide (DMSO) for PCR as solvent	NEB Carl Roth
Dithiothreitol (DTT)	Carl Roth
dNTP mix	Bioline
Ethanol (EtOH) denatured pure	Richter Chemie Carl Roth
Ethylenediaminetetraacetic acid (EDTA)	Carl Roth
D(+)-Galactose	Carl Roth
D(+)-Glucose, monohydrate	Carl Roth
Glycerol	Carl Roth
Glycine, Bioscience grade	Carl Roth
HABA (2-(4-Hydroxyphenylazo)benzoic acid)	Sigma Aldrich
Hydrochloric acid 37 %	Carl Roth
Imidazole	Sigma Aldrich
Iron(II) sulfate ($FeSO_4$)	Carl Roth
Isopropanol	Carl Roth
Isopropyl β-D-1-thiogalactopyranoside (IPTG)	Carl Roth
Kanamycin sulfate	Carl Roth
Lactose	Carl Roth
Magnesium chloride ($MgCl_2$)	Carl Roth
Magnesium sulfate ($MgSO_4$)	Merck KGaA
Manganese(II) chloride ($MnCl_2$)	Merck KGaA
Methanol, blotting grade	Carl Roth
Midori Green Advance	Nippon genetics
Nickel(II) sulfate ($NiSO_4$)	Carl Roth
β-Mercaptoethanol	Carl Roth
Peptone from casein	Carl Roth
Ortho-phosphoric acid, 85 %	Carl Roth
Potassium chloride (KCl)	Carl Roth
Potassium hydroxide pellets (KOH)	Carl Roth
Potassium phosphate (KH_2PO_4/K_2HPO_4)	Carl Roth
L(+)-Rhamnose, monohydrate	Carl Roth
ROTI®Blue (5x Coomassie staining reagent)	Carl Roth
ROTI® Nanoquant (5x Bradford reagent)	Carl Roth
Rotiphorese® Gel 30 (37.5:1)	Carl Roth
Salmon sperm DNA sodium salt	Carl Roth

Sodium chloride (NaCl)	Carl Roth
Sodium dodecyl sulfate (SDS)	Carl Roth
Sodium hydroxide pellets (NaOH)	Carl Roth
Sodium phosphate (NaH_2PO_4/Na_2HPO_4)	Carl Roth
Sodium propionate ($CH_3CH_2CO_2Na$)	Sigma Aldrich
Sulfuric acid, smoking (H_2SO_4)	Carl Roth
Spectinomycin dihydrochloride pentahydrate	Sigma Aldrich
Streptomycin sulfate, BioScience Grade	Carl Roth
Tetramethylethylenediamine (TEMED)	Carl Roth
Thiamine hydrochloride	Carl Roth
Tris(hydroxymethyl)-aminomethan (Tris)	Carl Roth
Triton® X 100	Carl Roth
Tween®20	Carl Roth
Yeast extract, micro granulated	Carl Roth
Zinc sulfate ($ZnSO_4$)	AppliChem

6.1.10. Media

If required sterile filtered antibiotics were added. Ampicillin was added to a final concentration of 100 μg/mL, kanamycin at 50 μg/mL, chloramphenicol 25 μg/mL, lastly spectinomycin 50 μg/mL.

- Lysogenic broth (LB) medium [112]
    - 0.5 %(w/v) yeast extract, 1 %(w/v) peptone, 1%(w/v) NaCl, pH 7.4, steam sterilized and stored at RT, after antibiotics added stored at 4 °C
- LB agar [112]
    - 0.5 % (w/v) yeast extract, 1 %(w/v) peptone, 1% (w/v) NaCl, pH 7.4, 1.5 %(w/v) agar, steam sterilized and stored at RT, prior to casting agar was melt in a microwave and cooled to lukewarm temperature before adding antibiotics and subsequent casting

Super Optimal broth with Catabolite repression (SOC) medium [113]

- 2 %(w/v) peptone, 0.5 %(w/v) yeast extract, 10 mM NaCl, 2.5 mM KCl, 10 mM $MgCl_2$, 20 mM $MgSO_4$, 20 mM glucose
    - Magnesium and glucose were added from sterile filtered stock solutions under laminar flow after stream sterilization to avoid precipitation and Maillard product formation respectively.

M9 minimal medium

- 0.6 %(w/v) Na_2PO_4, 0.3 %(w/v) KH_2PO_4, 0.5 %(w/v) NaCl, 0.1 %(w/v) NH_4Cl, pH 7.4. After steam sterilization 0.2 %(w/v) glucose, 3nM $(NH_4)_6Mo_7O_{24}$, 0.4 μM H_3BO_3, 30 nM $CoCl_2$, 10 nM $CuSO_4$, 80 nM $MnCl_2$, 10 nM $ZnSO_4$, 1 mM $MgSO_4$, 100 μM $CaCl_2$ and 1 μM $FeSO_4$ were added.

6.1.11. Technical Equipment and devices

Table 13 Technical equipment used in this work

Instrument	Model	Manufacturer
Agarose gel chambers	Perfectblue Mini S/M with various combs	peqlab
Automatic coffee machine	Magnifica	Delonghi
Bench top centrifuge	Microstar 17	VWR
Bench top centrifuge	Minispin plus	Eppendorf
Bench top incubator	HT Ecotron	Infors
Bench top rocker	Rocker 3D digital	IKA
Bench-top vortex	Vortex genie 2	Neo Lab
Block heater	Touch Screen Block Heater	Thermo Fisher Scientific
Blue light LED table	Illuminator	Nippon Genetics
Cell density measurement device	ULTROSPEC© 10 cell density meter	Biochrom
Cell homogenizer With external air compressor	EmulsiFlex-C3 Super Silent compressor	Avestin Aerotech
Electric pipetting aid	Powerpipette pro	VWR
Electroporation device	Gene pulser II with capacitance extender plus	Bio-Rad
FPLC	Äcta Pure	GE Healthcare
Gel documentation (blue light LEDs)	E-BOX	Vilber
Gel documentation (epi-fluorescence, chemo-luminescence)	Amersham Imager 600 RGB	GE Healthcare
Graduated glass pipettes	VWR collection (5 mL, 10 mL, 20 mL)	VWR
Incubator for microtiter plates	Titramax 1000 & Inkubator 1000	Heidolph
Incubator for petri dishes	Icubat Typ 80	Melag Apparate
Lab Scale	SE 1202	VWR
Large-scale Incubator	HT Unitron	Infors
Low volume UV/Vis spectrophotomerter	Nanodrop OneC	Thermo Fisher Scientific
Magnetic stirrer With heating plate	LabDisc S040 LabDisc VMS-A S040	VWR
Microtiter plate reader	Spark	Tecan
Microwave oven	Inverter	Sharp
PCR cycler	Labcycler	Sensoquest
pH meter	pHenomenal pH1102	VWR
Piston pipettes	Research Plus (2.5 µL, 10 µL, 100 µL, 1000 µL, 5 mL)	Eppendorf
Platform shakers with incubator hood	Cetromat R/HK	B. Braun Melsungen AG
Power Supply for agarose and SDS gels	PowerPac Basic	Bio-Rad
Refrigerated centrifuge With various rotors	Allegra X-30R Centrifuge	Beckman Coulter
Sonicator	CL-18	Qsonica sonicators
Thermal shaker	Cooling Thermal Shaker Touch	VWR
Vacuum pump	VP100	VWR
Western blot device	Trans-Blot® Turbo™	Bio-Rad

6.1.12. Software

Table 14 Software used in this work

Software	Originator	Reference
UCSF Chimera	University of California San Francisco	[114-124]
Microsoft® Office	Mircrosoft	
SnapGene®	GSL Biotech LLC	
GraphPad Prism	GraphPad Software	
Affinity Designer	Serif	
Fiji	Johannes Schindelin, Albert Cardona, Mark Longair, Benjamin Schmid, and others	[125-127]

6.2. Methods

6.2.1. *E. coli* cultivation

Required solutions:

- Lysogenic broth (LB)
    - 5 % (w/v) yeast extract, 1 %(w/v) peptone, 1%(w/v) NaCl, pH 7.4
- LB agar
    - 5 % (w/v) yeast extract, 1 %(w/v) peptone, 1%(w/v) NaCl, pH 7.4, 1.5 %(w/v) agar
- Appropriate antibiotics
    - Usually prepared as sterile filtered 1000x stock in appropriate solvent

E. coli cells were cultivated in lysogenic broth (LB) medium containing the appropriate antibiotics at 37 °C shaking at 200 rpm. For protein production cultures were incubated at 30 °C to reduce growth rates as well as thermal denaturing of the proteins of interest. Broth cultures were inoculated with single colonies from agar plates, scrapped material from glycerol stocks, or from pre-cultures depending on the situation. For plasmid preparation 5 mL broth cultures were inoculated in standard glass tubes with metallic lids. For library generation 20 to 50 mL broth cultures in 50 to 200 mL Erlenmeyer flasks were performed. Lastly for the purification of proteins for *in vitro* characterizations 500 mL broth cultures in 1 L Erlenmeyer flasks were used. All flasks were covered with aluminum foil cut outs.

6.2.2. Chemo-competent *E. coli* cells and heat shock transformation

Required solutions:

- $CaCl_2$ solution
    - 80 mM $CaCl_2$, autoclaved, pre-cooled to 4 °C
- Cryo solution
    - 80 mM $CaCl_2$, 20 %(v/v) glycerol, autoclaved, pre-cooled to 4 °C

5 mL LB broth containing appropriate antibiotics, if necessary, were inoculated with a single colony or with material scrapped off a cryo-stock. Pre-cultures were incubated overnight at 37 °C shaking at 180 rpm. On the following morning 200 mL LB broth containing the same antibiotics as before were inoculated with 2 mL overnight culture (1:100 dilution). The main culture was incubated as stated before until an OD_{600} of ~0.5 was reached. Cultures were split

into 50 mL reaction tubes. Subsequently, tubes were incubated on ice for 30 min. After cooling cells were harvested by centrifugation (2500xg, 4 °C, 30 min). All following steps were performed on ice. The supernatant was decanted and the precipitated cells were resuspended in 5 mL cold $CaCl_2$ solution and transferred to a fresh pre-cooled 50 mL tube. Then, suspensions were filled up with $CaCl_2$ solution to a final volume of 50 mL and were incubated for another 30 min on ice. Cells were harvested once again (parameters as before) and the supernatant was discarded. The precipitated cells were gently resuspended in 3.5 mL cold cryo solution. 100 μL aliquots in sterile 1.5 mL were prepared, snap-frozen in liquid nitrogen and stored at -80 °C.

Frozen aliquots were thawed for three to five minutes on ice. For heat-shock transformation 20 ng plasmid DNA per 100 μL of chemo-competent cells were used. Plasmid DNA solution was added by carefully pipetting and subsequently gently stirring the transformation mix with the pipette tip. Afterwards transformation mixes were incubated on ice for 30 min. Following the incubation, a heat-shock was performed by incubating the tubes at 42 °C in a dry bath for 45 s. After heat-shock, cells were cooled down on ice for 5 min. 9 volume equivalents of SOC medium were added to the transformation mix and cells were incubated at 37 °C and 200 rpm for ~1h to allow expression of the selection marker. Following phenotypic expression transformants were selected on LB agar plates containing the appropriate antibiotics. LB agar plates were incubated upside down at 37 °C. Usually, colonies were obtained the day after the transformation.

6.2.3. Room temperature electro-competent *E. coli* cells and electroporation transformation

Required solutions:

- Sterile ddH_2O
- DNA preparation in DNase free H_2O

Pre- and main cultures were prepared as describe for chemo-competent *E. coli* cells (see **Chapter 6.2.2**). Once an OD_{600} of ~0.5 was reached cultures were immediately harvested without an incubation on ice. Centrifugation itself was performed the same way as for chemo-competent cells except that cells were sedimented at RT (see **Chapter 6.2.2**). Harvested cells were resuspended in 5 mL sterile ddH_2O before adjusting the final suspension volume with sterile ddH_2O to 50 mL. All following steps were performed at room temperature. Subsequently cells were precipitated as described earlier. Cells were washed a second time with 50 mL sterile ddH_2O. Finally, cells were resuspended in 1 mL ddH_2O. For electroporation 1 μL of 20 ng/μL DNA preparation in DNase free H_2O (NEB) was provided in a sterile 1mm electroporation cuvette (VWR). The DNA preparation was pipetted onto one of the two short walls of the cavity. Afterwards 80 μL electro-competent cell suspension were gently pipetted over the DNA solution droplet. This procedure ensured thorough mixture of DNA solution and cell suspension whilst omitting extensive sheering forces. Lastly cell suspension was pulsed using the following parameters with a Gene pulser II with a capacitance extender plus (Bio-Rad; 300 Ω, 25 μF, 1.8 kV). Usually time constants of four to eight milliseconds were achieved. If visible or audible electrical discharge was observed, or the time constant was below three milliseconds the transformation was repeated. In case of multiple discharges occurred using the same DNA solution a fresh one was prepared. In event of multiple discharges occurred with different DNA solutions the cell suspension was washed once again with 50 mL sterile ddH_2O.

6.2.4. DNA purification from *E. coli* cells

Plasmid DNA was prepared from fresh grown overnight cultures of *E. coli* using the appropriate kits from Macherey-Nagel. For 5 to 20 mL cultures the NucleoSpin® NoLid Mini-Prep kit was chosen, for larger cultures (up to 200 mL) the NucleoBond® Xtra Midi kit was chosen and lastly for the isolation of genomic DNA the NucleSpin® Microbial DNA kit was used.

6.2.5. Phusion® High-Fidelity DNA Polymerase -recombinant expression, purification and storage

All credit for this protocol belongs to A. Gräwe

Required solutions:

- TB medium
    - Tryptone 12 g/L, Yeast extract 24 g/L, K_2HPO_4 9.4 g/L, KH_2PO_4 2.2 g/L, autoclaved
- 1000x IPTG stock solution
    - 500 mM IPTG, sterile filtered
- Buffer A
    - 50 mM Tris pH 7.4, 10%(v/v) glycerol, autoclaved
- Buffer B
    - 50 mM Tris pH 7.4, 300 mM NaCl, 30 mM Imidazole, sterile filtered and degassed
- Buffer B2
    - 50 mM Tris pH 7.4, 1 M NaCl, 30 mM Imidazole, sterile filtered and degassed
- Buffer C
    - 50 mM Tris pH 7.4, 1 M NaCl, 300 mM Imidazole (optimal: use highly pure from Sigma → no absorption at 280 nm), sterile filtered and degassed
- Buffer D
    - 100mM Tris pH 8.2, 0.1mM EDTA, 1mM DTT
- Buffer E
    - 0.1 mM EDTA, 1mM DTT, 0.2%(v/v) IGEPAL® CA-630, 0.2%(v/v) Tween20 in glycerol
    - This is just a virtual specification of buffer E, in reality simply add all components aside from glycerol to Phusion® preparations in buffer D to a final concentration equal to twice the values shown here and than add one volume equivalent of glycerol.

Expression

E. coli BL21(DE3) cells were co-transformed with plasmids pPhusion and pSJS1240 following the regular protocol for the transformation of chemo-competent *E. coli* cells until regeneration. Due to cells were transformed with two plasmids at once regeneration time had to be prolonged to at least 90 min. Prolonged regeneration was mandatory to allow transformed cells to sufficiently express both resistance genes. Otherwise no transformants would have been obtained on LB Amp/Spec dual selection plates. A single colony from the selection plate was used to inoculate 10 mL TB Amp/Spec medium in a glass tube as a pre-culture. Once the pre-culture was visibly turbid it was used to inoculated up to 2 L TB Amp/Spec medium in a sufficiently large flak or in multiple flasks. The main-culture(s) was (were) grown to an optical density at 600 nm of approximately 1. Then expression was induced by adding IPTG to a final concentration of 1 mM to the culture medium. Protein expression was performed for 12 h at 37 °C while vigorously shaking. Cells where harvested by centrifugation and resuspend in 25 mL Buffer A per liter culture volume. Subsequently cell suspension was transferred to 50 mL tubes. One tube per 25 mL of cell suspension was used. If needed cells were precipitated again and the received cell precipitates were stored at -20 °C until cell lysis.

Purification

Independent whether cells were stored after harvesting or not, it was ensured that cells were suspended in 25 mL Buffer A per liter culture volume before proceeding with the protocol. Triton X-100 was added to a final concentration of 0.1 %(v/v), likewise $MgSO_4$ was added to a final concentration of 5 mM as well as a few milligrams of DNase (or Barnase) and Lysozyme were added. Subsequently cells are lysed by sonication (4x 1 min 75 % amplitude intercepted by 1 min rests). Cell debris was precipitated by centrifugation (30 min, 35000xg). The supernatant was transferred into fresh 50 mL tubes and endogenous host proteins were denatured at 85 °C for 30 min. Denatured proteins were precipitated by centrifugation (30 min, 40000xg). The supernatant was transferred into fresh 50 mL tubes. During the last centrifugation step Ni-NTA sepharose columns were equilibrated with 10 column volumes (CV) buffer B (flow rate: 1 mL/min). Prior to loading the supernatant from the last centrifugation step was filtered through a 0.45 μm sterile filters to remove any solid particles large enough to damage the column. If multiple tubes had to be used for centrifugation, the filtration step was used to pool them into one tube. Lastly the supernatant was loaded onto the column (flow rate: 0.1 mL/min). Following the load, the sample tubing was placed into a Buffer B reservoir and flushed with 3 CV (flow rate: 1 mL/min). This step was included to compensated for the dead volume of the FPLC. Subsequently the column was washed with 2 CV Buffer B2.

Followed by a second washing step with 3 CV Buffer B. Now Phusion® High-Fidelity DNA polymerase was eluted from the column with Buffer C in fractions equal to 1 CV. Elution was continued until no more protein was eluted for at least 5 CV. All protein containing fractions were pooled and a Vivaspin 20 (MWCO 10 kDa) column was used to exchange Buffer C with Buffer D. At least two concentration steps were executed according to manufacturer's instruction to ensure complete buffer exchange. Finally, protein content was measured using the Bradford assay with a BSA standard curve to calibrate the assay. For storage the eluate was diluted to 0.4 $mg_{protein}$/mL with Buffer D. Lastly the Phusion® High-Fidelity DNA polymerase solution was mixed with one volume equivalent Buffer E. Usually the resulting Phusion® High-Fidelity DNA polymerase of these preparation was approximately 2 U/μL. 1 mL Aliquots were prepared in sterile 1.5 mL screw cap tubes and snap frozen in liquid nitrogen. For long term storage aliquots were stored at -80 °C. The working aliquot was stored at -20 °C.

6.2.6. Clonetregration for the genomic integration of protease constructs into the genome of *E. coli* Bl21(DE3)

The integration of protease constructs into the genome of BL21 (DE3) cells followed the general protocol published by St. Pierre *et al.* [102] slightly modified by M. Röder. The modified protocol is found in the supplement of this thesis (**see Chapter 13.3.1**).

6.2.7. Polymerase chain reaction (PCR)

All PCRs in this work were performed with Phusion® High-Fidelity DNA polymerase produced in house (see **Chapter 6.2.5**). The tables below show reaction mixes as well as the standard cycler program used in this work. By default, 5x HF buffer was used. If this led to failed PCRs or undesired product formation 5x GC buffer was used or DMSO was added in concentrations varying from 0.5 to 4 %(v/v).

Table 15 Phusion® High Fidelity DNA polymerase reaction mix

Component	Volume [µL]	Final concentration
5x HF/GC buffer	10	1x
10 mM dNTP mix	1	0.2 mM
10 µM forward primer	2.5	25 pmol / 50 µL
10 µM reverse primer	2.5	25 pmol / 50 µL
Template	1 µL	≤20 ng / 50 µL
(DMSO)	(0.25 to 2)	(0.5 to 4 %(v/v))
2 U/µL Phusion® High-Fidelity DNA Polymerase	0.5	1 U/ 50 µL
ddH_2O	ad 50	-

Table 16 Standard thermocycler program for Phusion® High Fidelity DNA Polymerase

Step		Temperature [°C]	Time [s]	Cycles
Initial denaturing		98	300	
	Denaturing	98	30	
	Annealing	52 to 72 depending on primer pair used	30	30
	Extension	72	45/kb	
Final extension		72	600	
Hold		4 to 12	∞	

colony PCR

Colony PCRs were run to screen transformants for correct construct integrity or correct integration into the genome. The template for colony PCRs was prepared as follows. Some colony material was resuspended in 10 μL ddH_2O in a 0.2 mL reaction tube. Cells were thermo-lysed at 98 °C for 5 min in a thermocycler. Subsequently 1 μL lysate was used as the template for the colony PCR.

overlap extension PCR (oePCR)

Overlap extension PCRs were utilized to form one long PCR product from two or more shorter ones. Among other things oePCRs were used to insert multiple mutations in a DNA sequence at once or to avoid undesired PCR products through self-priming events. In the first step multiple standard PCRs were run in parallel. Primers for these initial PCR were designed to yield in internal homologous overhangs. These overhangs were used to define the order in which the individual fragments were fused together. The length of the overhangs was chosen to be as similar as possible within the standard annealing temperature range for primers. Therefore, those overhangs were able to mimic primers in the actual oePCR. This PCR was identical to a standard PCR with the following changes. First, instead of one template all initial PCR products were used as templates. Initial PCR products were added in equimolar concentrations with a total amount of template DNA of 20 ng. Second, the forward primer annealed to 5' end of the most upstream template while the reverse primer annealed to the 3' end of the most downstream template. Consequently, through regular priming and internal self-priming of the homologues overhangs all fragments were fused into one full-length product. Third and last the amplification cycle was split into two cycles if the annealing temperatures of the overhangs were incompatible to the annealing temperatures of the used primer pair. The first ten cycles used an annealing temperature optimal for annealing of the internal overhangs to drive formation of full-length product, through overhang extension, forward. The subsequent twenty cycles used an annealing temperature optimal for the flanking primer pair to force amplification of the full-length product. The resulting thermocycler program is found in **Table 17**.

Table 17 Thermocycler program for oePCRs with two separated cycles.

Step	Temperature [°C]	Time [s]	Cycles
Initial denaturing	98	300	
Denaturing	98	30	10
Annealing	52 to 72 depending on internal overhangs	30	
Extension	72	45/kb of full-length product	
Denaturing	98	30	20
Annealing	52 to 72 depending on primer pair used	30	
Extension	72	45/kb of full-length product	
Final extension	72	600	
Hold	4	∞	

6.2.8. Agarose gel electrophoresis

Required solutions:

- 0.5 to 2 %(w/v) agarose in 1x TAE
    - usually 300 mL 1 %(w/v) agarose was prepared in a 500 mL blue cap bottle
- Midori Green (Nippon genetics)

Agarose gel electrophoresis was carried out in PerfectBlue Mini chambers (peglab). Agarose stocks were melted in a microwave and approx. 30 to 50 mL or 50 to 80 mL were used to cast gels in MiniS or MiniM chambers respectively. A standard beaker was used to estimate the agarose volume. Prior to casting 2 μL Midori Green (Nippon Genetics) were added to the melted agarose. The pipette tip used for transferring Midori Green was used to stir it into the agarose to avoid the formation of air bubbles. Prior to loading, samples were prepared with 6x QuickLoad® purple loading dye (NEB). For the most part Quick-Load® 1 kb Plus DNA Ladder 1kb plus functioned as a size standard. Exceptions are noted in chapter 6.1.4. Electrophoresis was performed at a constant voltage of 130 V for approximately 35 min. Gels were documented using the E-BOX gel documentation (Vilber). DNA bands were excised using standard scalpels on a blue light LED table with an in-built eye protection screen (Nippon Genetics). DNA was extracted from the gel slices with the NucleoSpin Gel and PCR Clean-up kit (Macherey-Nagel).

6.2.9. iFLinkC

All parts to be used in iFLinkC assemblies must be cloned into the corresponding storage vector first. pFD for so called functional domains which are proteins or peptide motives that introduce functionalities to the multi-domain fusion protein to be assembled. Linkers are cloned into pL2 vector. Once all required parts were present within the appropriate storage vectors an iterative and hierarchical assembly procedure was abided. First the coding sequence (CDS) of either a linker or of a functional domain was selected as the upstream sequence. The upstream sequence was always restricted with BsrDI the second enzyme was chosen to yield in well separable restriction fragments for easier excision of bands. Either SpeI, EcoRI or MfeI served as the second restriction enzyme. The CDS of the other part became the downstream sequence. The downstream sequence was always restricted with BtsI. The second enzyme used had to be the same as used for the upstream sequence. BsrDI and BtsI required elevated temperatures for full activity, 65 °C and 55 °C respectively. Therefore, the second enzymes were added to the reaction mixes once they were cooled down to RT from the first digestion step. Both restriction reactions were routinely performed for 90 min in a total reaction volume of 50 to 100 μL. Shrimp phosphatase (rSAP) was added to the restriction mix generating the fragment carrying the origin of replication (ori) to reduce the number of recyclized original backbone propagated after the transformation. For the steps at higher temperatures a thermocycler was used to prevent evaporation of the reaction mix. Once restriction was completed the resulting fragments were separated on an agarose gel (0.5 to 1.5 %(w/v) depending on size of the fragments). The desired fragments were extracted from gel slices using the appropriate kit from Macherey & Nagel. Following the extraction fragments were ligated using T4 DNA ligase (NEB) in total reaction volumes of 10 to 25 μL using 50 to 125 ng of linear DNA fragments. If fragments were generated using either SpeI or MfeI the fragment lacking ori and selection marker was added in a threefold molecular excess. If EcoRI was used creating one fragment which was baring the ori while the other fragment carried the selection marker fragments were used in equimolar concentration. Ligation was performed either at 16 °C for one hour or overnight. In rare cases ligation was performed at RT for 15 min. Up to 100 μL of competent cells were transformed with up to 10 μL of ligation mix. For linker library generation two times 80 μL RT electro-competent DH10β cells (NEB) were transformed with 10 μL ligation mix each. For individual constructs 25 μL of chemo-competent DH10β cells (NEB) were transformed using 5 μL ligation mix. Transformants were selected on LB ager plates containing 50 μg/mL kanamycin. In addition to the actual cloning reactions controls were performed as well. For this controls competent cells were transformed with ligation mixes missing the non-dephosphorylated part. If at least 5 times more colony forming units per milliliter ligation and microgram DNA used

(CFU*$mL_{ligation\ mix}^{-1}$*μg_{DNA}^{-1}) were received for the cloning compared to the control two clones were picked and used to inoculate overnight broth cultures for plasmid preparation. Lastly the integrity of construct was verified using Sanger sequencing (SeqLab, MicroSynth). If libraries were cloned only 100 μL of 1:100 and $1:10^4$ dilution of the regenerated transformation cultures were plated. The remainder was used to inoculate 50 mL broth cultures containing 50 μg/mL kanamycin. From these cultures midi-preps were performed to recover the library. Controls were carried out as above and used to calculate the approximately fraction of recyclized clones within the library. If this fraction was equal to or greater than 10 % the library was discarded and cloning was repeated. In order to estimate diversity within the library five clones received from plating of the dilutions were analyzed *via* Sanger sequencing.

Because the initial restriction sites, ori and selection markers were regenerated after each round of cloning with iFLinkC the constructs from the initial cloning step were suitable parts for a second round. Parts with an upstream linker CDS acted as linkers in the subsequent cloning steps. Accordingly, parts where the most upstream CDS was a functional domain acted as functional domains. Once the desired construct or library was completely assembled the CDS was cloned into an expression vector of choice. CDSs were cloned directly in an iFLinkC expression vector (pFLinkC-XE, various available) or were cloned into other expression vectors such as pPRO24 or pCtrl2. Latter might require adapter cloning to convert the iFLinkC restriction enzyme generated overhangs to overhangs of restriction enzymes present in the desired non-iFLinkC expression vector.

6.2.10. DNA sequencing

The Economy Run service of Sequence Laboratories (SeqLab, MicroSynth) was exclusively tasked for DNA sequencing throughout this work. According to service provider's recommendation samples containing 18 ng PCR product per 100 kb fragment length or approximately 960 ng plasmid DNA in a total volume of 12 μL 5 mM TrisHCl buffer were prepared. Prior to shipping DNA samples were mixed with 3 μL of a 10 μM solution of the desired primer in a 1.5 mL reaction tube. Samples were shipped in standard sample bags.

6.2.11. High pressure cell homogenization

Required solutions:

- ≥35 mL cell suspension
- cell resuspension buffer of choice
- ddH_2O
- Ethanol

- 80 %(v/v)
- 20 %(v/v)

- 100 mM NaOH

High pressure cell homogenization was performed with the EmulsiFlex-C3 (Avestin). First the external compressor was set to provide the homogenizer with 8 bar system pressure. Influx of air into the homogenizer was carefully omitted during all further steps. This meant adding the next solutions when bottom of the sample beaker still was covered with residual liquid from previous step. Second the system was washed three times with ½ sample beaker volume (SBV) ddH_2O. Third the system was primed with two times ½ SBV of the given cell resuspension buffer. Forth the homogenization pressure was adjusted while the second ½ SBV cell resuspension buffer still was being pumped through the system. Homogenization pressure was adjusted to 1.2 to 1.5 kbar for *E. coli* cells. The system flow was stopped and cell suspension was added to a maximum of one ¾ SBV. If sample volume exceeded this value cell suspension was added stepwise. During sample homogenization the pressure was constantly readjusted to keep it within the before mentioned boundaries. Additionally, the cooler spiral of the outlet tubing as well as the collection tube were placed in an ice bath to prevent thermal denaturing of the protein of interest. Usually samples were processed three times to ensure near to complete cell lysis. Afterwards the system was washed with ~10 mL resuspension buffer to flush the remaining cell homogenate out of the system. After this step the pressure was released to the system pressure provided by the external compressor. This is crucial to prolong the life span of the homogenizer. Subsequently the device was cleaned with ½ SBV of 100 mM NaOH to remove and inactivate any intact cells or cell debris left in the system. The remaining caustic soda was flushed out with ¾ SBV of ddH_2O prior to disinfection of the system. Disinfection was performed with ½ SBV of 80 % (v/v) ethanol. Lastly the system was filled with 20 % (v/v) ethanol (~ ½ SBV left in the sample beaker). The sample beaker was sealed with the lid and the outlet tubing was sealed with a clamp to prevent evaporation of the ethanol in the system. The external compressor was switched of and the remaining pressure was carefully released through the exhaust valve of the compressor.

6.2.12. Protein Purification

Recombinant protein expression was performed with *E. coli* BL21(DE3) cells transformed with an expression vector. All expression vectors bored an, in BL21(DE3) cells, inducible promotor in order to separate biomass generation (growth) from heterologous protein overexpression. For scouting runs recombinant proteins were produced in 50 mL broth cultures within 200 mL Erlenmeyer flasks. Actual expression cultures varied from 200 mL broth cultures in 1 L flasks to

1 L broth cultures in 3 L flasks (culture volume equal to or less than ⅓ flask volume). Appropriate pre-cultures were used to inoculate an expression culture to a starting OD_{600} of 0.05 to 0.1. Expression cultures were incubated shaking at 180 rpm to an OD_{600} of around 0.6 prior to induction of protein overexpression. During protein overexpression cultures were incubated at 30 °C and 220 rpm. The reduced incubation temperature was chosen to hempen cell division and thereby foster protein production. The higher revelation speed increased oxygen saturation in the medium and thereby increasing the cellular productivity.

Cells were harvested by centrifugation (4255xg, 60 min, 4 °C) after at least three hours of induced protein overexpression. In most cases proteins were expressed overnight (~12 to 16 h). Following harvesting, cells were washed once by resuspending them in ¼ total culture volume of pre-cooled resuspension buffer (His-tag: His binding buffer; Strep®-TagII: Buffer W). Cells were precipitated once again as stated for harvesting. Subsequently cells were resuspended in $^{1}/_{20}$ total culture volume. For scouting runs this resulted in cell suspension volumes below 35 mL. Therefore, cells were lysed using a sonicator (see **Chapter 6.2.5 - Expression**). For actual expression cultures if $^{1}/_{20}$ total cultures volume was below 35 mL resuspension buffer was added to increase the total volume to 35 mL. Cells were homogenized as described in **Chapter 6.2.11**). Solid particles, including cell debris, were separated from the liquid phased by centrifugation (25000xg, 60 min, 4 °C). In parallel the Äkta® Pure FPLC system (GE Healthcare) was prepared for the purification run as described in the following subchapters. The supernatant of the last centrifugation step was loaded onto the appropriate 1 mL column. From here the appropriate chromatography protocols were executed.

Immobilized metal ion affinity chromatography (IMAC)

Required solution:

- His binding buffer
    - 20 mM NaH_2PO_4, 500 mM NaCl, 30 mM imidazole, pH 7.4, prepared as 5x stock, steam sterilized stored at RT, 1x working stock degassed and particle free
- His elution buffer
    - 20 mM NaH_2PO_4, 500 mM NaCl, 300 mM imidazole, pH 7.4, prepared from 5x His binding buffer, degassed and particle free
- Ni solution
    - 100 mM $Ni(II)SO_4$
- Stripping solution
    - 20 mM NaH_2PO_4, 500 mM NaCl, 50 mM EDTA, pH 7.4, degassed and particle free

- 20 % (w/v) Ethanol
    - Degassed and particle free
- ddH_2O
    - degassed and particle free

IMAC was performed using the Äkta™ Pure FPLC system (GE health care) with 1 mL Protino Ni-NTA 1 mL FPLC columns (Macherey-Nagel). Prior to all runs all tubing was extensively rinsed with ddH_2O. Rinsing was essential to remove any remaining ethanol used as a preservative during off-times. Residual ethanol mixed with salt containing buffer could have led to hazardous precipitation within the system. Following the rinse, the column was installed and washed with ten CV of ddH_2O (flow-rate 1 mL/min). If the column was not loaded with nickel a loading step was performed where the column was filled with Ni solution. Once filled the column was incubated for one hour to allow complete formation of the Ni-NTA complexes on the sepharose matrix. Following the incubation, the column was washed with 15 CV ddH_2O to remove any excess nickel. Nickel removal was monitored on the conductivity chromatogram. If the conductivity was not on the baseline (ddH_2O) level, the washing step was prolonged until baseline level was reached again. Subsequently all tubes were filled with the appropriate buffer, bypassing the column, until stable UV and conductivity values were detected. Now the system was filled with His binding buffer. Once all preparations were done the column was equilibrated with binding buffer (flow-rate 1 mL/min) until UV and conductivity values were once again stable. Afterwards the sample was loaded onto the column (flow rate 1 mL/min). Approximately 95 % of the total sample volume were loaded to prevent accidentally pumping of air into the system. Following the load, 10 CV binding buffer were pumped through the sample inlet, using the sample pump, to load any leftover sample in the flow path onto the column (flow rate 1 mL/min). Protein was eluded from the column using a linear gradient from 0 t0 100 % (v/v) elution buffer (30 to 300 mM imidazole) over a length of 10 CV whilst collection fraction of 0.5 CV (20 fractions in total). After the gradient was completed, elution was continued isocratically with 300 mM imidazole over 6 CV to ensure all protein was eluded from the column. Following the isocratic step, the column was prepared for storage. For short term storage, to be used for the same protein in the near future, the column was washed with 15 CV ddH_2O and subsequently filled with 20 %(v/v) ethanol until stable UV and conductivity chromatograms were achieved. Now the column was removed under flow to avoid influx of air. Once the column was removed the exterior of all tubing was rinsed with ddH_2O and all tubing was placed in the water reservoir. Now the whole system was cleaned by manually executing pump washes for all used inlets, including the sample pump. Afterwards the outside of all inlet tubing was rinsed with 20 %(v/v) ethanol and all tubing was placed in the 20 %(v/v) ethanol

reservoir. Like before manual pump washes were executed to disinfect the system. All tubing remained in the ethanol reservoir until the next run. Alternative to the simple cleaning of all tubing, the column was stripped of its nickel content for either long-term storage or if the column was to be re-used for a different protein. Stripping was considered essential to remove any traces of the previously purified protein from the column matrix in order to prevent cross contamination of protein preparations. For stripping the column was washed with ddH_2O identically to the short-term storage protocol. Subsequently the column was stripped from nickel by administering stripping solution until the blue coloration of the column was entirely lost (at least 10 CV). Afterwards the column was washed another time with 15 CV ddH_2O and from here on the same procedure as for short-term storage was followed.

Affinity chromatography using the Strep-Tag®II/Strep-Tactin system

Required solutions:

- Buffer W
    - 100 mM Tris/HCl pH 8.0, 150 mM NaCl 1 mM EDTA, prepared as 10x stock, steam sterilized and stored at RT, 1x working stock degassed and particle free
- Buffer E
    - 100 mM Tris/HCl pH 8.0, 150 mM NaCl,1 mM EDTA, 2.5 mM desthiobiotin, freshly prepared from 10x Buffer W, degassed and particle free
- Buffer R
    - 100 mM Tris/HCl pH 8.0, 150 mM, NaCl, 1 mM EDTA, 1 mM HABA, freshly prepared from 10x Buffer W, degassed and particle free
- 100 mM Tris
    - Degassed and particle free
- 20 % (v/v) ethanol
    - Degassed and particle free
- ddH_2O
    - degassed and particle free

Strep-Tag®II/Strep-Tactin affinitiy chromatography was performed using the Äkta™ Pure FPLC system (GE health care) with 1 mL Strep-Tactin columns (iba). Prior to all runs all tubing was extensively rinsed with ddH_2O to remove any ethanol (see previous subchapter for further details). Following the rinse, the column was installed and washed with 10 CV of ddH_2O (flow-rate 1 mL/min). Subsequently all tubing was filled with the appropriate buffer, bypassing the column, until stable UV and conductivity values were detected. Now the system was filled with Buffer W. Once all preparations were done the column was equilibrated with Buffer W

(flow-rate 1 mL/min) until UV and conductivity values were once again stable. Afterwards, the sample was loaded onto the column (flow rate 1 mL/min). Approximately 95 % of the total sample volume were loaded to prevent accidently pumping of air into the system. Following the load 15 CV Buffer W were pumped through the sample inlet using the sample pump to load any leftover sample in the flow path onto the column (flow rate 1 mL/min). Now the column was washed with 8 CV Buffer W (flow rate 1 mL/min). Protein was isocratically eluded from the column with 3 CV Buffer E (flow rate 0.5 mL/min) whilst collection fractions equal to 0.5 CV (six fractions in total). Once elution was complete the column was regenerated with Buffer R (flow rate 1 mL/min) until the column showed an equally distributed strong red coloration (at least 15 CV). Generally, the more often a column had been used already the more Buffer R was required. After regeneration the column was rinsed with 100 mM Tris until the red color was removed completely. Subsequently the column was washed with 15 CV ddH_2O. Now the column was prepared for storage by adding 20 %(v/v) Ethanol until a stable UV signal was detected. The column was removed under flow to prevent air form entering the column. Strep®-Tactin columns were stored at 4 °C and used multiple times as long as the same protein was purified. After the column was removed the system was washed with ddH_2O to completely flush out any residual buffers. Lastly the system as well as all pumps and tubing were filled with 20 %(v/v) ethanol to prevent contamination.

Quality control and storage

To verify the purity of protein preparations SDS-PAGE was performed with samples taken from the supernatant of the last centrifugation step (“load”), from the efflux during sample load (“flow-through”), from the efflux during washing (“wash”) and from all protein containing elution fractions (“E_i”). Elution fractions were assumed to be protein containing according to peak size and morphology in the chromatogram (UV trace). If a fluorescent protein was purified protein content was instead estimated through visual inspection of the elution fractions (yellowish color for GFP derivatives, orange color for mKO_κ derivates and pinkish color for mCherry derivates). All sufficiently pure and protein of interest containing fractions, according to apparent molecular weight estimated with SDS-PAGE and subsequent Coomassie staining, were pooled. After the pooling a buffer exchange was performed using PD10 gravity flow columns (GE Healthcare). Proteins were eluted from the PD10 columns with 3.5 mL Buffer W and fractions of 500 μL (10 droplets) were collected. The protein concentration of the PD10 elution fractions was measured *via* UV/Vis spectroscopy (NanoDrop1000). Yet again if a fluorescent protein was purified visual inspection was performed to sort out the desired fractions. Protein concentrations were calculated using the proteins specific extinction coefficient at either 280 nm (non-fluorescent proteins) or at their respective absorption maxima

(fluorescent proteins). If a fusion protein comprised of multiple fluorescent proteins the concentration was calculated based on the absorption of the most C-terminal fluorescent protein domain. This way the calculated concentration was considered to most truthfully represent the actual concentration of full-length protein in the preparation. Finally, all satisfactory fractions were pooled sterile filtered. Subsequently glycerol was added to a final concentration of 25 %(v/v) from a steam sterilized 50 %(v/v) glycerol in 1x Buffer W stock. If necessary the protein solution was diluted further with 25 % (v/v) glycerol in 1x Buffer W to a final concentration of 100 nM. For storage protein preparations were split into 20 μL aliquots and subsequently snap frozen in liquid nitrogen. Frozen aliquots were transferred from the liquid nitrogen to 50 mL reactions tubes for easy labeling and handling. Storage tubes were kept at -80 °C for long-term storage. Individual aliquots were stored at -20 °C during experiments.

6.2.13. Sodium dodecyl sulfate polyacrylamide gel electrophoresis (SDS-PAGE) and Western blotting

SDS-PAGE

Required solutions:

- Separation buffer
    - 1.5 M Tris, 0.4 %(w/v) SDS, pH 8.8
- Stacking buffer
    - 0.5 M Tris, 0.4 %(w/v) SDS, pH 6.6
- Rotiphorese® Gel 30 (Carl Roth)
    - Stored at 4 °C
- APS
    - 15 to 20 %(w/v) APS, freshly prepared
- TEMED
    - Stored at 4 °C
- ddH_2O
- SDS running buffer
    - 3.02 g/L Tris, 14.4 g/L glycine, 0.1 %(w/v) SDS, prepared as a 10x stock stored at RT
- 2x loading dye
    - 200 mM Na_3PO_4, 4 %(w/v) SDS, 20 %(v/v) glycerol, 0.002 %(w/v) bromophenol blue

All SDS-gels were casted with the Mini-PROTEAN® system using short plates together with 1 mm spacers. Separation gels were casted first to a height of approximately six cm. The casted separation gels were covered with isopropanol while hardening to smoothen the top edge and absorb excess water released during the process. Separation gel hardening was followed by observing the remainder casting solution as well as the appearing of a visible line between hardened gel and the isopropanol layer on top. Once the polymerization of the gel was complete the isopropanol layer was aspirated and the stacking gel was casted on top of the separation gel to a level just below the opening of the chamber. Immediately after casting the comb (usually 15 wells) was inserted into the gel casting chamber. Polymerization progress was monitored as before. Fully polymerized gels were either used directly or stored covered in moist paper towels at 4 °C to prevent dehydration. Excess polymer (displaced upon comb insertion) was removed before placing the gels into a Mini-Protein® Tetra cell (Bio-Rad). **Table 18** shows the composition of the SDS gels used in this work.

Table 18 Composition of SDS-Gels used in this worked. Volumes listed here suffice for two gels.

	Volume [mL]	
Component	**Stacking gel (5 %)**	**Separation gel (12 %)**
ddH_2O	2.65	2.9
Separation buffer	-	2.79
Stacking buffer	1.25	-
Rotiphorese® Gel 30 (Carl Roth)	0.83	5.37
APS (15 to 20 % (w/v))	0.2	0.17
TEMED	0.01	0.007

SDS-PAGE was performed either to analyze the outcome of protein purification experiments or evaluate the expression of recombinant proteins. Samples were prepared by taking the volume equivalent of cells corresponding to an OD_{600} of 5 in 40 μL from broth cultures. Subsequently, cells were harvested by centrifugation at 13000xg for one minute. The supernatant was carefully removed and if necessary cell pellets were transferred in to 1.5 mL reaction tubes or directly snap-frozen in liquid nitrogen. Frozen samples were stored at -20 °C until SDS-PAGE was performed. Thawed samples were resuspended in 20 μL of sterile water and 20 μL 2x loading dye was added. Sample were denatured at 95 °C for 5 min or semi-denatured at 72 °C for 3 min. Samples were semi-denatured to retain the fluorescence properties of fluorescent proteins. 20 μL of a sample were loaded per well. Electrophoresis was performed at 200 V for 45 min with Mini Protean system (BioRad) in 1x running buffer.

Following separation, protein bands were visualized with either epi-fluorescence in an Amersham Imager 600 RGB (epi-fluorescence mode, all channels, automatic exposure with

maximum dynamic range protocol), or by Coomassie staining using RotiBlue (Carl-Roth), or by western blotting. Coomassie stained gels were imaged in an E-BOX Stand-Alone Gel Documentation Imaging station equipped with a blue light LED transillumination table (Vilber). Western Blots were imaged in an Amersham Imager 600 RGB (chemiluminescence mode, colored marker, automatic exposure with maximum dynamic range protocol).

Western blotting

Required solutions:

- Blotting buffer
    - 48 mM Tris, 39 mM glycine, stored at RT
- 1x PBS
    - 4 mM KH_2PO_4, 16 mM Na_2HPO_4, 115 mM NaCl, pH 7.4, prepared as 10x stock, steam sterilized and stored at RT
- PBS blocking buffer
    - 3 %(w/v) BSA, 0.5 %(v/v) Tween20 in 1x PBS, freshly prepared from 10x PBS stock
- PBS Tween buffer
    - 0.1 %(v/v) Tween20 in 1x PBS, freshly prepared from 10x PBS stock

After electrophoretic separation of samples on polyacrylamide gels proteins were transferred onto 0.2 μm PVDF membranes *via* semi-dry blotting (Trans-Blot® Turbo, Bio-Rad). Blotting was performed at a constant current of 200 mA for 30 min. Subsequently, membranes were blocked by gently shaking in 20 mL PBS blocking buffer overnight at 4 °C or for one hour at RT. Afterwards membranes were washed two times with 20 mL PBS Tween buffer to remove excess BSA. If not stated otherwise, washing steps were performed by gently shaking the membrane in PBS Tween buffer for five minutes at room temperature. POIs were detected with primary antibodies diluted 1:2000 in 10 mL PBS Tween buffer. Antibody incubation steps were performed for one hour at room temperature while gently shaking. Excess antibodies were removed by two subsequent washing steps. Secondary antibody-HRP-conjugates targeting the primary antibodies were used to visualize the detected protein bands. Alternative, if POIs possessed a Strep-Tag II, POI were directly detected and visualized with Strep-Tactin HRP conjuagtes (BioRad). Secondary antibody incubation was performed as stated for the primary antibodies with the exception of secondary antibodies were diluted 1:5000. As before excess

antibodies were removed by two washing steps. Finally, membranes were washed once with 10 mL 1x PBS to prevent Tween20 interference during the chemiluminescence reaction. Chemiluminescence reaction was performed using the Clarity™ Western ECL substrate (Bio-Rad). Chemiluminescence was detected using the Amersham Imager 600 RGB (Amersham) with automatic exposure (maximum dynamic range protocol). Alternative to HRP conjugated secondary antibodies Alexa Fluor 633 conjugated antibodies were used when two different proteins were to be detected in the same sample.

6.2.14. *In vivo* protease assays for live *E. coli* cells based on degrons

Fluorescence rescue in *E. coli*

A dual plasmid-based expression system was utilized to co-express protease variants together with mNeonGreen (mNG) derivates. The mNeonGreen constructs comprised of the mNG domain, a recruitment domain – either SH3, FKBP or FRB. pPro24 was used to produce the protease variant under the control of the propionate inducible promoter. pCtrl2 was used to produce the sensors under the control of the T7 promoter or mutants thereof. pPro24 bore the pB332 ori which is a class A ori which is compatible with pCtrl2's class B p15A ori. Therefore, stable propagation of both plasmids was ensured. To avoid strong background fluorescence the M9 minimal medium was used to grow broth cultures. Cultures were cultivated overnight at 37 °C in 96 deep well plates (200 μL culture volume) or 24 well plates (1 mL culture volume) depending on the experiment. For the measurements, cultures were cultivated in black 96 well plates with flat and transparent bottoms. The black plates omitted transillumination between wells while the clear bottom facilitated transmission measurements through the wells to allow online measurements of the optical density of the cultures. Latter was crucial to allow the normalization of the measured mNG fluorescence to the optical density of the cultures. 190 or 195 μL assay cultures were inoculated to an OD_{600} of 0.1 (190 μL if two inducers were used; 195 μL if a single inducer was added). Subsequently plates were covered with a lid and incubated for two to six hours. The lid was fixated with tape to prevent sliding during incubation. This prove to be crucial to prevent abrasion of the lid. Otherwise particles grated off from the lid might have fallen into the wells. Protein overexpression was induced by adding 5 μL inducer stock solution per well (final concentrations: 500 μM IPTG or 25 mM sodium propionate). After the first inducer was added the plates were incubated for 2 h at 1050 rpm at 30 °C. Lastly the second inducers were addend and immediately afterwards plates were placed in a TECAN Spark plate reader. mNG fluorescence ((485 ±20) nm / (535 ± 20) nm; 10 flashes; gain = 70) and optical density at 600 nm were measured in intervals of 15 min over the course of six hours. In between measurements plates were shook with double orbital movements

(2 mm amplitude, 185 rpm). To account for possible alterations in *E. coli* auto-fluorescence due to dual overexpression a control was included. This control co-expressed mKOκ instead of a mNeonGreen sensor together with the protease/mock construct in question. mKOκ fluorescence was omitted through the emission filter setting (see **Chapter 13.3.2**). Therefore, the change in auto-fluorescence in response to the expression of a monomeric fluorescent protein was measured exclusively.

The measured fluorescence intensities were normalized to the respective optical densities at 600 nm. This was necessary because a higher cell density per well led to higher total fluorescence intensities per well.

$$\frac{mNeonGreenfluorescence}{opticaldensityat600nm} - \frac{auto-fluorescenceundermKO_{\kappa}expression}{opticaldensityat600nm}$$

The normalized data were plotted against the time and the range of linear increase in fluorescence was estimated. Usually linear increase fluorescence occurred in between two and four to five hours after induction of the sensor. A linear regression analysis was performed within this range. The received slopes were deemed a sufficient measure for the apparent *in vivo* activity of the tested construct. Thereafter the fold change in slope of a protease construct compared to the corresponding mock construct was calculated. For each biological multiplicate the fold changes were averaged to estimate the biological variance of the system. In most cases the standard deviation from the mean values were equal to or less than two percent of the mean values.

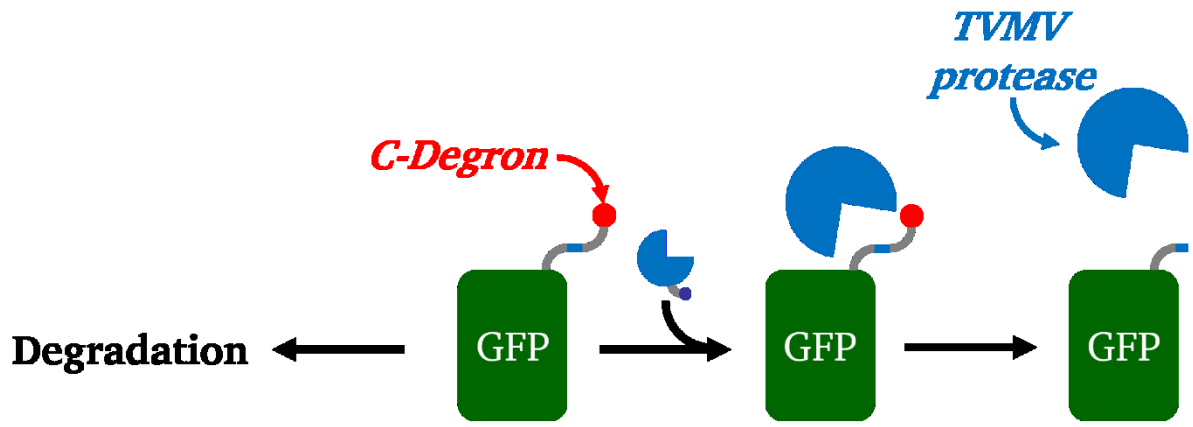

Scheme 22 Fluorescence rescue *in vivo* assay based on conditionally active C-degrons.

Ratiometric assay in *E. coli*

This assay was based on the fluorescence rescue assay as described in the previous subchapter. The aim was to access a more robust normalization condition as well as the discrimination of non-expression of the sensor from total abolishment of apparent fluorescence through efficient degradation. Thus the C-terminal degrons were replaced by cryptic N-terminal degrons published by the Voight lab [21]. The N-terminal degron was masked with mNeonGreen. The linker contained the protease cleavage site. The first amino acid of the degron was cloned at the P1' position of the cleavage site. Accordingly, upon protease cleavage the degron containing part of the fusion protein was released without any additional amino acids N-terminally of the degron which might had interfered with degron activity. The tested degrons were FLFVQ and YLFVQ respectively. C-terminally of the N-degron mCherry was cloned (see **Scheme 23**). Therefore, upon successful protease cleavage rapid degradation of mCherry should have occurred while mNeonGreen fluorescence should have remained unaffected by protease cleavage. In this case the mCherry fluorescence was normalized to mNeonGreen fluorescence. In contrast to the fluorescence rescue assay the loss of fluorescence over time was used to quantify the apparent *in vivo* activity of the protease constructs.

$$\frac{mCherryfluorescence}{mNeonGreenfluorescence}$$

Due to faster maturation time and higher photon quantum yield the mCherry fluorescence values were significantly lower compared to the mNeonGreen fluorescence values. This was true even after the gain for mCherry flourescence was increased from 70 to 100. This resulted in small quotients between both fluorescence intensities. Nevertheless, the fold change between the slopes of the linear regressions were calculated and compared as beforehand.

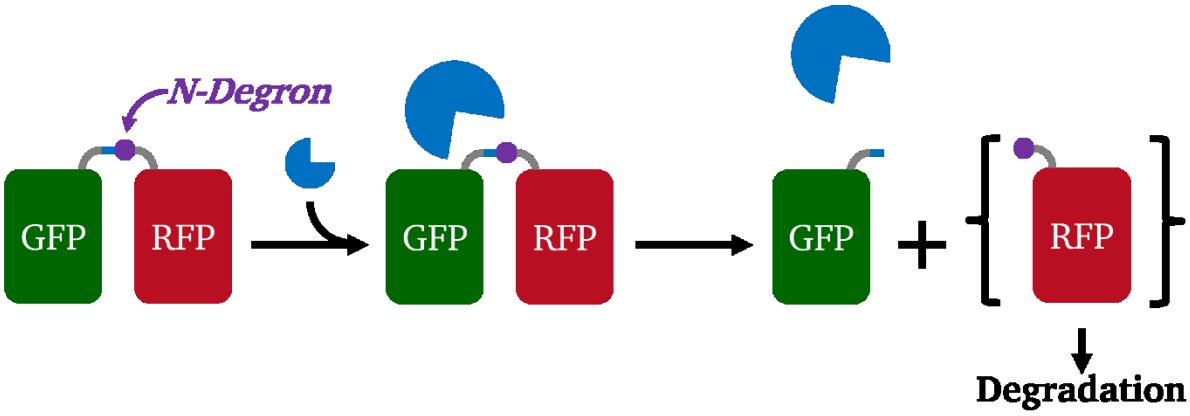

Scheme 23 Ratiometric *in vivo* protease assay based on Cryptic. N-degron.

7. References

1. Stein, V. and K. Alexandrov, *Protease-based synthetic sensing and signal amplification.* Proceedings of the National Academy of Sciences, 2014. **111**(45): p. 15934-15939.
2. Stein, V. and K. Alexandrov, *Synthetic protein switches: design principles and applications.* Trends in Biotechnology, 2015. **33**(2): p. 101-110.
3. Stein, V., M. Nabi, and K. Alexandrov, *Ultrasensitive Scaffold-Dependent Protease Sensors with Large Dynamic Range.* ACS Synthetic Biology, 2017. **6**(7): p. 1337-1342.
4. Gräwe, A., et al., *Engineering artificial signalling functions with proteases.* Current Opinion in Biotechnology, 2020. **63**: p. 1-7.
5. Müller, K., M.D. Zurbriggen, and W. Weber, *Control of gene expression using a red- and far-red light-responsive bi-stable toggle switch.* Nat Protoc, 2014. **9**(3): p. 622-32.
6. Zhang, F., J.M. Carothers, and J.D. Keasling, *Design of a dynamic sensor-regulator system for production of chemicals and fuels derived from fatty acids.* Nat Biotechnol, 2012. **30**(4): p. 354-9.
7. Slusarczyk, A.L., A. Lin, and R. Weiss, *Foundations for the design and implementation of synthetic genetic circuits.* Nat Rev Genet, 2012. **13**(6): p. 406-20.
8. Ivask, A., T. Rõlova, and A. Kahru, *A suite of recombinant luminescent bacterial strains for the quantification of bioavailable heavy metals and toxicity testing.* BMC Biotechnol, 2009. **9**: p. 41.
9. Bayer, T.S., et al., *Synthesis of methyl halides from biomass using engineered microbes.* J Am Chem Soc, 2009. **131**(18): p. 6508-15.
10. Emanuelsson, O., et al., *Locating proteins in the cell using TargetP, SignalP and related tools.* Nat Protoc, 2007. **2**(4): p. 953-71.
11. Burgess-Beusse, B., et al., *The insulation of genes from external enhancers and silencing chromatin.* Proc Natl Acad Sci U S A, 2002. **99 Suppl 4**(Suppl 4): p. 16433-7.
12. Win, M.N. and C.D. Smolke, *Higher-order cellular information processing with synthetic RNA devices.* Science, 2008. **322**(5900): p. 456-60.
13. Chen, X., J.L. Zaro, and W.C. Shen, *Fusion protein linkers: property, design and functionality.* Adv Drug Deliv Rev, 2013. **65**(10): p. 1357-69.
14. Szymczak-Workman, A.L., K.M. Vignali, and D.A. Vignali, *Design and construction of 2A peptide-linked multicistronic vectors.* Cold Spring Harb Protoc, 2012. **2012**(2): p. 199-204.
15. Moon, T.S., et al., *Genetic programs constructed from layered logic gates in single cells.* Nature, 2012. **491**(7423): p. 249-53.
16. Sohka, T., et al., *An externally tunable bacterial band-pass filter.* Proc Natl Acad Sci U S A, 2009. **106**(25): p. 10135-40.
17. Guido, N.J., et al., *A bottom-up approach to gene regulation.* Nature, 2006. **439**(7078): p. 856-60.
18. Rinaudo, K., et al., *A universal RNAi-based logic evaluator that operates in mammalian cells.* Nat Biotechnol, 2007. **25**(7): p. 795-801.
19. Leisner, M., et al., *Rationally designed logic integration of regulatory signals in mammalian cells.* Nat Nanotechnol, 2010. **5**(9): p. 666-70.
20. Wang, Y.-H., K.Y. Wei, and C.D. Smolke, *Synthetic Biology: Advancing the Design of Diverse Genetic Systems.* Annual Review of Chemical and Biomolecular Engineering, 2013. **4**(1): p. 69-102.
21. Fernandez-Rodriguez, J. and C.A. Voigt, *Post-translational control of genetic circuits using Potyvirus proteases.* Nucleic Acids Research, 2016. **44**(13): p. 6493-6502.
22. Fink, T., et al., *Design of fast proteolysis-based signaling and logic circuits in mammalian cells.* Nature Chemical Biology, 2018.
23. Gao, X.J., et al., *Programmable protein circuits in living cells.* Science, 2018. **361**(6408): p. 1252-1258.

24. Gao, C., et al., *Programmable biomolecular switches for rewiring flux in Escherichia coli.* Nature Communications, 2019. **10**(1): p. 3751.
25. Durante-Rodríguez, G., V. de Lorenzo, and P.I. Nikel, *A Post-translational Metabolic Switch Enables Complete Decoupling of Bacterial Growth from Biopolymer Production in Engineered Escherichia coli.* ACS Synthetic Biology, 2018. **7**(11): p. 2686-2697.
26. Sedlmayer, F., D. Aubel, and M. Fussenegger, *Synthetic gene circuits for the detection, elimination and prevention of disease.* Nature Biomedical Engineering, 2018. **2**(6): p. 399-415.
27. Roquet, N. and T.K. Lu, *Digital and analog gene circuits for biotechnology.* Biotechnol J, 2014. **9**(5): p. 597-608.
28. Zhang, J., et al., *Creating new fluorescent probes for cell biology.* Nat Rev Mol Cell Biol, 2002. **3**(12): p. 906-18.
29. Binkowski, B., F. Fan, and K. Wood, *Engineered luciferases for molecular sensing in living cells.* Curr Opin Biotechnol, 2009. **20**(1): p. 14-8.
30. van der Meer, J.R. and S. Belkin, *Where microbiology meets microengineering: design and applications of reporter bacteria.* Nat Rev Microbiol, 2010. **8**(7): p. 511-22.
31. Deans, T.L., C.R. Cantor, and J.J. Collins, *A tunable genetic switch based on RNAi and repressor proteins for regulating gene expression in mammalian cells.* Cell, 2007. **130**(2): p. 363-72.
32. Liu, C., et al., *Sequential establishment of stripe patterns in an expanding cell population.* Science, 2011. **334**(6053): p. 238-41.
33. Lu, T.K. and J.J. Collins, *Dispersing biofilms with engineered enzymatic bacteriophage.* Proc Natl Acad Sci U S A, 2007. **104**(27): p. 11197-202.
34. Siddiqui, M.S., et al., *Advancing secondary metabolite biosynthesis in yeast with synthetic biology tools.* FEMS Yeast Res, 2012. **12**(2): p. 144-70.
35. Phan, J., et al., *Structural Basis for the Substrate Specificity of Tobacco Etch Virus Protease.* Journal of Biological Chemistry, 2002. **277**(52): p. 50564-50572.
36. Sun, P., et al., *Structural determinants of tobacco vein mottling virus protease substrate specificity.* Protein Science, 2010. **19**(11): p. 2240-2251.
37. Hellmann, G.M., J.G. Shaw, and R.E. Rhoads, *In vitro analysis of tobacco vein mottling virus Nla cistron: Evidence for a virus-encoded protease.* Virology, 1988. **163**(2): p. 554-562.
38. Hwang, D.C., et al., *Characterization of Active-Site Residues of the NIa Protease from Tobacco Vein Mottling Virus.* Molecules and Cells, 2000. **10**(5): p. 505-511.
39. ADAMS, M.J., J.F. ANTONIW, and F. BEAUDOIN, *Overview and analysis of the polyprotein cleavage sites in the family Potyviridae.* Molecular Plant Pathology, 2005. **6**(4): p. 471-487.
40. Yoon, H.Y., et al., *Proteolytic Processing of Oligopeptides Containing the Target Sequences by the Recombinant Tobacco Vein Mottling Virus NIa Proteinase.* Molecules and Cells, 2000. **10**(2): p. 213-219.
41. Hwang, D.C., et al., *Molecular Cloning, Expression, and Purification of Nuclear Inclusion A Protease from Tobacco Vein Mottling Virus.* Molecules and Cells, 2000. **10**(2): p. 148-155.
42. Fang, L., et al., *An improved strategy for high-level production of TEV protease in Escherichia coli and its purification and characterization.* Protein Expression and Purification, 2007. **51**(1): p. 102-109.
43. Mak, P., et al., *Reconstitution of hepatitis C virus protease activities in yeast.* FEBS Letters, 2001. **503**(1): p. 13-18.
44. Love, R.A., et al., *The Crystal Structure of Hepatitis C Virus NS3 Proteinase Reveals a Trypsin-like Fold and a Structural Zinc Binding Site.* Cell, 1996. **87**(2): p. 331-342.

45. Gräwe, A., et al., *iFLinkC: an iterative functional linker cloning strategy for the combinatorial assembly and recombination of linker peptides with functional domains.* Nucleic Acids Research, 2020. **48**(4): p. e24-e24.
46. Brian, D.A. and R.S. Baric, *Coronavirus genome structure and replication.* Curr Top Microbiol Immunol, 2005. **287**: p. 1-30.
47. Zhang, L., et al., *Crystal structure of SARS-CoV-2 main protease provides a basis for design of improved α-ketoamide inhibitors.* Science, 2020. **368**(6489): p. 409-412.
48. Mairhofer, J., et al., *Comparative transcription profiling and in-depth characterization of plasmid-based and plasmid-free Escherichia coli expression systems under production conditions.* Appl Environ Microbiol, 2013. **79**(12): p. 3802-12.
49. Dong, H., L. Nilsson, and C.G. Kurland, *Gratuitous overexpression of genes in Escherichia coli leads to growth inhibition and ribosome destruction.* Journal of Bacteriology, 1995. **177**(6): p. 1497-1504.
50. Novick, R.P., *Plasmid incompatibility.* Microbiol Rev, 1987. **51**(4): p. 381-95.
51. Nicholls, S.B., et al., *Mechanism of a Genetically Encoded Dark-to-Bright Reporter for Caspase Activity.* Journal of Biological Chemistry, 2011. **286**(28): p. 24977-24986.
52. Nicholls, S.B. and J.A. Hardy, *Structural basis of fluorescence quenching in caspase activatable-GFP.* Protein Science : A Publication of the Protein Society, 2013. **22**(3): p. 247-257.
53. Wu, P., Samantha B. Nicholls, and Jeanne A. Hardy, *A Tunable, Modular Approach to Fluorescent Protease-Activated Reporters.* Biophysical Journal, 2013. **104**(7): p. 1605-1614.
54. Do, K. and S.G. Boxer, *Thermodynamics, Kinetics, and Photochemistry of Beta-Strand Association and Dissociation in a Split-GFP System.* Journal of the American Chemical Society, 2011. **133**(45): p. 18078-18081.
55. Do, K. and S.G. Boxer, *GFP Variants with Alternative β-Strands and Their Application as Light-driven Protease Sensors: A Tale of Two Tails.* Journal of the American Chemical Society, 2013. **135**(28): p. 10226-10229.
56. Algar, W.R., et al., *FRET as a biomolecular research tool — understanding its potential while avoiding pitfalls.* Nature Methods, 2019. **16**(9): p. 815-829.
57. Takai, A., et al., *Expanded palette of Nano-lanterns for real-time multicolor luminescence imaging.* Proceedings of the National Academy of Sciences, 2015. **112**(14): p. 4352-4356.
58. Hiblot, J., et al., *Luciferases with Tunable Emission Wavelengths.* Angewandte Chemie, 2017. **129**(46): p. 14748-14752.
59. Suzuki, K., et al., *Five colour variants of bright luminescent protein for real-time multicolour bioimaging.* Nature Communications, 2016. **7**: p. 13718.
60. Arts, R., S.J.A. Aper, and M. Merkx, *Chapter Three - Engineering BRET-Sensor Proteins*, in *Methods in Enzymology*, R.B. Thompson and C.A. Fierke, Editors. 2017, Academic Press. p. 87-114.
61. Dacres, H., et al., *Direct comparison of fluorescence- and bioluminescence-based resonance energy transfer methods for real-time monitoring of thrombin-catalysed proteolytic cleavage.* Biosensors and Bioelectronics, 2009. **24**(5): p. 1164-1170.
62. Nguyen, A.W. and P.S. Daugherty, *Evolutionary optimization of fluorescent proteins for intracellular FRET.* Nature Biotechnology, 2005. **23**(3): p. 355-360.
63. Vinkenborg, J.L., et al., *Enhanced Sensitivity of FRET-Based Protease Sensors by Redesign of the GFP Dimerization Interface.* ChemBioChem, 2007. **8**(10): p. 1119-1121.
64. Zhang, B., *Design of FRET-based GFP probes for detection of protease inhibitors.* Biochemical and Biophysical Research Communications, 2004. **323**(2): p. 674-678.
65. den Hamer, A., et al., *Bright Bioluminescent BRET Sensor Proteins for Measuring Intracellular Caspase Activity.* ACS Sensors, 2017. **2**(6): p. 729-734.

66. Ding, Y., et al., *Ratiometric biosensors based on dimerization-dependent fluorescent protein exchange.* Nat Meth, 2015. **12**(3): p. 195-198.
67. Hahlbrock, A., D. Gößwein, and R.H. Stauber, *Protein Translocation Assays to Probe Protease Function and Screen for Inhibitors*, in *Protein Terminal Profiling: Methods and Protocols*, O. Schilling, Editor. 2017, Springer New York: New York, NY. p. 227-241.
68. Pu, J., et al., *A Panel of Protease-Responsive RNA Polymerases Respond to Biochemical Signals by Production of Defined RNA Outputs in Live Cells.* Journal of the American Chemical Society, 2015. **137**(51): p. 15996-15999.
69. Boch, J. and U. Bonas, *Xanthomonas AvrBs3 family-type III effectors: discovery and function.* Annu Rev Phytopathol, 2010. **48**: p. 419-36.
70. Copeland, M.F., et al., *A transcription activator-like effector (TALE) induction system mediated by proteolysis.* Nat Chem Biol, 2016. **12**(4): p. 254-260.
71. Lonzarić, J., et al., *Locked and proteolysis-based transcription activator-like effector (TALE) regulation.* Nucleic Acids Research, 2016. **44**(3): p. 1471-1481.
72. Köhler, F., *A yeast-based growth assay for the analysis of site-specific proteases.* Nucleic Acids Research, 2003. **31**(4): p. e16.
73. Varshavsky, A., *The N-end rule pathway of protein degradation.* Genes to Cells, 1997. **2**(1): p. 13-28.
74. Varshavsky, A., *The N-end rule: functions, mysteries, uses.* Proc Natl Acad Sci USA, 1996. **93**.
75. Varshavsky, A., *The N-end rule.* Cell, 1992. **69**.
76. Chen, S.-J., A. Melnykov, and A. Varshavsky, *Evolution of Substrates and Components of the Pro/N-Degron Pathway.* Biochemistry, 2020. **59**(4): p. 582-593.
77. Varshavsky, A., *N-degron and C-degron pathways of protein degradation.* Proceedings of the National Academy of Sciences of the United States of America, 2019. **116**(2): p. 358-366.
78. Nishimura, K. and K.J. van Wijk, *Organization, function and substrates of the essential Clp protease system in plastids.* Biochimica et Biophysica Acta (BBA) - Bioenergetics, 2015. **1847**(9): p. 915-930.
79. Yu, G., et al., *Pac-Man for biotechnology: co-opting degrons for targeted protein degradation to control and alter cell function.* Current Opinion in Biotechnology, 2015. **36**: p. 199-204.
80. Sekar, K., et al., *N-Terminal-Based Targeted, Inducible Protein Degradation in Escherichia coli.* PLOS ONE, 2016. **11**(2): p. e0149746.
81. Imburgio, D., et al., *Studies of Promoter Recognition and Start Site Selection by T7 RNA Polymerase Using a Comprehensive Collection of Promoter Variants.* Biochemistry, 2000. **39**(34): p. 10419-10430.
82. Olins, P.O. and S.H. Rangwala, *A novel sequence element derived from bacteriophage T7 mRNA acts as an enhancer of translation of the lacZ gene in Escherichia coli.* J Biol Chem, 1989. **264**(29): p. 16973-6.
83. Banaszynski, L.A., C.W. Liu, and T.J. Wandless, *Characterization of the FKBP·Rapamycin·FRB Ternary Complex.* Journal of the American Chemical Society, 2005. **127**(13): p. 4715-4721.
84. Diaz, G.A., C.A. Raskin, and W.T. McAllister, *Hierarchy of Base-Preference in the Binding Domain of the Bacteriophage T7 Promoter.* Journal of Molecular Biology, 1993. **229**(4): p. 805-811.
85. Shaner, N.C., et al., *A bright monomeric green fluorescent protein derived from Branchiostoma lanceolatum.* Nature Methods, 2013. **10**(5): p. 407-409.
86. Kemmerer, K. and J.E. Weigand, *Hypoxia reduces MAX expression in endothelial cells by unproductive splicing.* FEBS Letters, 2014. **588**(24): p. 4784-4790.
87. Lee, S.K. and J.D. Keasling, *A Propionate-Inducible Expression System for Enteric Bacteria.* Applied and Environmental Microbiology, 2005. **71**(11): p. 6856-6862.

88. Ponchon, L., et al., *Co-expression of RNA–protein complexes in Escherichia coli and applications to RNA biology.* Nucleic Acids Research, 2013. **41**(15): p. e150-e150.
89. Aidelberg, G., et al., *Hierarchy of non-glucose sugars in Escherichia coli.* BMC Systems Biology, 2014. **8**(1): p. 133.
90. Davis, J.H., T.A. Baker, and R.T. Sauer, *Small-Molecule Control of Protein Degradation Using Split Adaptors.* ACS Chemical Biology, 2011. **6**(11): p. 1205-1213.
91. Tu, G.-F., et al., *C-terminal Extension of Truncated Recombinant Proteins in Escherichia coli with a 10Sa RNA Decapeptide.* Journal of Biological Chemistry, 1995. **270**(16): p. 9322-9326.
92. Keiler, K.C., P.R.H. Waller, and R.T. Sauer, *Role of a Peptide Tagging System in Degradation of Proteins Synthesized from Damaged Messenger RNA.* Science, 1996. **271**(5251): p. 990-993.
93. Neupert, J., D. Karcher, and R. Bock, *Design of simple synthetic RNA thermometers for temperature-controlled gene expression in Escherichia coli.* Nucleic Acids Research, 2008. **36**(19): p. e124-e124.
94. Posern, G., et al., *Development of highly selective SH3 binding peptides for Crk and CRKL which disrupt Crk-complexes with DOCK180, SoS and C3G.* Oncogene, 1998. **16**(15): p. 1903-1912.
95. Shaner, N.C., et al., *Improved monomeric red, orange and yellow fluorescent proteins derived from Discosoma sp. red fluorescent protein.* Nature Biotechnology, 2004. **22**(12): p. 1567-1572.
96. Kawano, F., et al., *Engineered pairs of distinct photoswitches for optogenetic control of cellular proteins.* Nature Communications, 2015. **6**: p. 6256.
97. Zoltowski, B.D., et al., *Conformational switching in the fungal light sensor Vivid.* Science (New York, N.Y.), 2007. **316**(5827): p. 1054-1057.
98. Baumschlager, A., S.K. Aoki, and M. Khammash, *Dynamic Blue Light-Inducible T7 RNA Polymerases (Opto-T7RNAPs) for Precise Spatiotemporal Gene Expression Control.* ACS Synthetic Biology, 2017. **6**(11): p. 2157-2167.
99. !!! INVALID CITATION !!! [1, 3, 45].
100. Hörner, M., et al., *Production of Phytochromes by High-Cell-Density E. coli Fermentation.* ACS Synthetic Biology, 2019.
101. Shimizu-Sato, S., et al., *A light-switchable gene promoter system.* Nature Biotechnology, 2002. **20**(10): p. 1041-1044.
102. St-Pierre, F., et al., *One-Step Cloning and Chromosomal Integration of DNA.* ACS Synthetic Biology, 2013. **2**(9): p. 537-541.
103. Tsutsui, H., et al., *Improving membrane voltage measurements using FRET with new fluorescent proteins.* Nature Methods, 2008. **5**(8): p. 683-685.
104. Hochuli, E., et al., *Genetic Approach to Facilitate Purification of Recombinant Proteins with a Novel Metal Chelate Adsorbent.* Bio/Technology, 1988. **6**(11): p. 1321-1325.
105. Duplay, P., et al., *Sequences of the malE gene and of its product, the maltose-binding protein of Escherichia coli K12.* J Biol Chem, 1984. **259**(16): p. 10606-13.
106. Schmidt, T.G. and A. Skerra, *The Strep-tag system for one-step purification and high-affinity detection or capturing of proteins.* Nat Protoc, 2007. **2**(6): p. 1528-35.
107. Skerra, A. and T.G.M. Schmidt, *[18] Use of the Strep- tag and streptavidin for detection and purification of recombinant proteins*, in *Methods in Enzymology*. 2000, Academic Press. p. 271-304.
108. Munro, S. and H.R. Pelham, *Use of peptide tagging to detect proteins expressed from cloned genes: deletion mapping functional domains of Drosophila hsp 70.* Embo j, 1984. **3**(13): p. 3087-93.
109. Cabrita, L.D., et al., *Enhancing the stability and solubility of TEV protease using in silico design.* Protein Science, 2007. **16**(11): p. 2360-2367.

110. Ingallinella, P., et al., *Optimization of the P'-Region of Peptide Inhibitors of Hepatitis C Virus NS3/4A Protease.* Biochemistry, 2000. **39**(42): p. 12898-12906.
111. Protocols, C.S.H., *Sodium phosphate.* Cold Spring Harbor Protocols, 2006. **2006**(1): p. pdb.rec8303.
112. *LB (Luria-Bertani) liquid medium.* Cold Spring Harbor Protocols, 2006. **2006**(1): p. pdb.rec8141.
113. *SOC Medium.* Cold Spring Harbor Protocols, 2018. **2018**(3): p. pdb.rec098863.
114. Hertig, S., et al., *Multidomain Assembler (MDA) Generates Models of Large Multidomain Proteins.* Biophysical Journal, 2015. **108**(9): p. 2097-2102.
115. Chen, J.E., C.C. Huang, and T.E. Ferrin, *RRDistMaps: a UCSF Chimera tool for viewing and comparing protein distance maps.* Bioinformatics, 2015. **31**(9): p. 1484-1486.
116. Huang, C.C., et al., *Enhancing UCSF Chimera through web services.* Nucleic Acids Research, 2014. **42**(W1): p. W478-W484.
117. Yang, Z., et al., *UCSF Chimera, MODELLER, and IMP: An integrated modeling system.* Journal of Structural Biology, 2012. **179**(3): p. 269-278.
118. Pintilie, G.D., et al., *Quantitative analysis of cryo-EM density map segmentation by watershed and scale-space filtering, and fitting of structures by alignment to regions.* Journal of Structural Biology, 2010. **170**(3): p. 427-438.
119. Morris, J.H., et al., *structureViz: linking Cytoscape and UCSF Chimera.* Bioinformatics, 2007. **23**(17): p. 2345-2347.
120. Goddard, T.D., C.C. Huang, and T.E. Ferrin, *Visualizing density maps with UCSF Chimera.* Journal of Structural Biology, 2007. **157**(1): p. 281-287.
121. Meng, E.C., et al., *Tools for integrated sequence-structure analysis with UCSF Chimera.* BMC Bioinformatics, 2006. **7**(1): p. 339.
122. Couch, G.S., D.K. Hendrix, and T.E. Ferrin, *Nucleic acid visualization with UCSF Chimera.* Nucleic Acids Research, 2006. **34**(4): p. e29-e29.
123. Goddard, T.D., C.C. Huang, and T.E. Ferrin, *Software Extensions to UCSF Chimera for Interactive Visualization of Large Molecular Assemblies.* Structure, 2005. **13**(3): p. 473-482.
124. Pettersen, E.F., et al., *UCSF Chimera—A visualization system for exploratory research and analysis.* Journal of Computational Chemistry, 2004. **25**(13): p. 1605-1612.
125. Rueden, C.T., et al., *ImageJ2: ImageJ for the next generation of scientific image data.* BMC Bioinformatics, 2017. **18**(1): p. 529.
126. Schneider, C.A., W.S. Rasband, and K.W. Eliceiri, *NIH Image to ImageJ: 25 years of image analysis.* Nature Methods, 2012. **9**(7): p. 671-675.
127. Schindelin, J., et al., *Fiji: an open-source platform for biological-image analysis.* Nature Methods, 2012. **9**(7): p. 676-682.

8. List of Publications

1) Gräwe, Alexander; Ranglack, Jan Weyrich, Anastasia; Stein, Viktor, iFLinkC: an iterative functional linker cloning strategy for the combinatorial assembly and recombination of linker peptides with functional domains. Nucleic Acids Research, 2020. **48**(4): p. e24-e24.
2) Gräwe, Alexander; Ranglack, Jan; Weber, Wadim; Stein, Viktor, Engineering artificial signalling functions with proteases. Current Opinion in Biotechnology, 2020. **63**: p. 1-7.

9. List of Abbreviations

A	alanine
AHT	anhydrotetracycline
AI	auto-inhibiting
AmpR	ampicillin resistance
APS	Ammonium persulfate
BRET	bioluminescence resonance energy transfer
BSA	bovine serum albumin
C	cysteine
CamR	chloramphenicol resistance
C-degron	C-terminal degradation tag
CDS	coding sequence
CFU	colony forming units
ClpX	caseinolytic protease complex
COVID19	corona virus ID 2019
SARS-CoV2 ^{M}Pro	Severe acute respiratory syndrome corona virus 2 main protease
C-terminal	located at the C-terminus
C-terminus	Carboxy-Terminus
CV	column volume
D	glutamic acid
Degron	degradation tag
DMSO	Dimethyl sulfoxide
DNA	desoxyribonucleic acid
DNase	desoxyribonuclease
dNTP	Desoxyribonucleotide triphosphate
DTT	dithiothreitol
E	aspartic acid
E. coli	*Escherichia coli*
E118min	minimal variant of E118-134
EC	enzyme class (IUPAC)
ECL	enhanced chemiluminescence
EDTA	Ethylenediaminetetraacetic acid
F	phenylalanine
FACS	fluorescence activated cell sorting
FAD	flavin adenine dinucleotide
FK506	tacrolimus
FKBP	FK506 binding protein
FP	fluorescent protein
FPLC	flow pressure liquid chromatography
FPX	fluorescent protein exchange

FRB	FKBP rapamycin binding protein
FRET	Förster resonance energy transfer
G	glycine
GFP	green fluorescent protein
H	histidine
HABA	2-[4 -hydroxy-benzeneazo]benzoic acid
HCV	hepatitis C virus, also as synonym for HCV protease
His	histidine
HRP	horseradish peroxidase
I	isoleucine
IDT	Integrated DNA Technologies
iFLinkC	iterative Functional Linker Cloning
IGEPAL	octylphenoxypolyethoxyethanol
IMAC	Immobilized metal ion affinity chromatography
IPTG	Isopropyl-β-D-thiogalactopyranosid
K	lysine
kDa	kilo Dalton
L	leucine
Lac	lactose
lacI	lac repressor
lacO	lac operator
LB	lysogenic broth
lonp	lon protease
LVA	derivate of ssrA
M	methionine
M9	minimal medium 9
mAB	monoclonal antibody
MBP	maltose binding protein
mCh	mCherry
mCherry	monomeric Cherry
MCS	multiple cloning site
mKO_{κ}	monomeric Kusabira-Orange kappa
mNeonGreen	monomeric NeonGreen
mNG	mNeonGreen
MWCO	molecular weight cut off
N	asparagine
NanoLuc	nano luciferase
NaPro	sodium propionate
N-degron	N-terminal degradation tag
NEB	New England Biolabs
NES	nuclear export sequence

Ni-NTA	nickel nitrilotriacetic acid
NLS	nuclear localization sequence
nMag	negative magnet
N-terminal	located at the N-terminus
N-terminus	amino terminus
OD_{600}	optical density at 600 nm
oePCR	overlap extension PCR
ori	origin of replication
P	proline
PAA	polyacrylamide
pAB	polyclonal antibody
PBS	phosphate buffered saline
PCB	phycocyanobillin
PCR	polymerase chain reaction
pFD	plasmid for functional domains
PhyB	phytochrome B
PIF6	phytochrome interacting factor 6
pL2	plasmid for Linkers 2
pMag	positive magnet
POI	protein of interest
Pols	polymerases
prp	propionate
PVDF	polyvinylidene difluoride
Q	glutamine
R	arginine
R^2	coefficient of determination
Rap	rapamycin
Ras	rat sarcoma
RBS	ribosome binding site
RFP	red fluorescent protein
RGB	red green blue color space
RNA	ribonucleic acid
rSAP	Shrimp Alkaline Phosphatase
RT	room temperature
S	serine
SBOL	Synthetic Biology Open Language
SBV	sample beaker volume
SDS	sodium dodecyl sulfate
sfGFP	super folder GFP
SH3	Src Homology 3
SOC	Super optimal broth with catabolite supression

sSH3L	strong SH3 ligand
ssOligos	single stranded oligo nucleotides
ssoverhang	single stranded (DNA) overhang
ssrA	small stable RNA A
SuMMV	sunflower mild mosaic virus, also as synoym for SuMMV protease
SynBio	Synthetic Biology
T	threonine
TAE	Tris-acetate-EDTA
TALE	transcription activator-like effector
TB	terrific broth
TEMED	Tetramethyl ethylenediamine
TEV	tobacco etch virus, also as synonym for TEV protease
TVMV	tobacco vein mottling virus, also as synonym for TVMV protease
Tween20	Polyoxyethylene (20) sorbitan monolaurate
UV	ultraviolet
V	valine
W	tryptophan
wSH3L	weak SH3 ligand
xSH3L	strong or weak SH3 ligand
Y	tyrosine
YFP	yellow fluorescent protein

10. List of Figures

Figure 28 Direct comparison of three different proteases with the LVA C-degron based assay. **A:** Schematic depiction of the experiment: The basic C-degron assay was performed as explained in **Chapter 4.2** with three site-specific proteases TEV, TVMV and HCV in direct comparison. **B:** Real-time kinetic data of *in vivo* protease activity measured over the course of 8 hours; Colors and symbols as in **Figure 15,** proteases and corresponding inactive variants are listed above the corresponding graphs, sensors are listed in the central legend, data points represent the mean values of dependent biological quadruplicates measured, error areas depict the SEM. **C:** Fold changes between active and inactive protease variant, bars represent the mean slopes of the protease dependent increase in mNeonGreen fluorescence, error bars depict the SEM, filled bars for active proteases, empty bars for inactive proteases, brackets above the paired bars state the corresponding fold changes in slope. Constructs used: pPRO24_MBP-^{TVMV}sSH3L-TVMV-Strep, pPRO24_MBP-^{TVMV}sSH3L-TVMV^{C151A}-Strep, pPRO24_MBP-^{TVMV}sSH3L-TEV-Strep, pPRO24_MBP-^{TVMV}sSH3LTEV^{C151A}-Strep, pPRO24_MBP-^{TVMV}sSH3L-HCV-Strep, pPRO24_MBP-^{TVMV}sSH3L-HCV^{S152A}-Strep, pCtrl2_T7.03_U9_myc-SH3-mNG-^{TVMV}, pCtrl2_T7.03_U9_myc-SH3-mNG-^{TVMV}LVA, pCtrl2_T7.03_U9_myc-SH3-mNG-^{TEV}, pCtrl2_T7.03_U9_myc-SH3-mNG-^{TEV}LVA, pCtrl2_T7.03_U9_myc-SH3-mNG-^{HCV}, pCtrl2_T7.03_U9_myc-SH3-mNG-^{HCV}LVA, pCtrl2_mKO$_\kappa$. Protein Sequences are stated in the supplement (see **13.4.9**). TEV and HCV related constructs were cloned by C. Rühmkorff; all data shown in this figure were generated by C. Rühmkorff under my supervision. 70

Figure 29 Western blot analysis of protease expression under assay conditions. Double transformed *E. coli* BL21(DE3) cultures were grown in M9 at 37 °C for 2 h. Subsequently, protease expression was induced with 25 mM sodium propionate and cultures were incubated at 30 °C. Another two hours later, the expression of the sensor was induced with 1 mM IPTG. Samples were taken before protease induction (2h timepoint), before sensor induction (4h timepoint) and 6 h after sensor induction (10 h timepoint, the usually endpoint of the *in vivo* assays). Then 20 μL cell suspension with an OD_{600} = 5 were loaded per lane. The pictograms to the right of the individual Western blots show the expected protease bands, the upper band around 68 kDa when the MBP solubility tag is not cleaved off and the lower band around 28 kDa for the autocatalytically processed protease construct. The weak band at 35 kDa belongs to BirA which corresponds to the the biotin ligase of *E. coli* and is always detected through Strep-Tactin. The +/- refers to the presence of the LVA C-Degron in the co-expressed sensor constructs. The expression of the sensor was generally included to fully mimic the assay conditions during expression tests.

11. List of Schemes

12. List of Tables

13. Supplement

13.1. List of supplementary figures

pCtrl2_T7.03_sRBS_FKBP-mNG-^{TVMV}, pCtrl2_ T7.03_sRBS_FKBP-mNG-^{TVMV}-E118-134, pCtrl2_ T7.03_sRBS_mKO$_{κ}$, pCtrl2_T7.03_U9_FKBP-mNG-^{TVMV}, pCtl2_T7.03_U9_FKBP-mNG-^{TVMV}E118-134, pCtrl2_T7.03_U9_mKO$_{κ}$ Protein Sequences are stated in supplement (see **13.4.3**). 181

Figure S17 Comparison of all three considered pCtrl2 variants using the LVA C-Degron. Symbols, colors and constructs as in **Figure 16**. Transcription was reduced either by reducing the distance between T7 promoter and Start-Codon (T7.wt to T7.100) or by introducing a mutation to the native T7 promoter that reduced transcription to approx. 3 % [84]; alternatively the previously used RBS (sRBS) was replaced with the synthetic U9 RNA thermometer that possessed a approx. 5 % probability to adopt the open conformation at 30 °C [93]; Data points represent the mean values of dependent biological triplicates measured, the error areas depict the SEM, pCtrl2 derivate used stated above the corresponding graph, legend at the bottom refers to all graphs. Constructs used: pPRO24_MBP-^{TVMV}TVMV-FRB, MBP-^{TVMV}TVMV^{C151A}-FRB, pCtrl2_FKBP-mNG-^{TVMV}, pCtrl2_FKBP-mNG-^{TVMV}-LVA, pCtrl2_mKO$_{κ}$, pCtrl2_T7.100_FKBP-mNG-^{TVMV}, pCtrl2_T7.100_FKBP-mNG-^{TVMV}-LVA, pCtrl2_T7.100_mKO$_{κ}$, pCtrl2_T7.03_sRBS_FKBP-mNG-^{TVMV}, pCtrl2_ T7.03_sRBS_FKBP-mNG-^{TVMV}- LVA, pCtrl2_ T7.03_sRBS_mKO$_{κ}$, pCtrl2_T7.03_U9_FKBP-mNG-^{TVMV}, pCtl2_T7.03_U9_FKBP-mNG-^{TVMV}LVA, pCtrl2_T7.03_U9_mKO$_{κ}$ Protein Sequences are stated in supplement (see **13.4.3**). 182

Figure S18 Comparison of the E118-134 C-degron with its triple minimal version and the LVA C-degron raw data. Constructs, colors and symbols as in **Figure 22**. Graphs depict the real-time data of the protease activity dependent alteration in mNGs fluorescence, the respective sensors used shown in the respective pictograms, data points represent the mean values of dependent biological quadruplicates measured, error areas depict the SEM, the legend uses placeholder colors for the constructs with degrons fused, in the respective graph the placeholder colors are replaced with the colors according to degron (matching **Figure 22**, excepts striped bars for (E118min)$_3$ are replaced with half-filled triangles). Constructs used: pPRO24_MBP-^{TVMV}sSH3L-TVMV-Strep, pPRO24_MBP-^{TVMV}sSH3L-TVMV^{C151A}-Strep, pCtrl2_T7.03_U9_myc-SH3-mNG-^{TVMV}, pCtrl2_T7.03_U9_myc-SH3-mNG-^{TVMV}E118.134, pCtrl2_T7.03_U9_myc-SH3-mNG-^{TVMV}LVA, pCtrl2_T7.03_U9_myc-SH3-mNG-TVMV(E118min)$_3$, pCtrl2_T7.03_U9_mKO$_{κ}$. Protein Sequences are stated in the supplement (see **12.4.5**) 183

Figure S19 Raw data Orientation screen ratiometric *in vivo* protease assay based on cryptic N-degrons. **A:** Schematic depiction of the experiment. **B:** Normalized mCherry fluorescences

13.2. Supplementary Figures

13.2.1. Orientation screen FKBP/FRB

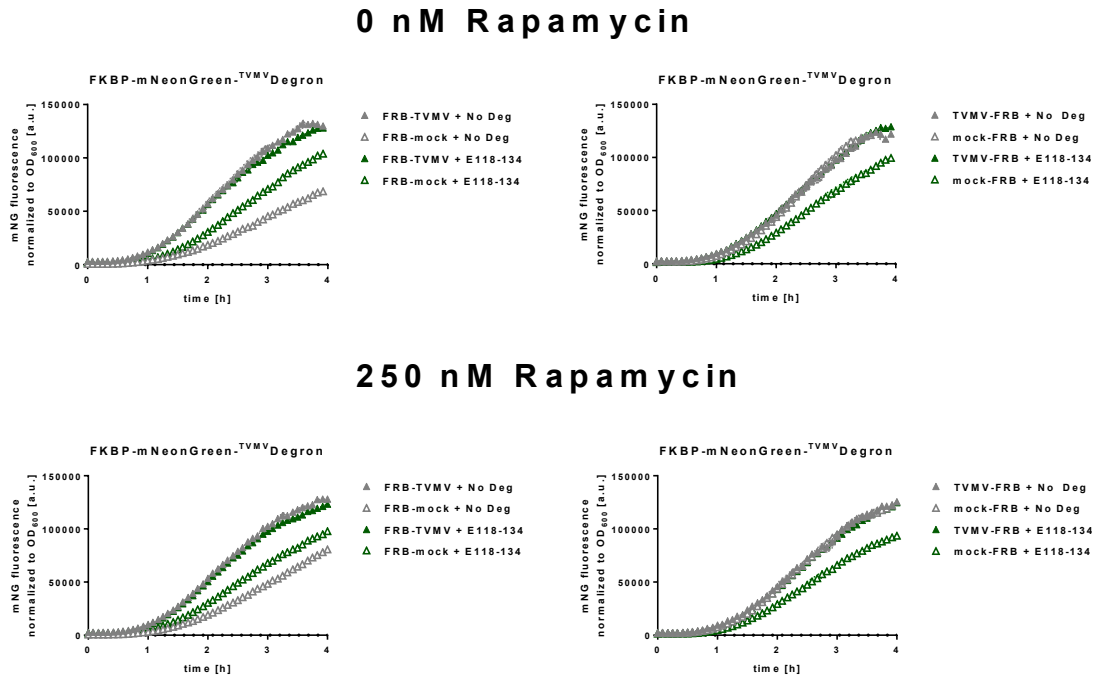

Figure S1 TVMV-FRB and FRB-TVMV probed with FKBP-mNeonGreen-^{TVMV}E118-134 sensor. Top: without addition of Rapamycin. Bottom: With addition of 250 nM Rapamycin. Left: FRB-TVMV with FRB-mock control with and without degron present at the sensor. Right: TVMV-FRB with mock-FRB control with and without degron present at the sensor. Filled triangles: active protease, empty triangles: mock protease, grey: no degron present at the sensor, green: degron present at the sensor. Constructs used: pCtrl2_FKBP-mNG-^{TVMV}, pCtrl2_FKBP-mNG-^{TVMV}E118-134, pCtrl2_mKO$_{\kappa}$, pPRO24_MBP-^{TVMV}TVMV-FRB, pPRO24_MBP-^{TVMV}TVMV^{C151A}-FRB, pPRO24_MBP-^{TVMV}FRB-TVMV, pPRO24_MBP-^{TVMV}FRB-TVMV^{C151A}.

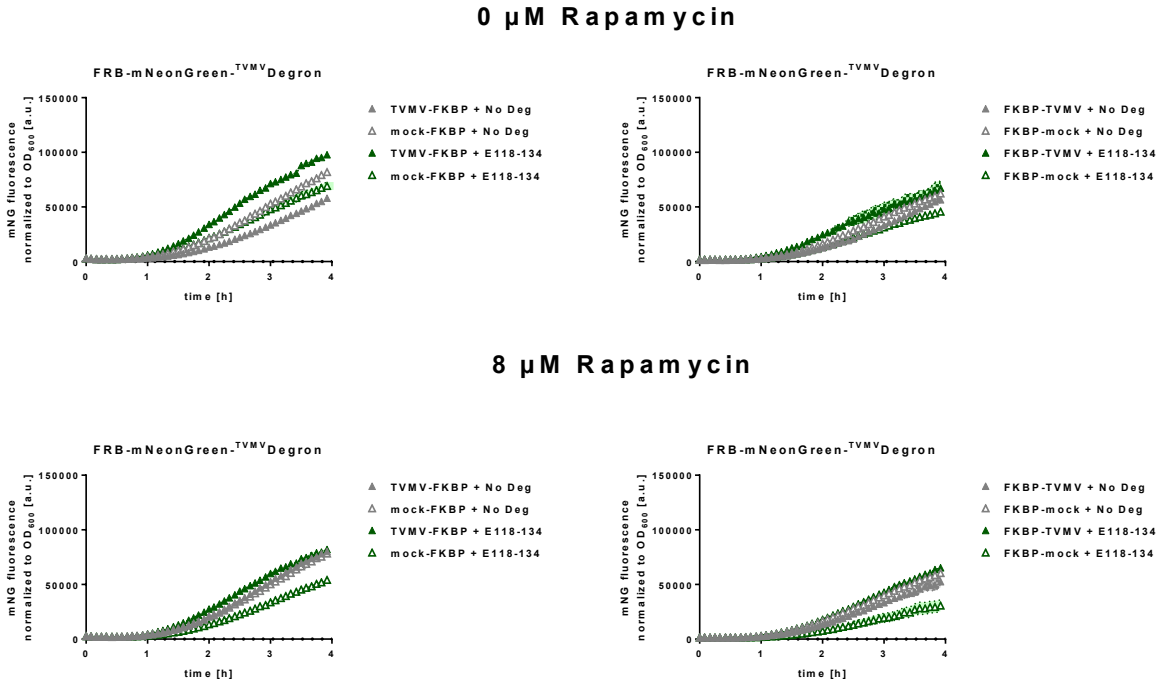

Figure S2 TVMV-FKBP and FKBP-TVMV probed with FRB-mNeonGreen-^{TVMV}E118-134 sensor. Top: without addition of Rapamycin. Bottom: With addition of 8 µM Rapamycin. Left: TVMV-FKBP with FRB-mock control with and without degron present at the sensor. Right: FKBP-TVMV with mock-FRB control with and without degron present at the sensor. Filled triangles: active protease, empty triangles: mock protease, grey: no degron present at the sensor, green: degron present at the sensor. Constructs used: pCtrl2_FRB-mNG-^{TVMV}, pCtrl2_FRB-mNG-^{TVMV}E118-134, pCtrl2_mKO$_K$, pPRO24_MBP-^{TVMV}TVMV-FKBP, pPRO24_MBP-^{TVMV}TVMV^{C151A}-FKBP, pPRO24_MBP-^{TVMV}FKBP-TVMV, pPRO24_MBP-^{TVMV}FKBP-TVMV^{C151A}.

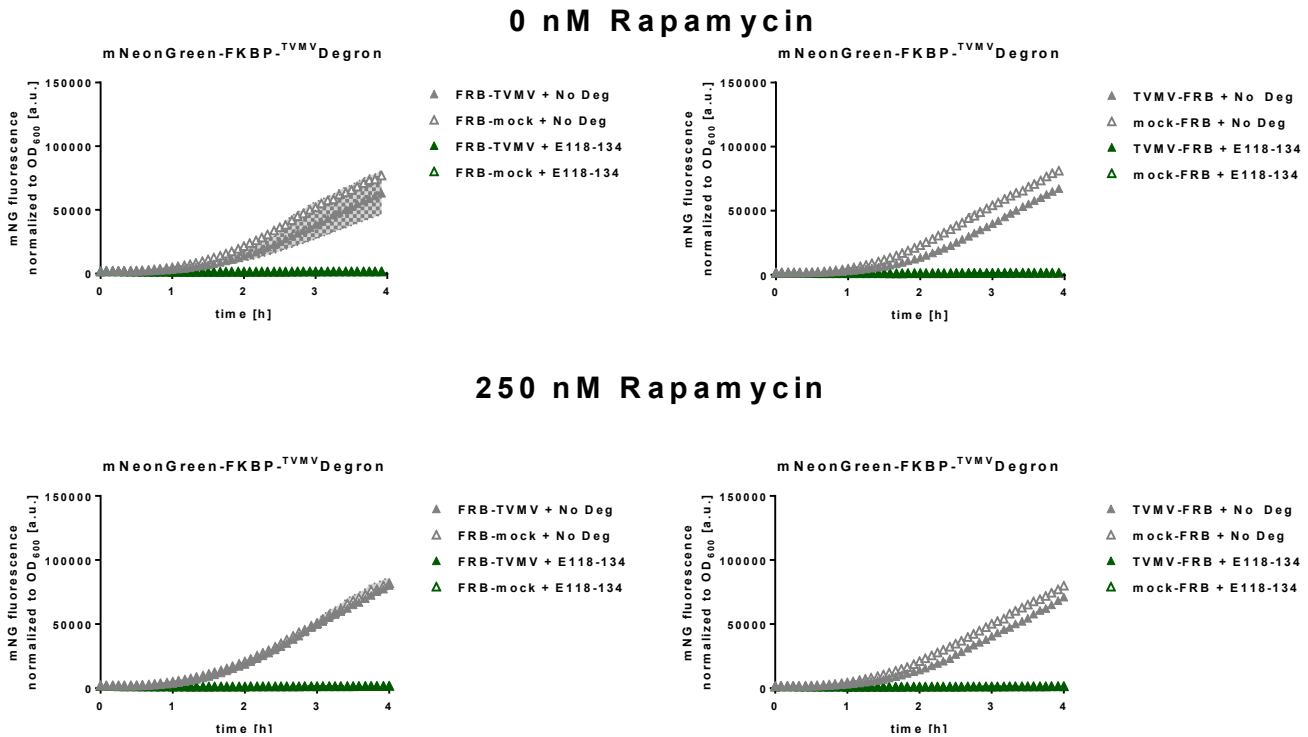

Figure S3 FRB-TVMV and TVMV-FRB probed with mNeonGreen-FKBP-^{TVMV}E118-134 sensor. Top: without addition of Rapamycin. Bottom: With addition of 250 nM Rapamycin. Left: FRB-TVMV with FRB-mock control with and without degron present at the sensor. Right: TVMV-FRB with mock-FRB control with and without degron present at the sensor. Filled triangles: active protease, empty triangles: mock protease, grey: no degron present at the sensor, green: degron present at the sensor. Constructs used: pCtrl2_mNG-FKBP^{TVMV}, pCtrl2_ mNG-FKBP^{TVMV}E118-134, pCtrl2_mKO$_K$, pPRO24_MBP-^{TVMV}TVMV-FRB, pPRO24_MBP-^{TVMV}TVMV^{C151A}-FRB, pPRO24_MBP-^{TVMV}FRB-TVMV, pPRO24_MBP-^{TVMV}FRBd-TVMV^{C151A}.

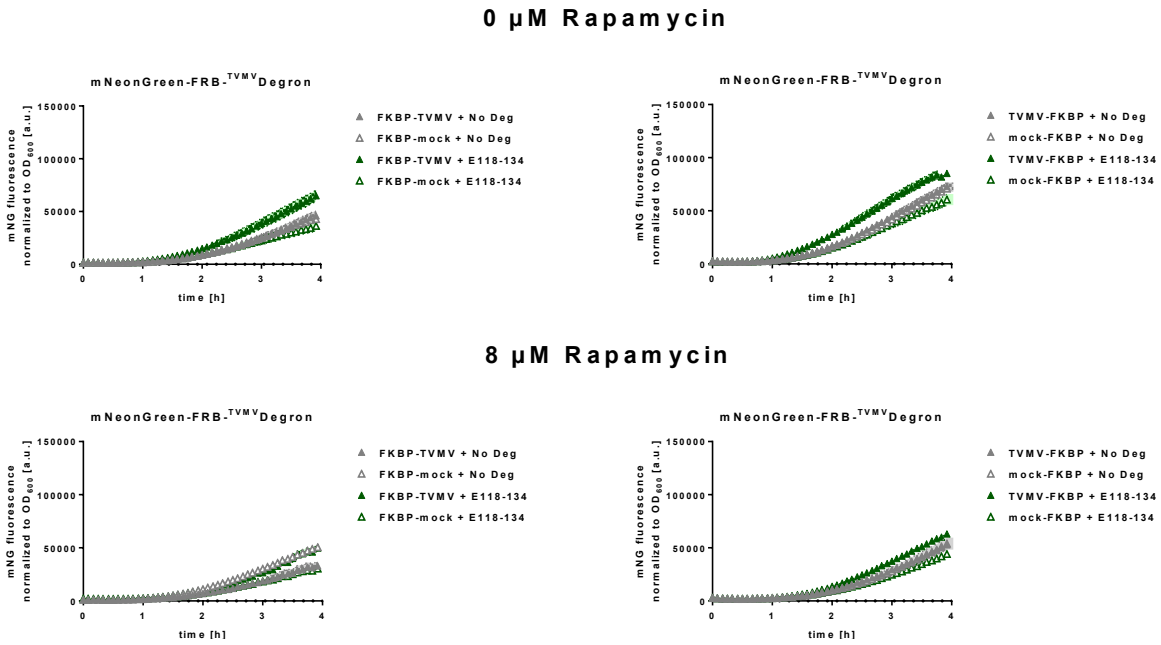

Figure S4 FKBP-TVMV and TVMV-FKBP probed with mNeonGreen-FRB-^{TVMV}E118-134 sensor. Top: without addition of Rapamycin. Bottom: With addition of 8 µM Rapamycin. Left: FKBP-TVMV with FKBP-mock control with and without degron present at the sensor. Right: TVMV-FKBP with mock-FKBP control with and without degron present at the sensor. Filled triangles: active protease, empty triangles: mock protease, grey: no degron present at the sensor, green: degron present at the sensor. Constructs used: pCtrl2_mNG-FRB^{TVMV}, pCtrl2_mNG-FRB^{TVMV}E118-134, pCtrl2_mKO$_{\kappa}$, pPRO24_MBP-^{TVMV}TVMV-FKBP, pPRO24_MBP-^{TVMV}TVMV^{C151A}-FKBP, pPRO24_MBP-^{TVMV}FKBP-TVMV, pPRO24_MBP-^{TVMV}FKBP-TVMV^{C151A}.

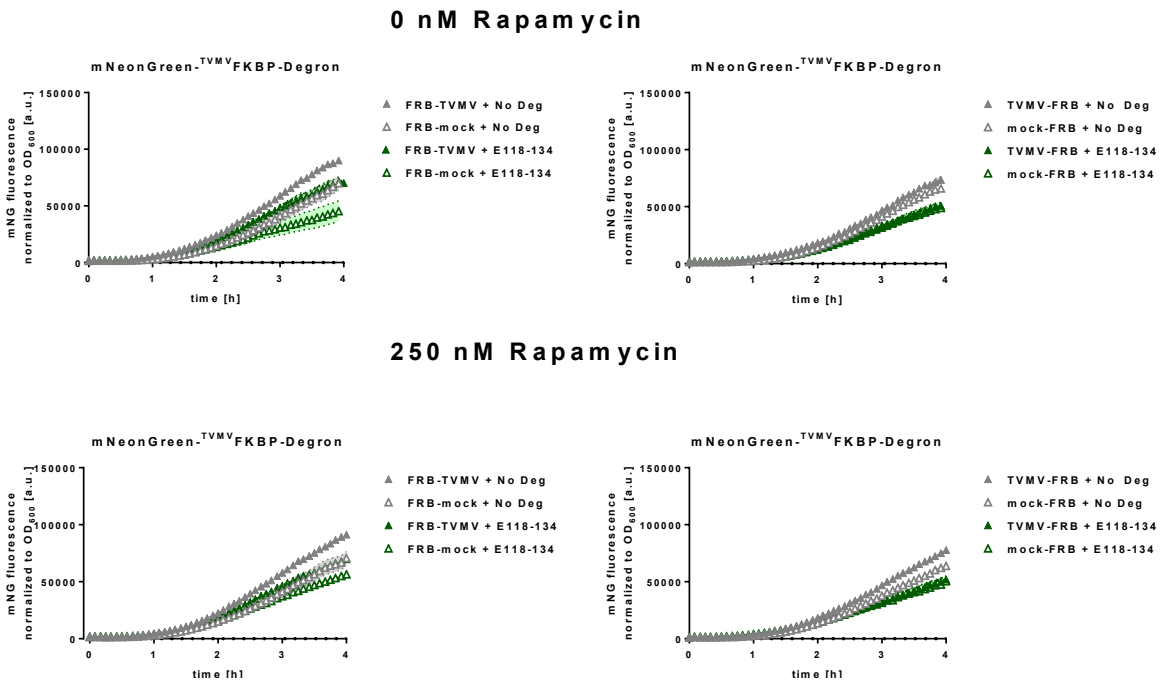

Figure S5 FRB-TVMV and TVMV-FRB probed with mNeonGreen-^{TVMV}FKBP-E118-134 sensor. Top: without addition of Rapamycin. Bottom: With addition of 250 nM Rapamycin. Left: FRB-TVMV with FRB-mock control with and without degron present at the sensor. Right: TVMV-FRB with mock-FRB control with and without degron present at the sensor. Filled triangles: active protease, empty triangles: mock protease, grey: no degron present at the sensor, green: degron present at the sensor. Constructs used: pCtrl2_mNG-^{TVMV}FKBP, pCtrl2_mNG-^{TVMV}FKBP-E118-134, pCtrl2_mKO$_{\kappa}$, pPRO24_MBP-^{TVMV}TVMV-FRB, pPRO24_MBP-^{TVMV}TVMV^{C151A}-FRB, pPRO24_MBP-^{TVMV}FRB-TVMV, pPRO24_MBP-^{TVMV}FRB-TVMV^{C151A}.

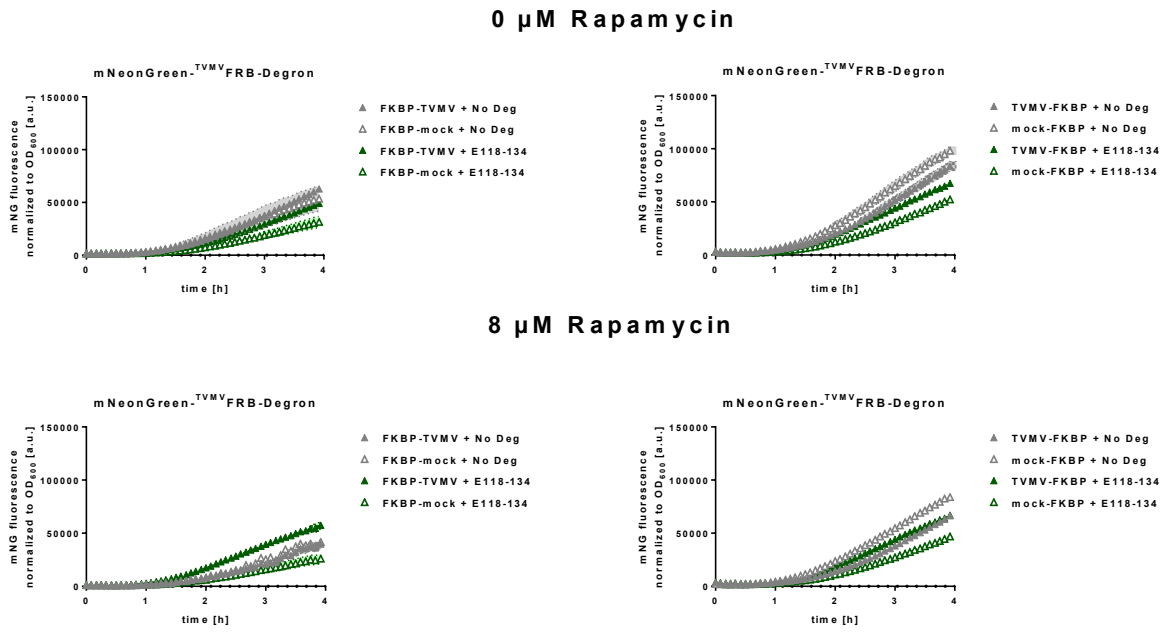

Figure S6 FKBP-TVMV and TVMV-FKBP probed with mNeonGreen-^{TVMV}FRB-E118-134 sensor. Top: without addition of Rapamycin. Bottom: With addition of 8 µM Rapamycin. Left: FKBP-TVMV with FKBP-mock control with and without degron present at the sensor. Right: TVMV-FKBP with mock-FKBP control with and without degron present at the sensor. Filled triangles: active protease, empty triangles: mock protease, grey: no degron present at the sensor, green: degron present at the sensor.

13.2.2. IPTG - Titration

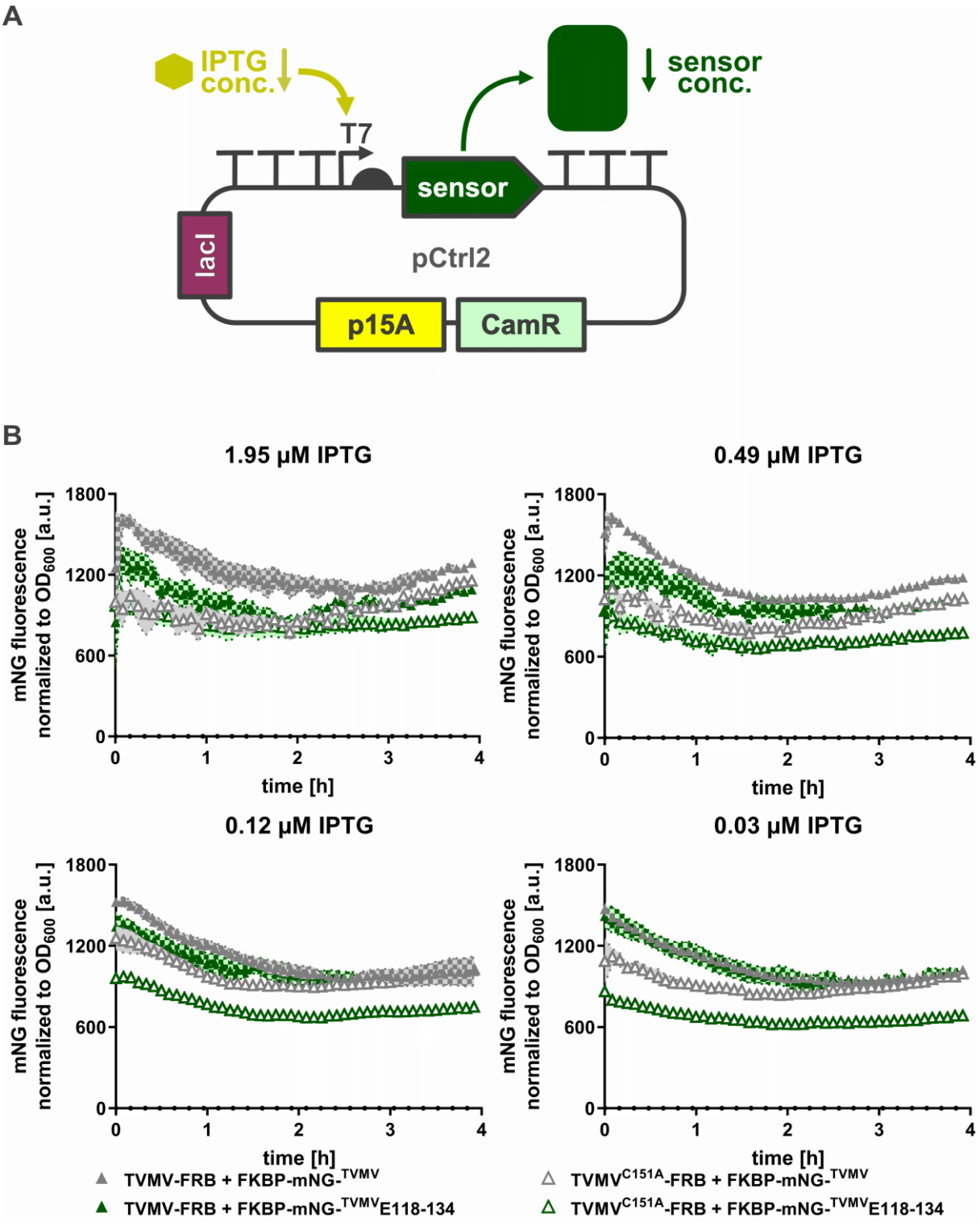

Figure S7 IPTG concentration from 1.95 µM to 0.03 µM in 1:4 dilution steps. Constructs, colors and symbols as in **Figure 13**. **A:** Schematic depiction of the experiment. **B:** Experimental results for the lowest IPTG concentrations tested. Constructs used: pPRO24_MBP-^{TVMV}TVMV-FRB, pPRO24_MBP-^{TVMV}TVMV^{C151A}-FRB, pCtrl2_FKBP-mNG-^{TVMV}, pCtrl2_FKBP-mNG-^{TVMV}-E118-134, pCtrl2_mKO$_{\kappa}$ Protein Sequences are stated in supplement (see 13.4.1).

13.2.3. Orientation screen C-degron based assay with SH3 based recruitment

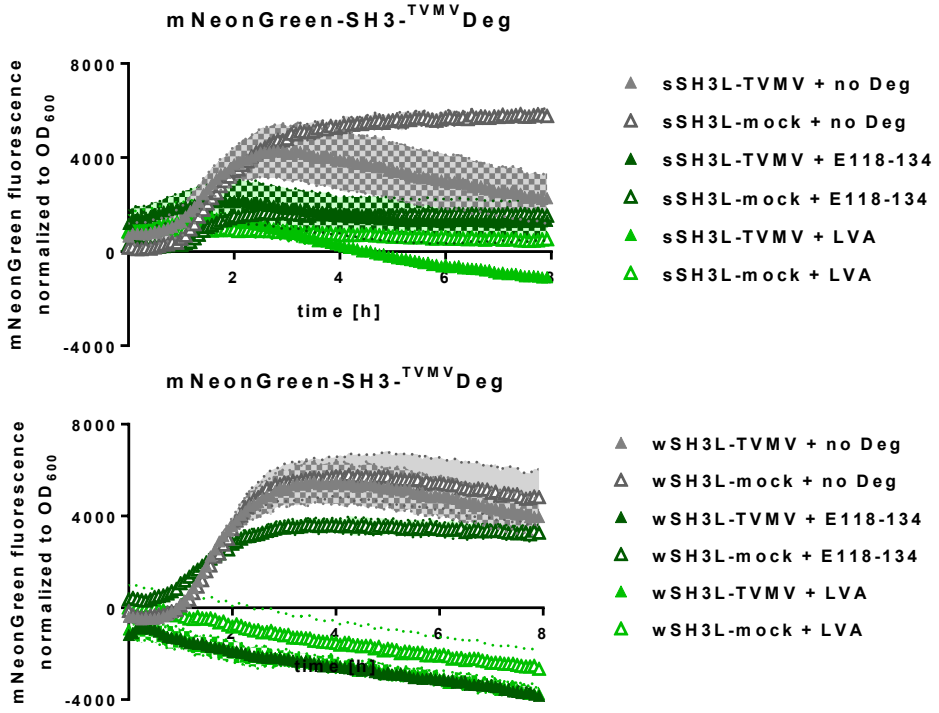

Figure S8 Fluorescence rescue assay with two C-degrons. Results for N-terminal SH3 Ligand combined with mNeonGreen-SH3-^{TVMV}degron orientation.

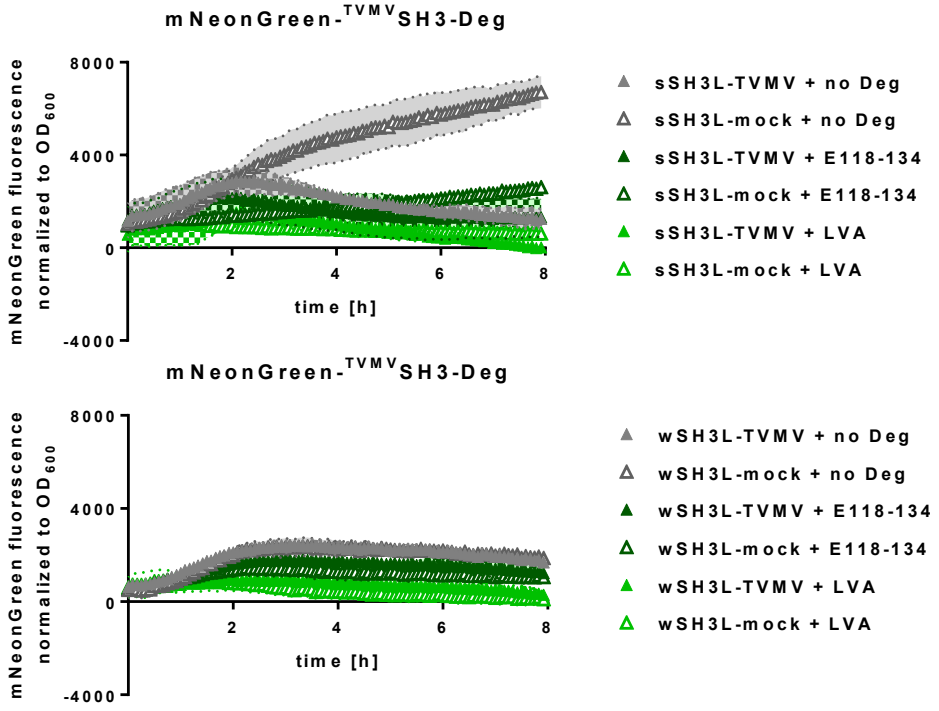

Figure S9 Fluorescence rescue assay with two C-degrons. Results for N-terminal SH3 Ligand combined with mNeonGreen-^{TVMV}SH3-degron orientation.

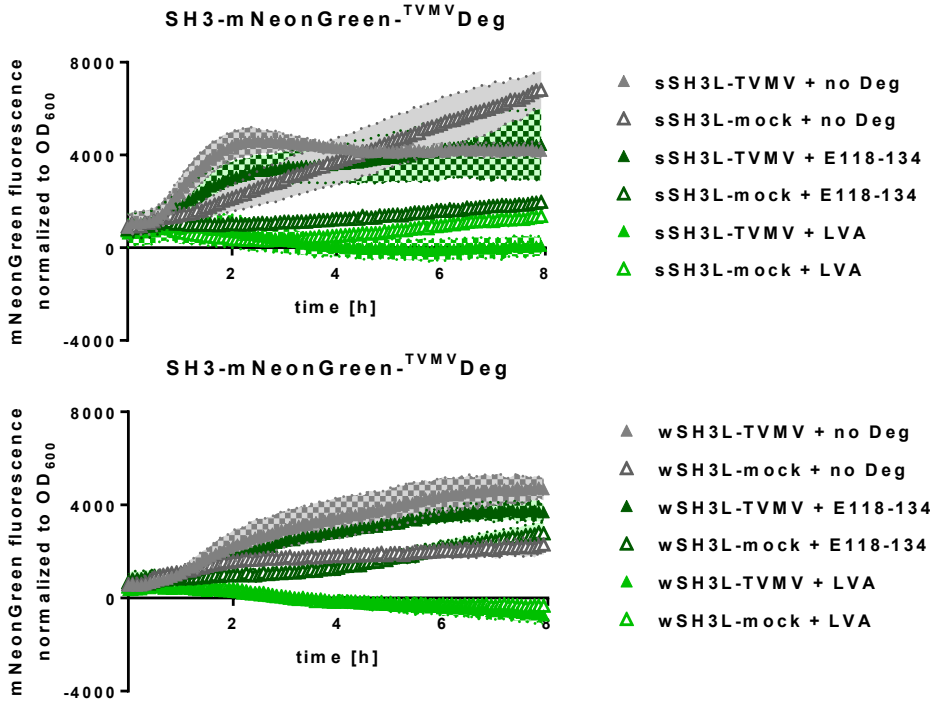

Figure S10 Fluorescence rescue assay with two C-degrons. Results for N-terminal SH3 Ligand combined with SH3-mNeonGreen-^{TVMV}degron orientation.

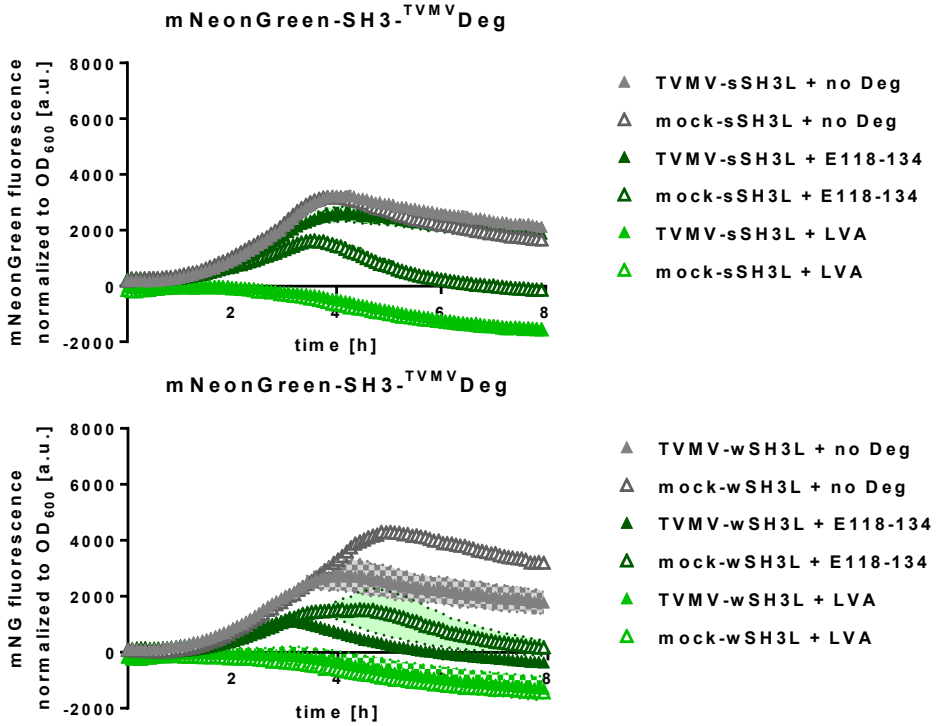

Figure S11 Fluorescence rescue assay with two C-degrons. Results for C-terminal SH3 Ligand combined with mNeonGreen-SH3-^{TVMV}degron orientation.

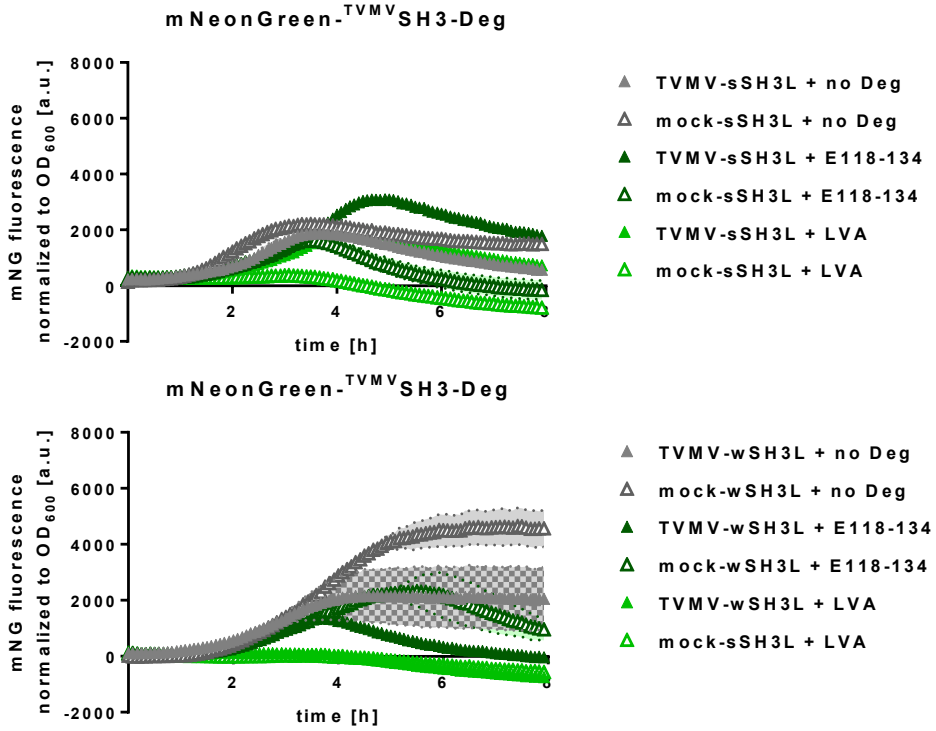

Figure S12 Fluorescence rescue assay with two C-degrons. Results for C-terminal SH3 Ligand combined with mNeonGreen-^{TVMV}SH3-degron orientation.

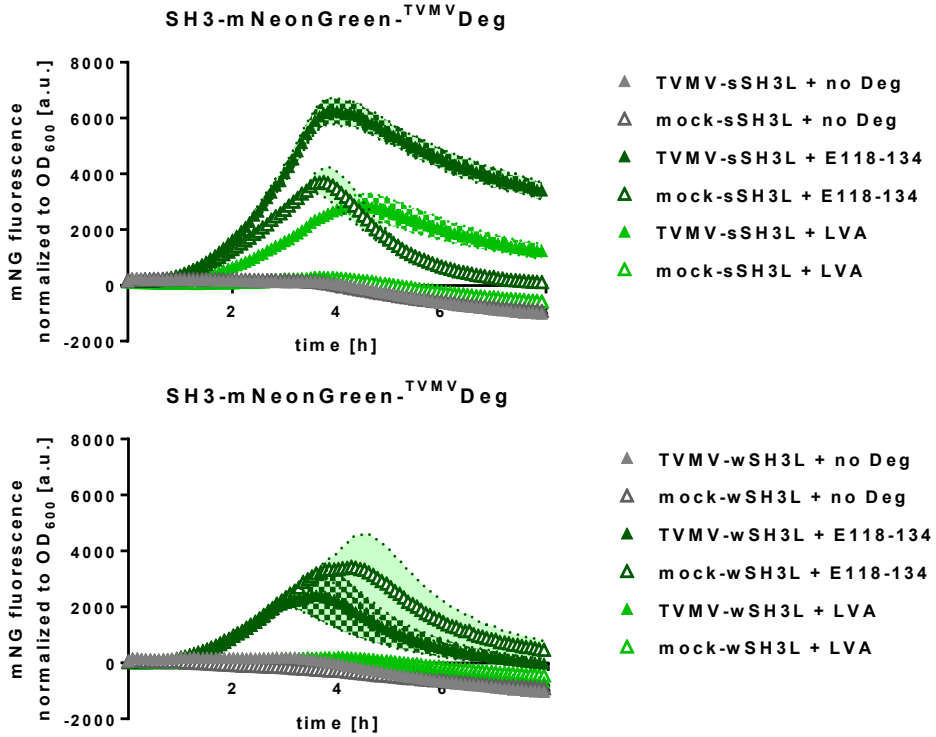

Figure S13 Fluorescence rescue assay with two C-degrons. Results for C-terminal SH3 Ligand combined with SH3-mNeonGreen-^{TVMV}degron orientation.

13.2.4. New C-degron LVA – raw data

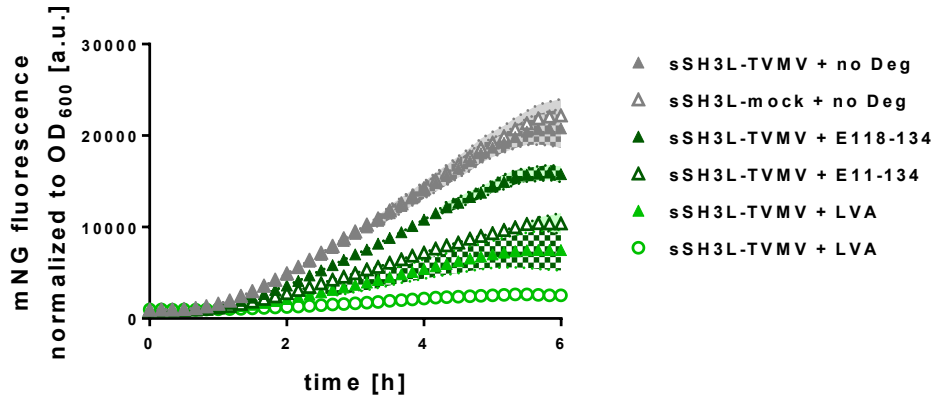

Figure S14 Fluorescence rescue assay with two C-degrons. Results for the re-tested orientation of sSH3L-protease and SH3-mNeonGreen-^{TVMV}C-degron.

13.2.5. Optimizing the expression of the protease sensor

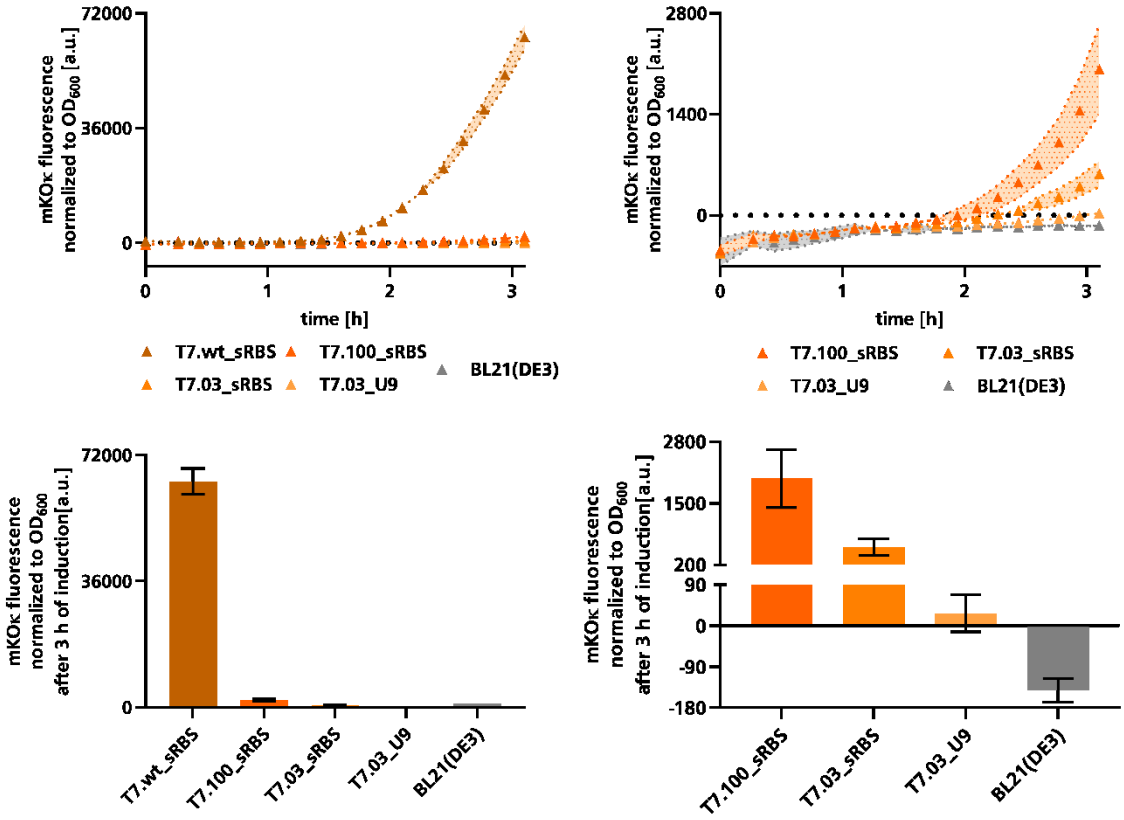

Figure S15 Expression control of the considered pCtrl2. Graphs depicted the fluorescence intensities for the mKO_{κ} reporter gene under control of two different T7 promoter variants and two different ribosome biding sites (RBS). T7.wt_sRBS is the native pCtrl2 vector architecture. T7.100 is the same wild type promoter but with reduced distance between lac operator and RBS, T7.03 poses a T-to-C two nucleotides upstream of the transcription start, U9 is a synthetic RNA thermometer that masks the Shine-Dalgarno (SD) sequence with an anti-SD sequence *via* stem loop formation at temperatures below 37 °C. Data points depict the mean values measured for dependent biological quadruplicates measured, error bars/areas show the standard error of the mean (SEM). Top: Graphs show mKO_{κ} reporter fluorescence after the first 3 hours of induction with 500 µM IPTG, on the left including the native pCtrl2 (named T7.wt_sRBS in this data set) and on the right without the native pCtrl2 for better differentiation of the considered pCtrl2 variants. Bottom: Bar plots show the fluorescence after 3 hours, error bars depict the SEM, on left including native pCtrl2 and on the right without it for better differentiation of the considered pCtrl2 variants. All data shown here were generated by W. Weber the creator of pCtrl2 and all its variants.

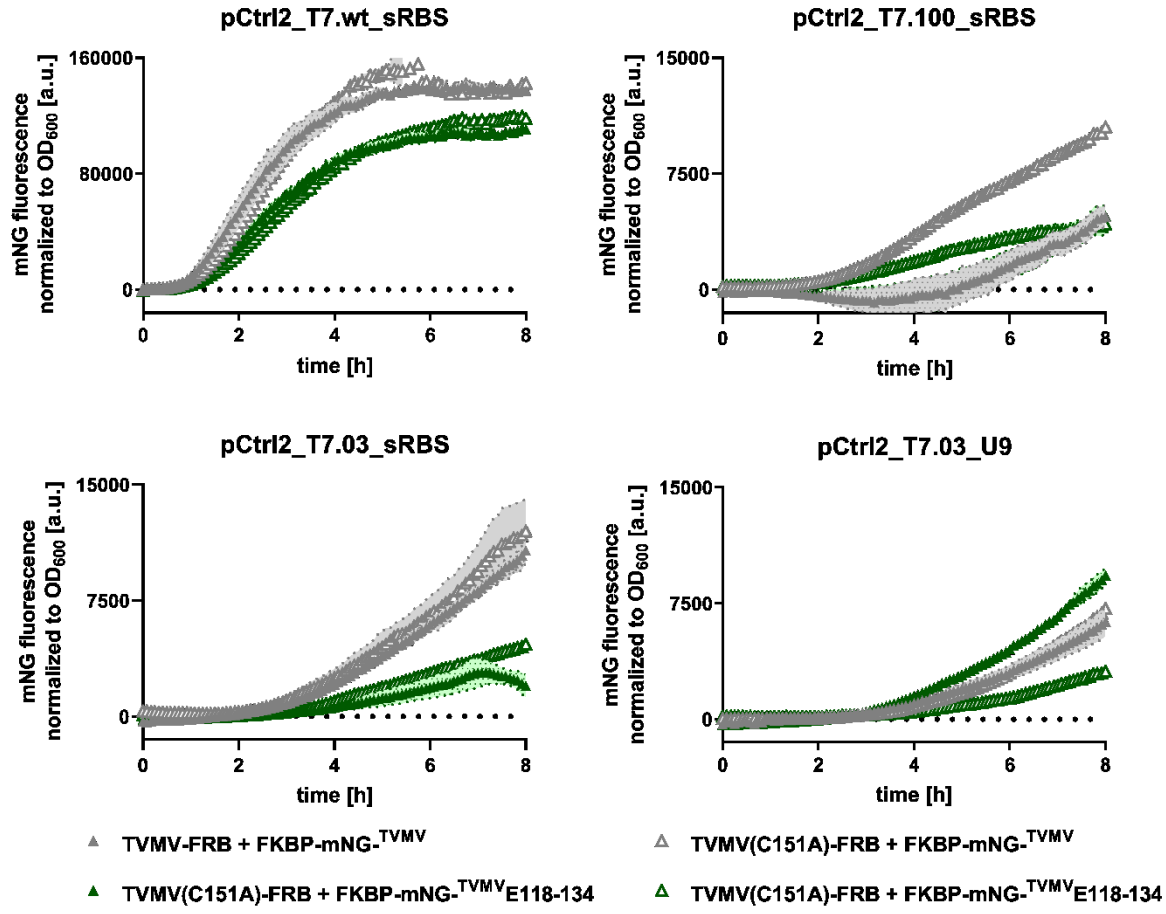

Figure S16 Comparison of all three considered pCtrl2 variants using the E118-134 C-Degron. Symbols, colors and constructs as in **Figure 16**. Transcription was reduced either by reducing the distance between T7 promoter and Start-Codon (T7.wt to T7.100) or by introducing a mutation to the native T7 promoter that reduced transcription to approx. 3 % [84]; alternatively the previously used RBS (sRBS) was replaced with the synthetic U9 RNA thermometer that possessed a approx. 5 % probability to adopt the open conformation at 30 °C [93]; Data points represent the mean values of dependent biological triplicates measured, the error areas depict the SEM, pCtrl2 derivate used stated above the corresponding graph, legend at the bottom refers to all graphs. Constructs used: pPRO24_MBP-^{TVMV}TVMV-FRB, MBP-^{TVMV}TVMV^{C151A}-FRB, pCtrl2_FKBP-mNG-^{TVMV}, pCtrl2_FKBP-mNG-^{TVMV}-E118-134, pCtrl2_mKO$_κ$, pCtrl2_T7.100_FKBP-mNG-^{TVMV}, pCtrl2_T7.100_FKBP-mNG-^{TVMV}-E118-134, pCtrl2_T7.100_mKO$_κ$, pCtrl2_T7.03_sRBS_FKBP-mNG-^{TVMV}, pCtrl2_ T7.03_sRBS_FKBP-mNG-^{TVMV}-E118-134, pCtrl2_ T7.03_sRBS_mKO$_κ$, pCtrl2_T7.03_U9_FKBP-mNG-^{TVMV}, pCtl2_T7.03_U9_FKBP-mNG-^{TVMV}E118-134, pCtrl2_T7.03_U9_mKO$_κ$ Protein Sequences are stated in supplement (see **13.4.3**).

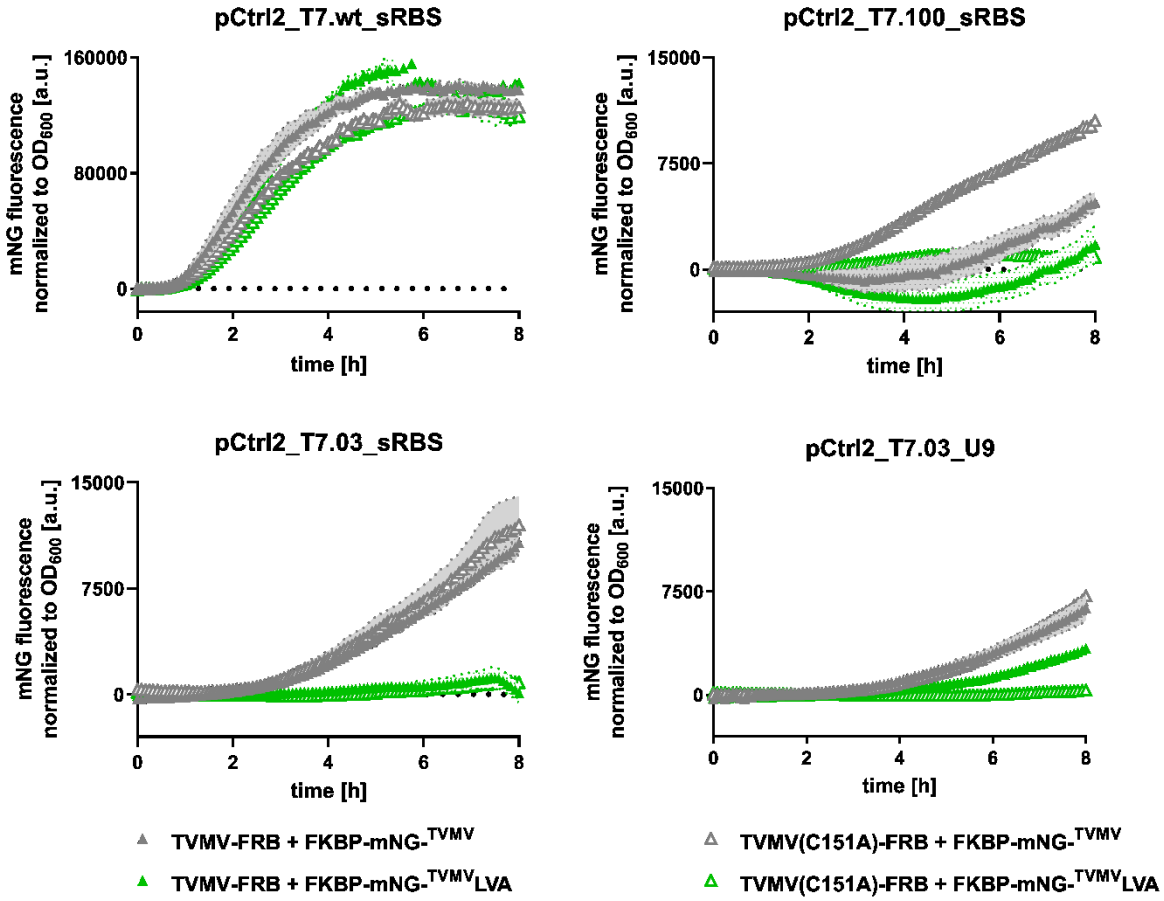

Figure S17 Comparison of all three considered pCtrl2 variants using the LVA C-Degron. Symbols, colors and constructs as in **Figure 16**. Transcription was reduced either by reducing the distance between T7 promoter and Start-Codon (T7.wt to T7.100) or by introducing a mutation to the native T7 promoter that reduced transcription to approx. 3 % [84]; alternatively the previously used RBS (sRBS) was replaced with the synthetic U9 RNA thermometer that possessed a approx. 5 % probability to adopt the open conformation at 30 °C [93]; Data points represent the mean values of dependent biological triplicates measured, the error areas depict the SEM, pCtrl2 derivate used stated above the corresponding graph, legend at the bottom refers to all graphs. Constructs used: pPRO24_MBP-^{TVMV}TVMV-FRB, MBP-^{TVMV}TVMV^{C151A}-FRB, pCtrl2_FKBP-mNG-^{TVMV}, pCtrl2_FKBP-mNG-^{TVMV}-LVA, pCtrl2_mKO$_κ$, pCtrl2_T7.100_FKBP-mNG-^{TVMV}, pCtrl2_T7.100_FKBP-mNG-^{TVMV}-LVA, pCtrl2_T7.100_mKO$_κ$, pCtrl2_T7.03_sRBS_FKBP-mNG-^{TVMV}, pCtrl2_ T7.03_sRBS_FKBP-mNG-^{TVMV}- LVA, pCtrl2_ T7.03_sRBS_mKO$_κ$, pCtrl2_T7.03_U9_FKBP-mNG-^{TVMV}, pCtl2_T7.03_U9_FKBP-mNG-^{TVMV}LVA, pCtrl2_T7.03_U9_mKO$_κ$ Protein Sequences are stated in supplement (see **13.4.3**).

13.2.6. Triple minimal E118-134 – raw data

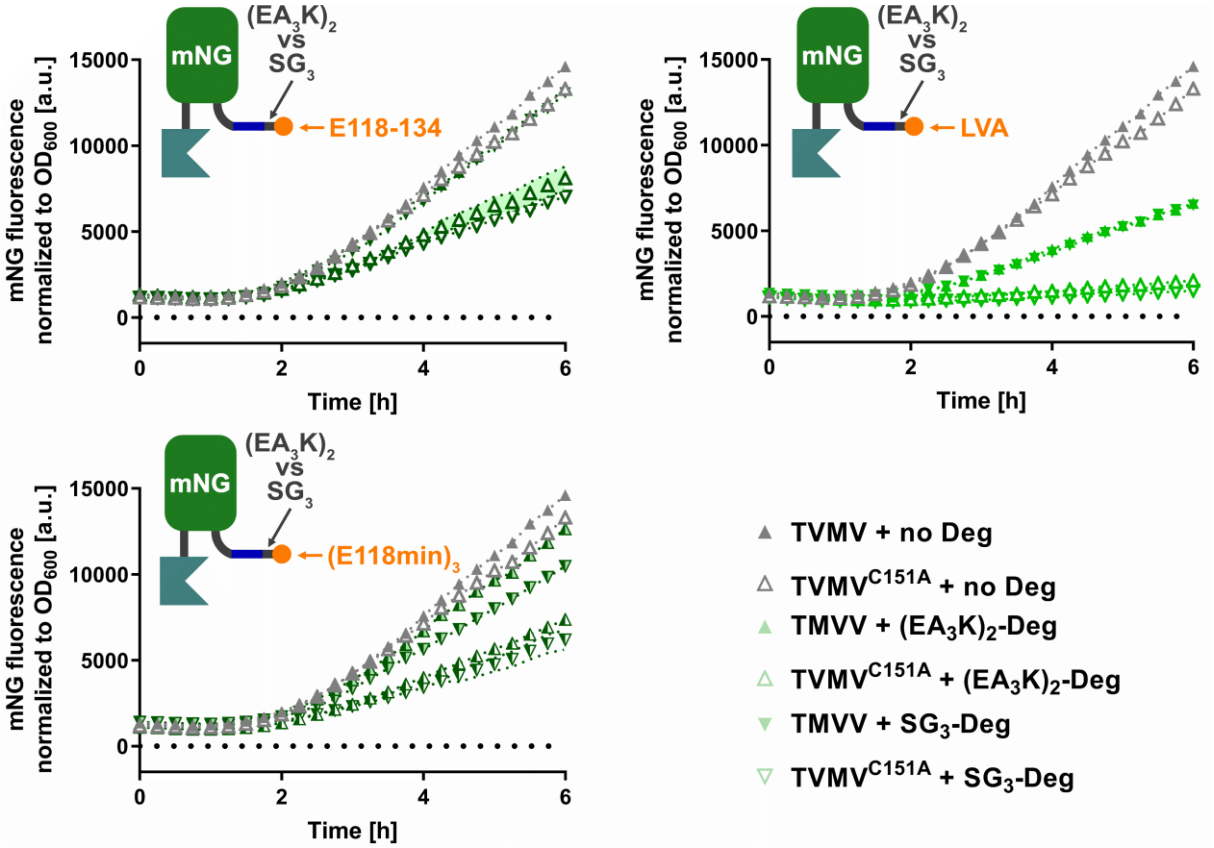

Figure S18 Comparison of the E118-134 C-degron with its triple minimal version and the LVA C-degron raw data. Constructs, colors and symbols as in **Figure 22**. Graphs depict the real-time data of the protease activity dependent alteration in mNGs fluorescence, the respective sensors used shown in the respective pictograms, data points represent the mean values of dependent biological quadruplicates measured, error areas depict the SEM, the legend uses placeholder colors for the constructs with degrons fused, in the respective graph the placeholder colors are replaced with the colors according to degron (matching **Figure 22**, excepts striped bars for $(E118min)_3$ are replaced with half-filled triangles). Constructs used: pPRO24_MBP-^{TVMV}sSH3L-TVMV-Strep, pPRO24_MBP-^{TVMV}sSH3L-TVMV^{C151A}-Strep, pCtrl2_T7.03_U9_myc-SH3-mNG-^{TVMV}, pCtrl2_T7.03_U9_myc-SH3-mNG-^{TVMV}E118.134, pCtrl2_T7.03_U9_myc-SH3-mNG-^{TVMV}LVA, pCtrl2_T7.03_U9_myc-SH3-mNG-TVMV$(E118min)_3$, pCtrl2_T7.03_U9_mKO$_\kappa$. Protein Sequences are stated in the supplement (see **12.4.5**)

13.2.7. Orientation Screen ratiometric

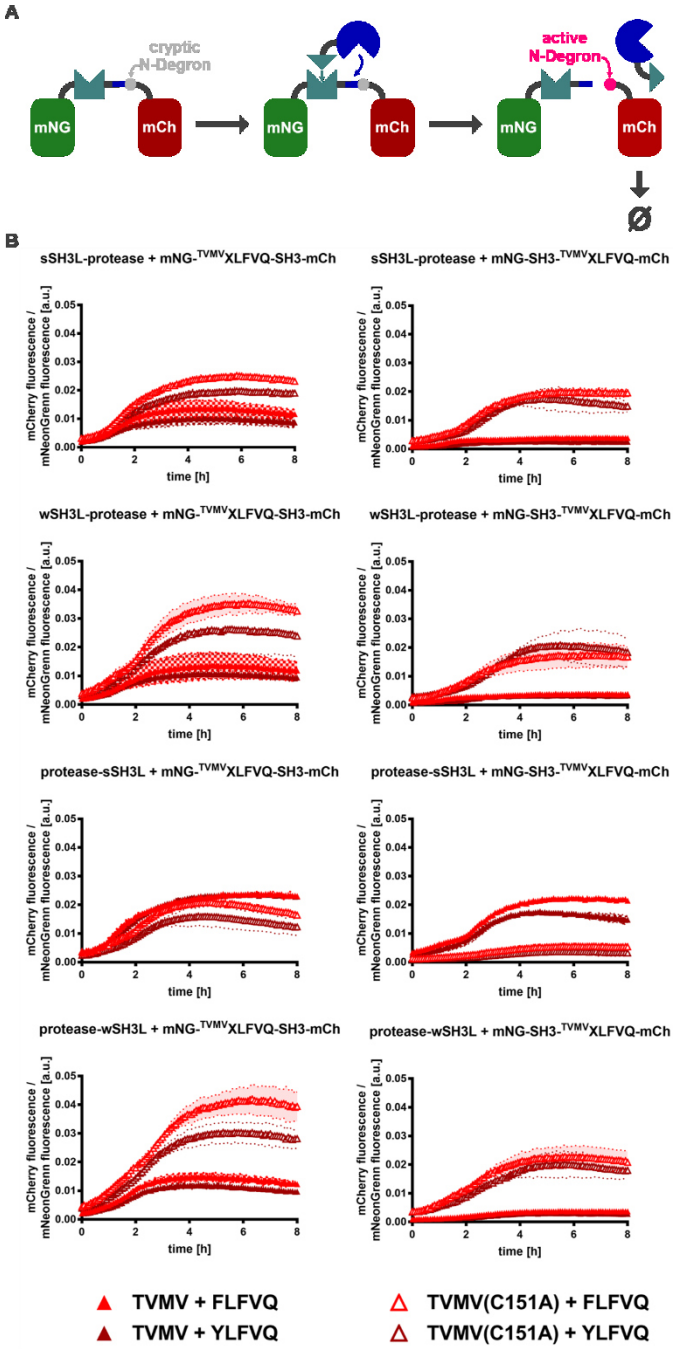

Figure S19 Raw data Orientation screen ratiometric *in vivo* protease assay based on cryptic N-degrons. **A:** Schematic depiction of the experiment. **B:** Normalized mCherry fluorescences order by combination of relative orientations, data points represent the mean values of the dependent biological triplicates measured, error areas depict the SEM. Constructs used: pPRO24_MBP-^{TVMV}sSH3L-TVMV-Strep, pPRO24_MBP-^{TVMV}sSH3L-TVMV^{C151A}-Strep, pPRO24_MBP-^{TVMV}wSH3L-TVMV-Strep, pPRO24_MBP-^{TVMV}wSH3L-TVMV^{C151A}-Strep, pPRO24_MBP-^{TVMV}TVMV-sSH3L-Strep, pPRO24_MBP-^{TVMV}TVMV^{C151A}-sSH3L-Strep, pPRO24_MBP-^{TVMV}TVMV-wSH3L-Strep, pPRO24_MBP-^{TVMV}TVMV^{C151A}-wSH3L-Strep, pCtrl2_T7.03_U9_myc-mNG-SH3-^{TVMV}FLFVQ-mCh-Strep, pCtrl2_T7.03_U9_myc-mNG-SH3-^{TVMV}YLFVQ-mCh-Strep. Protein Sequences are stated in the supplement (see **12.4.7**)

13.2.8. Preliminary Results opto-switch – custom-made blue LED panel

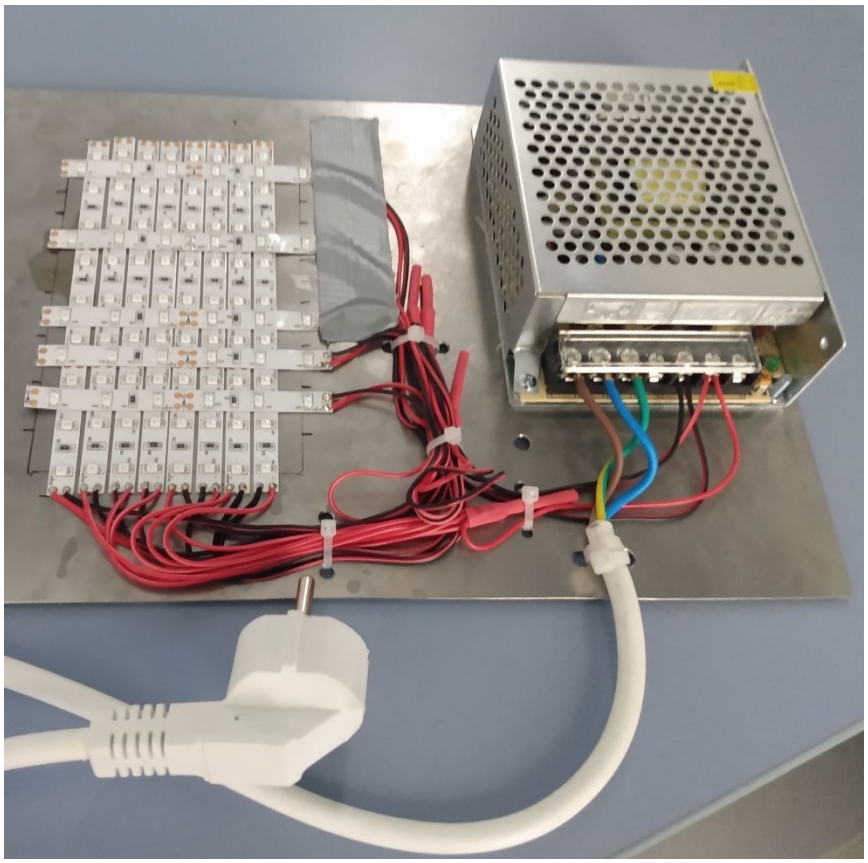

Figure S20 Custom-made LED panel for irradiating the blue light switch library.

13.3. Supplementary Methods

13.3.1. Modified clonetegration protocol

All credit for this modified protocol goes to our former master student Mr. Markus Röder. The original protocol is found in One-Step Cloning and Chromosomal Integration of DNA by St. Pierre *et al.*, 2013, ACS Synth. Biol. 2013, 2, 537−541.

http://pubs.acs.org/doi/abs/10.1021/sb400021j

Introduction

One-step cloning and chromosomal Integration of DNA is a method for integration DNA into prokaryotic chromosomes that approaches the simplicity of cloning DNA within extrachromosomal vectors. With a single transformation step, efficient integration is achieved. Therefore, the working group developed new vectors combining integrase-expression and integration plasmid: **O**ne-**S**tep **I**ntegration **P**lasmid, pOSIP (**Figure S21**).

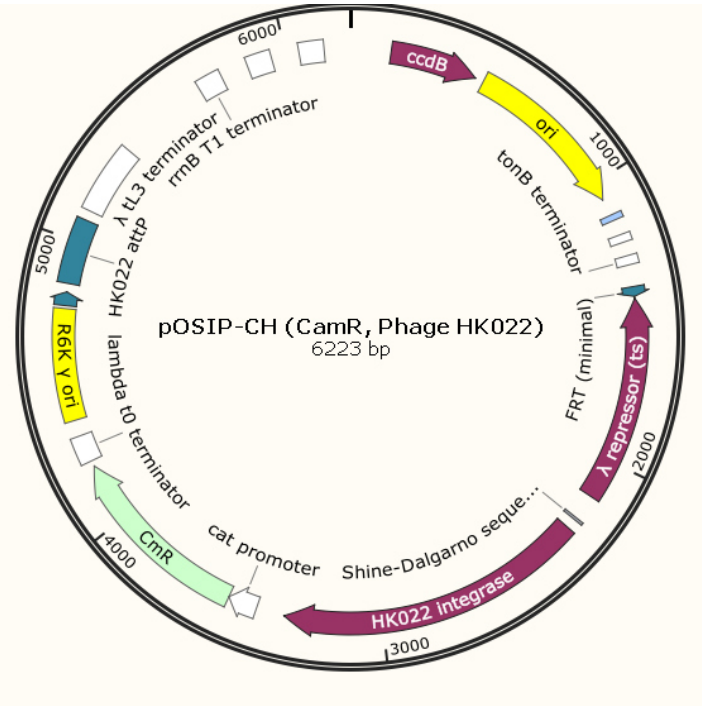

Figure S21 Plasmid map of pOSIP-CH. Created with SnapGene.

The genes for *ccdb* and ori resemble the multiple cloning site. For chromosomal integration, both *ccdb* and ori have to be deleted. ccdb is a potent toxin preventing usual cloning and expression strains from growing. The ori is not needed anymore since you only want colonies with successful integration. Note, that a second ori (R6Kγ ori) is present. The *pir*-dependent R6Kγ origin is unnecessary for clonetegration, but allows the user to maintain a plasmid version of the pOSIP clone in a *pir*-containing strain (*E. coli* BW23474 is able to propagate this ori and is currently available in the working group of Stein). The multiple cloning site is flanked by forward and reverse transcription terminators to isolate integrated OSIP plasmid from transcription in chromosomal regions flanking integration site and vice versa. The arrangement of terminators is depicted in **Figure S22**.

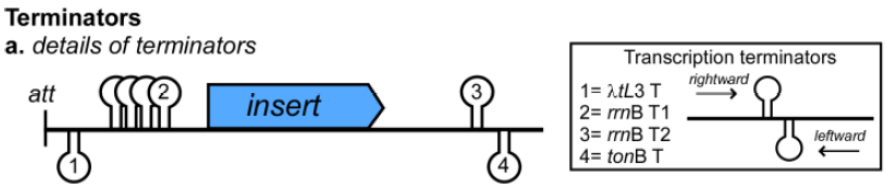

Figure S22 The identity and direction of the transcriptional terminators protecting the cloning module of pOSIP are shown.

For plasmid propagation of original pOSIPS, use a ccdb resistant *E. coli* strain (e.g. DB3.1). See **Table S1** for OSIP plasmids which are currently used in the working group of Stein. DB3.1 is also available.

Table S1 Details of OSIP plasmids currently available in the working group of Stein

Plasmid	Origin of integrase	*E. coli* strain for propagation	Antibiotics	Growth temperature	Copy number	Addgene links
pOSIP-CH	HK022	DB 3.1	chloramphenicol	30 °C	high copy	http://www.addgene.org/45980/
pOSIP-KO	186	DB 3.1	kanamycin	30 °C	high copy	http://www.addgene.org/45985/
pE-FLP	-	E811	ampicillin 50 µg/ml	30 °C	low copy	http://www.addgene.org/45978/

The integration of properly assembled pOSIP-insert molecules occurs during post-transformation outgrowth. Verification of integration can be performed by colony PCR using sets of primers that were optimized from the original CRIM set. In this work, primers for colony PCR are modified for *E. coli* BL21(DE3). When using a different strain check for primer binding first.

Methods

One-Step chromosomal integration

Like standard plasmid cloning, clonetegration requires the initial assembly of one or multiple DNA fragments into pOSIP using one's favourite cloning technique, such as Gibson assembly, Clonetech In-Fusion®, or traditional restriction digest and ligation. Resulting cloning mixtures are then directly transformed into chemically competent *E. coli* BL21(DE3) cells. You can also use electro-competent cells for higher efficiency. After transformation, let your cells regenerate at 37 °C for 1 h under shaking like a "normal" transformation. Integration of properly assembled pOSIP-insert molecules occurs during post-transformation outgrowth at 30 °C. Use 15 μg/ml chloramphenicol or kanamycin only. Due to low copy number of antibiotic resistance transcripts, growth will be slow and can take up to 20 h until colonies show up.

Verification of integration

For verification of integration use the cost-efficient colony PCR. The colony PCR is designed to run with four primers simultaneously resulting in two PCR products. Primer arrangement is shown in **Figure S23**.

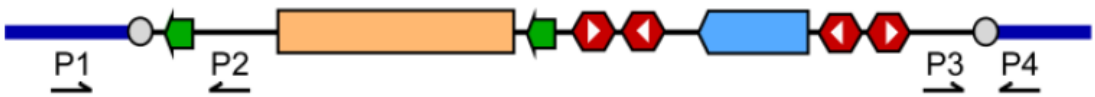

Figure S23 Following successful site-specific recombination between the pOSIP attP sequence and chromosomal attB site, single integration produces two fragments, one from P1 and P2, and one from P3 and P4. Blue (genome), grey circles (attP and attB sites), green (FRT sites), beige (integration module), red (terminators), light blue (insert). P is for primer.

Following primers are currently available (**Table S2**).

Table S2 Primer sequences for colony PCR and insert extraction for BL21(DE3) strain.

Primer name	Primer sequence (5'->3')	Use for plasmid
P2 seq pOSIPs	ACTTAACGGCTGACATGG	all
P3 seq pOSIPs	ACGAGTATCGAGATGGCA	all
P1 seq HK022	GGAATCAATGCCTGAGTG	pOSIP-CH
P4 seq HK022	GGCATCAACAGCACATTC	pOSIP-CH
P1 seq 186_IS2	CCCTGGAGCCAAAATATCC	pOSIP-KO
P4 seq 186_IS2_mod	TCCGGAATGCCCGCATTG	pOSIP-KO
pOSIP seq for	CAAGAATTAATTCCCAATTCCCCAGG	all
pOSIP seq rev	ATTACTCAACAGGTAAGGCG	all

When using pOSIP-CH use primers P2 seq pOSIPs, P3 seq pOSIPs, P1 seq HK022 and P4 seq HK022. When using pOSIP-KO use primers P2 seq pOSIPs, P3 seq pOSIPs, P1 seq 186_IS2 and P4 seq 186_IS2_mod. All primers can be found in the "clonetegration" box in a -20 °C freezer.

You can use the following pipette scheme and cycling program (adjusted to Phusion polymerase):

Table S3 Pipette scheme and cycling program for colony PCR

P1 (10 μM)	2.5 μl
P4 (10 μM)	2.5 μl
P2 (10 μM)	2.5 μl
P3 (10 μM)	2.5 μl
H_2O	28.7 μl
dNTPs (10 mM)	1 μl
HF-Buffer (10x)	10 μl
Phusion	0.3 μl

5 min	98 °C	
30 sec	98 °C	30x
20 sec	50 °C	
50 sec	72 °C	
5 min	72 °C	
∞	4 °C	

Note, that the elongation time is independent of your insert and does not need further adjustment.

The use of different pOSIPs will grant you bands of different sizes. For single integration following bands are expected (**Figure S24**):

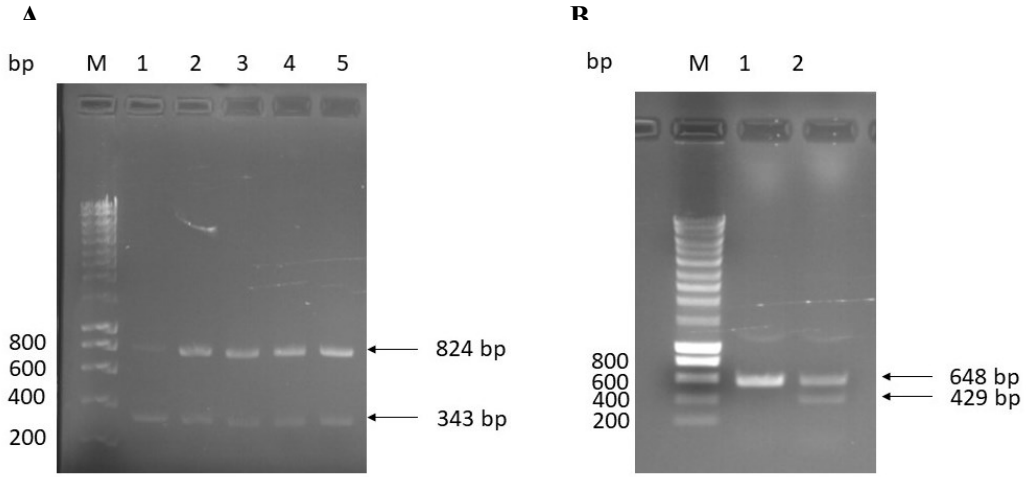

Figure S24 Colony-PCR of randomly picked colonies after one-step chromosomal integration. A, chromosomal integration with pOSIP-CH. M, SmartLadder by eurogentec; 1-5, randomly picked colonies. B, chromosomal integration with pOSIP-KO. M, SmartLadder by eurogentec; 1-2, randomly picked colonies. *E. coli* BL21(DE3) was used. Bp are for *E. coli* K12-MG1655.

However, as seen in **Figure S24**, B lane 1, only one band is shown at around 600 bp, while a second distinct band is missing. I encountered this numerous times that only one band was shown even though that both bands were shown before when testing the same clone. Hence, a negative colony PCR does not mean the colony is negative. You might have to consider to repeat the colony PCR multiple times. After checking for single integration by colony PCR you might want to check for activity of your protein. Furthermore, your insert should be sequenced.

Sequencing of DNA Constructs

For sequencing, amplify your insert from colonies by PCR. Use primers pOSIP seq for and pOSIP seq rev from **Table S4**. Choose an elongation time suitable for your insert. You can use the following pipette scheme and cycling program (adjusted to Phusion polymerase):

Table S4 Pipette scheme and cycling program for PCR.

pOSIP seq for (10 µM)	2.5 µl
pOSIP seq rev (10 µM)	2.5 µl
H_2O	33.7 µl
dNTPs (10 mM)	1 µl
HF-Buffer (10x)	10 µl
Phusion	0.3 µl

5 min	98 °C	
30 sec	98 °C	30x
20 sec	59 °C	
X sec	72 °C	
5 min	72 °C	
∞	4 °C	

You can simply clean your amplified product by a PCR clean-up kit and prepare it for sequencing. Both primers can be used for sequencing, but you will want to tick “GC-rich sequence” in your sequencing options. Also consider designing primers which bind within your insert!

Excision of integration module

Remember that antibiotic resistance is also integrated using pOSIPs. To excise the integration module, prepare chemically competent cells of your colonies containing your sequenced insert. Now, transform at least 50 μl of your competent cells with pE-FLP (>50 ng) to excise everything between the FRT sites (**Figure S23** Following successful site-specific recombination between the pOSIP attP sequence and chromosomal attB site, single integration produces two fragments, one from P1 and P2, and one from P3 and P4. Blue (genome), grey circles (attP and attB sites), green (FRT sites), beige (integration module), red (terminators), light blue (insert). P is for primer. **Figure S23**, green arrows). After transformation, incubate your cells in SOC-medium for 3 h at 30 °C. This turned out to be a critical step. After regeneration, centrifuge the transformation mix and resuspend the pellet in a smaller volume. Now plate half of the volume on LB-agar plates (10 μg/ml ampicillin) and incubate your plates at 30 °C overnight. Plate

untransformed cells as well as a control onto plates with same antibiotic concentration. Since the antibiotic concentration is really low you might want to stamp your cells onto LB-agar plates with higher ampicillin concentration to make sure no satellite colonies show up. Also stamp your colonies onto LB-agar plates supplemented with either chloramphenicol or kanamycin to make sure the cells lost their resistance. The excision efficiency is reported to be 100%. You can also run a colony PCR with P1 and P4 suitable for your original plasmid. pE-FLP contains a temperature-sensitive replicon of pCP20, meaning that the plasmid is only propagated at 30 °C. Simply grow your colonies at 37 °C to prevent any further pE-FLP propagation. Inoculate 5 ml LB-media without antibiotics with a colony and incubate it overnight at 37 °C. Next day, plate your cells onto LB-agar plates without antibiotics, LB-agar with ampicillin (5 μg/ml, 25 μg/ml) and again chloramphenicol/kanamycin. Meanwhile prepare a glycerol stock of your colonies. When no colonies show up on plates with antibiotics you can be sure that the resistance was excised efficiently and that the pE-FLP plasmid is lost.

13.3.2. *In vivo* protease assays

Plate reader specifications fluorescence rescue assay for *E. coli*

Table S5 Plate reader settings for the mNG C-degron assay

Parameter			Value
Plate			[COR96fb clear bottom] - Corning 96 Flat Black
Lid lifter			No lid
Humidity Cassette			No humidity cassette
Smooth mode			Selected
Temperature control			On
Target temperature			30 °C
Mode			Kinetic
	Kinetic duration		6 h
	Interval time		15 min
	Mode		Absorbance
		Name	OD600
		Measurement wavelength	600 nm
		Number of flashes	10
		Settle time	50 ms
	Mode		Fluorescence Top Reading
		Name	mNeonGreen
		Excitation	Monochromator
		Excitation wavelength	485 nm
		Excitation bandwidth	20 nm
		Emission	Monochromator
		Emission wavelength	535 nm

	Emission bandwidth	20 nm
	Gain	70
	Mirror	Automatic (Dichroic 510)
	Number of flashes	10
	Integration time	40 µs
	Lag time	0
	Settle time	0
	Z-Position	20000 µm
	Z-Position mode	Manual
Shaking (Double Orbital) Duration		Continuous
Shaking (Double Orbital) Position		Current
Shaking (Double Orbital) Amplitude		1 mm
Shaking (Double Orbital) Frequency		270 rpm

Plate reader setting for the ratiometric assay

Table S6 Plate reader settings for the ratiometric mNG-mCh N-degron assay

Parameter			Value
Plate			[COR96fb clear bottom] - Corning 96 Flat Black
Lid lifter			No lid
Humidity Cassette			No humidity cassette
Smooth mode			Selected
Temperature control			On
Target temperature			30 °C
Mode			Kinetic
	Kinetic duration		6 h
	Interval time		15 min
	Mode		Absorbance
		Name	OD600
		Measurement wavelength	600 nm
		Number of flashes	10
		Settle time	50 ms
	Mode		Fluorescence Top Reading
		Name	mNeonGreen
		Excitation	Monochromator
		Excitation wavelength	485 nm
		Excitation bandwidth	20 nm
		Emission	Monochromator
		Emission wavelength	535 nm
		Emission bandwidth	20 nm

	Gain	70
	Mirror	Automatic (Dichroic 510)
	Number of flashes	10
	Integration time	40 µs
	Lag time	0
	Settle time	0
	Z-Position	20000 µm
	Z-Position mode	Manual
	Mode	Fluorescence Top Reading
	Name	mCherry
	Excitation	Monochromator
	Excitation wavelength	578 nm
	Excitation bandwidth	20 nm
	Emission	Monochromator
	Emission wavelength	619 nm
	Emission bandwidth	20 nm
	Gain	100
	Mirror	Automatic (Dichroic 510)
	Number of flashes	10
	Integration time	40 µs
	Lag time	0
	Settle time	0
	Z-Position	20000 µm
	Z-Position mode	Manual
Shaking (Double Orbital) Duration		Continuous

	Shaking (Double Orbital) Position	Current
	Shaking (Double Orbital) Amplitude	1 mm
	Shaking (Double Orbital) Frequency	270 rpm

Plate reader settings for the mCherry C-degron assay

Table S7 Plate reader settings for the mCh C-degron assay

Parameter			**Value**
Plate			[COR96fb clear bottom] - Corning 96 Flat Black
Lid lifter			No lid
Humidity Cassette			No humidity cassette
Smooth mode			Selected
Temperature control			On
Target temperature			30 °C
Mode			Kinetic
	Kinetic duration		6 h
	Interval time		15 min
	Mode		Absorbance
		Name	OD600
		Measurement wavelength	600 nm
		Number of flashes	10
		Settle time	50 ms
	Mode		Fluorescence Top Reading
		Name	mCherry
		Excitation	Monochromator
		Excitation wavelength	578 nm

	Excitation bandwidth	20 nm
	Emission	Monochromator
	Emission wavelength	619 nm
	Emission bandwidth	20 nm
	Gain	100
	Mirror	Automatic (Dichroic 510)
	Number of flashes	10
	Integration time	40 µs
	Lag time	0
	Settle time	0
	Z-Position	20000 µm
	Z-Position mode	Manual
Shaking (Double Orbital) Duration		Continuous
Shaking (Double Orbital) Position		Current
Shaking (Double Orbital) Amplitude		1 mm
Shaking (Double Orbital) Frequency		270 rpm

13.4. Constructs used in this work

The constructs used for the experiments shown in Results Chapter are listed below ordered by the respective figures.

13.4.1. Figure 10

FKBP-mNeonGreen-^{TVMV}

MSSGSSGVQVETISPGDGRTFPKRGQTCVVHYTGMLEDGKKFDSSRDRNKPFKFMLGKQEVIRGW
EEGVAQMSVGQRAKLTISPDYAYGATGHPGIIPPHATLVFDVELLKLEGGSGGSGVSKGEEDNMASL
PATHELHIFGSINGVDFDMVGQGTGNPNDGYEELNLKSTKGDLQFSPWILVPHIGYGFHQYLPYPD
GMSPFQAAMVDGSGYQVHRTMQFEDGASLTVNYRYTYEGSHIKGEAQVKGTGFPADGPVMTNSL
TAADWCRSKKTYPNDKTIISTFKWSYTTGNGKRYRSTARTTYTFAKPMAANYLKNQPMYVFRKTEL
KHSKTELNFKEWQKAFTDVMGMDELYKGGSGGSGETVRFQ|SGIA*

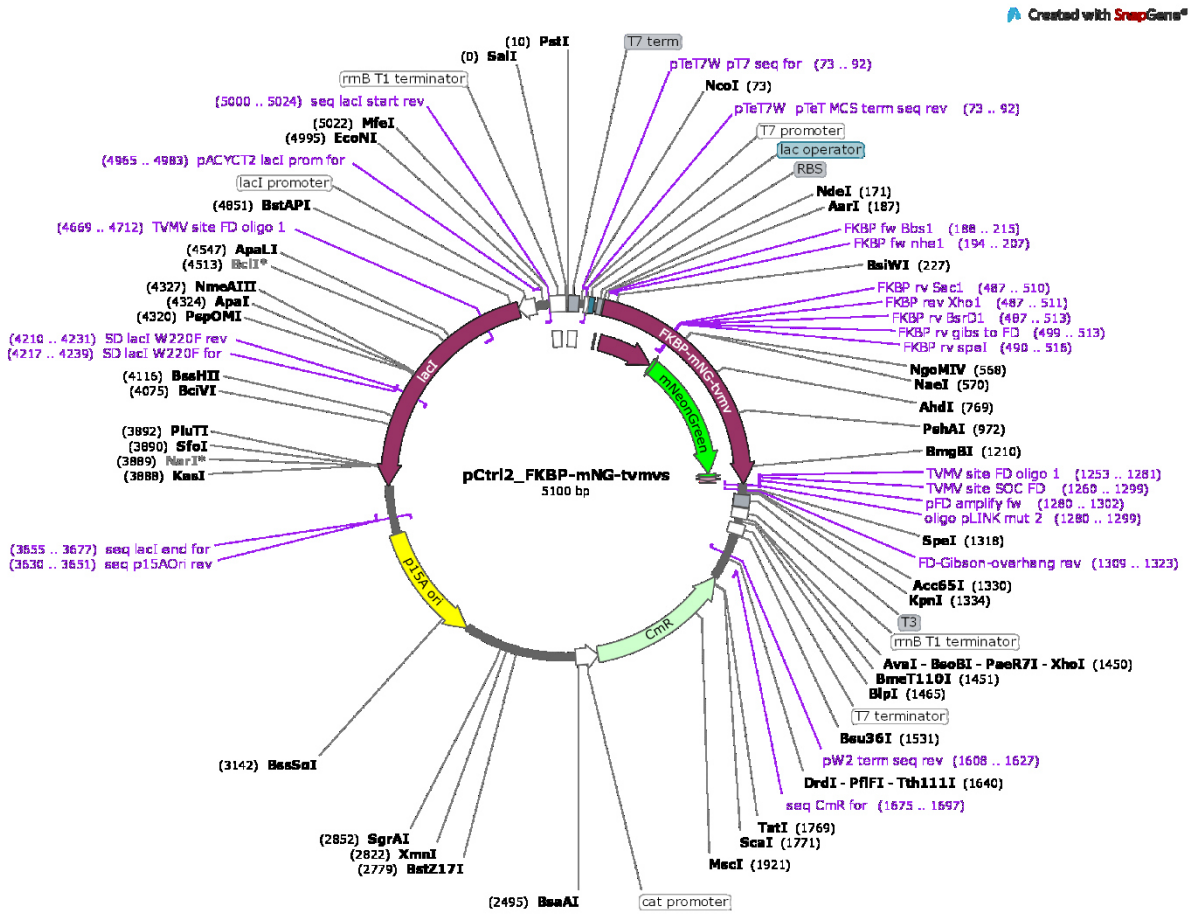

Figure S25 Vector map pCtrl2_FKBP-mNG-^{TVMV}. Figure generated with SnapGene (GSL Biotech LLC).

FKBP-mNeonGreen-^{TVMV}(E118-134)

MSSGSSGVQVETISPGDGRTFPKRGQTCVVHYTGMLEDGKKFDSSRDRNKPFKFMLGKQEVIRGW
EEGVAQMSVGQRAKLTISPDYAYGATGHPGIIPPHATLVFDVELLKLEGGSGGSGVSKGEEDNMASL
PATHELHIFGSINGVDFDMVGQGTGNPNDGYEELNLKSTKGDLQFSPWILVPHIGYGFHQYLPYPD
GMSPFQAAMVDGSGYQVHRTMQFEDGASLTVNYRYTYEGSHIKGEAQVKGTGFPADGPVMTNSL
TAADWCRSKKTYPNDKTIISTFKWSYTTGNGKRYRSTARTTYTFAKPMAANYLKNQPMYVFRKTEL
KHSKTELNFKEWQKAFTDVMGMDELYKGGSGGSGETVRFQ|SGGAEAAAKEAAAKAGGFGTWAC
RVRASHGVCAQ*

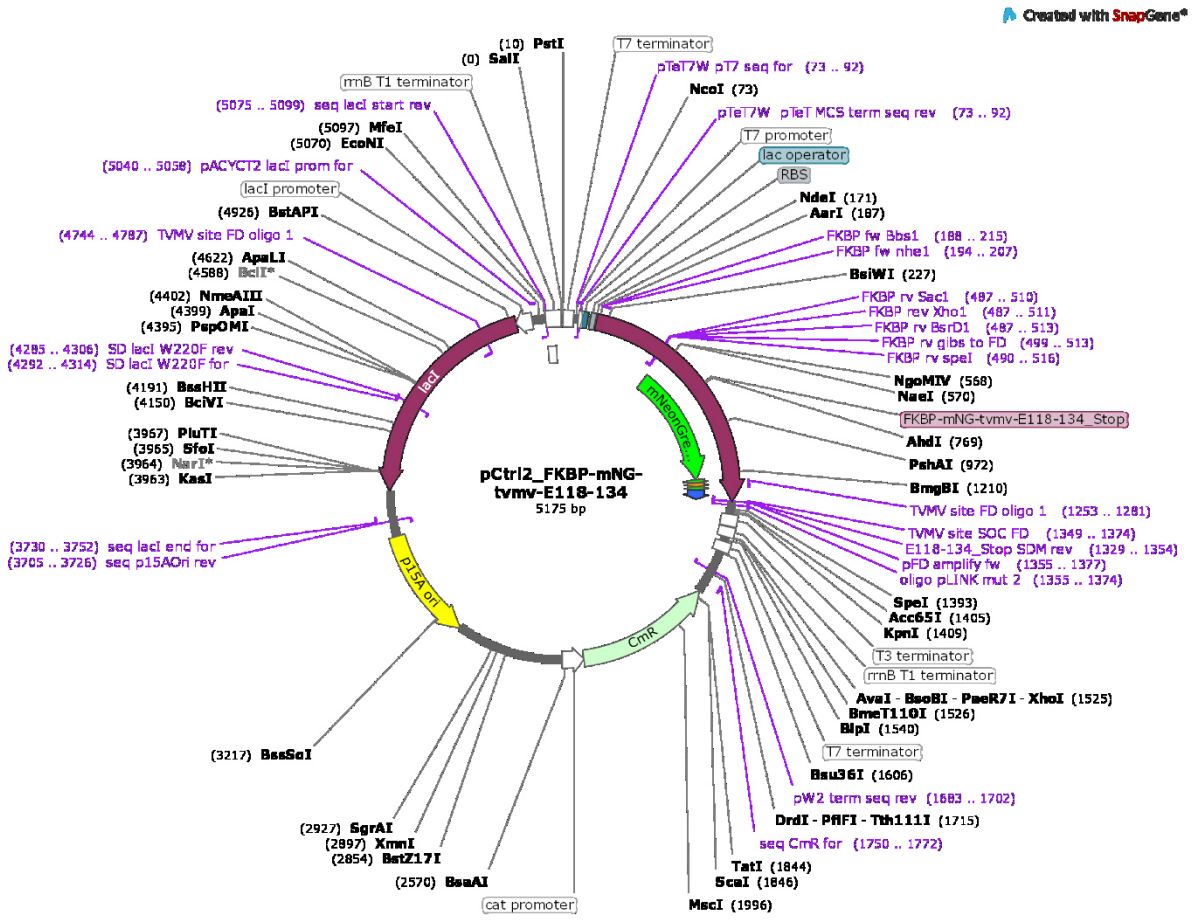

Figure S26 Vector map pCtrl2_FKBP-mNG-^{TVMV}E118-134. Figure generated with SnapGene (GSL Biotech LLC).

TVMV/TVMV(C151A)-FRB

MGSGSIGKIEEGKLVIWINGDKGYNGLAEVGKKFEKDTGIKVTVEHPDKLEEKFPQVAATGDGPDIIF
WAHDRFGGYAQSGLLAEITPDKAFQDKLYPFTWDAVRYNGKLIAYPIAVEALSLIYNKDLLPNPPKT
WEEIPALDKELKAKGKSALMFNLQEPYFTWPLIAADGGYAFKYENGKYDIKDVGVDNAGAKAGLTFL
VDLIKNKHMNADTDYSIAEAAFNKGETAMTINGPWAWSNIDTSKVNYGVTVLPTFKGQPSKPFVGV
LSAGINAASPNKELAKEFLENYLLTDEGLEAVNKDKPLGAVALKSYEEELVKDPRIAATMENAQKGEI
MPNIPQMSAFWYAVRTAVINAASGRQTVDEALKDAQTGLGGGSGGGSGGGSETGETVRFQ|SGG
ASPAGGSKALLKGVRDFNPISACVCLLENSSDGHSERLFGIGFGPYIIANQHLFRRNNGELTIKTMHG
EFKVKNSTQLQMKPVEGRDIIVIKMAKDFPPFPQKLKFRQPTIKDRVCMVSTNFQQKSVSSLVSESS
HIVHKEDTSFWQHWITTKDGQC/AGSPLVSIIDGNILGIHSLTHTTNGSNYFVEFPEKFVATYLDAAD
GWCKNWKFNADKISWGSFTLVEDAPEDGGASPAAPAPASPAAPAPSAPAGGILWHEMWHEGLEE
ASRLYFGERNVKGMFEVLEPLHAMMERGPQTLKETSFNQAYGRDLMEAQEWCRKYMKSGNVKDL
TQAWDLYYHVFRRIGIA*

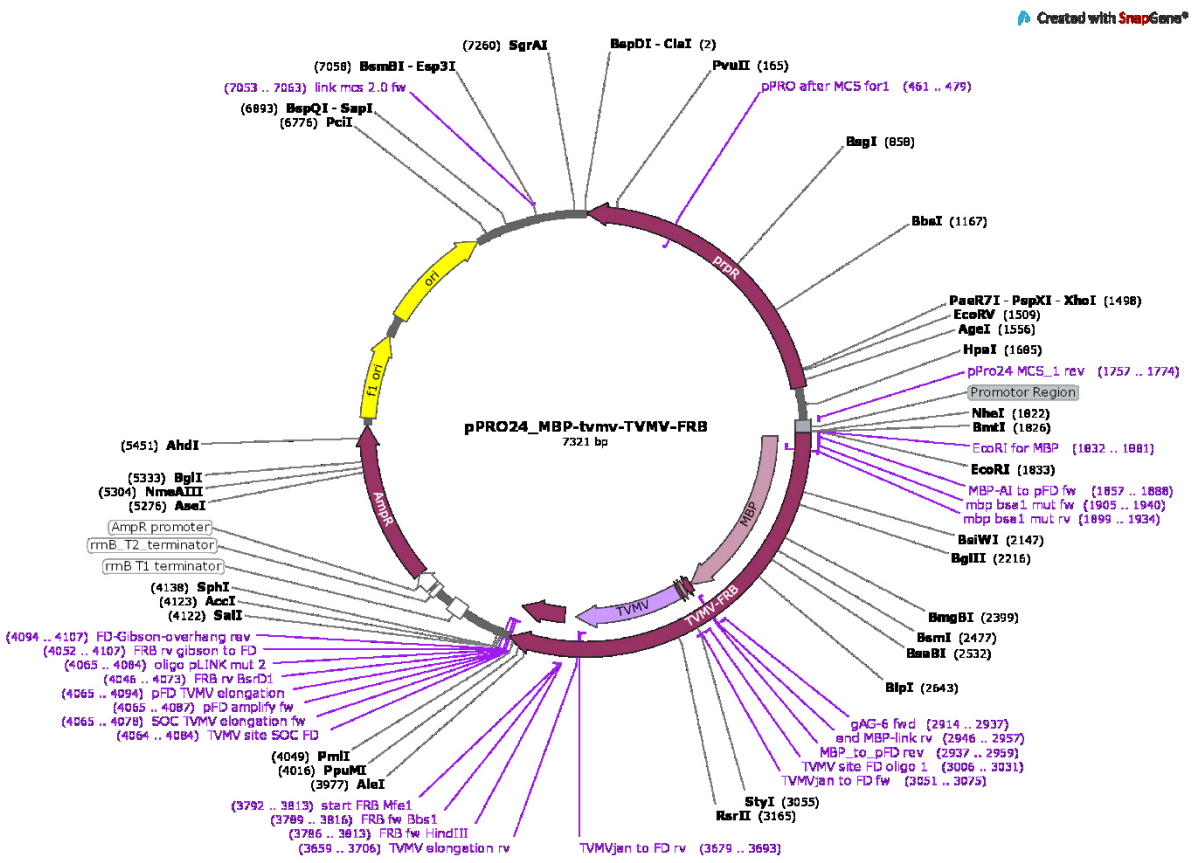

Figure S27 Vector map pPRO24_MBP-$^{TV>MV}$-TVMV-FRB. Figure generated with SnapGene (GSL Biotech LLC).

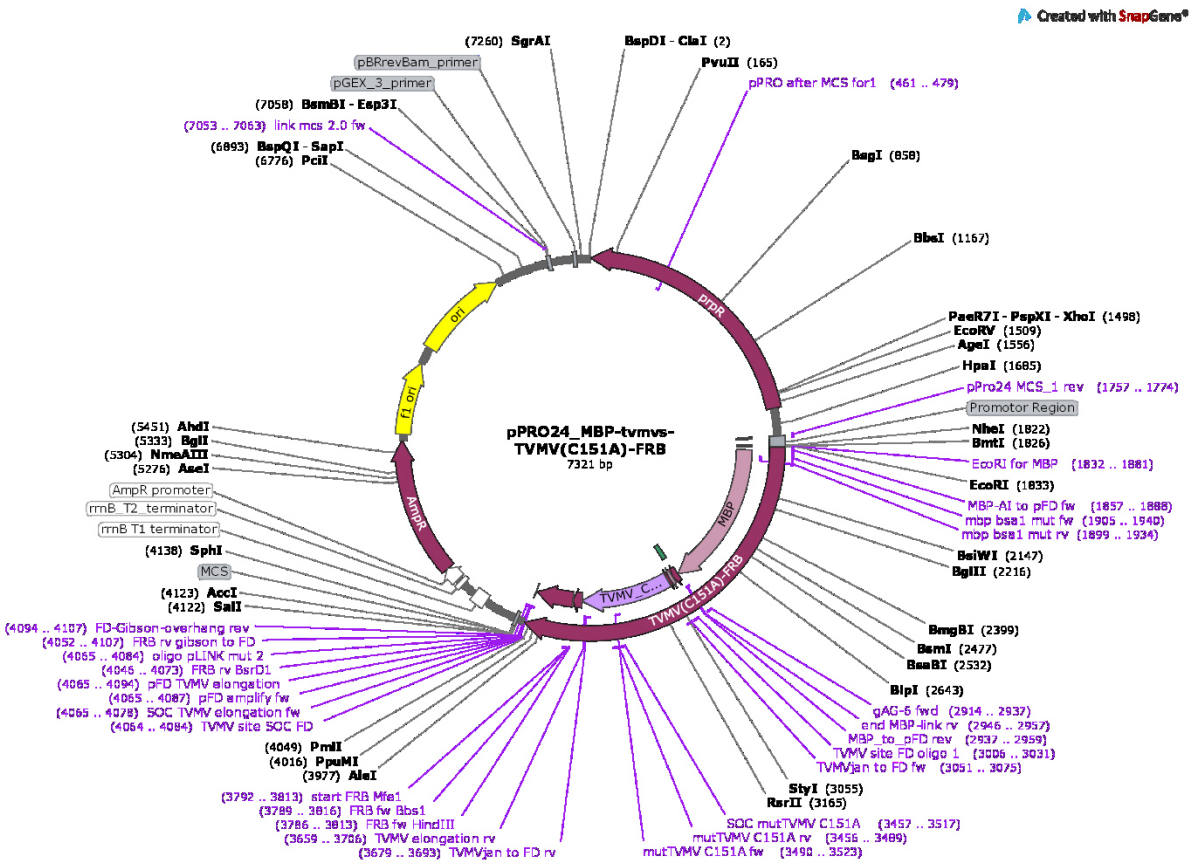

Figure S28 Vector map pPRO24_MBP-^{TVMV}-TVMV^{C151A}-FRB. Figure generated with SnapGene (GSL Biotech LLC).

13.4.2. Figure 15

FKBP-mNG-^{TVMV}LVA

MSSGSSGVQVETISPGDGRTFPKRGQTCVVHYTGMLEDGKKFDSSRDRNKPFKFMLGKQEVIRGW
EEGVAQMSVGQRAKLTISPDYAYGATGHPGIIPPHATLVFDVELLKLEGGSGGSGVSKGEEDNMASL
PATHELHIFGSINGVDFDMVGQGTGNPNDGYEELNLKSTKGDLQFSPWILVPHIGYGFHQYLPYPD
GMSPFQAAMVDGSGYQVHRTMQFEDGASLTVNYRYTYEGSHIKGEAQVKGTGFPADGPVMTNSL
TAADWCRSKKTYPNDKTIISTFKWSYTTGNGKRYRSTARTTYTFAKPMAANYLKNQPMYVFRKTEL
KHSKTELNFKEWQKAFTDVMGMDELYKGGSGGSGETVRFQ|SGGAEAAAKEAAAKAGGAANDEN
YALVAGIA*

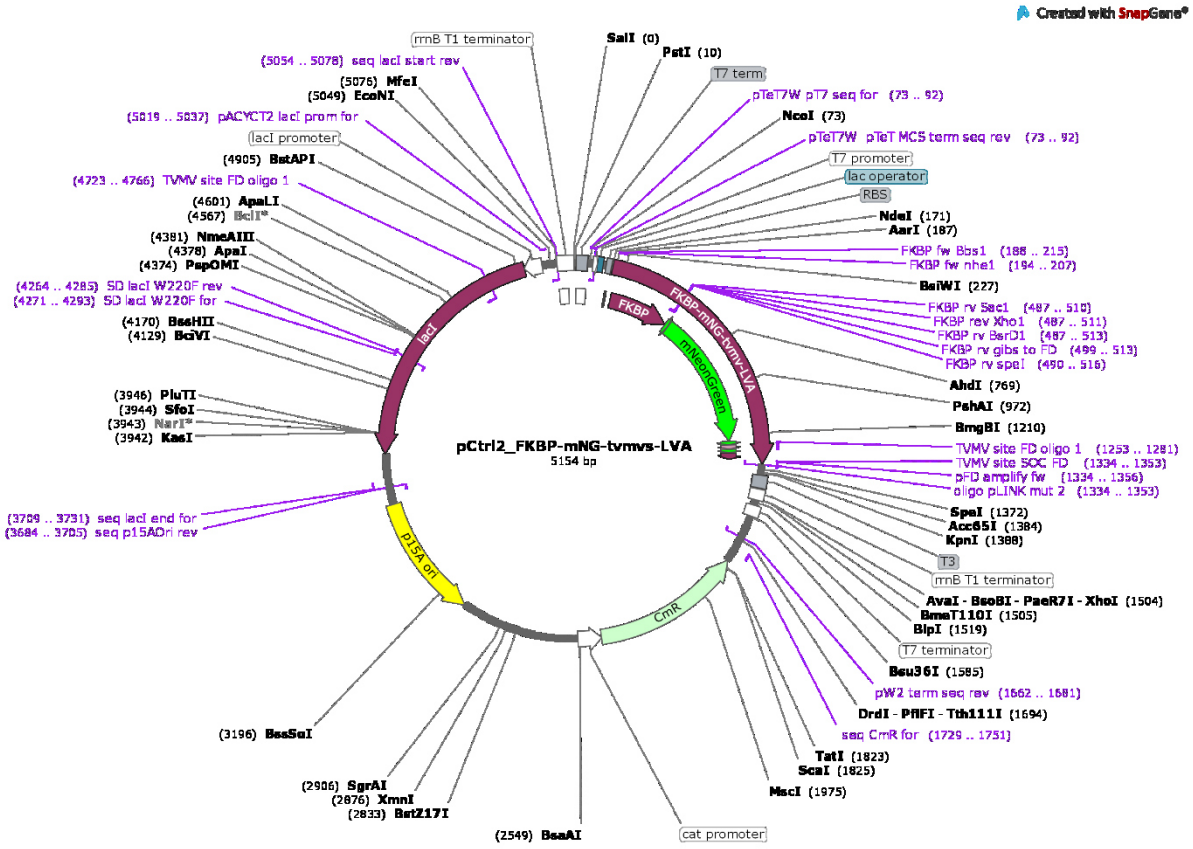

Figure S29 Vector map pCtrl2_FKBP-mNG-^{TVMV}LVA. Figure generated with SnapGene (GSL Biotech LLC).

13.4.3. Figure 16

pCtrl2_T7.03_U9_FKBP-mNG-^{TVMV}

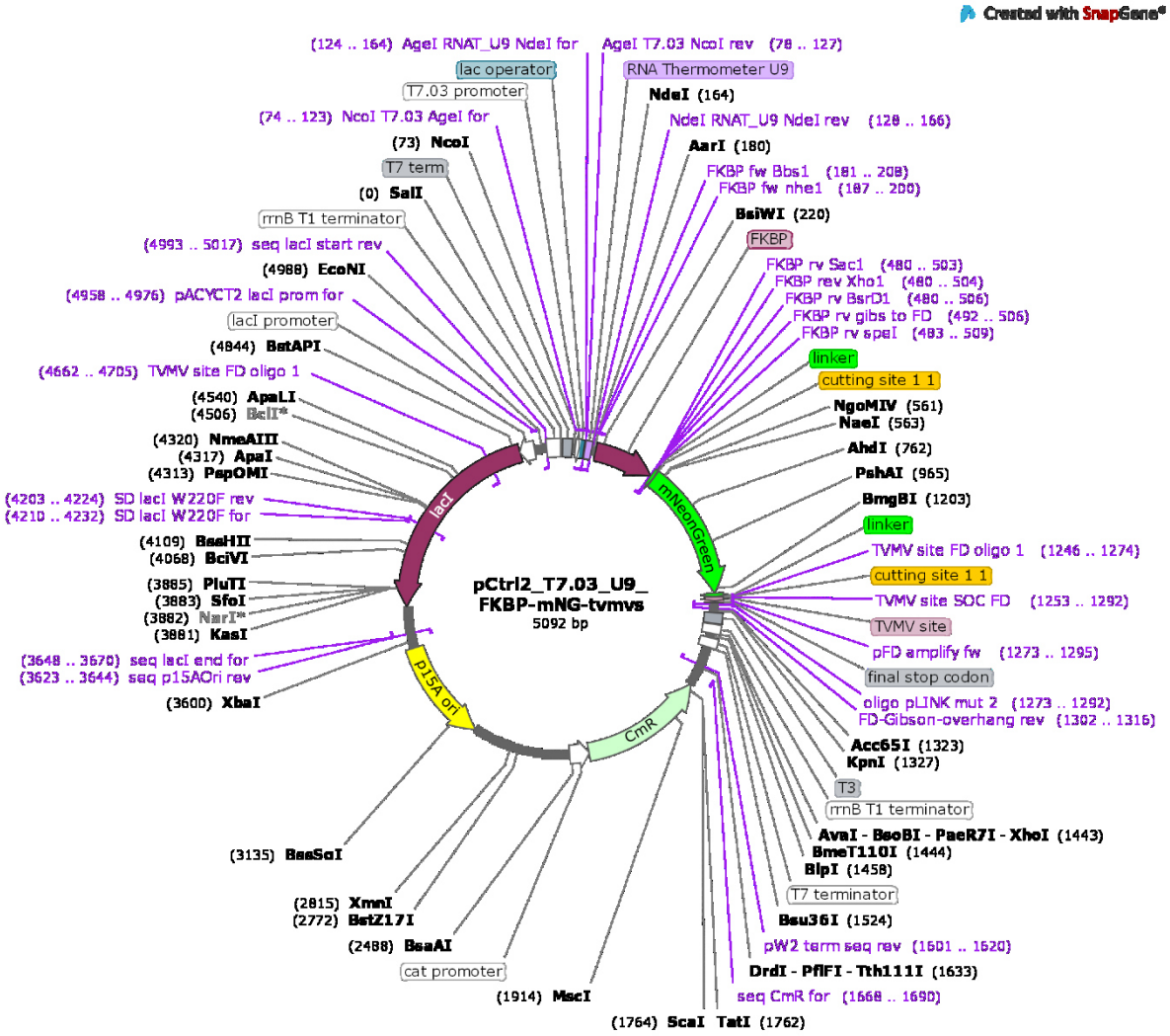

Figure S30 Vector map pCtrl2_T7.03_U9_FKBP-mNG-^{TVMV}. Figure generated with SnapGene (GSL Biotech LLC).

pCtrl2_T7.03_U9_FKBP-mNG-^{TVMV}E118-134

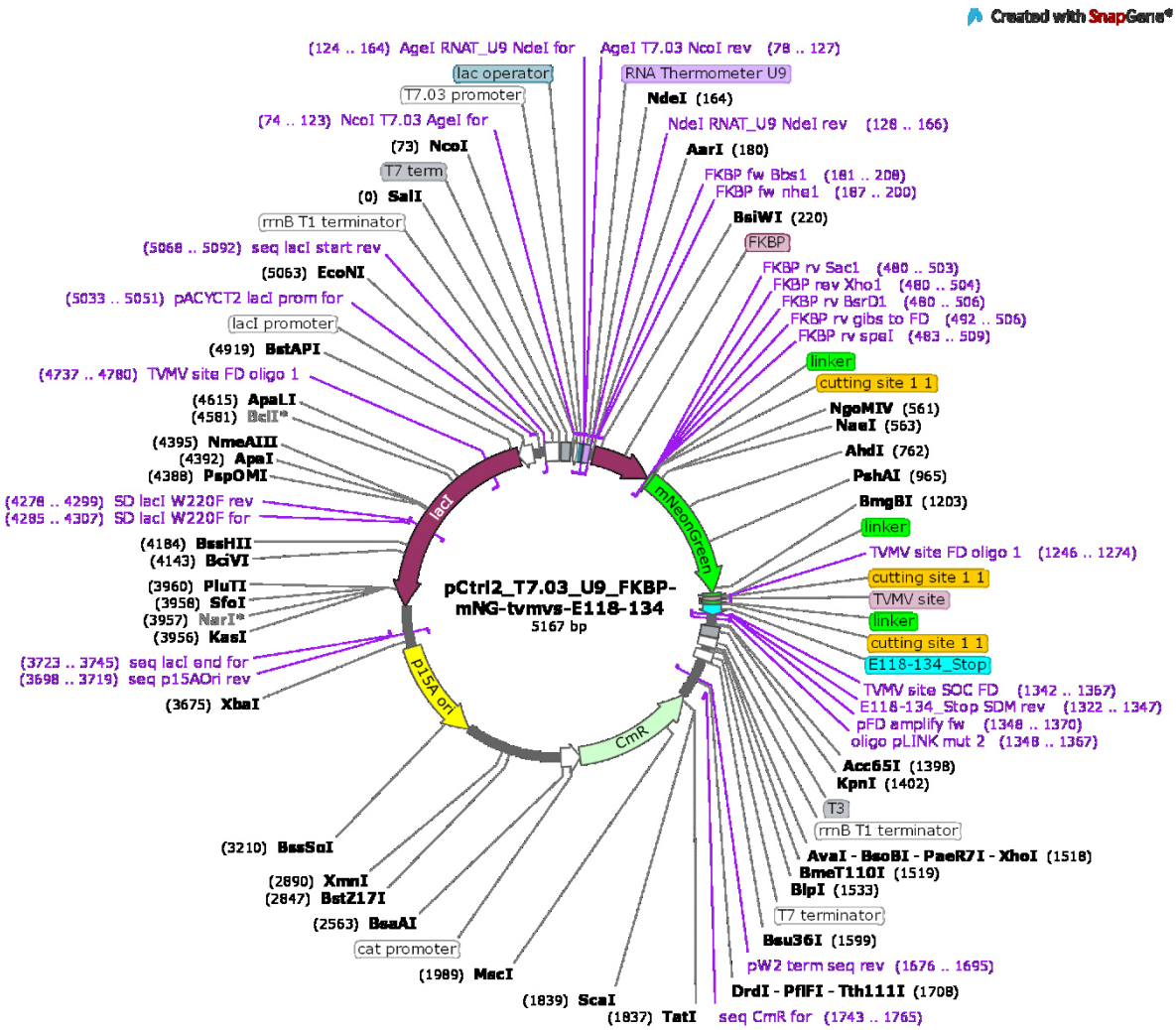

Figure S31 Vector map pCtrl2_T7.03_U9_FKBP-mNG-^{TVMV}E118-134. Figure generated with SnapGene (GSL Biotech LLC).

pCtrl2_T7.03_U9_FKBP-mNG-^{TVMV}LVA

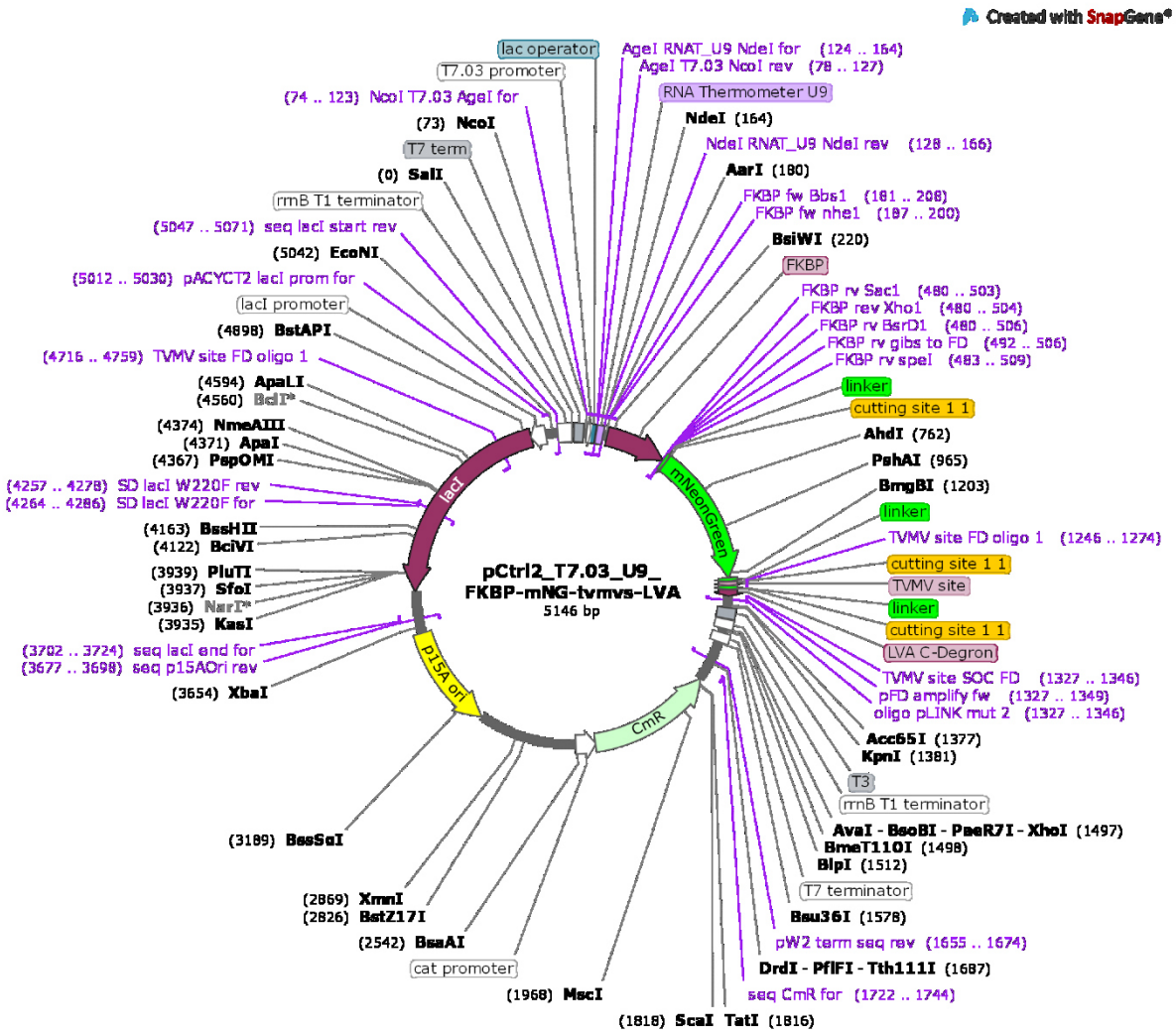

13.4.4. Figure 20

myc-SH3-mNG-^{TVMV}

MSSGSSGEQKLISEEDLGGASPAGGAEYVRALFDFNGNDEEDLPFKKGDILRIRDKPEEQWWNAED
SEGKRGMIPVPYVEKYGGASPAGGVSKGEEDNMASLPATHELHIFGSINGVDFDMVGQGTGNPND
GYEELNLKSTKGDLQFSPWILVPHIGYGFHQYLPYPDGMSPFQAAMVDGSGYQVHRTMQFEDGAS
LTVNYRYTYEGSHIKGEAQVKGTGFPADGPVMTNSLTAADWCRSKKTYPNDKTIISTFKWSYTTGN
GKRYRSTARTTYTFAKPMAANYLKNQPMYVFRKTELKHSKTELNFKEWQKAFTDVMGMDELYKG
GASPAAPAPAGETVRFQ|SGIA*

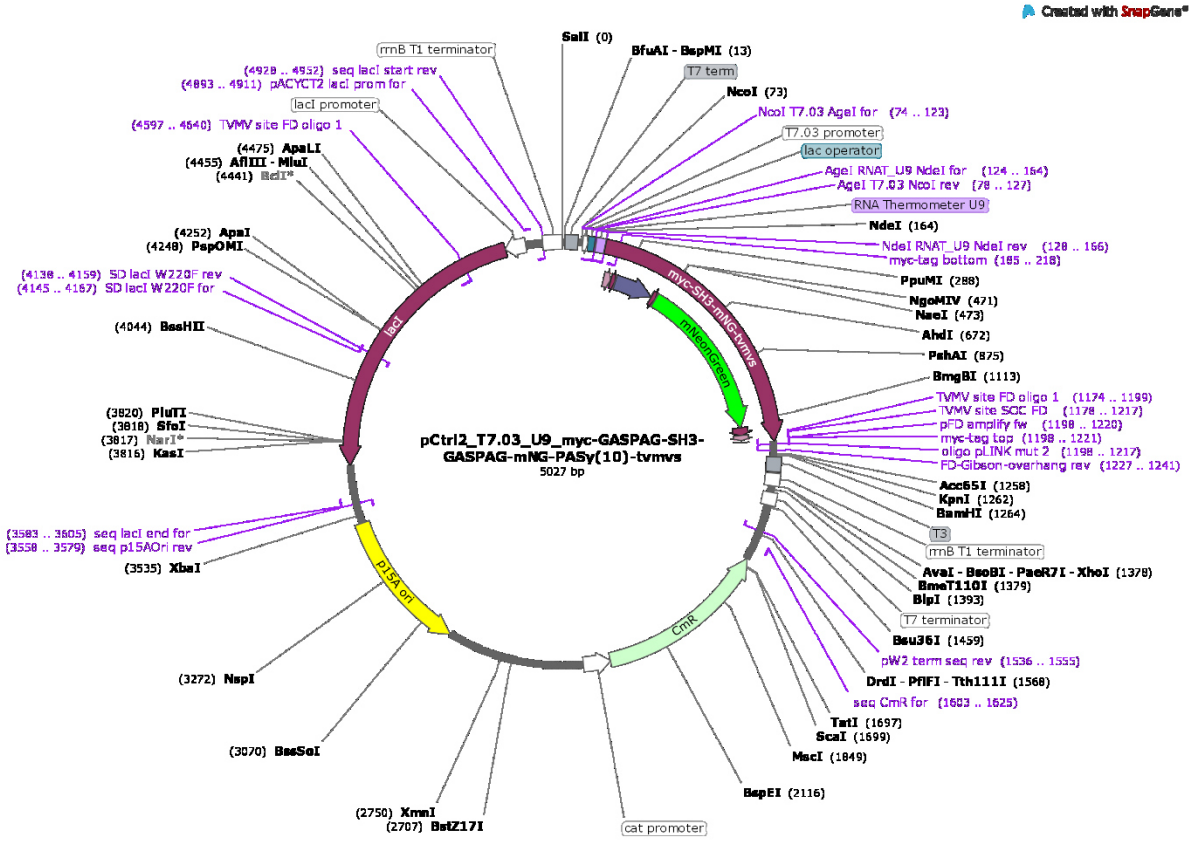

Figure S32 Vector map pCtrl2_T7.03_U9_myc-SH3- mNG^{TVMV}. Figure generated with SnapGene (GSL Biotech LLC).

myc-SH3-mNG-^{TVMV}(E118-134)/LVA

MSSGSSGEQKLISEEDLGGASPAGGAEYVRALFDFNGNDEEDLPFKKGDILRIRDKPEEQWWNAED
SEGKRGMIPVPYVEKYGGASPAGGVSKGEEDNMASLPATHELHIFGSINGVDFDMVGQGTGNPND
GYEELNLKSTKGDLQFSPWILVPHIGYGFHQYLPYPDGMSPFQAAMVDGSGYQVHRTMQFEDGAS
LTVNYRYTYEGSHIKGEAQVKGTGFPADGPVMTNSLTAADWCRSKKTYPNDKTIISTFKWSYTTGN
GKRYRSTARTTYTFAKPMAANYLKNQPMYVFRKTELKHSKTELNFKEWQKAFTDVMGMDELYKG
GASPAAPAPAGETVRFQ|SGGAEAAAKEAAAKAGGFGTWACRVRASHGVCAQ*/AANDENYALVA
GIA*

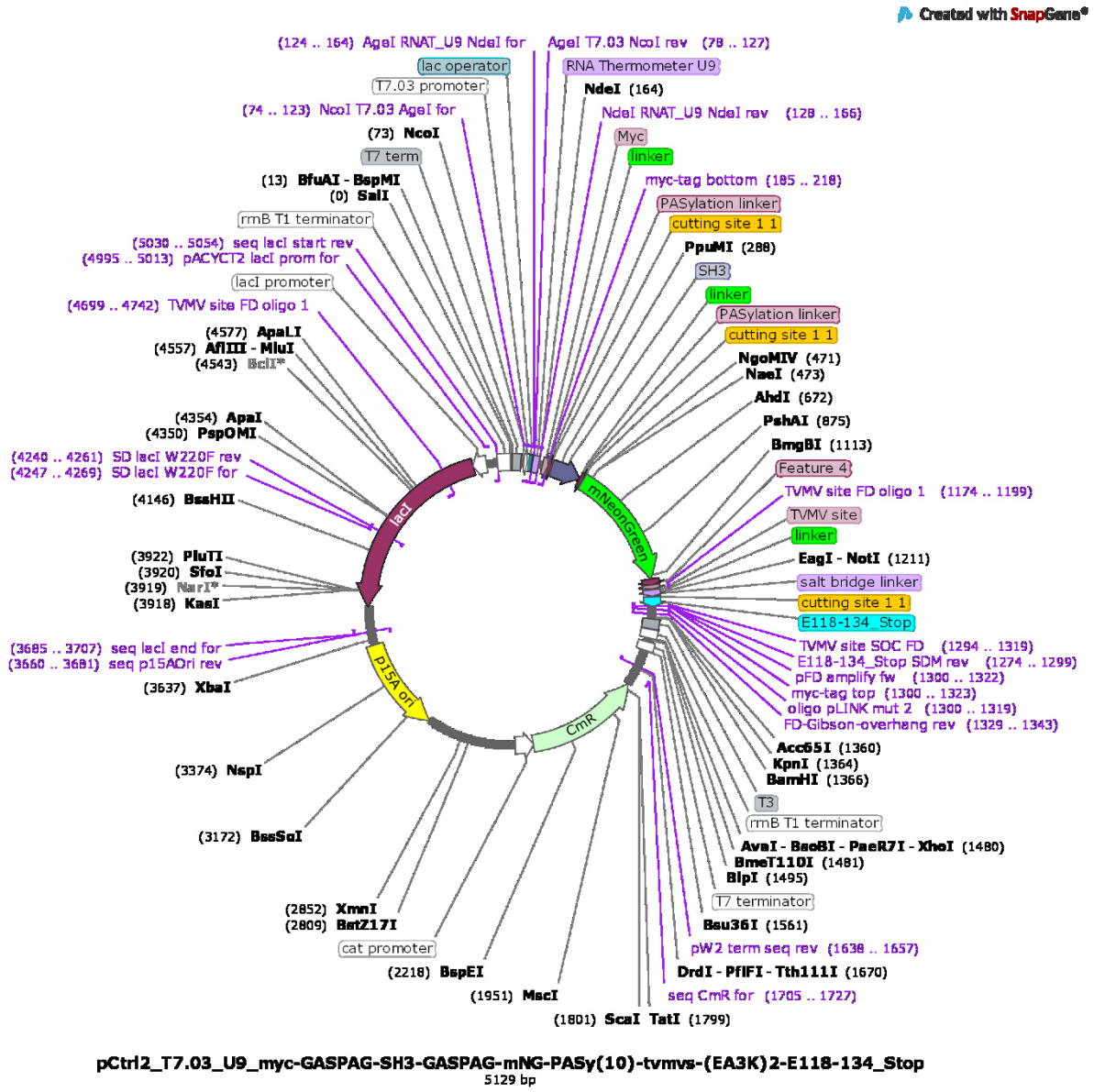

Figure S33 Vector map pCtrl2_T7.03_U9_myc-SH3- mNG^{TVMV}E118-134. Figure generated with SnapGene (GSL Biotech LLC).

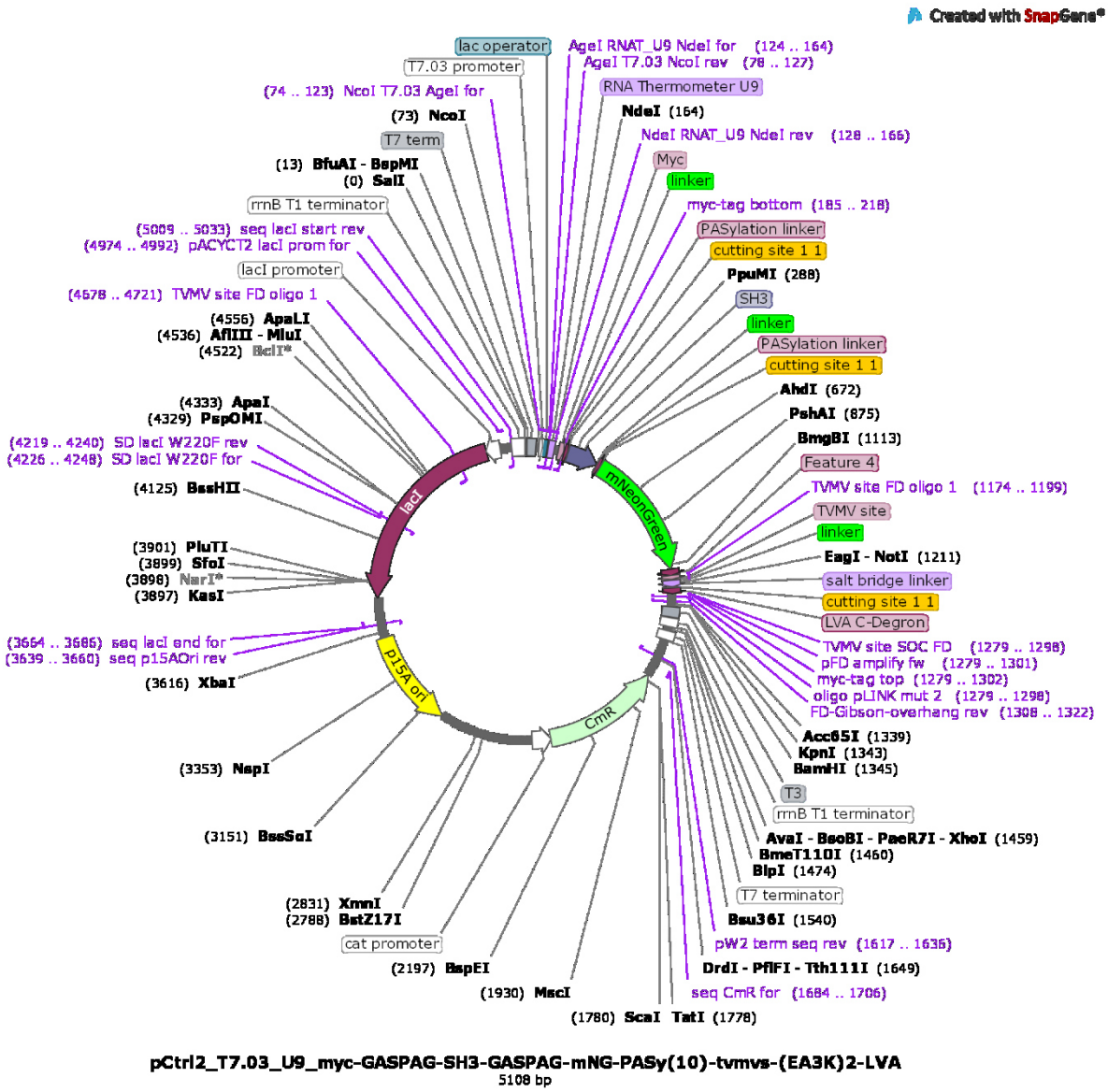

Figure S34 Vector map pCtrl2_T7.03_U9_myc-SH3- mNG^{TVMV}. Figure generated with SnapGene (GSL Biotech LLC).

MBP-^{TVMV}sSH3L-TVMV/TVMV(C151A)-Strep

MGSGSIGKIEEGKLVIWINGDKGYNGLAEVGKKFEKDTGIKVTVEHPDKLEEKFPQVAATGDGPDIIF
WAHDRFGGYAQSGLLAEITPDKAFQDKLYPFTWDAVRYNGKLIAYPIAVEALSLIYNKDLLPNPPKT
WEEIPALDKELKAKGKSALMFNLQEPYFTWPLIAADGGYAFKYENGKYDIKDVGVDNAGAKAGLTFL
VDLIKNKHMNADTDYSIAEAAFNKGETAMTINGPWAWSNIDTSKVNYGVTVLPTFKGQPSKPFVGV
LSAGINAASPNKELAKEFLENYLLTDEGLEAVNKDKPLGAVALKSYEEELVKDPRIAATMENAQKGEI
MPNIPQMSAFWYAVRTAVINAASGRQTVDEALKDAQTGLGGGSGGGSGGGSETGETVRFQ|SGNS
SSNNNNNNNNNNGPPPPLPPKRRRGGSGGSGGSGGSGGSGGSGGSGGSGSKALLKGVRDFNPISA
CVCLLENSSDGHSERLFGIGFGPYIIANQHLFRRNNGELTIKTMHGEFKVKNSTQLQMKPVEGRDIIV
IKMAKDFPPFPQKLKFRQPTIKDRVCMVSTNFQQKSVSSLVSESSHIVHKEDTSFWQHWITTKDGQ
C/AGSPLVSIIDGNILGIHSLTHTTNGSNYFVEFPEKFVATYLDAADGWCKNWKFNADKISWGSFTL
VEDAPEDGGSGGSGWSHPQFEKGIA*

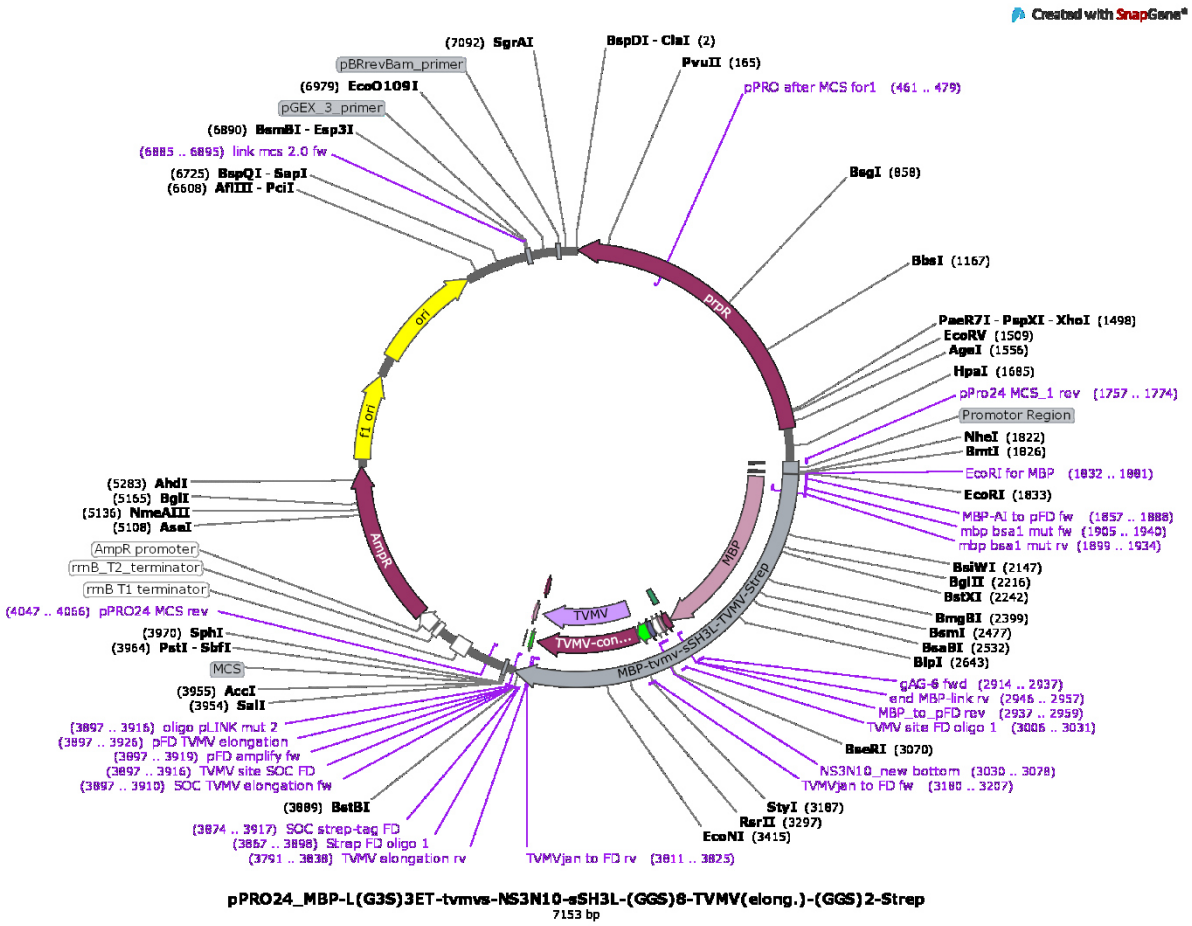

Figure S35 Vector map pPRO24_MBP-^{TVMV}sSH3L-TVMV-Strep. Figure generated with SnapGene (GSL Biotech LLC).

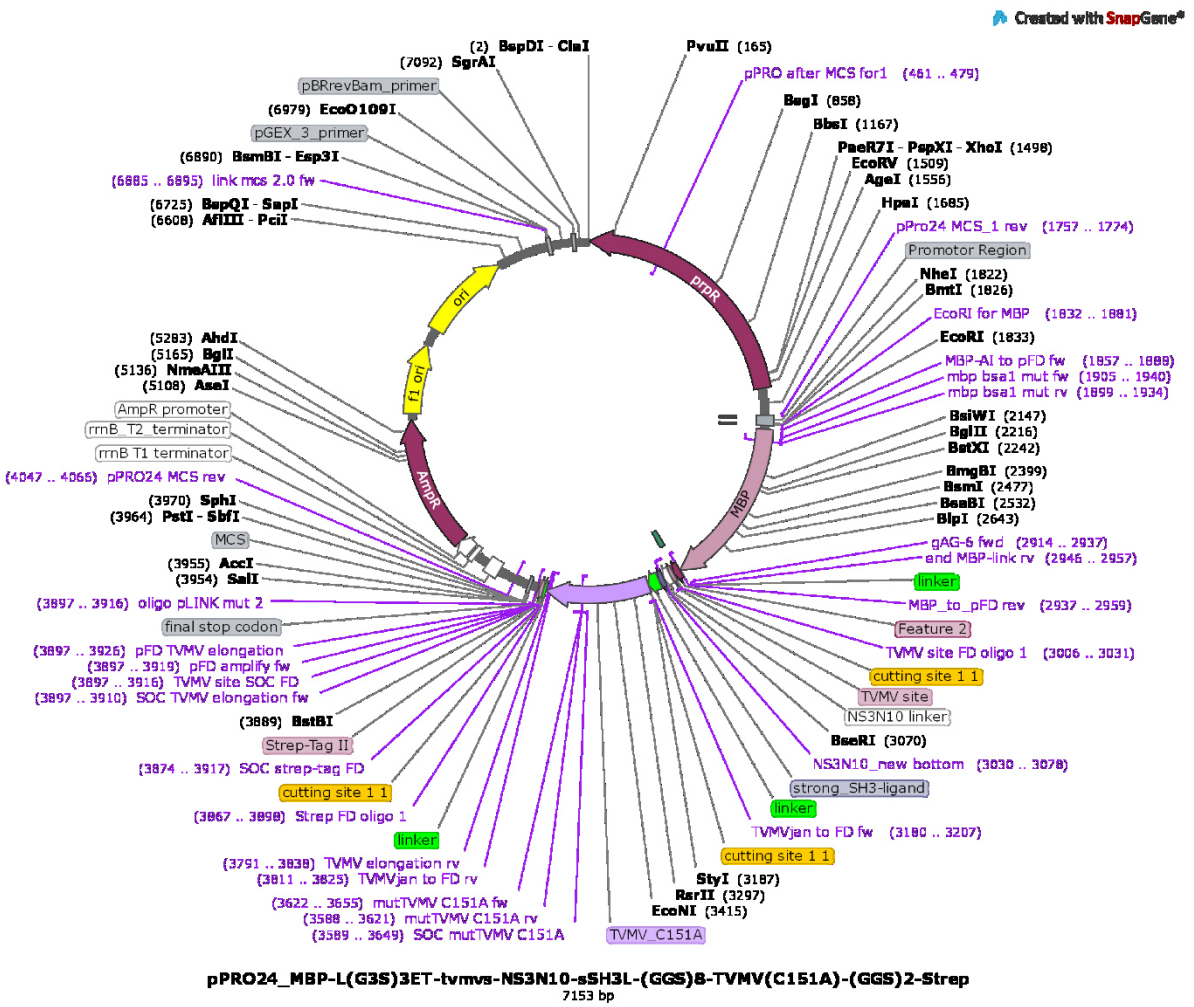

Figure S36 Vector map pPRO24_MBP-^{TVMV}sSH3L-TVMV^{C151A}-Strep. Figure generated with SnapGene (GSL Biotech LLC).

MBP-^{TVMV}wSH3L-TVMV/TVMV(C151A)-Strep

MGSGSIGKIEEGKLVIWINGDKGYNGLAEVGKKFEKDTGIKVTVEHPDKLEEKFPQVAATGDGPDIIF
WAHDRFGGYAQSGLLAEITPDKAFQDKLYPFTWDAVRYNGKLIAYPIAVEALSLIYNKDLLPNPPKT
WEEIPALDKELKAKGKSALMFNLQEPYFTWPLIAADGGYAFKYENGKYDIKDVGVDNAGAKAGLTFL
VDLIKNKHMNADTDYSIAEAAFNKGETAMTINGPWAWSNIDTSKVNYGVTVLPTFKGQPSKPFVGV
LSAGINAASPNKELAKEFLENYLLTDEGLEAVNKDKPLGAVALKSYEEELVKDPRIAATMENAQKGEI
MPNIPQMSAFWYAVRTAVINAASGRQTVDEALKDAQTGLGGGSGGGSGGGSETGETVRFQ|SGNS
SSNNNNNNNNNNGPPPALPPKKRGGSGGSGGSGGSGGSGGSGGSGGSGGSGSKALLKGVRDFNPISAC
VCLLENSSDGHSERLFGIGFGPYIIANQHLFRRNNGELTIKTMHGEFKVKNSTQLQMKPVEGRDIIVI
KMAKDFPPFPQKLKFRQPTIKDRVCMVSTNFQQKSVSSLVSESSHIVHKEDTSFWQHWITTKDGQC
/AGSPLVSIIDGNILGIHSLTHTTNGSNYFVEFPEKFVATYLDAADGWCKNWKFNADKISWGSFTLV
EDAPEDGGSGGSGWSHPQFEKGIA*

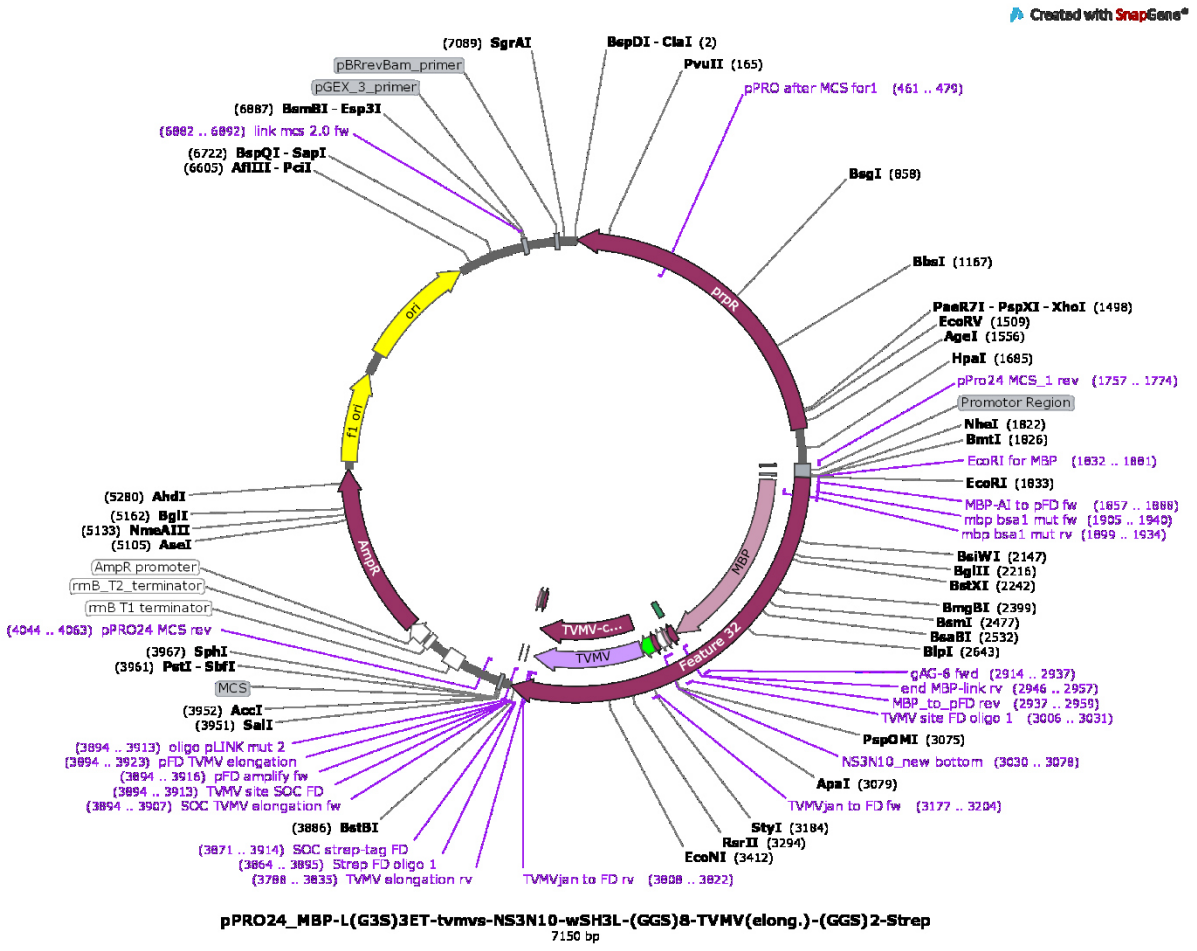

Figure S37 Vector map pPRO24_MBP-^{TVMV}wSH3L-TVMV-Strep. Figure generated with SnapGene (GSL Biotech LLC).

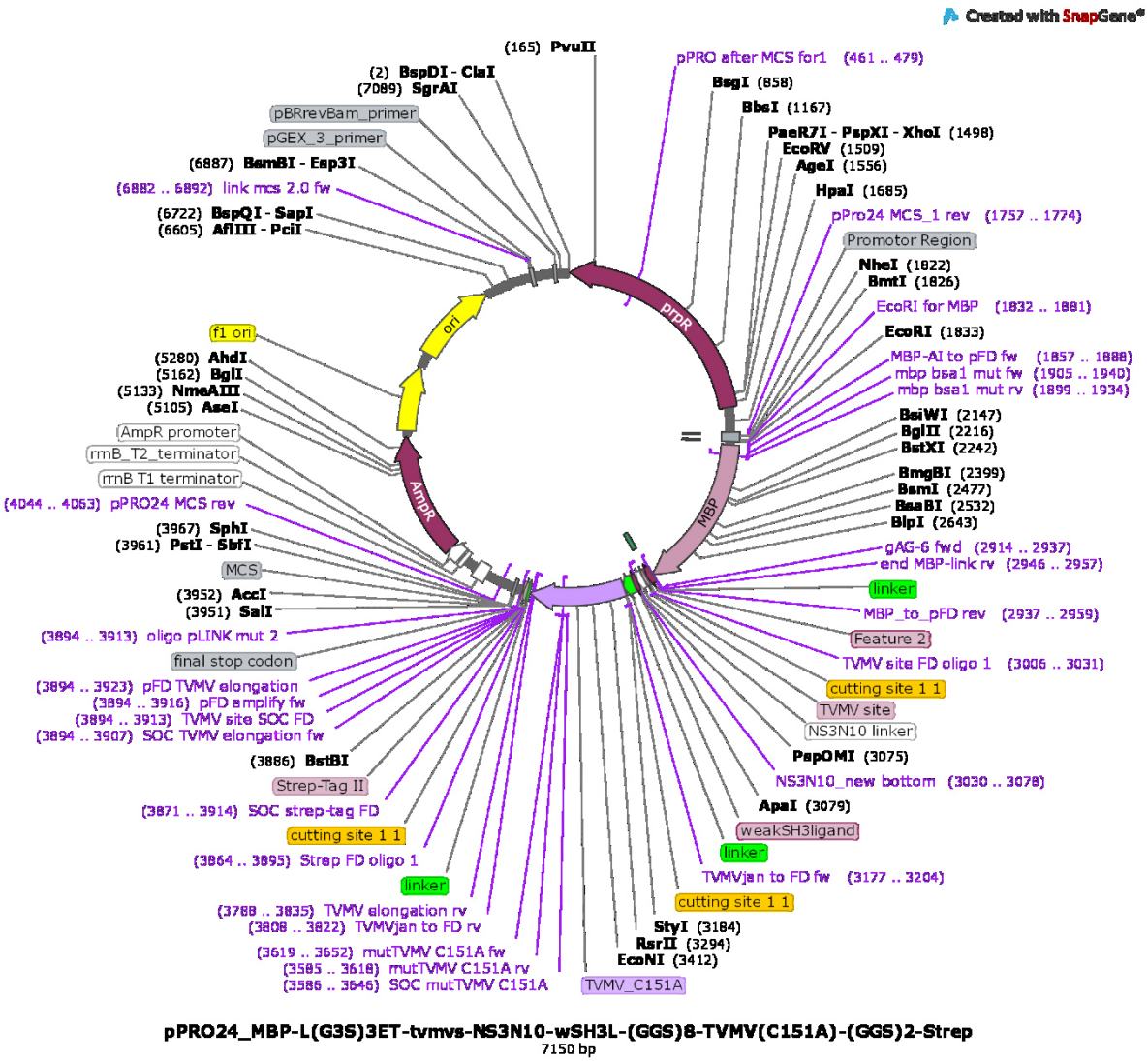

Figure S38 Vector map pPRO24_MBP-^{TVMV}wSH3L-TVMV^{C151A}-Strep. Figure generated with SnapGene (GSL Biotech LLC).

13.4.5. Figure 21

MBP-^{TVMV}TVMV/TVMV(C151A)-Strep

MGSGSIGKIEEGKLVIWINGDKGYNGLAEVGKKFEKDTGIKVTVEHPDKLEEKFPQVAATGDGPDIIF
WAHDRFGGYAQSGLLAEITPDKAFQDKLYPFTWDAVRYNGKLIAYPIAVEALSLIYNKDLLPNPPKT
WEEIPALDKELKAKGKSALMFNLQEPYFTWPLIAADGGYAFKYENGKYDIKDVGVDNAGAKAGLTFL
VDLIKNKHMNADTDYSIAEAAFNKGETAMTINGPWAWSNIDTSKVNYGVTVLPTFKGQPSKPFVGV
LSAGINAASPNKELAKEFLENYLLTDEGLEAVNKDKPLGAVALKSYEEELVKDPRIAATMENAQKGEI
MPNIPQMSAFWYAVRTAVINAASGRQTVDEALKDAQTGLGGGSGGGSGGGSETGETVRFQ|SGNS
SSNNNNNNNNNNGSKALLKGVRDFNPISACVCLLENSSDGHSERLFGIGFGPYIIANQHLFRRNNG
ELTIKTMHGEFKVKNSTQLQMKPVEGRDIIVIKMAKDFPPFPQKLKFRQPTIKDRVCMVSTNFQQKS
VSSLVSESSHIVHKEDTSFWQHWITTKDGQC/AGSPLVSIIDGNILGIHSLTHTTNGSNYFVEFPEKF
VATYLDAADGWCKNWKFNADKISWGSFTLVEDAPEDGGSGGSGWSHPQFEKGIA*

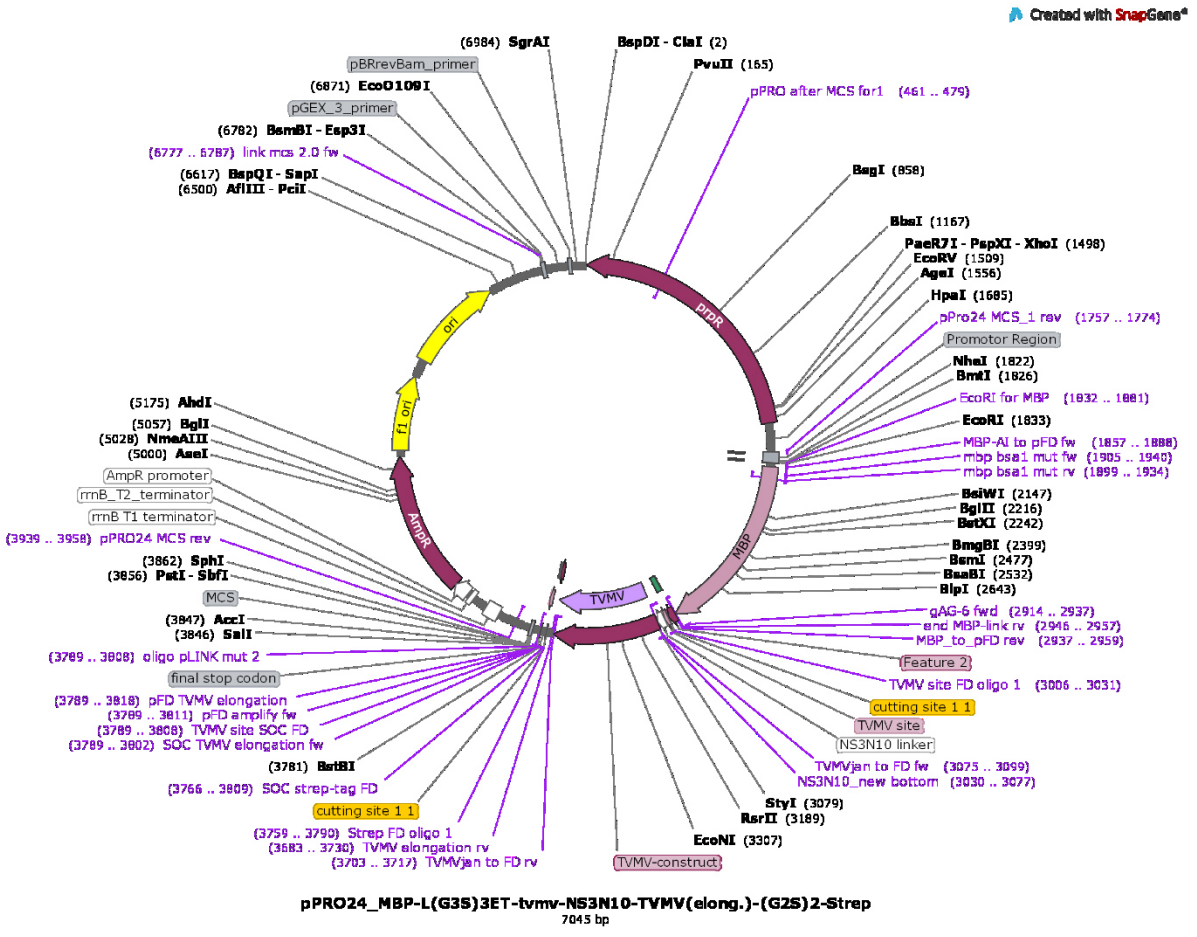

Figure S39 Vector map pPRO24_MBP-^{TVMV}TVMV-Strep. Figure generated with SnapGene (GSL Biotech LLC).

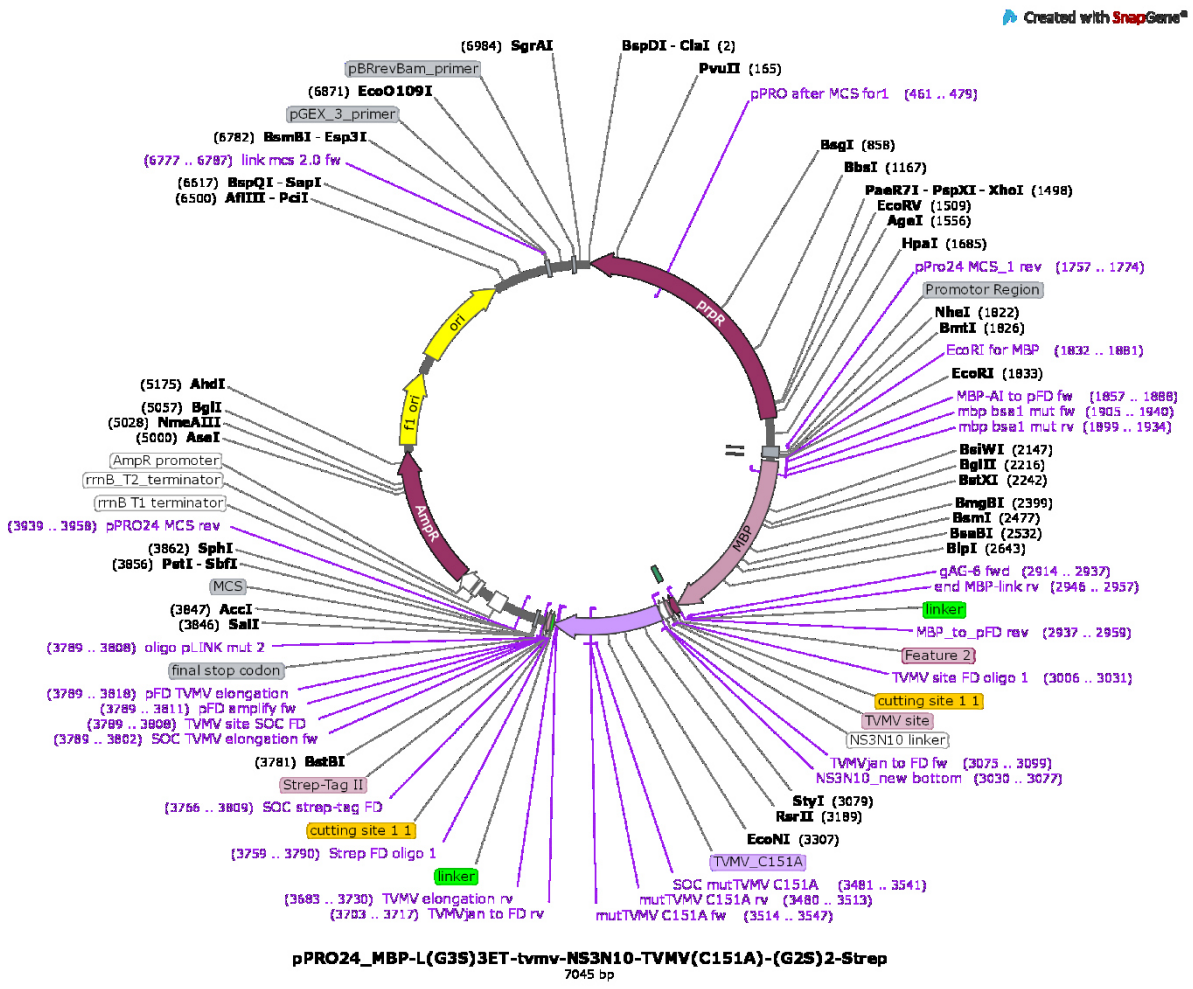

Figure S40 Vector map pPRO24_MBP-^{TVMV}TVMV^{C151A}-Strep. Figure generated with SnapGene (GSL Biotech LLC).

13.4.6. Figure 22

myc-SH3-mNG-^{TVMV}(E118-134)/LVA/(E118min)$_3$

MSSGSSGEQKLISEEDLGGASPAGGAEYVRALFDFNGNDEEDLPFKKGDILRIRDKPEEQWWNAED
SEGKRGMIPVPYVEKYGGASPAGGVSKGEEDNMASLPATHELHIFGSINGVDFDMVGQGTGNPND
GYEELNLKSTKGDLQFSPWILVPHIGYGFHQYLPYPDGMSPFQAAMVDGSGYQVHRTMQFEDGAS
LTVNYRYTYEGSHIKGEAQVKGTGFPADGPVMTNSLTAADWCRSKKTYPNDKTIISTFKWSYTTGN
GKRYRSTARTTYTFAKPMAANYLKNQPMYVFRKTELKHSKTELNFKEWQKAFTDVMGMDELYKG
GASPAAPAPAGETVRFQ|SGSGGGGFGTWACRVRASHGVCAQ*/AANDENYALVAGIA*/FGTWA
CRFGTWACRFGTWACR*

13.4.7. Figure 23

myc-mNG-SH3-^{TVMV}F/YLFVQ-mCherry-Strep

MSSGSSGEQKLISEEDLGPGVSKGEEDNMASLPATHELHIFGSINGVDFDMVGQGTGNPNDGYEEL
NLKSTKGDLQFSPWILVPHIGYGFHQYLPYPDGMSPFQAAMVDGSGYQVHRTMQFEDGASLTVNY
RYTYEGSHIKGEAQVKGTGFPADGPVMTNSLTAADWCRSKKTYPNDKTIISTFKWSYTTGNGKRYR
STARTTYTFAKPMAANYLKNQPMYVFRKTELKHSKTELNFKEWQKAFTDVMGMDELYKGGASPAG
GAEYVRALFDFNGNDEEDLPFKKGDILRIRDKPEEQWWNAEDSEGKRGMIPVPYVEKYGGASPAAP
APAGETVRFQ|F/YLFVQGGASPAAPAPAGVSKGEEDNMAIIKEFMRFKVHMEGSVNGHEFEIEGE
GEGRPYEGTQTAKLKVTKGGPLPFAWDILSPQFMYGSKAYVKHPADIPDYLKLSFPEGFKWERVMN
FEDGGVVTVTQDSSLQDGEFIYKVKLRGTNFPSDGPVMQKKTMGWEASSERMYPEDGALKGEIKQ
RLKLKDGGHYDAEVKTTYKAKKPVQLPGAYNVNIKLDITSHNEDYTIVEQYERAEGRHSTGGMDEL
YKGGSGGSGWSHPQFEKGIA*

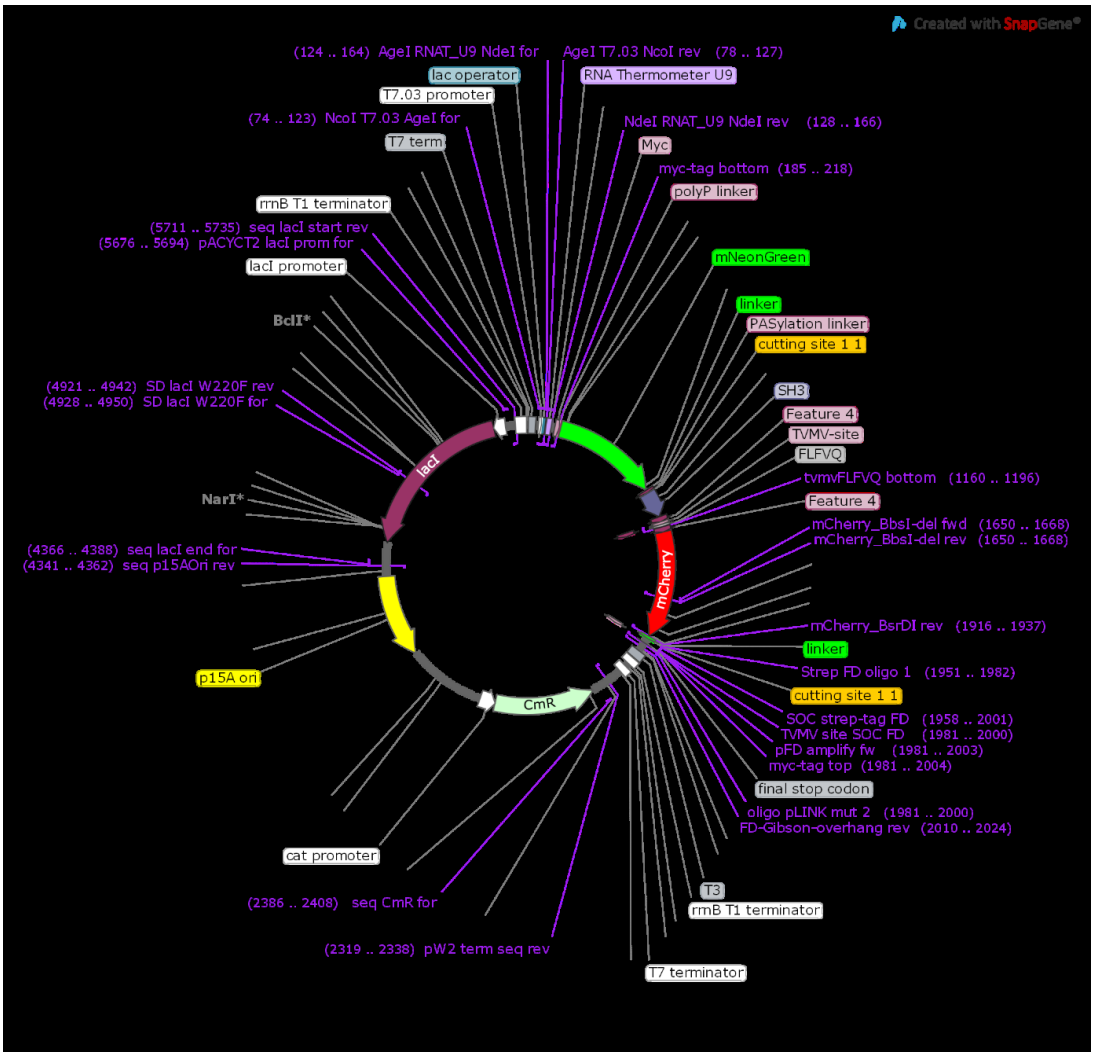

Figure S41 Vector map pCtrl2_T7.03_U9_myc-mNG-SH3-^{TVMV}FLFVQ-mCh-Strep. Figure generated with SnapGene (GSL Biotech LLC).

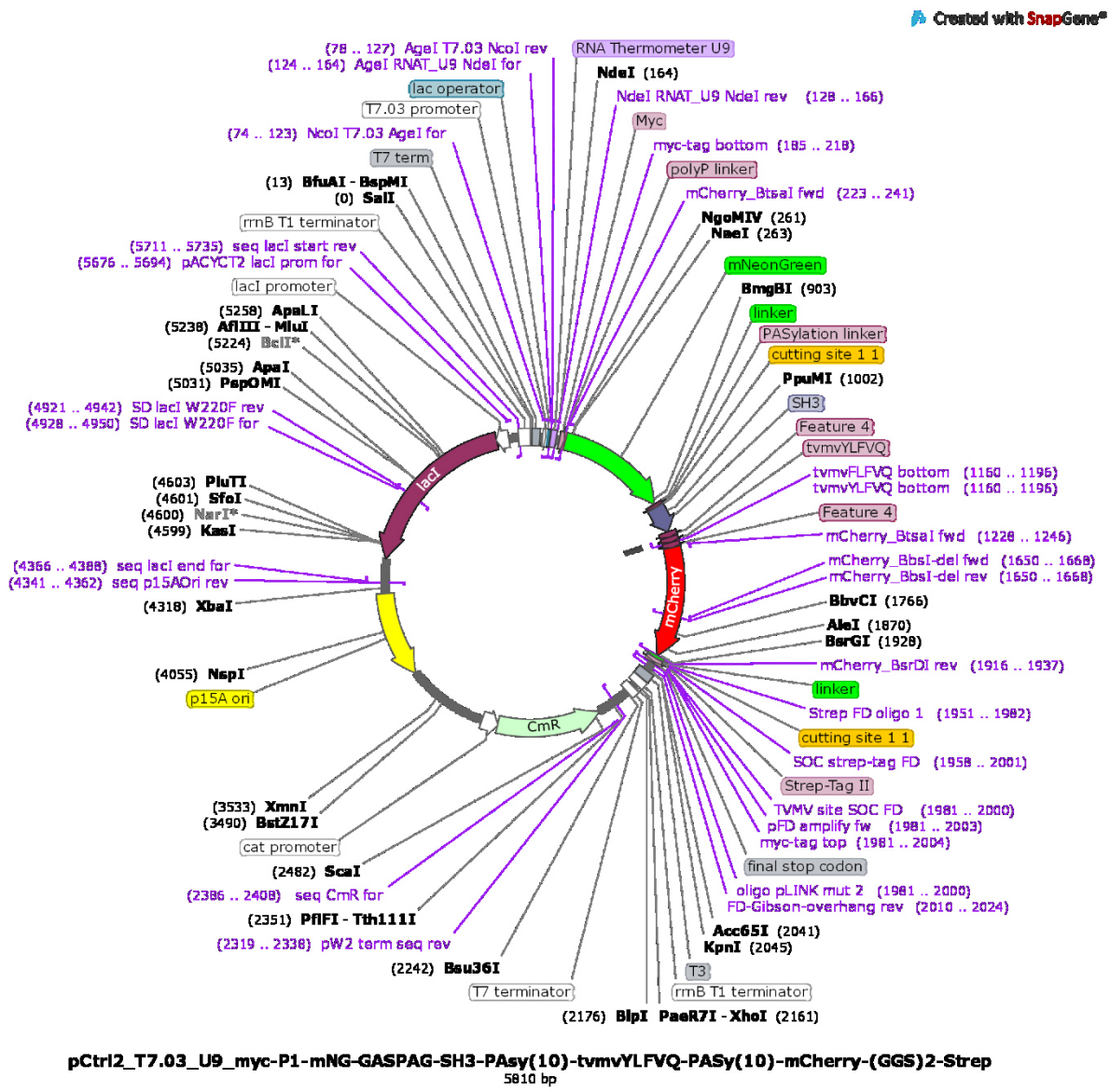

Figure S42 Vector map pCtrl2_T7.03_U9_myc-mNG-SH3-^{TVMV}YLFVQ-mCh-Strep. Figure generated with SnapGene (GSL Biotech LLC).

13.4.8. Figure 26

myc-mCh-^{TVMV}

MSSGSSGEQKLISEEDLGPGVSKGEEDNMAIIKEFMRFKVHMEGSVNGHEFEIEGEGEGRPYEGTQ
TAKLKVTKGGPLPFAWDILSPQFMYGSKAYVKHPADIPDYLKLSFPEGFKWERVMNFEDGGVVTVT
QDSSLQDGEFIYKVKLRGTNFPSDGPVMQKKTMGWEASSERMYPEDGALKGEIKQRLKLKDGGHY
DAEVKTTYKAKKPVQLPGAYNVNIKLDITSHNEDYTIVEQYERAEGRHSTGGMDELYKGGASPAGG
ETVRFQ|SGIA*

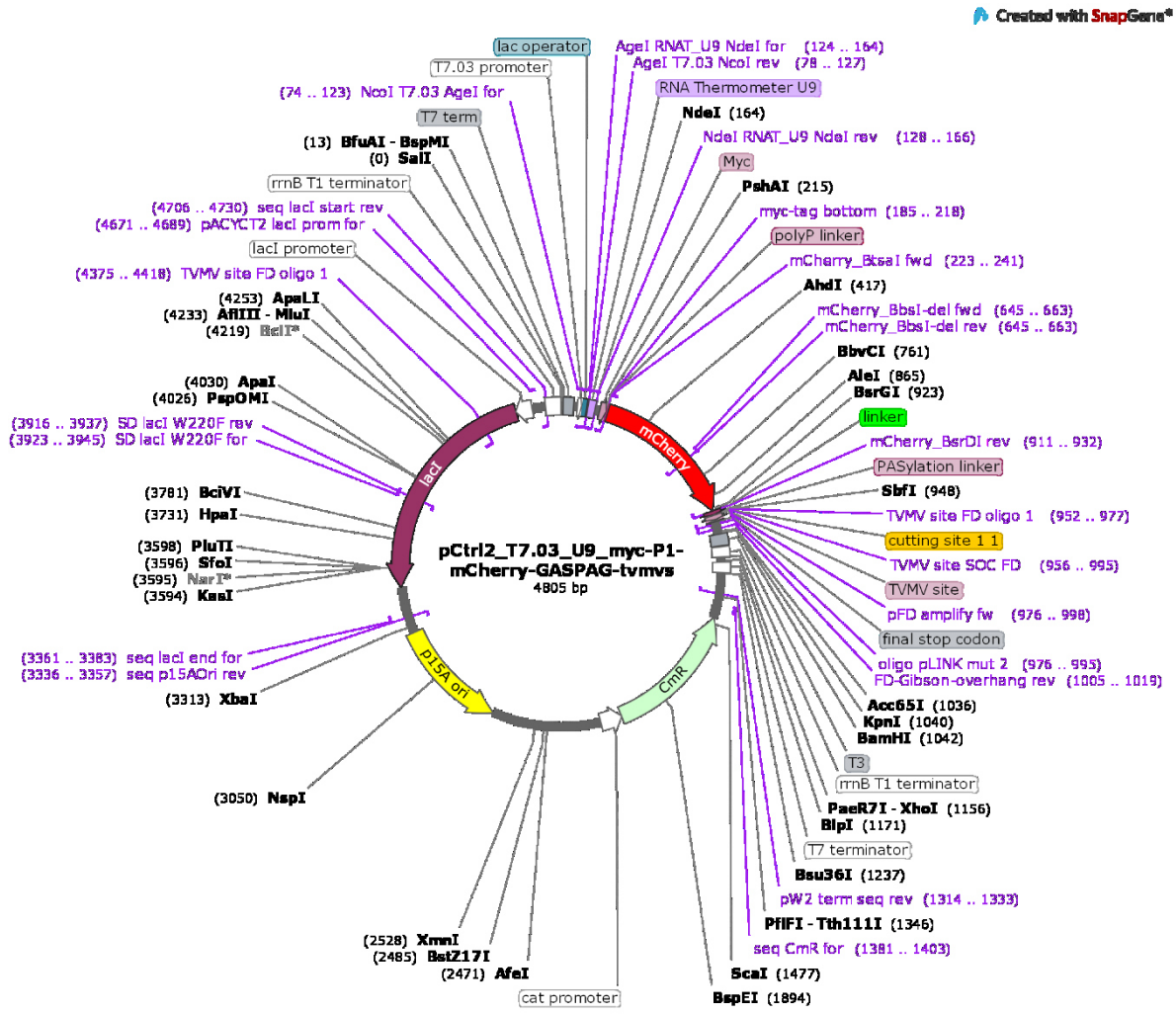

Figure S43 Vector map pCtrl2_T7.03_U9_myc-mCh^{TVMV}. Figure generated with SnapGene (GSL Biotech LLC).

myc-mCh-^{TVMV}-LVA

MSSGSSGEQKLISEEDLGPGVSKGEEDNMAIIKEFMRFKVHMEGSVNGHEFEIEGEGEGRPYEGTQ
TAKLKVTKGGPLPFAWDILSPQFMYGSKAYVKHPADIPDYLKLSFPEGFKWERVMNFEDGGVVTVT
QDSSLQDGEFIYKVKLRGTNFPSDGPVMQKKTMGWEASSERMYPEDGALKGEIKQRLKLKDGGHY
DAEVKTTYKAKKPVQLPGAYNVNIKLDITSHNEDYTIVEQYERAEGRHSTGGMDELYKGGASPAGG
ETVRFQ|SGSGGGGAANDENYALVAGIA*

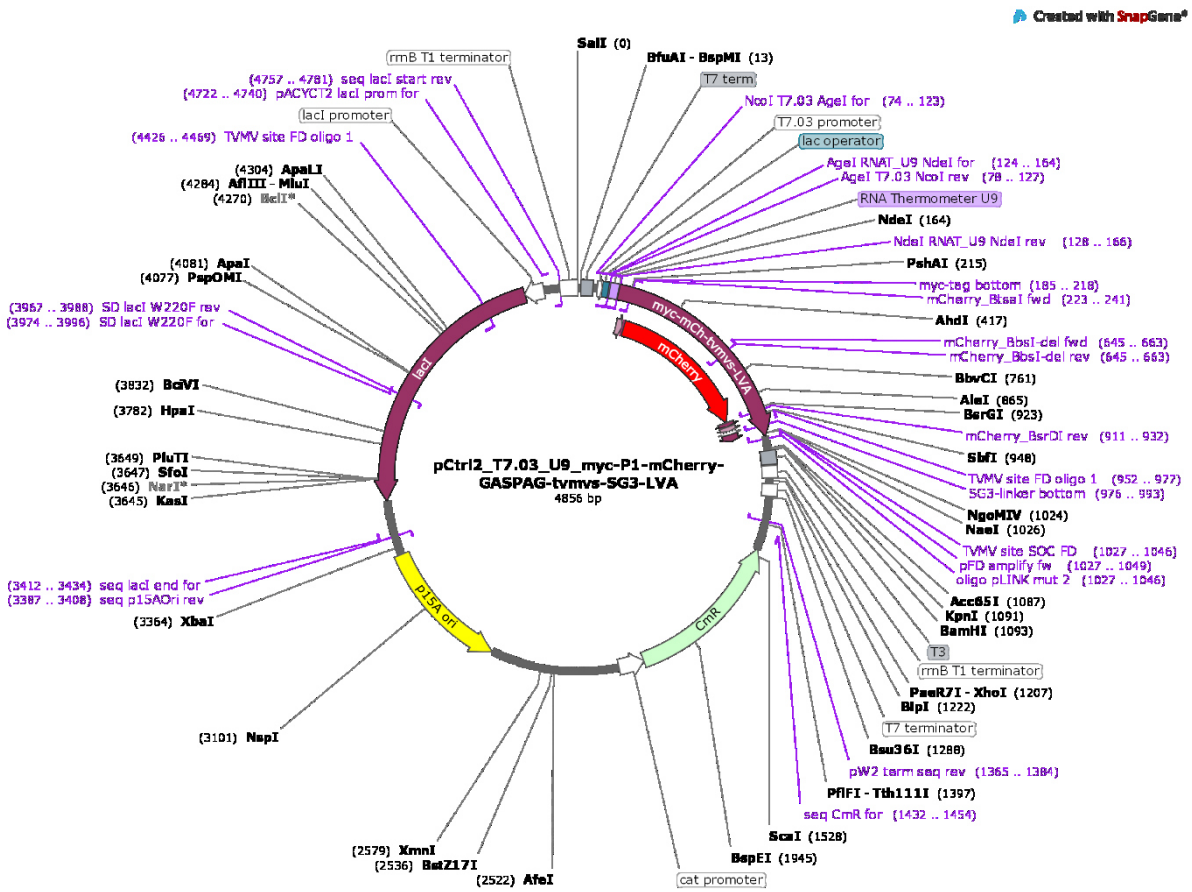

Figure S44 Vector map pCtrl2_T7.03_U9_myc-mCh^{TVMV}LVA. Figure generated with SnapGene (GSL Biotech LLC).

13.4.9. Figure 28

myc-SH3-mNG-^{TEV}

MSSGSSGEQKLISEEDLGGASPAGGAEYVRALFDFNGNDEEDLPFKKGDILRIRDKPEEQWWNAED
SEGKRGMIPVPYVEKYGGASPAGGVSKGEEDNMASLPATHELHIFGSINGVDFDMVGQGTGNPND
GYEELNLKSTKGDLQFSPWILVPHIGYGFHQYLPYPDGMSPFQAAMVDGSGYQVHRTMQFEDGAS
LTVNYRYTYEGSHIKGEAQVKGTGFPADGPVMTNSLTAADWCRSKKTYPNDKTIISTFKWSYTTGN
GKRYRSTARTTYTFAKPMAANYLKNQPMYVFRKTELKHSKTELNFKEWQKAFTDVMGMDELYKG
GASPAAPAPAGENLYFQ|SGIA*

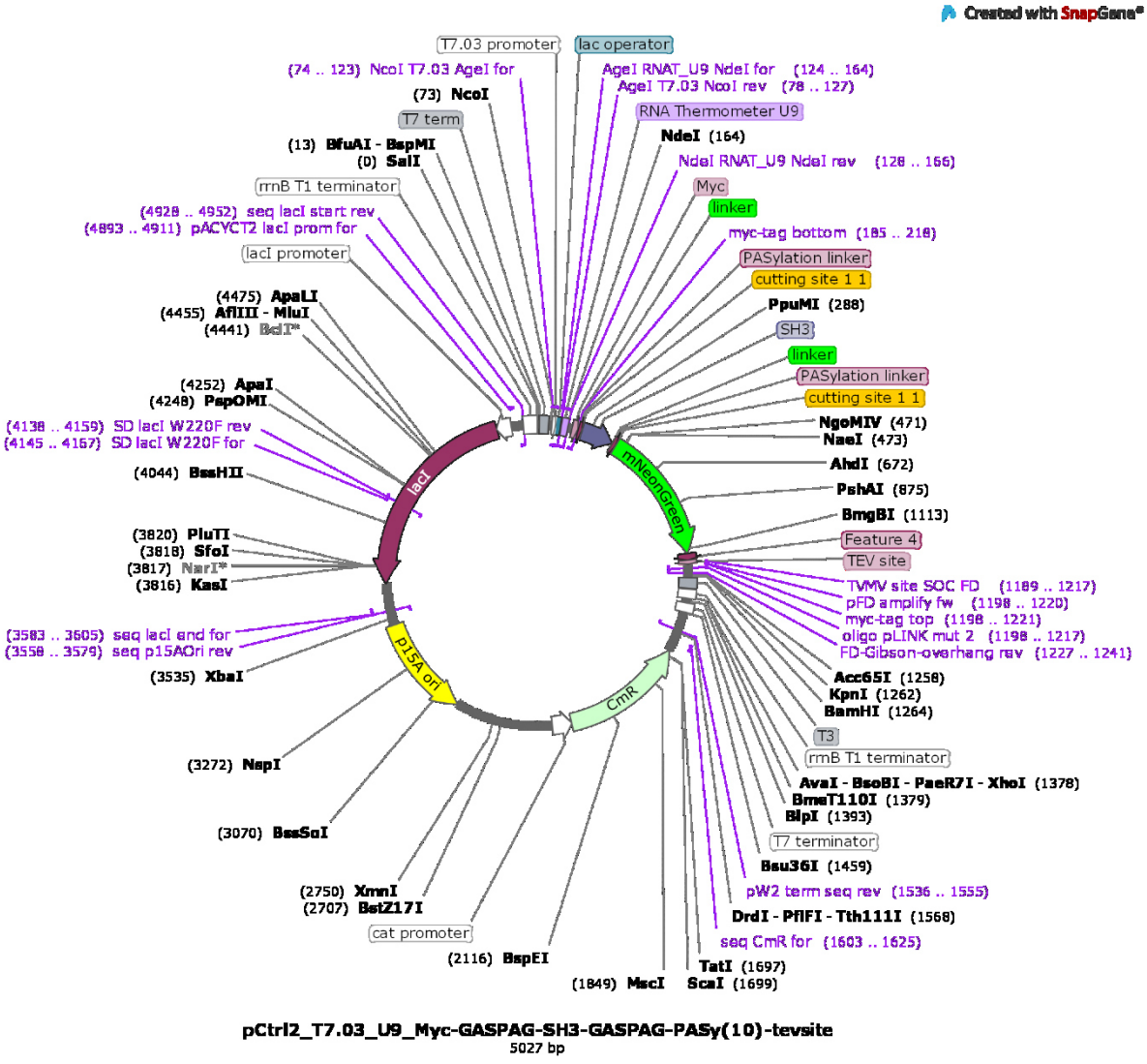

Figure S45 Vector map pCtrl2_T7.03_U9_myc-SH3-mNG-^{TEV}. Figure generated with SnapGene (GSL Biotech LLC).

myc-SH3-mNG-^{TEV}LVA

MSSGSSGEQKLISEEDLGGASPAGGAEYVRALFDFNGNDEEDLPFKKGDILRIRDKPEEQWWNAED
SEGKRGMIPVPYVEKYGGASPAGGVSKGEEDNMASLPATHELHIFGSINGVDFDMVGQGTGNPND
GYEELNLKSTKGDLQFSPWILVPHIGYGFHQYLPYPDGMSPFQAAMVDGSGYQVHRTMQFEDGAS
LTVNYRYTYEGSHIKGEAQVKGTGFPADGPVMTNSLTAADWCRSKKTYPNDKTIISTFKWSYTTGN
GKRYRSTARTTYTFAKPMAANYLKNQPMYVFRKTELKHSKTELNFKEWQKAFTDVMGMDELYKG
GASPAAPAPAGENLYFQ|SGGAEAAAKEAAAKAGGAANDENYALVAGIA*

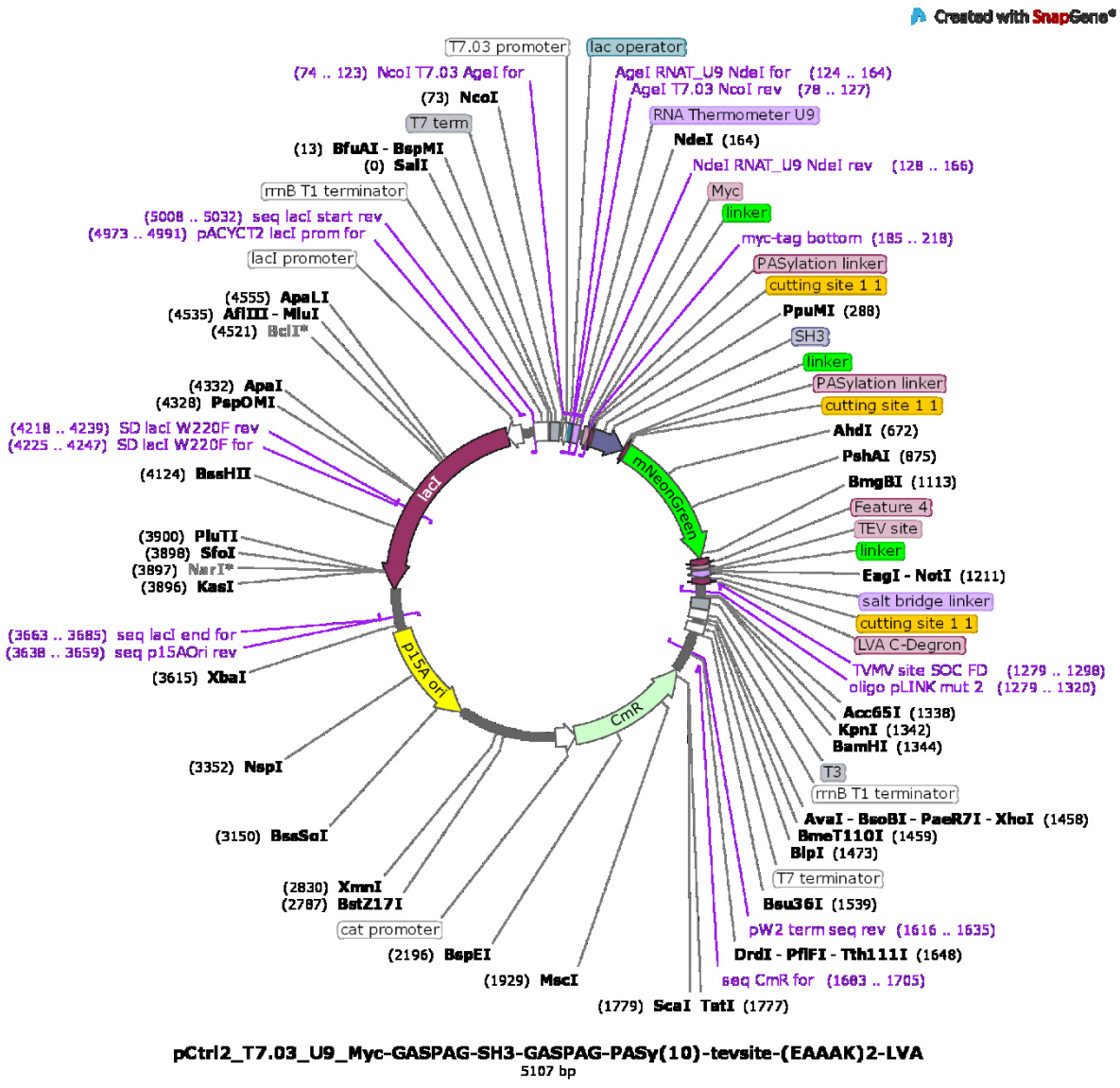

Figure S46 Vector map pCtrl2_T7.03_U9_myc-SH3-mNG-^{TEV}LVA. Figure generated with SnapGene (GSL Biotech LLC).

MBP-^{TEV}sSH3L-TEV/TEV(C151A)-Strep

MGSGSIGKIEEGKLVIWINGDKGYNGLAEVGKKFEKDTGIKVTVEHPDKLEEKFPQVAATGDGPDIIF
WAHDRFGGYAQSGLLAEITPDKAFQDKLYPFTWDAVRYNGKLIAYPIAVEALSLIYNKDLLPNPPKT
WEEIPALDKELKAKGKSALMFNLQEPYFTWPLIAADGGYAFKYENGKYDIKDVGVDNAGAKAGLTFL
VDLIKNKHMNADTDYSIAEAAFNKGETAMTINGPWAWSNIDTSKVNYGVTVLPTFKGQPSKPFVGV
LSAGINAASPNKELAKEFLENYLLTDEGLEAVNKDKPLGAVALKSYEEELVKDPRIAATMENAQKGEI
MPNIPQMSAFWYAVRTAVINAASGRQTVDEALKDAQTGLGGGSGGGSGGGSETGENLYQ|SGNSS
SNNNNNNNNNNGPPPPLPPKRRRGGSGGSGGSGGSGGSGGSGGSGGSGGSGGESLFKGPRDYNPISST
ICHLTNESDGHTTSLYGIGFGPFIITNKHLFRRNNGTLVVQSLHGVFKVKNTTTLQQHLIDGRDMIII
RMPKDFPPFPQKLKFREPQREERICLVTTNFQTKSMSSMVSDTSCTFPSGDGIFWKHWIQTKDGQC
/SGSPLVSTRDGFIVGIHSASNFTNTNNYFTSVPKNFMELLTNQEAQQWVSGWRLNADSVLWGGH
KVFMVKPEEPFQPVKEATQLMNELVYSQGGSGGSGWSHPQFEKGIA*

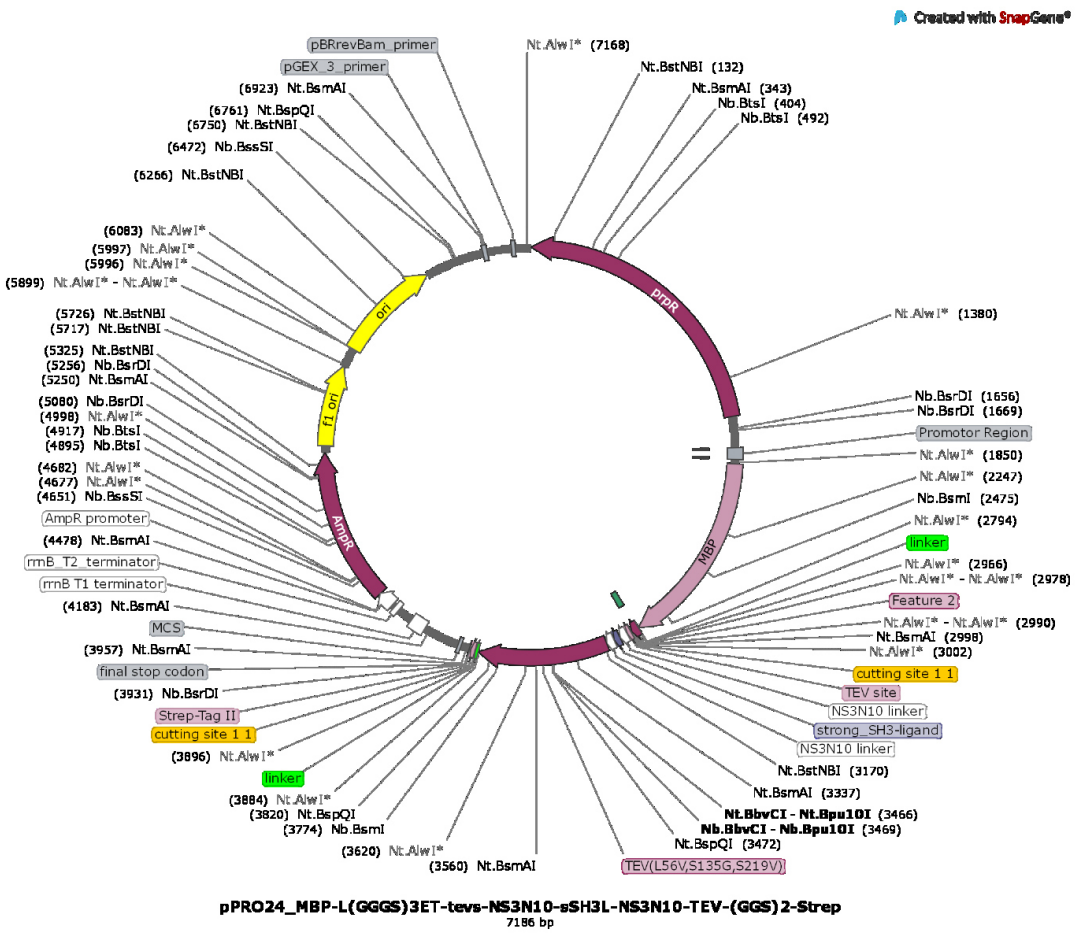

Figure S47 Vector map pPRO24_MBP-^{TEV}sSH3L-TEV-Strep. Figure generated with SnapGene (GSL Biotech LLC).

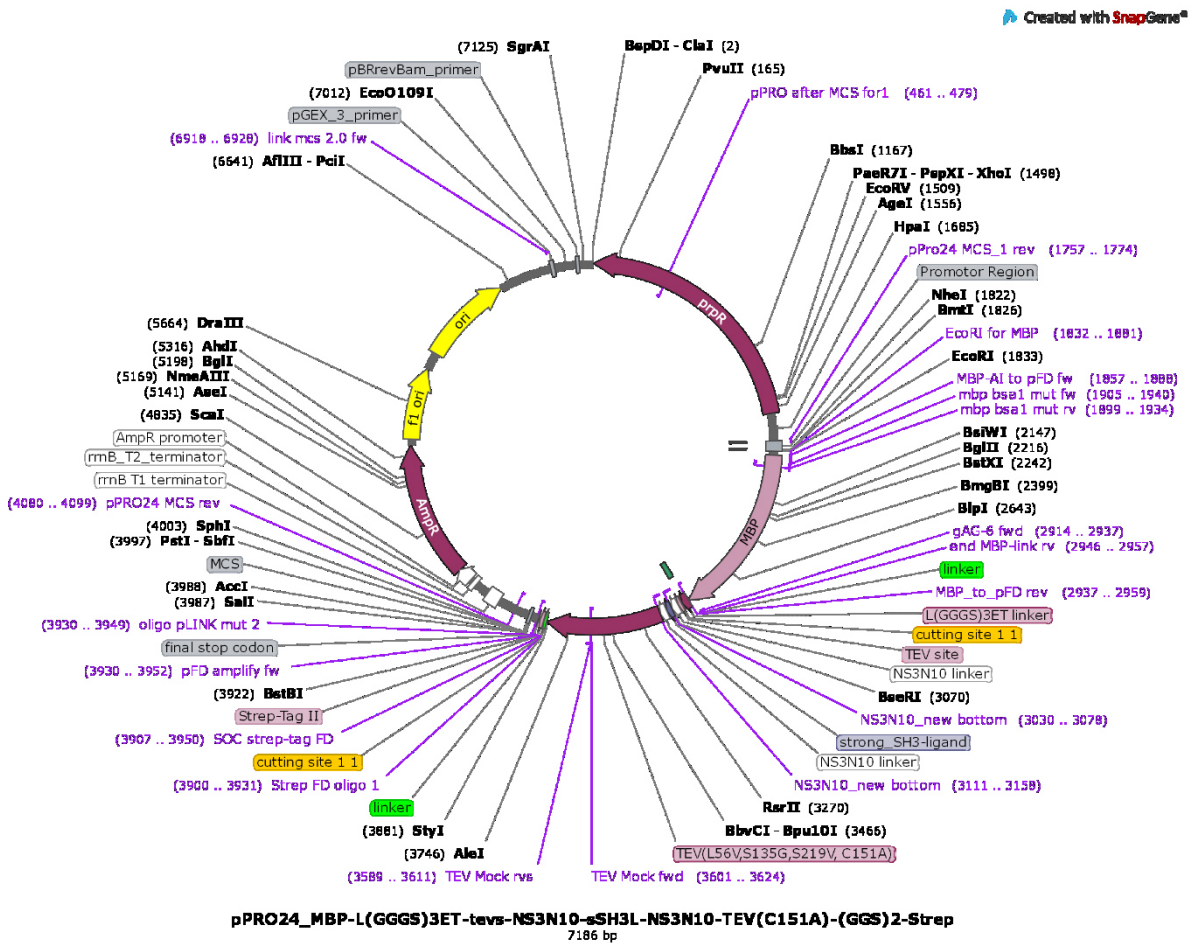

Figure S48 Vector map pPRO24_MBP-^{TEV}sSH3L-TEV^{C151A}-Strep. Figure generated with SnapGene (GSL Biotech LLC).

myc-SH3-mNG-^{HCV}

MSSGSSGEQKLISEEDLGGASPAGGAEYVRALFDFNGNDEEDLPFKKGDILRIRDKPEEQWWNAED
SEGKRGMIPVPYVEKYGGASPAGGVSKGEEDNMASLPATHELHIFGSINGVDFDMVGQGTGNPND
GYEELNLKSTKGDLQFSPWILVPHIGYGFHQYLPYPDGMSPFQAAMVDGSGYQVHRTMQFEDGAS
LTVNYRYTYEGSHIKGEAQVKGTGFPADGPVMTNSLTAADWCRSKKTYPNDKTIISTFKWSYTTGN
GKRYRSTARTTYTFAKPMAANYLKNQPMYVFRKTELKHSKTELNFKEWQKAFTDVMGMDELYKG
GASPAAPAPAGDDVTPCSM|SGIA*

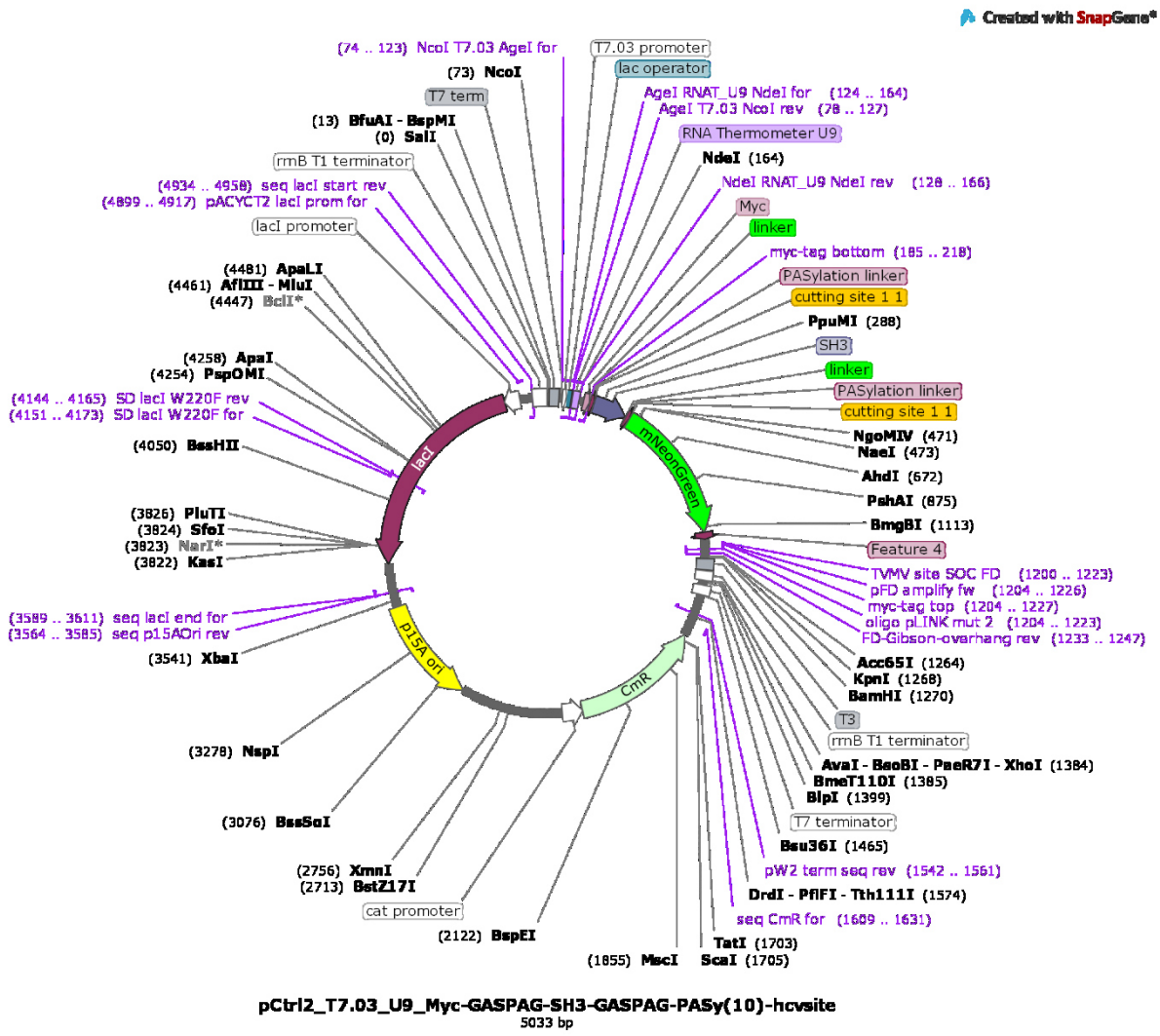

Figure S49 Vector map pCtrl2_T7.03_U9_myc-SH3-mNG-^{HCV}. Figure generated with SnapGene (GSL Biotech LLC).

myc-SH3-mNG-^{HCV}LVA

MSSGSSGEQKLISEEDLGGASPAGGAEYVRALFDFNGNDEEDLPFKKGDILRIRDKPEEQWWNAED
SEGKRGMIPVPYVEKYGGASPAGGVSKGEEDNMASLPATHELHIFGSINGVDFDMVGQGTGNPND
GYEELNLKSTKGDLQFSPWILVPHIGYGFHQYLPYPDGMSPFQAAMVDGSGYQVHRTMQFEDGAS
LTVNYRYTYEGSHIKGEAQVKGTGFPADGPVMTNSLTAADWCRSKKTYPNDKTIISTFKWSYTTGN
GKRYRSTARTTYTFAKPMAANYLKNQPMYVFRKTELKHSKTELNFKEWQKAFTDVMGMDELYKG
GASPAAPAPAGDDVTPCSM|SGGAEAAAKEAAAKAGGAANDENYALVAGIA*

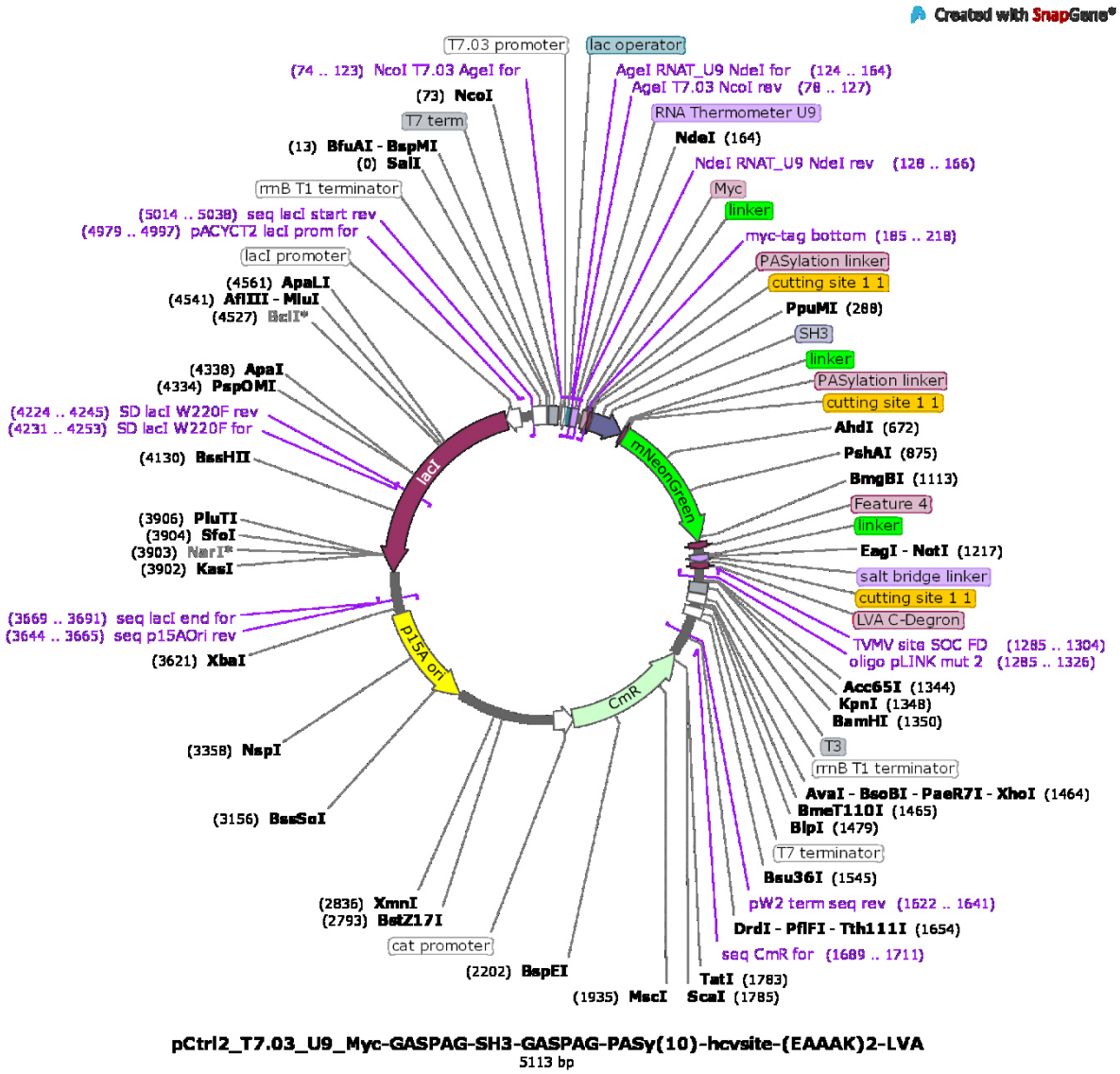

Figure S50 Vector map pCtrl2_T7.03_U9_myc-SH3-mNG-^{HCV}LVA. Figure generated with SnapGene (GSL Biotech LLC).

MBP-^{HCV}sSH3L-HCV/HCV(S151A)-Strep

MGSGSIGKIEEGKLVIWINGDKGYNGLAEVGKKFEKDTGIKVTVEHPDKLEEKFPQVAATGDGPDIIF
WAHDRFGGYAQSGLLAEITPDKAFQDKLYPFTWDAVRYNGKLIAYPIAVEALSLIYNKDLLPNPPKT
WEEIPALDKELKAKGKSALMFNLQEPYFTWPLIAADGGYAFKYENGKYDIKDVGVDNAGAKAGLTFL
VDLIKNKHMNADTDYSIAEAAFNKGETAMTINGPWAWSNIDTSKVNYGVTVLPTFKGQPSKPFVGV
LSAGINAASPNKELAKEFLENYLLTDEGLEAVNKDKPLGAVALKSYEEELVKDPRIAATMENAQKGEI
MPNIPQMSAFWYAVRTAVINAASGRQTVDEALKDAQTGLGGGSGGGSGGGSETGDDVTPCSM|S
GNSSSNNNNNNNNNNGPPPPLPPKRRRGGSGGSGGSGGSGGSGGSGGSGGSGAKGSVVIVGRINL
SGDTAYSQQTRGAAGIAATSATGRDKNQVDGEVQVLSTATQSFLATCVNGVCWTVYHGAGSKTLA
GPKGPITQMYTNVDQDLVGWPAPPGARSMTPCTCGSSDLYLVTRHADVIPVRRRGDSRGSLLSPRP
VSYLKGSS/AGGPLLCPSGHVVGIFRAAVCTRGVAKAVDFIPVESMETTMRGGSGGSGWSHPQFEK
GIA*

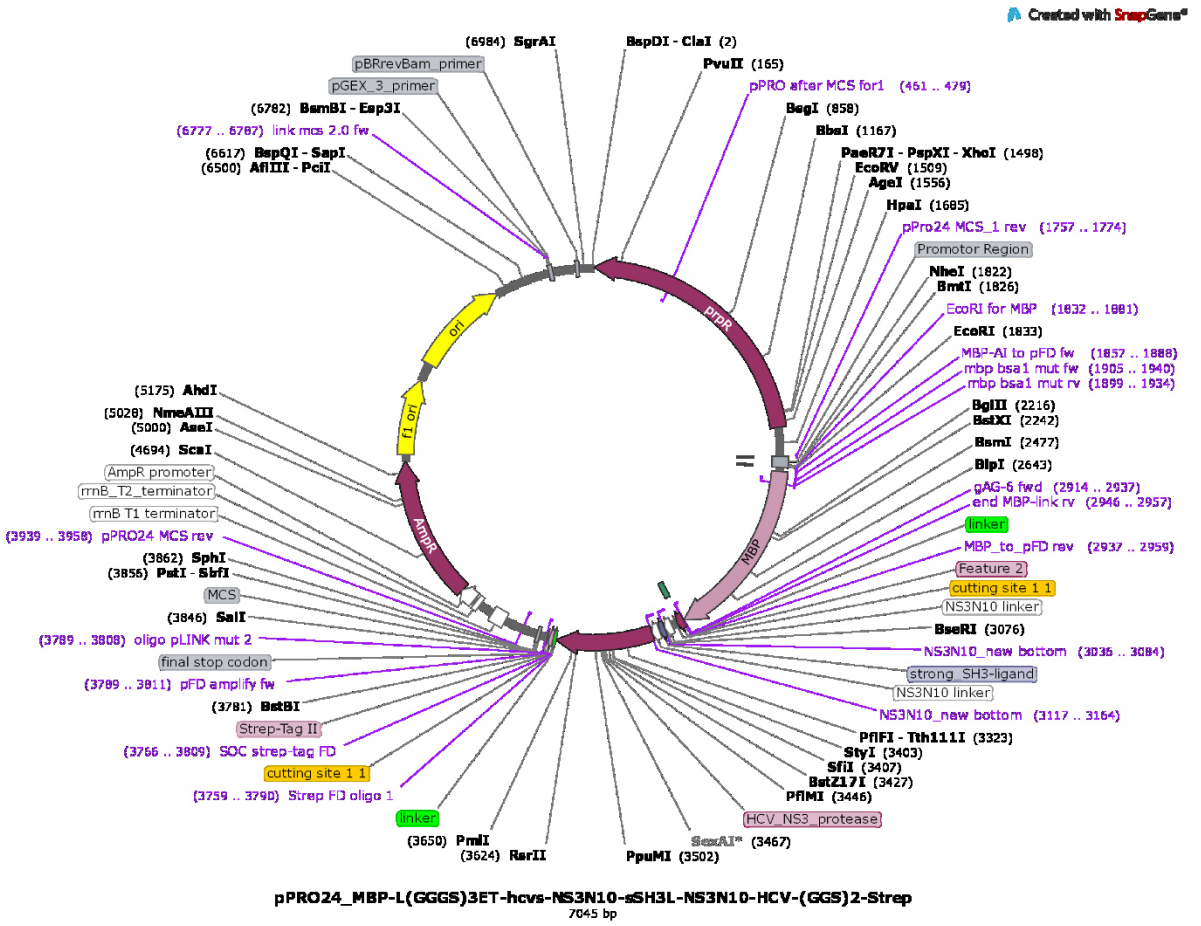

Figure S51 Vector map pPRO24_MBP-^{HCV}sSH3L-GCV-Strep. Figure generated with SnapGene (GSL Biotech LLC).

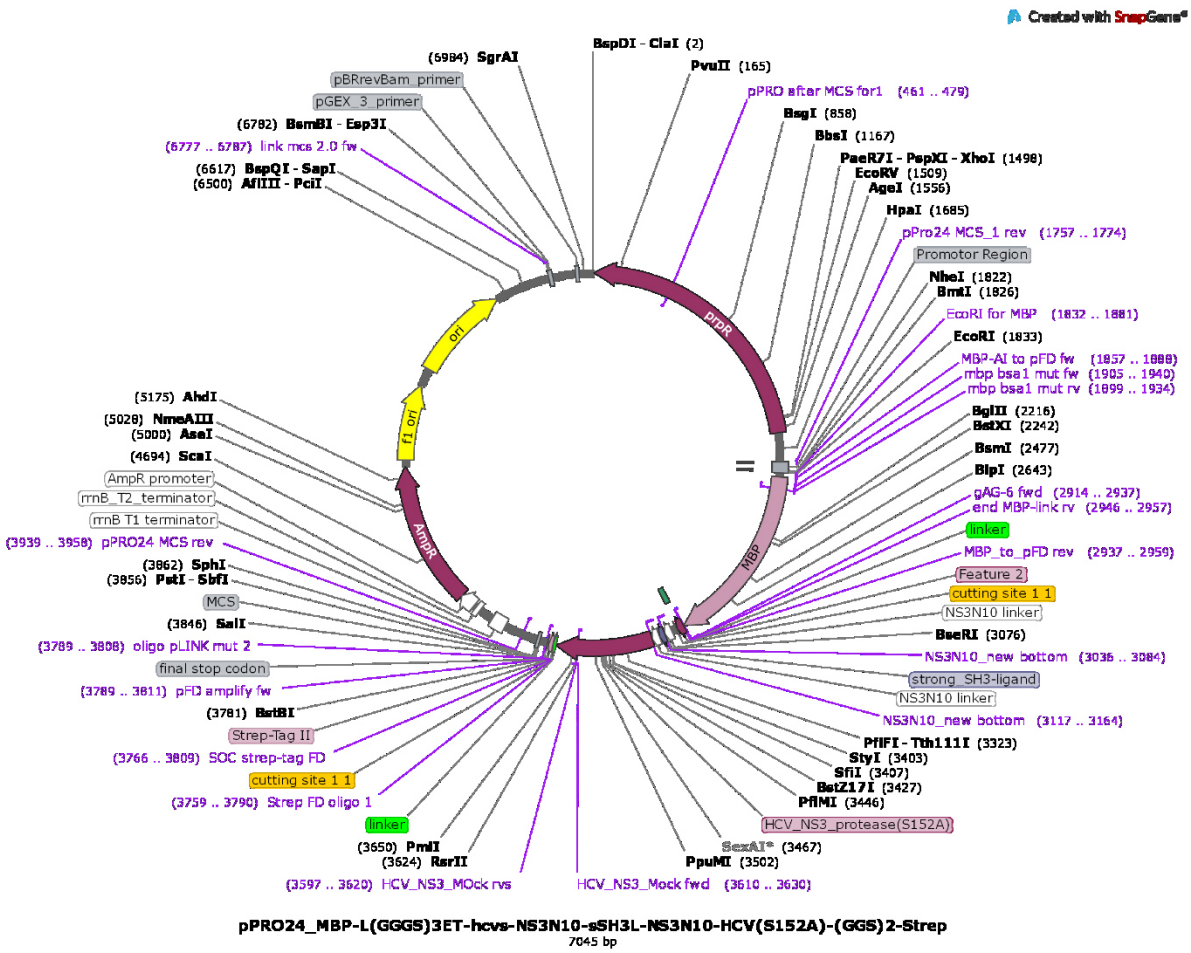

Figure S52 Vector map pPRO24_MBP-^{HCV}sSH3L-HCV-Strep. Figure generated with SnapGene (GSL Biotech LLC).

13.4.10. Figure 30

MBP-^{TVMV}AI-nMagHigh1-pMagF2-TVMV-Strep; clone D1 as example of the whole library

MGKIEEGKLVIWINGDKGYNGLAEVGKKFEKDTGIKVTVEHPDKLEEKFPQVAATGDGPDIIFWAHD
RFGGYAQSGLLAEITPDKAFQDKLYPFTWDAVRYNGKLIAYPIAVEALSLIYNKDLLPNPPKTWEEIPA
LDKELKAKGKSALMFNLQEPYFTWPLIAADGGYAFKYENGKYDIKDVGVDNAGAKAGLTFLVDLIKN
KHMNADTDYSIAEAAFNKGETAMTINGPWAWSNIDTSKVNYGVTVLPTFKGQPSKPFVGVLSAGIN
AASPNKELAKEFLENYLLTDEGLEAVNKDKPLGAVALKSYEEELVKDPRIAATMENAQKGEIMPNIPQ
MSAFWYAVRTAVINAASGRQTVDEALKDAQTGNSSSNNNNNNNNNNGETVRFQ|SGSGGGGREY
VRFAPGPGHTLYAPGGYDIMGYLDQIGNRPNPQVELGPVDTSCALILCDLKQKDTPIVYASEAFLYM
TGYSNAEVLGRNCRFLQSPDGMVKPKSTRKYVDSNTINTIRKAIDRNAEVQVEVVNFKKNGQRFVN
FLTIIPVRDETGEYRYSMGFQCETEGGASPAAPAPASPAAPAPSAPAGGHTLYAPGGYDIMGYLRQIR
NRPNPQVELGPVDTSCALVLCDLKQKDTPVVYASEAFLYMTGYSNAEVLGRNCRFLQSPDGMVKPK
STRKYVDSNTINTMRKAIDRNAEVQVEVVNFKKNGQRFVNFLTMIPVRDETGEYRYSMGFQCETEG
GGTKALLKGVRDFNPISACVCLLENSSDGHSERLFGIGFGPYIIANQHLFRRNNGELTIKTMHGEFKV
KNSTQLQMKPVEGRDIIVIKMAKDFPPFPQKLKFRQPTIKDRVCMVSTNFQQKSVSSLVSESSHIVHK
EDTSFWQHWITTKDGQCGSPLVSIIDGNILGIHSLTHTTNGSNYFVEFPEKFVATYLDAADGWCKN
WKFNADKISWGSFTLVEDAPEDGGSGGSGWSHPQFEKGIA*

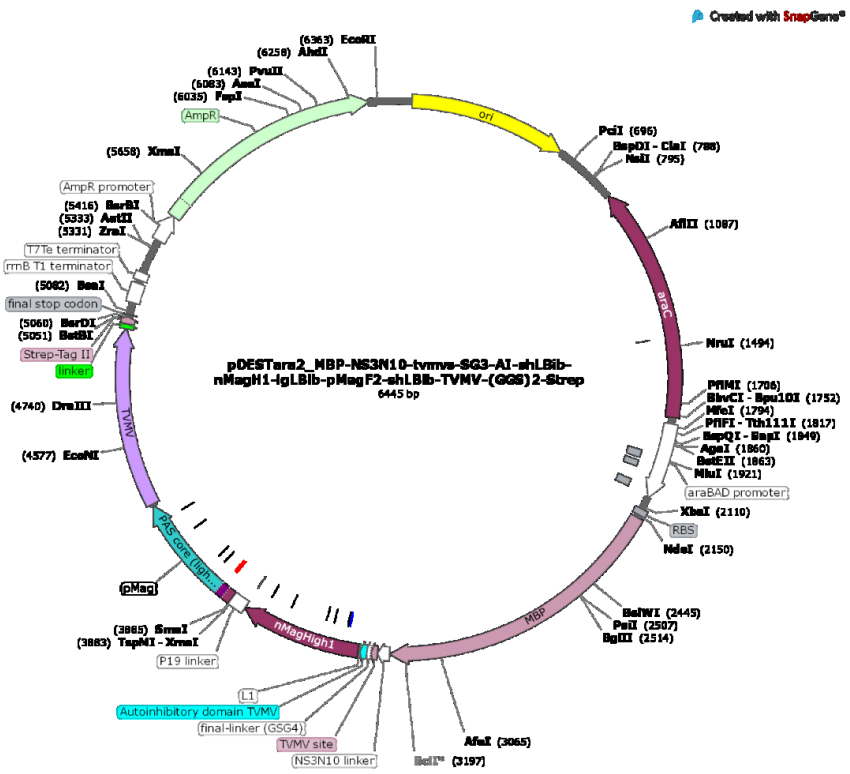

Figure S53 Vector map pDESTara2_MBP-^{TVMV}AI-L1-nMagHigh1-L2-pMagFast2-L3-TVMV-Strep. Figure generated with SnapGene (GSL Biotech LLC).

13.4.11. Figure 32

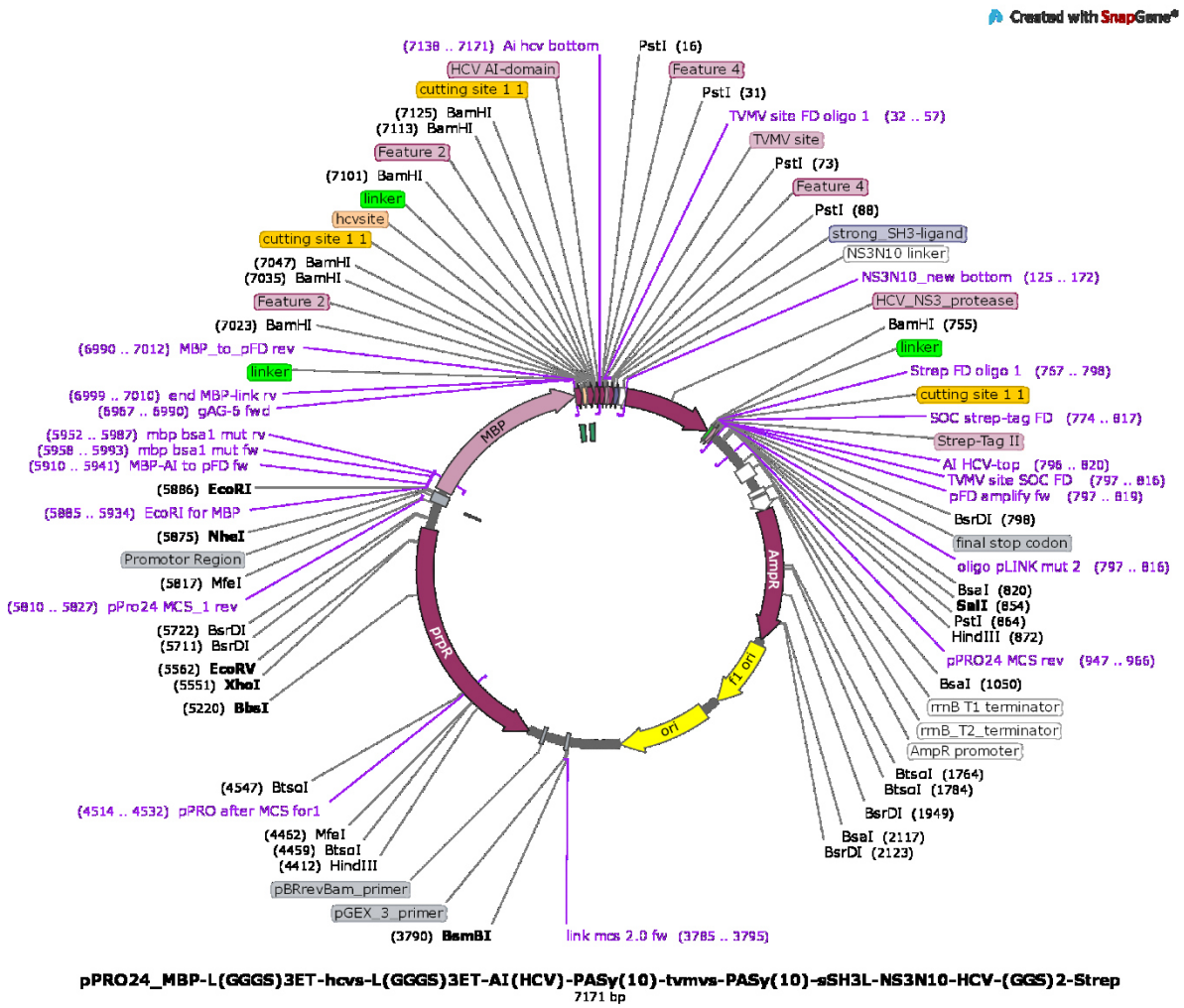

Figure S54 Vector map pPRO24_MBP-^{HCV}AI(HCV)^{TVMV}sSH3L-HCV-Strep. Figure generated with SnapGene (GSL Biotech LLC).

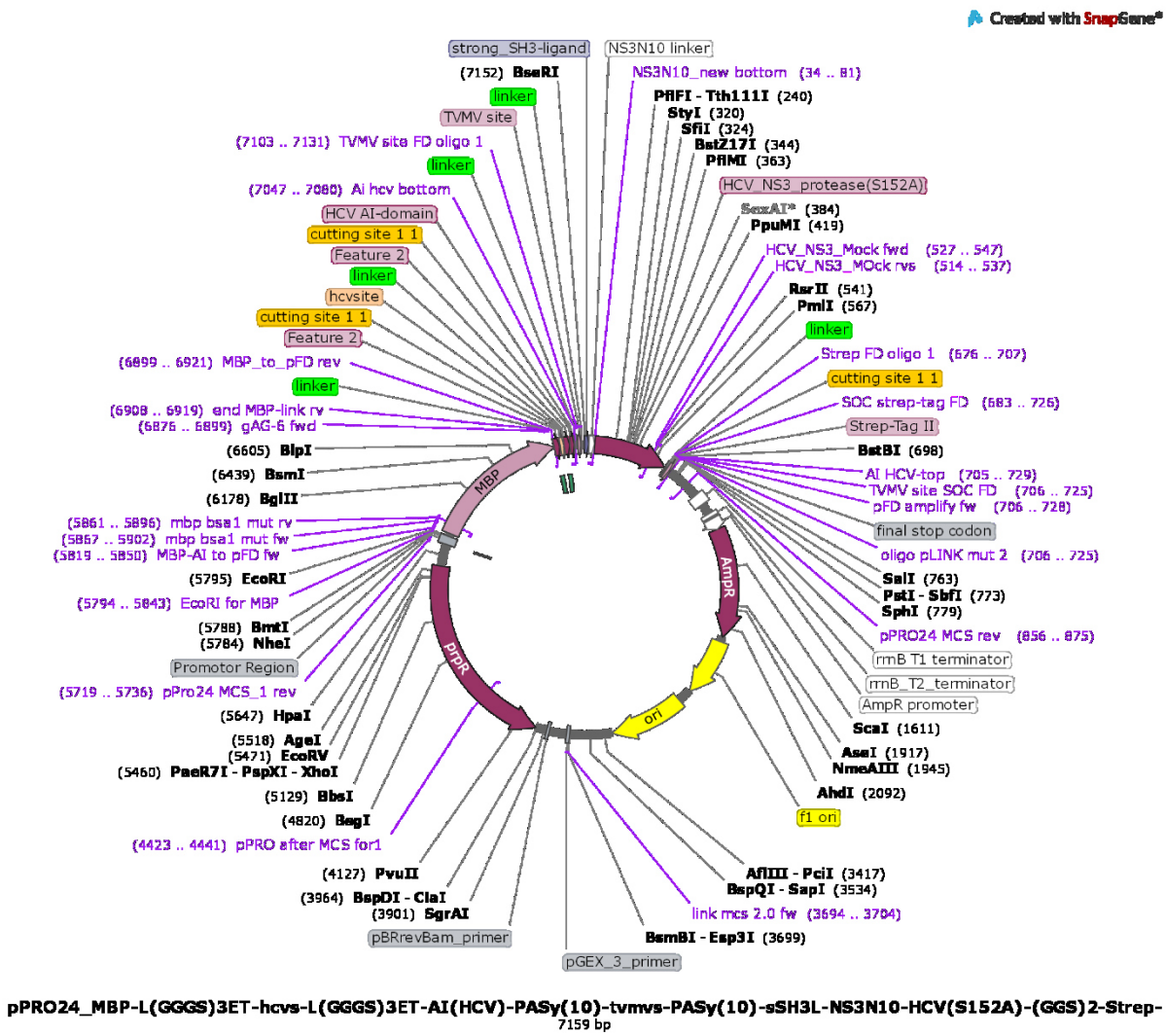

Figure S55 Vector map pPRO24_MBP-^{HCV}AI(HCV)^{TVMV}sSH3L-HCV^{S152A}-Strep. Figure generated with SnapGene (GSL Biotech LLC).

13.4.12. Figure S1

FKBP-mNG-^{TVMV}

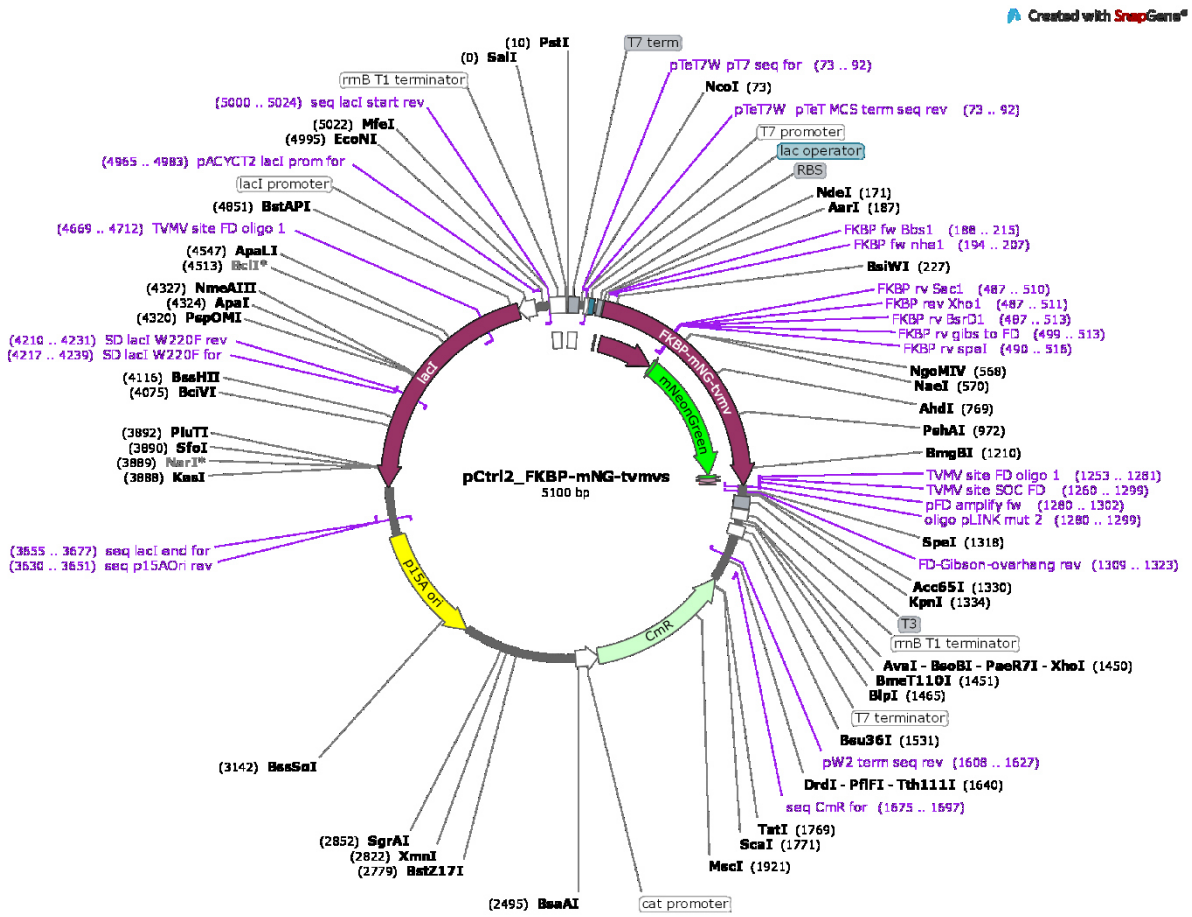

Figure S56 Vector map pCtrl2_FKBP-mNG-^{TVMV}. Figure generated with SnapGene (GSL Biotech LLC).

FKBP-mNG-^{TVMV}E118-134

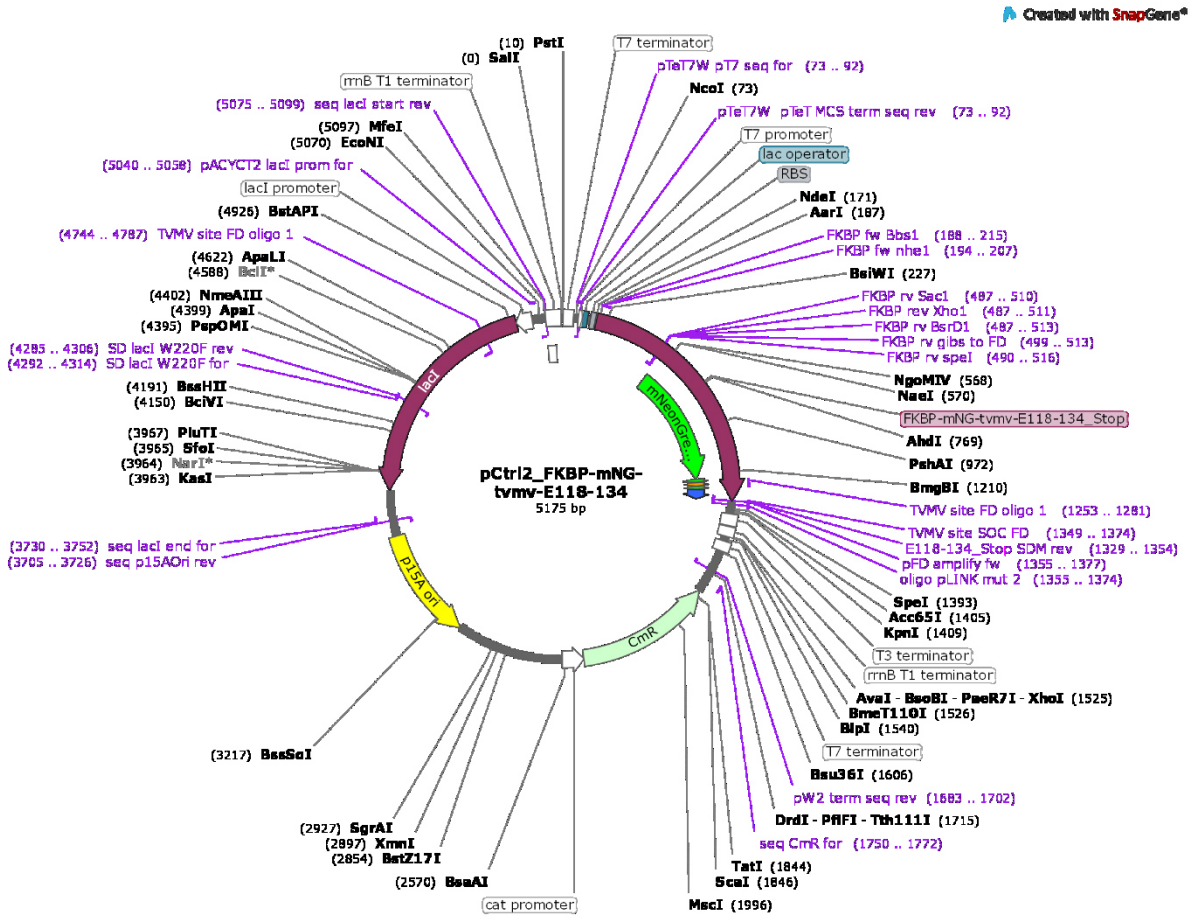

Figure S57 Vector map pCtrl2_FKBP-mNG-^{TVMV}E118-134. Figure generated with SnapGene (GSL Biotech LLC).

MBP-^{TVMV}FRB-TVMV

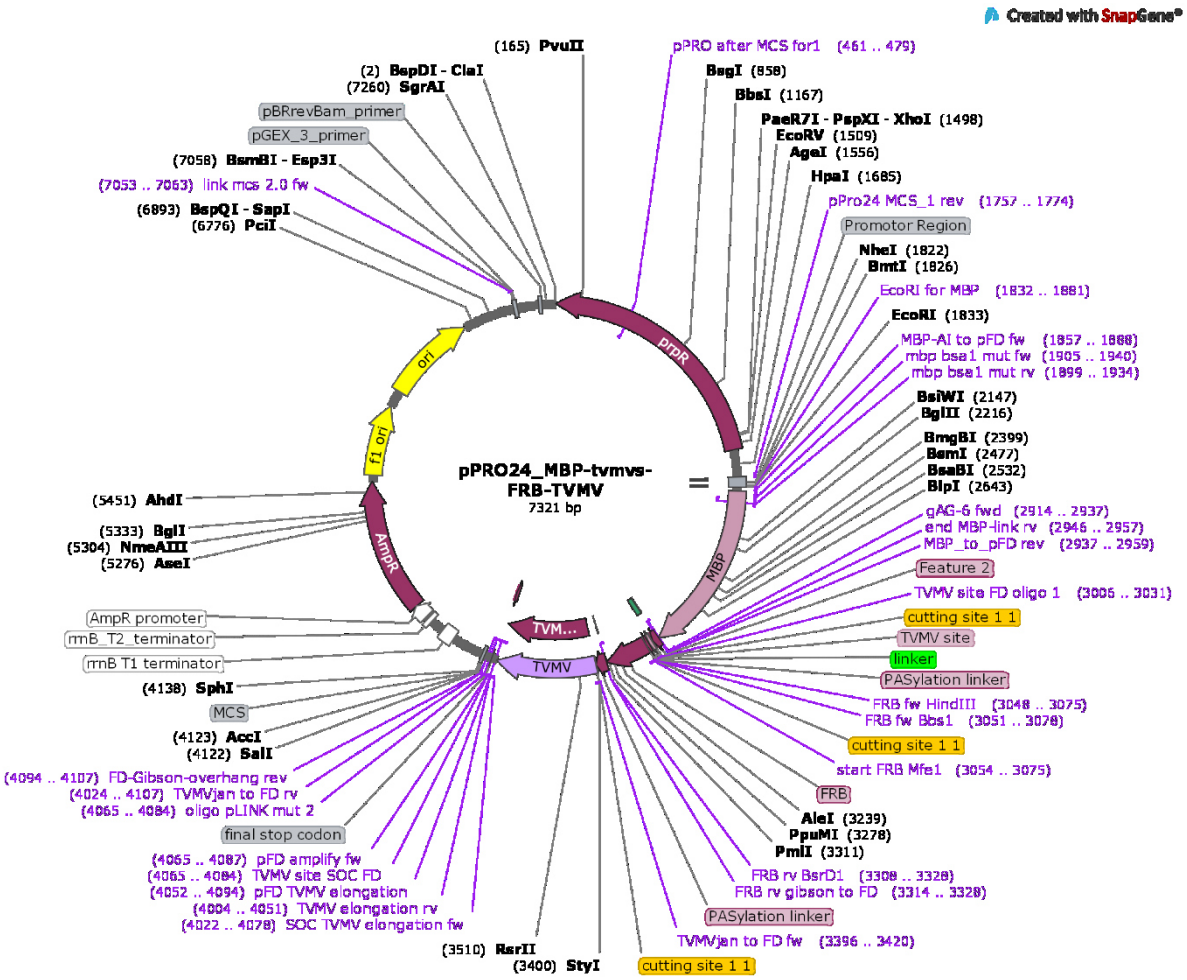

Figure S58 Vector map pPRO24_MBP-^{TVMV}FRB-TVMV. Figure generated with SnapGene (GSL Biotech LLC).

MBP-^{TVMV}FRB-TVMV^{C151A}

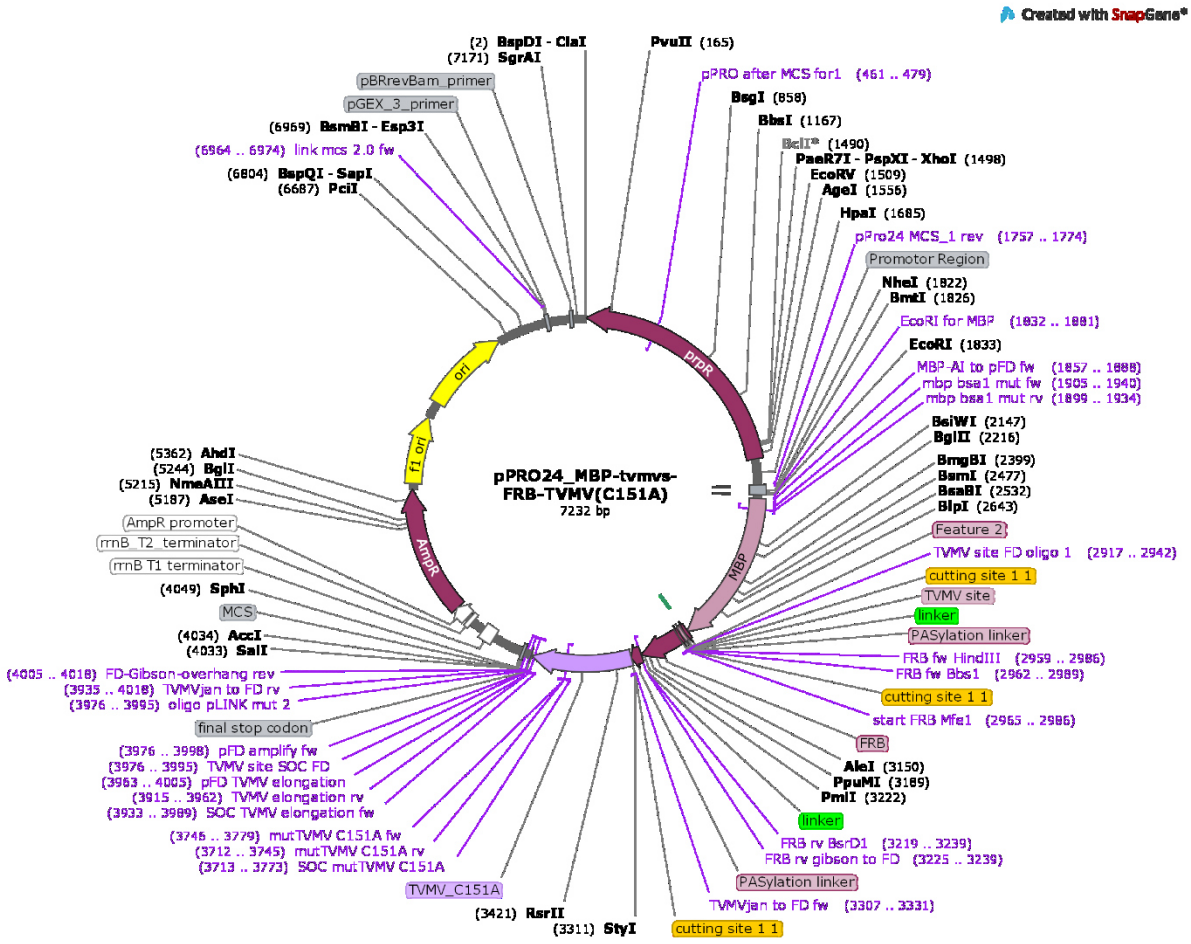

Figure S59 Vector map pPRO24_MBP-^{TVMV}FRB-TVMV^{C151A}. Figure generated with SnapGene (GSL Biotech LLC).

MBP-^{TVMV}TVMV-FRB

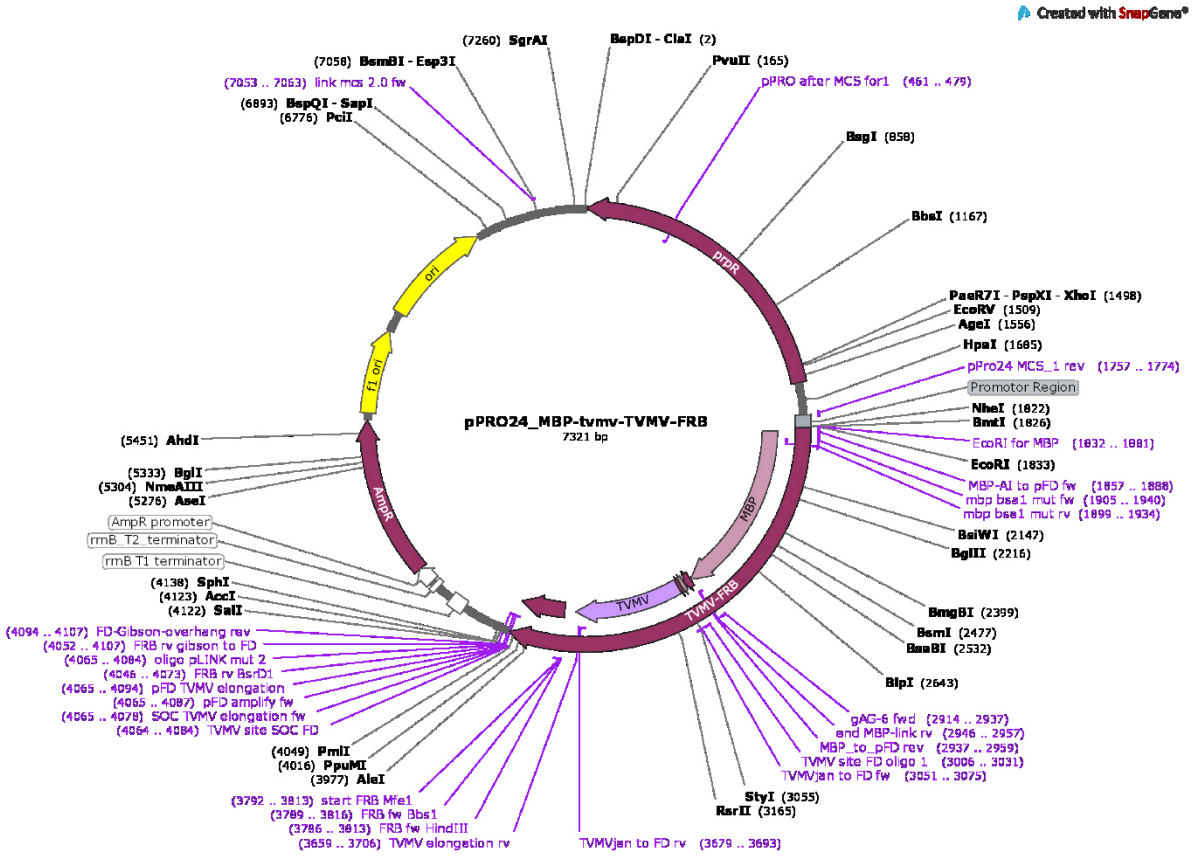

Figure S60 Vector map pPRO24_MBP-^{TVMV}TVMV-FRB. Figure generated with SnapGene (GSL Biotech LLC).

MBP-^{TVMV}TVMV^{C151A}-FRB

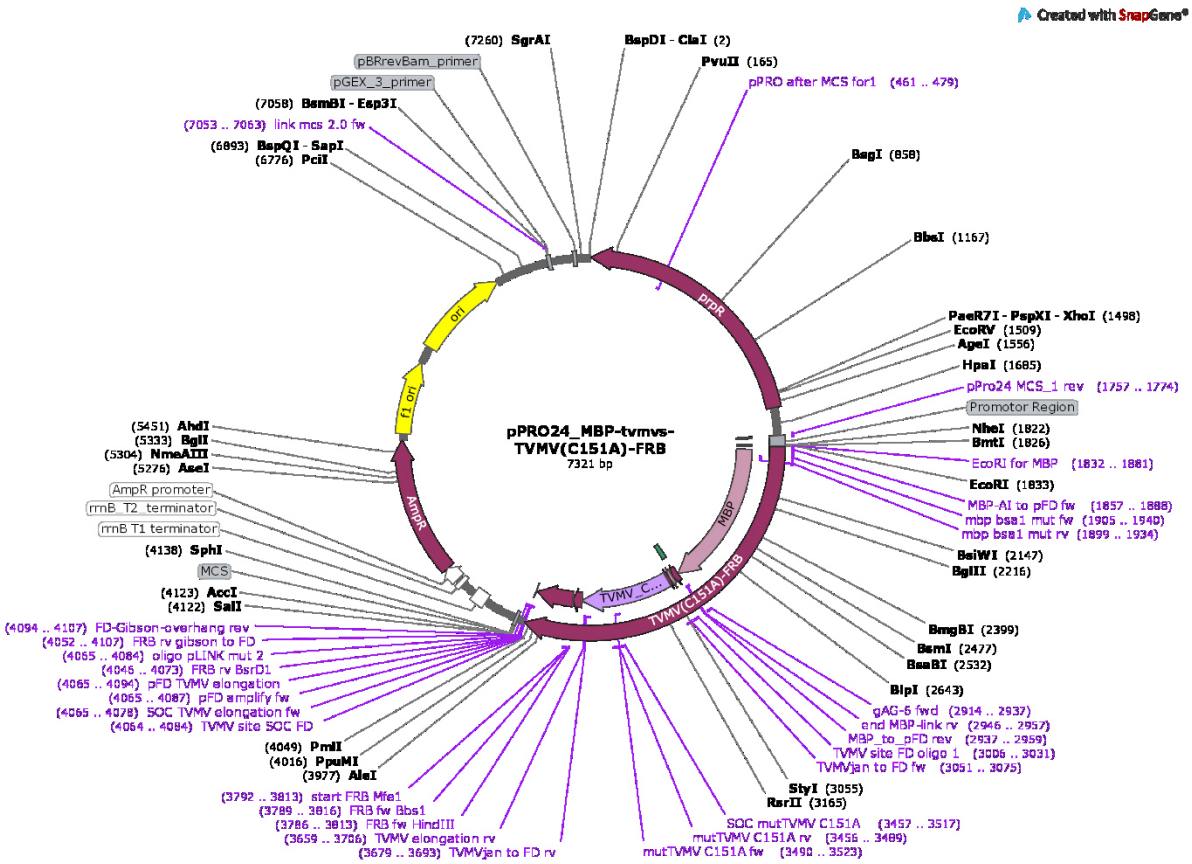

Figure S61 Vector map pPRO24_MBP-^{TVMV}TVMV^{C151A}-FRB. Figure generated with SnapGene (GSL Biotech LLC)

13.4.13. Figure S2

FRB-mNG-^{TVMV}

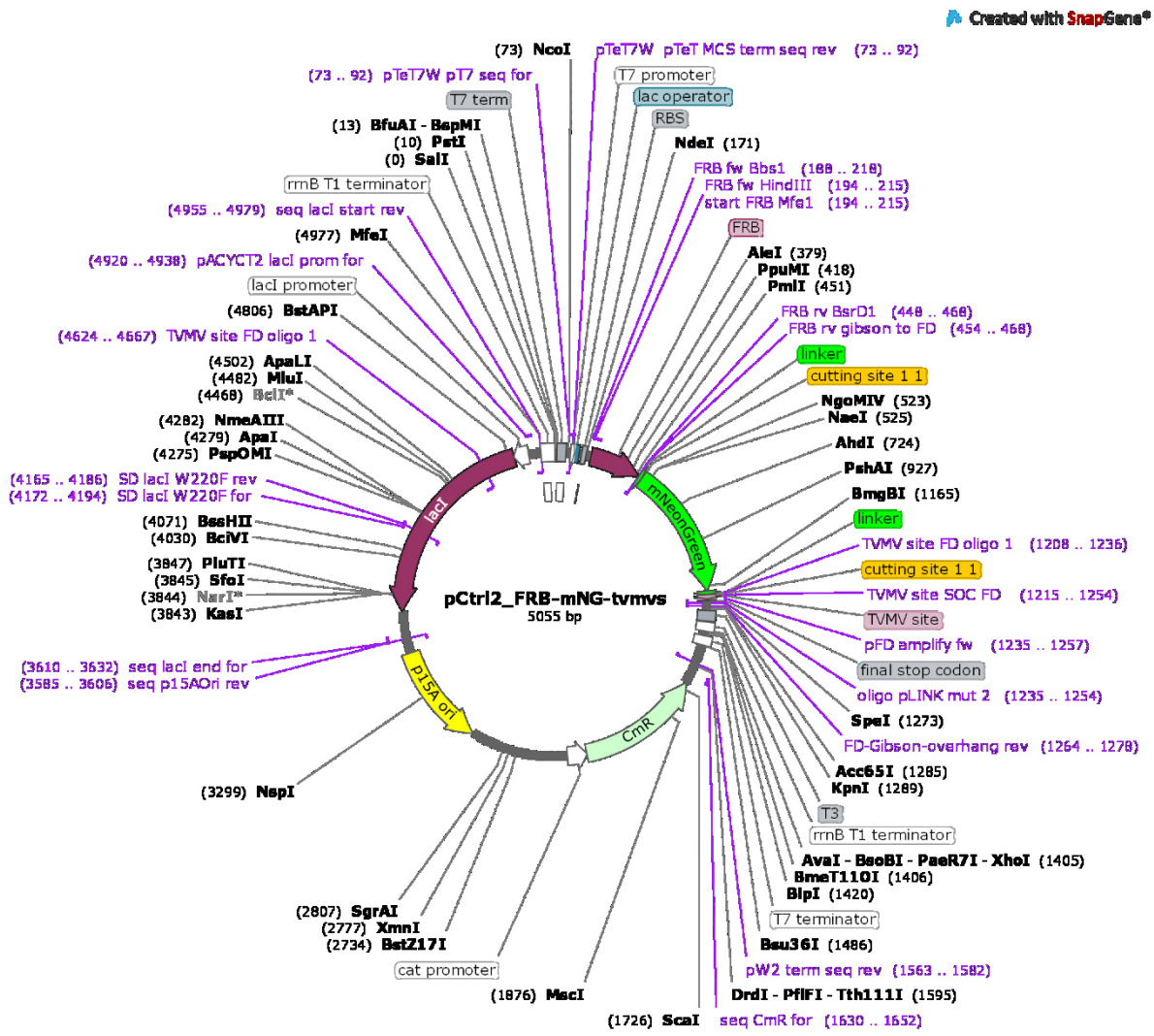

Figure S62 Vector map pCtrl2_FRB-mNG-^{TVMV} Figure generated with SnapGene (GSL Biotech LLC).

FRB-mNG-^{TVMV}E118-134

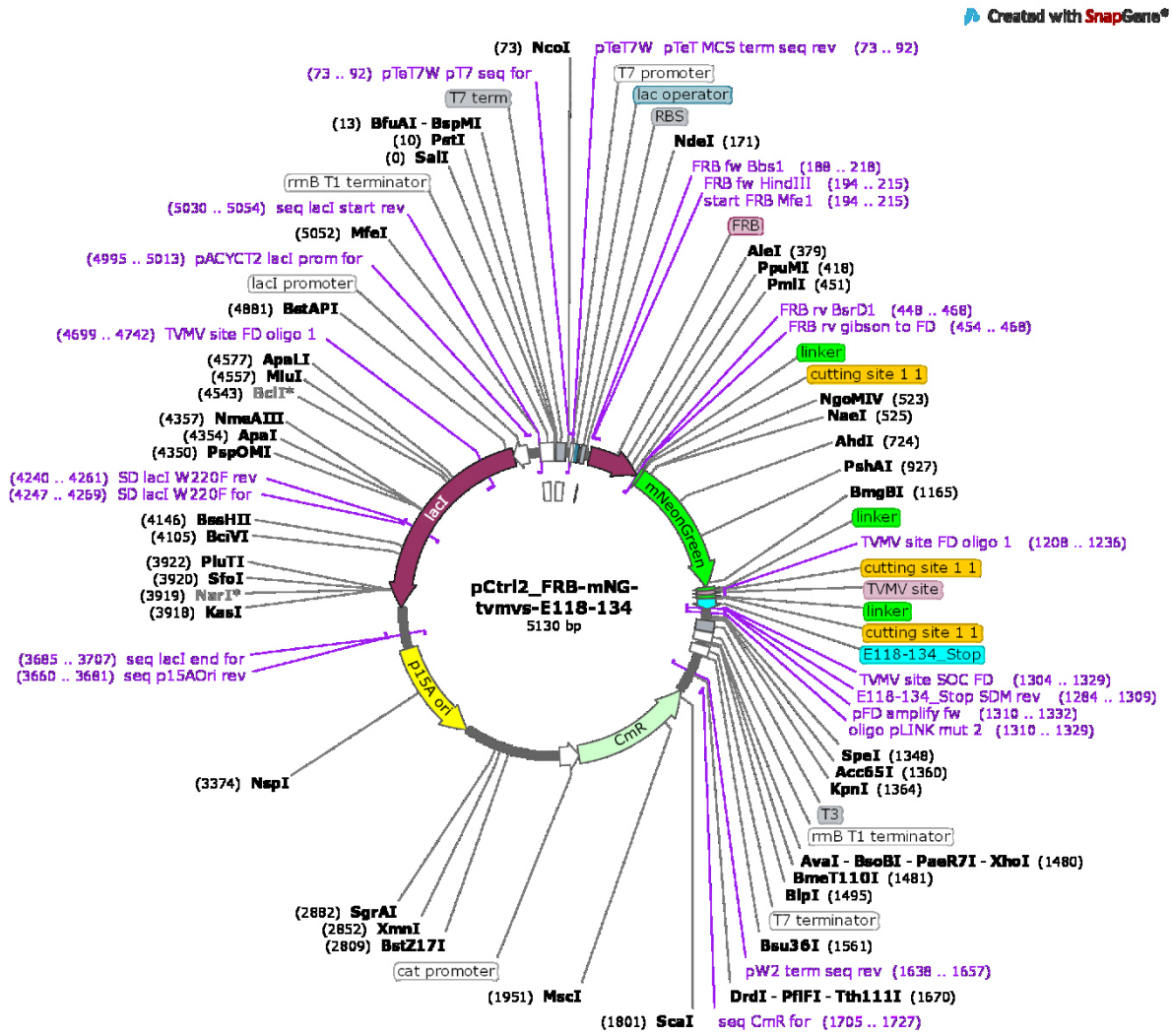

Figure S63 Vector map pCtrl2_FRB-mNG-^{TVMV}E118-134. Figure generated with SnapGene (GSL Biotech LLC).

MBP-^{TVMV}FKBP-TVMV

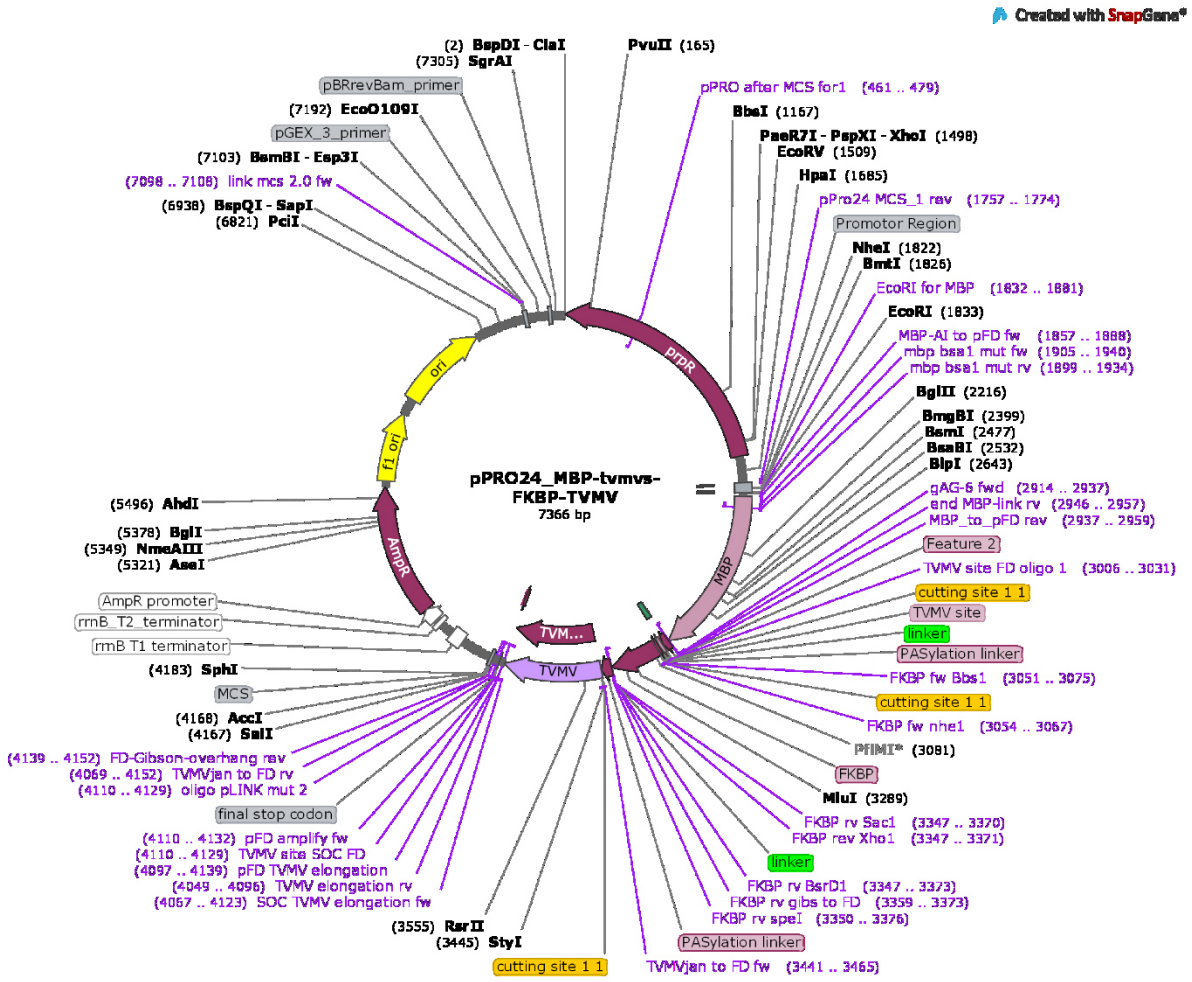

Figure S64 Vector map pPRO24_MBP-^{TVMV}FKBP-TVMV. Figure generated with SnapGene (GSL Biotech LLC)

MBP-^{TVMV}FKBP-TVMV^{C151A}

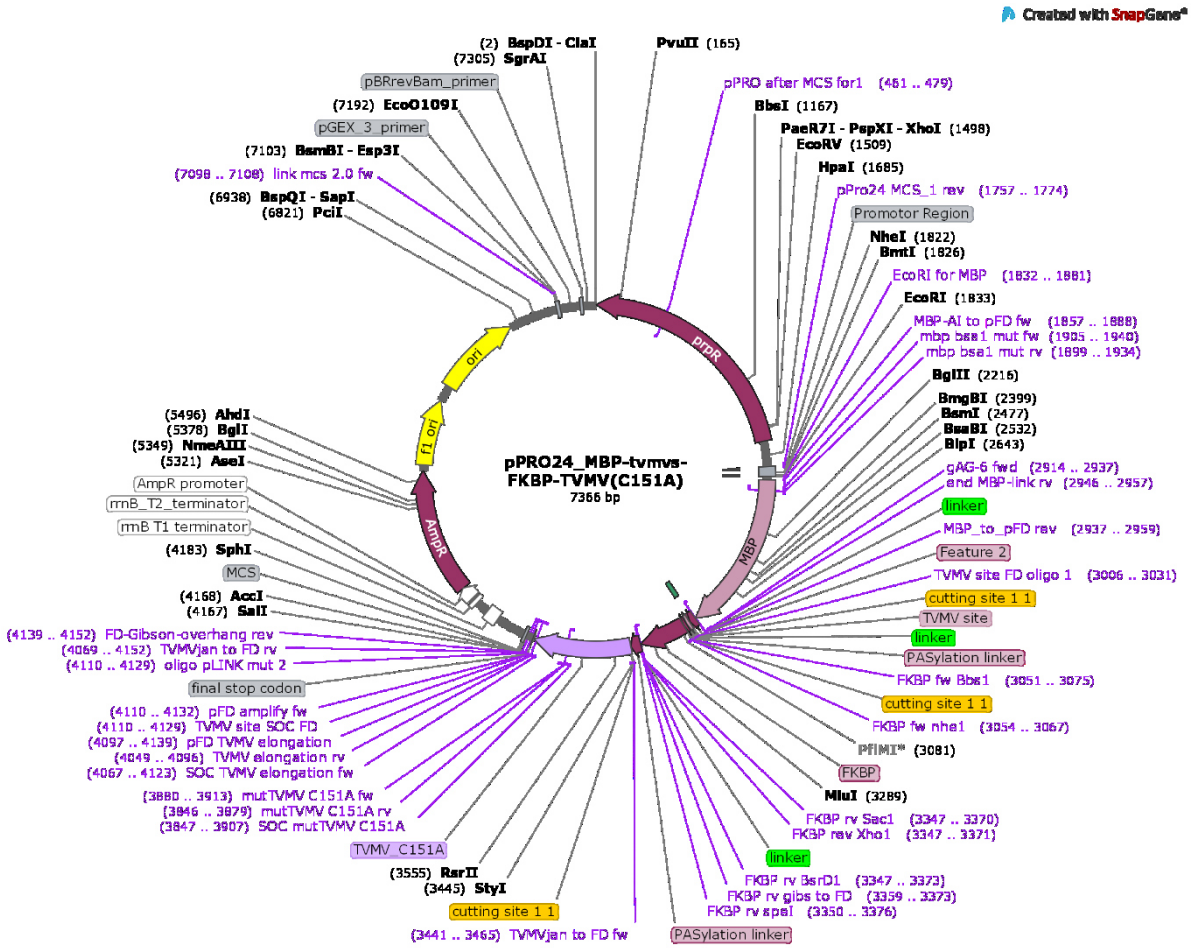

Figure S65 Vector map pPRO24_MBP-^{TVMV}FKBP-TVMV^{C151A}. Figure generated with SnapGene (GSL Biotech LLC)

MBP-^{TVMV}TVMV-FKBP

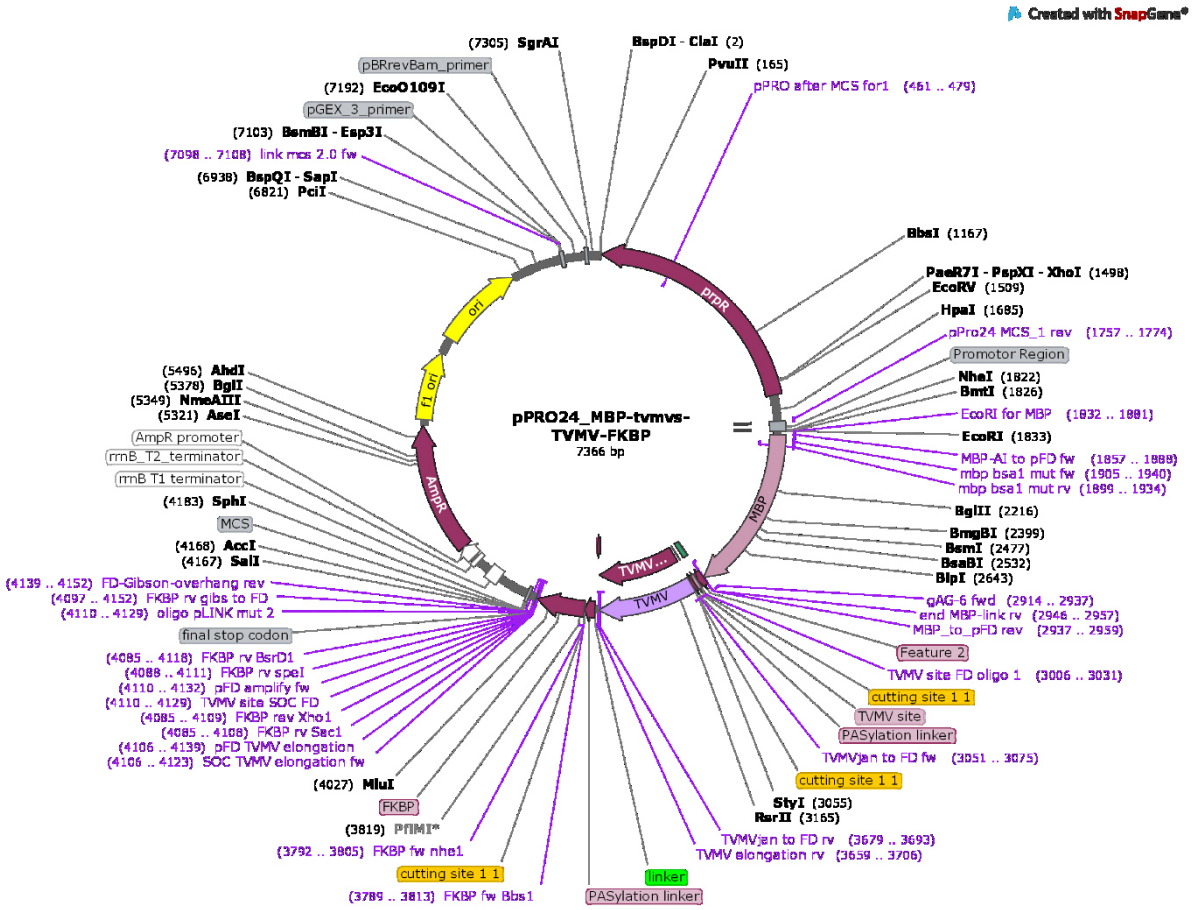

Figure S66 Vector map pPRO24_MBP-^{TVMV}TVMV-FKBP. Figure generated with SnapGene (GSL Biotech LLC)

MBP-^{TVMV}TVMV^{C151A}-FKBP

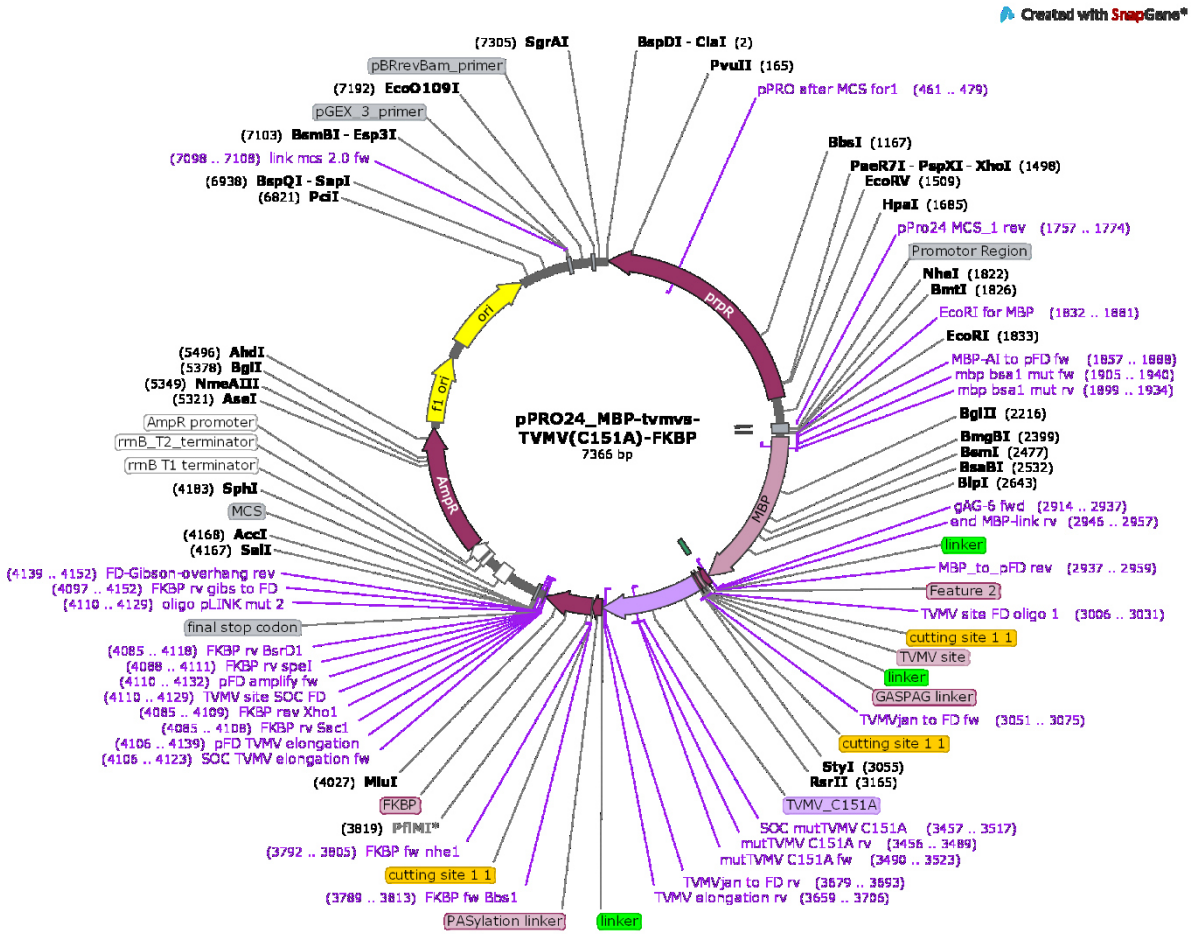

Figure S67 Vector map pPRO24_MBP-^{TVMV}TVMV^{C151A}-FKBP. Figure generated with SnapGene (GSL Biotech LLC)

13.4.14. Figure S3

For protease constructs see 13.4.12.

mNG-FKBP-^{TVMV}

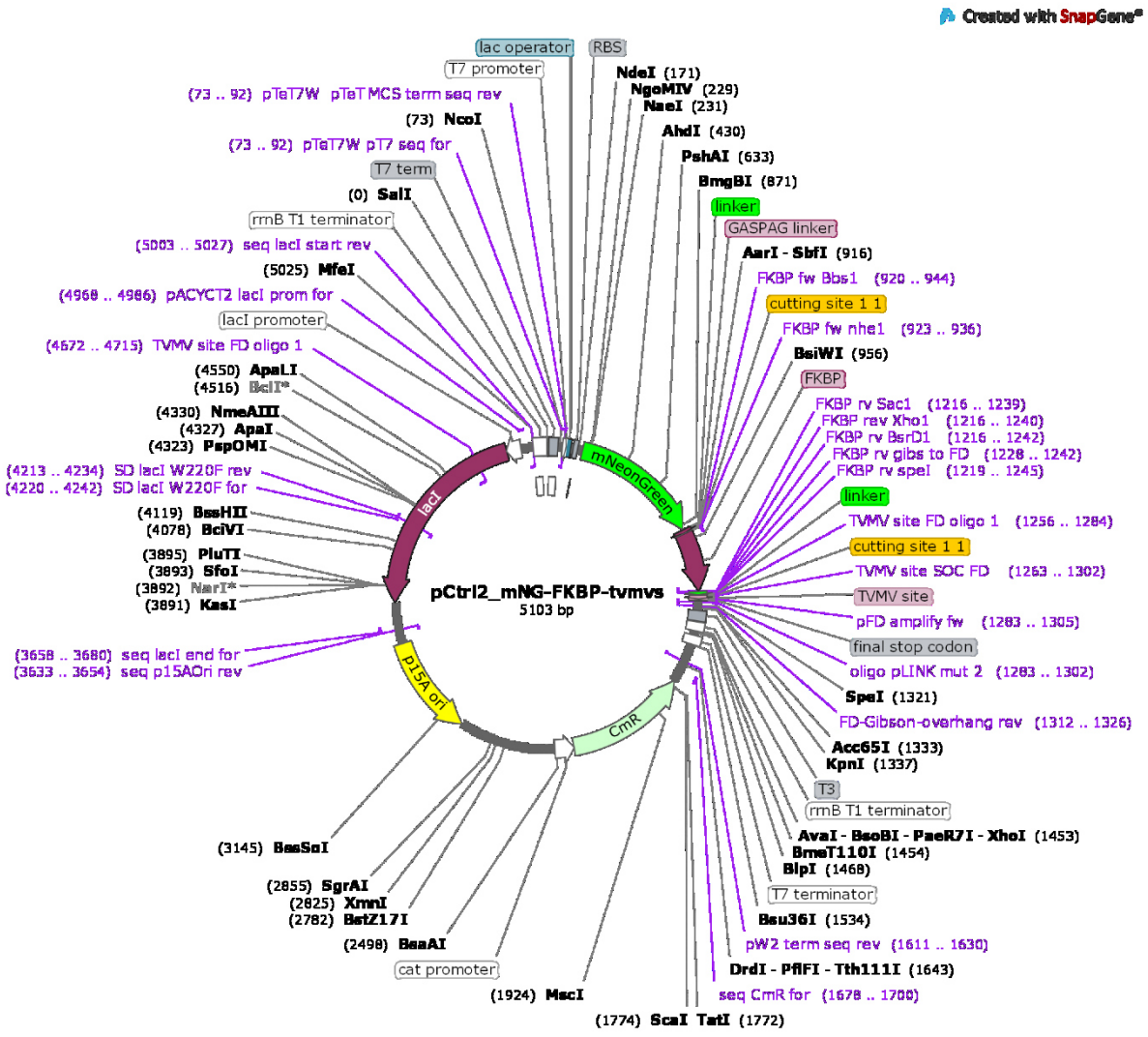

Figure S68 Vector map pCtrl2_mNG-FKBP^{TVMV}. Figure generated with SnapGene (GSL Biotech LLC).

mNG-FKBP-^{TVMV}E118

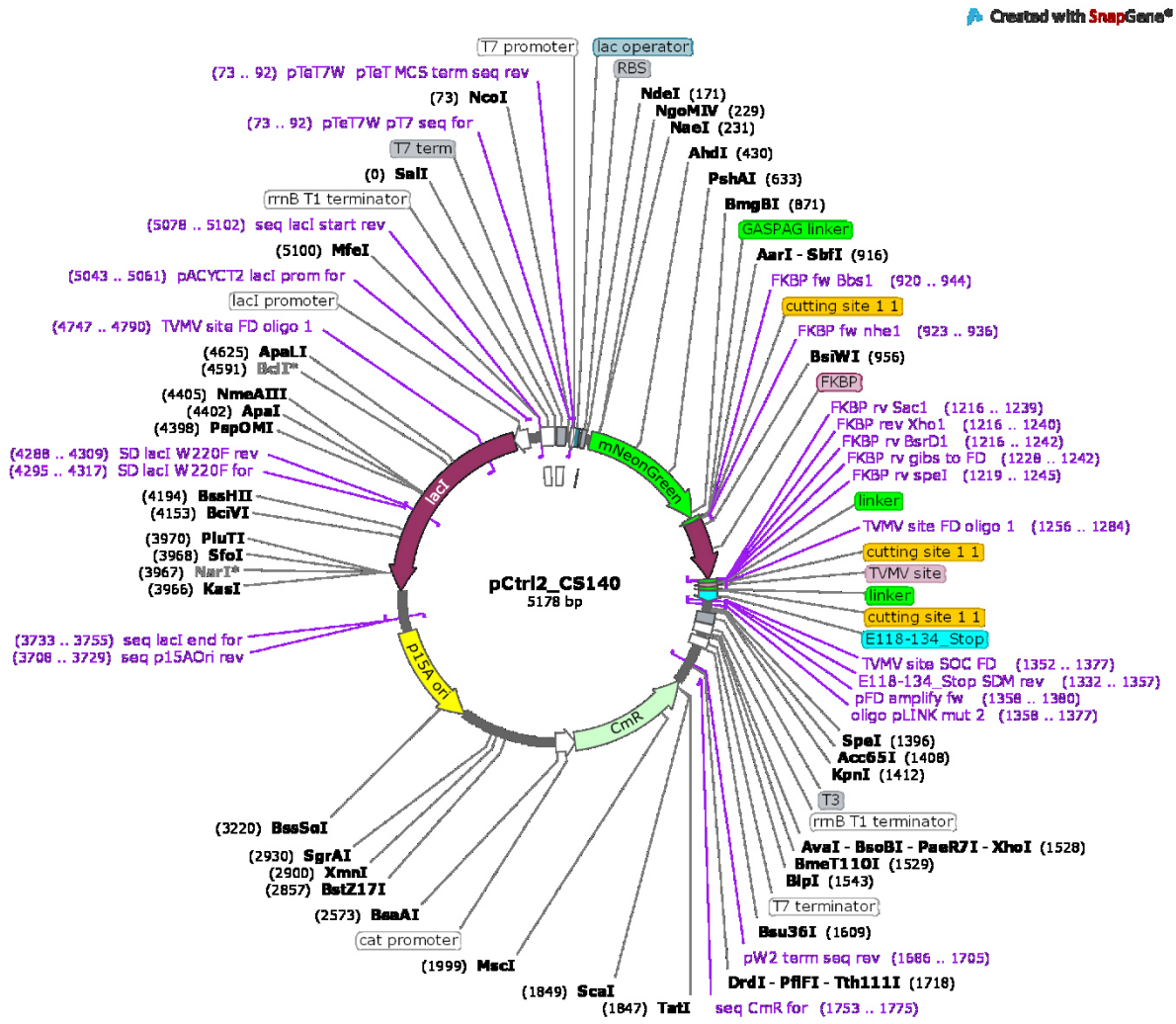

Figure S69 Vector map pCtrl2_mNG-FKBP-^{TVMV}E118-134. Figure generated with SnapGene (GSL Biotech LLC).

13.4.15. Figure S4

For protease constructs see 13.4.13.

mNG-FRB-^{TVMV}

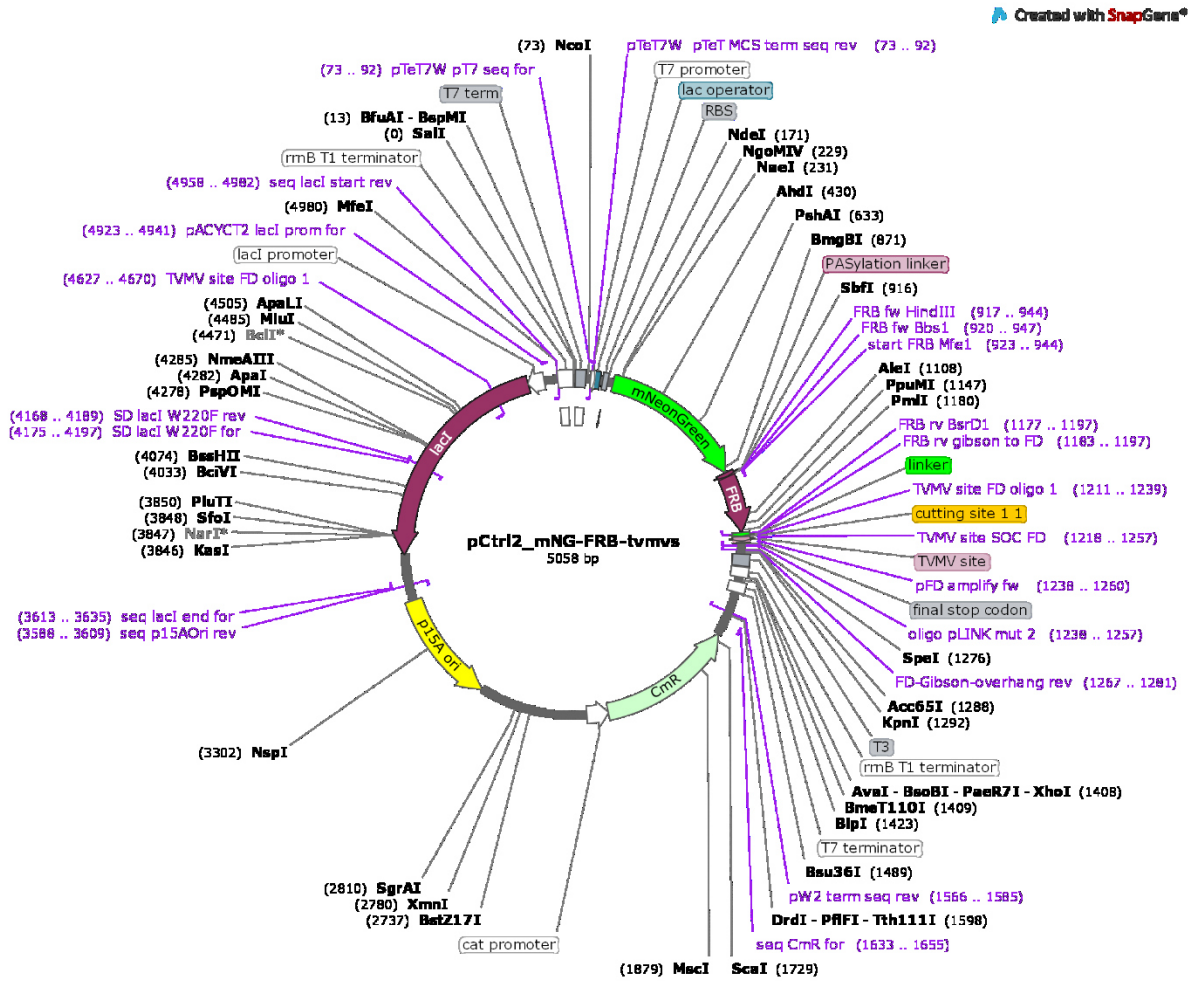

Figure S70 Vector map pCtrl2_mNG-FRB-^{TVMV}. Figure generated with SnapGene (GSL Biotech LLC).

mNG-FRB-^{TVMV}E118-134

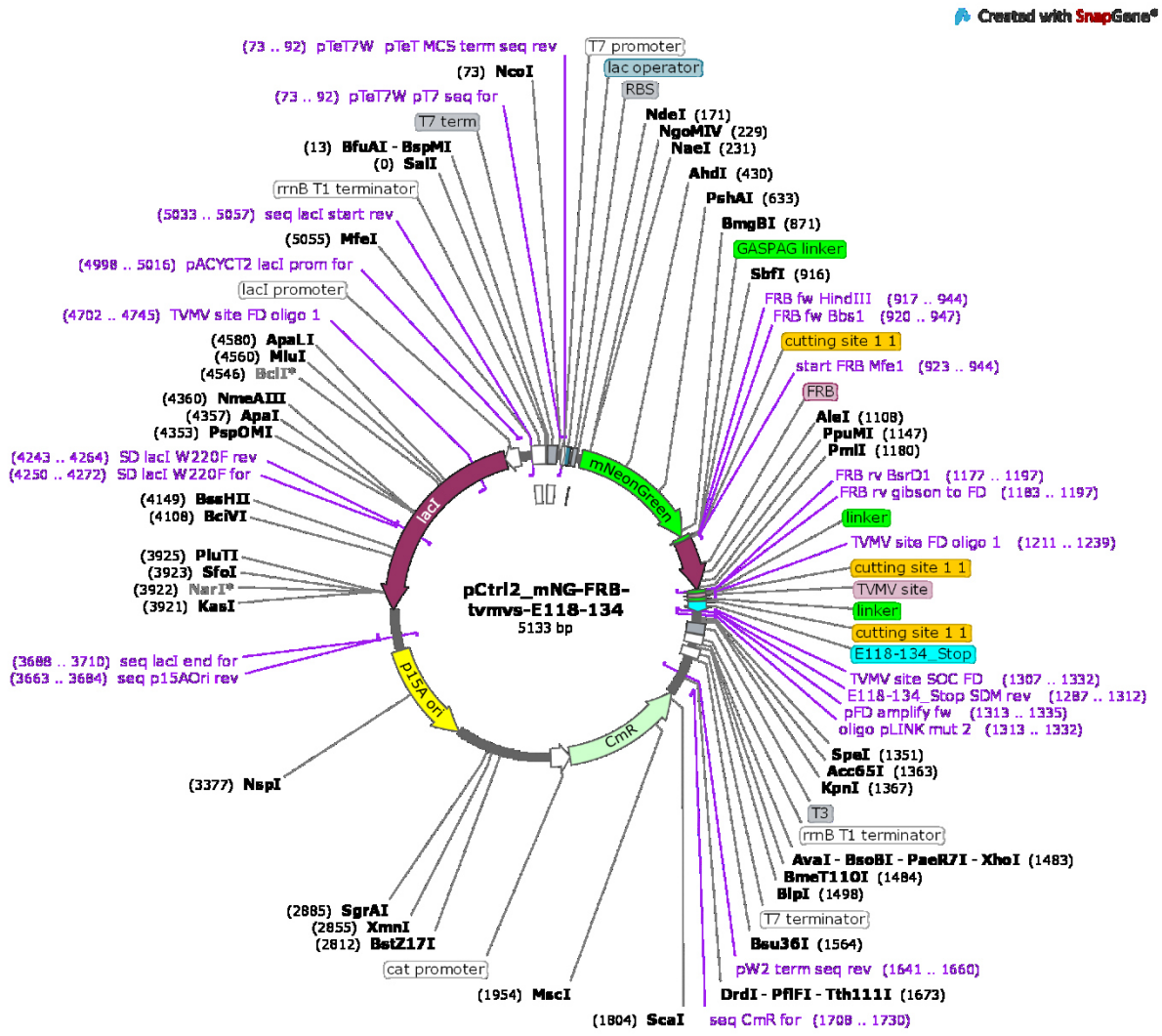

Figure S71 Vector map pCtrl2_mNG-FRB-^{TVMV}E118-134. Figure generated with SnapGene (GSL Biotech LLC).

13.4.16. Figure S5

For protease constructs see 13.4.12

mNG-^{TVMV}FKBP

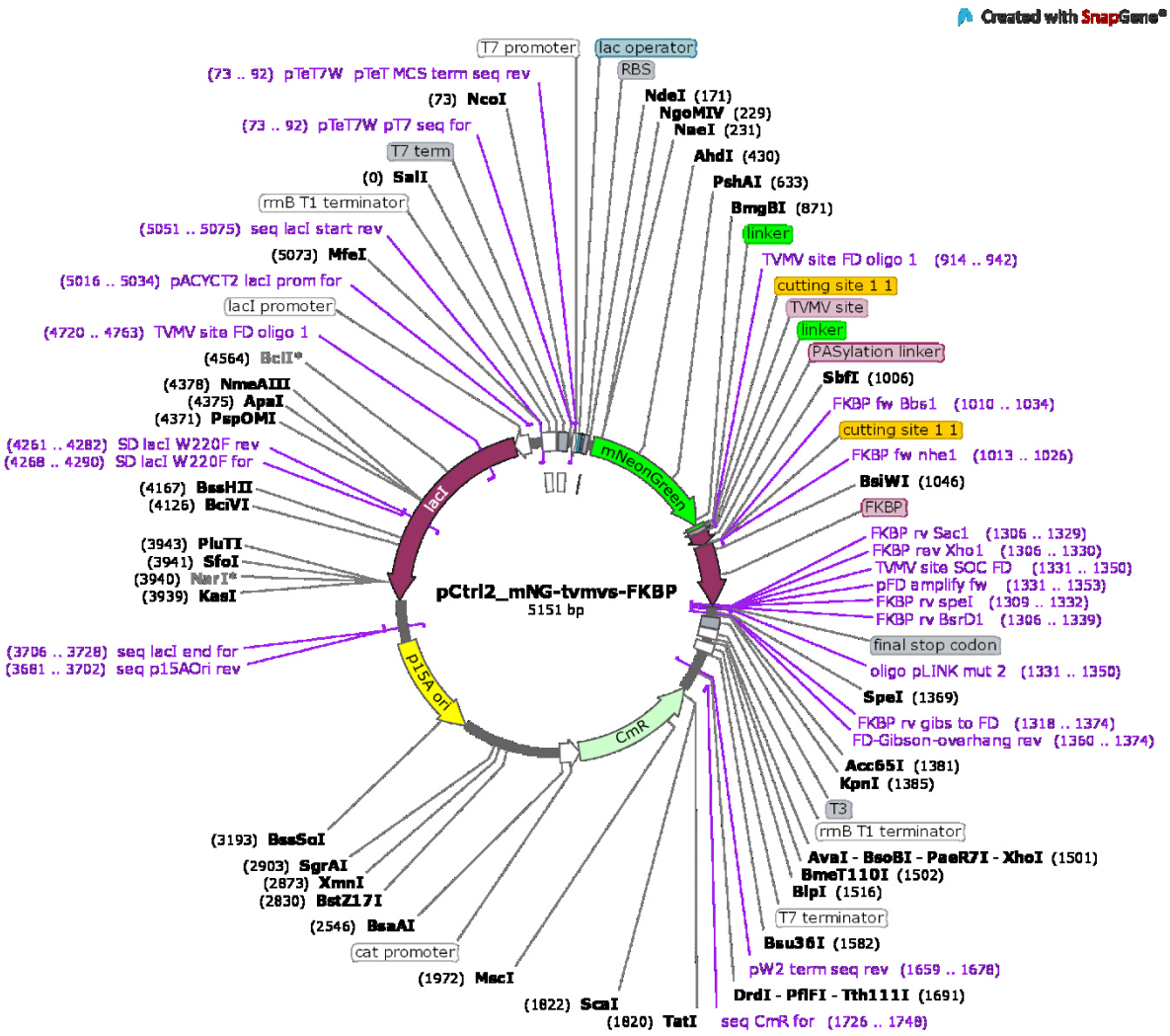

Figure S72 Vector map pCtrl2_mNG-^{TVMV}FKBP. Figure generated with SnapGene (GSL Biotech LLC).

mNG-^{TVMV}FKBP-E118-134

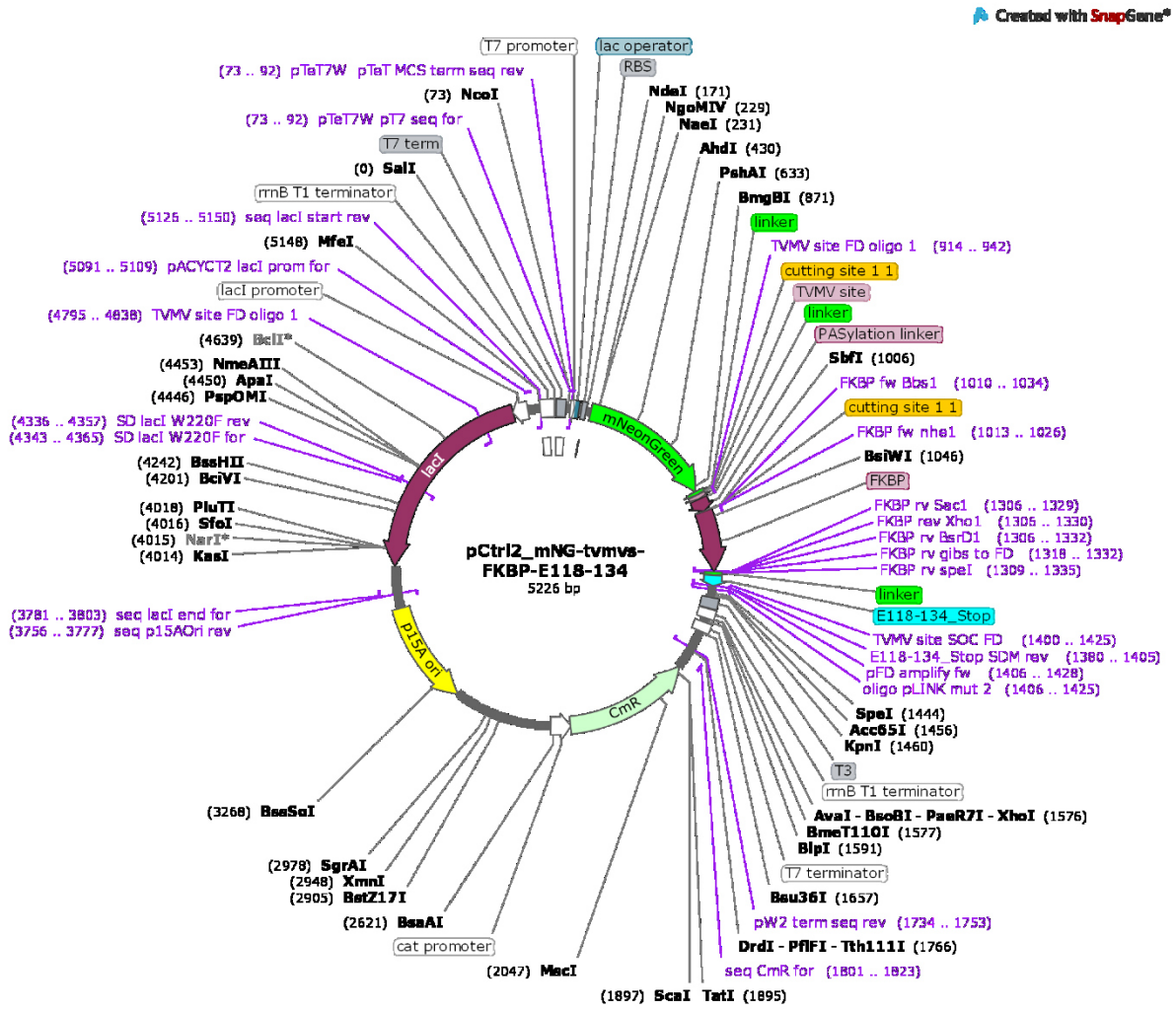

Figure S73 Vector map pCtrl2_mNG-^{TVMV}FKBP-E118-134. Figure generated with SnapGene (GSL Biotech LLC).

13.4.17. Figure S6

For protease constructs see 13.4.13

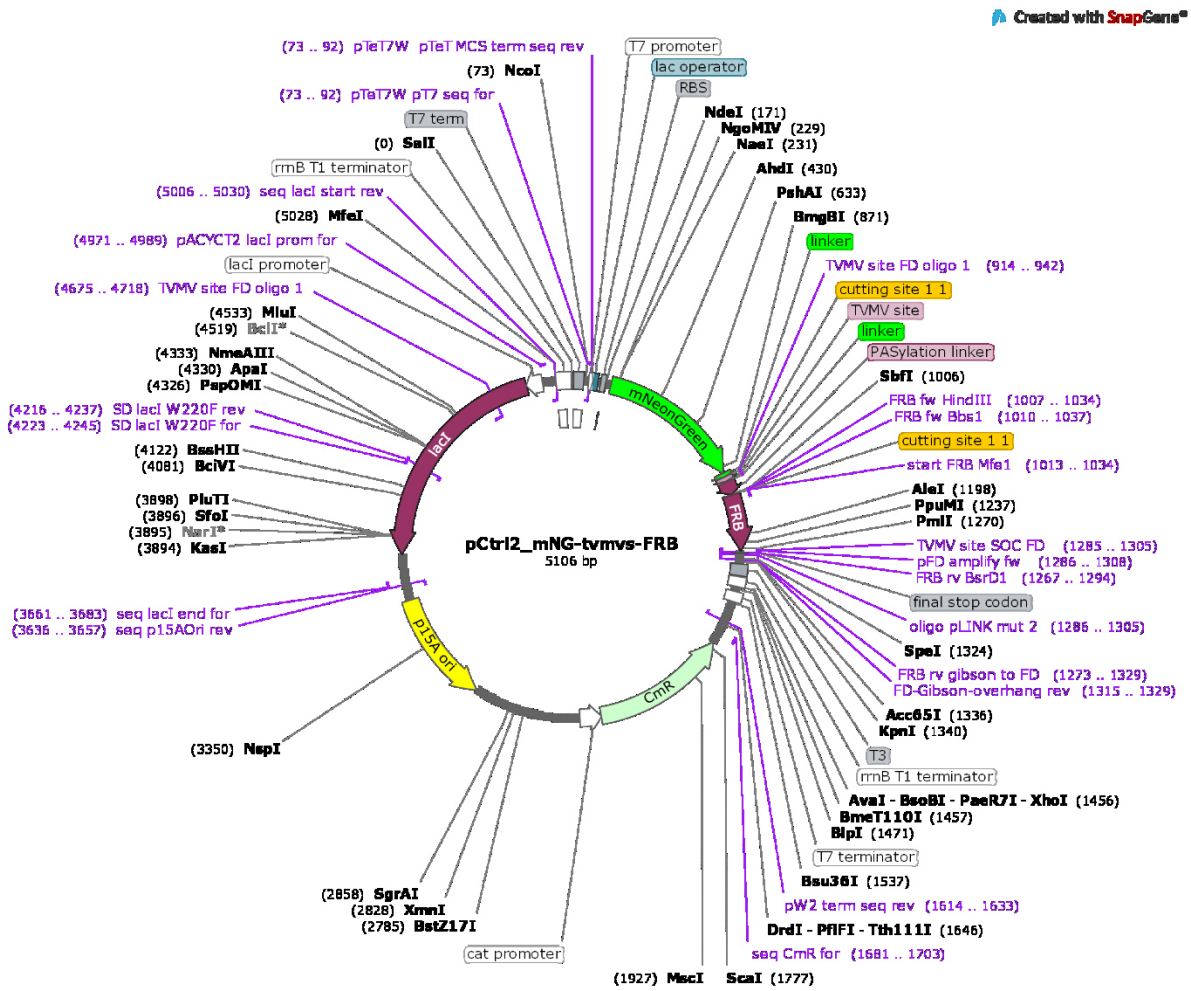

Figure S74 Vector map pCtrl2_mNG-^{TVMV}FRB. Figure generated with SnapGene (GSL Biotech LLC).

pCtrl2_mNG-^{TVMV}FRB-E118-134

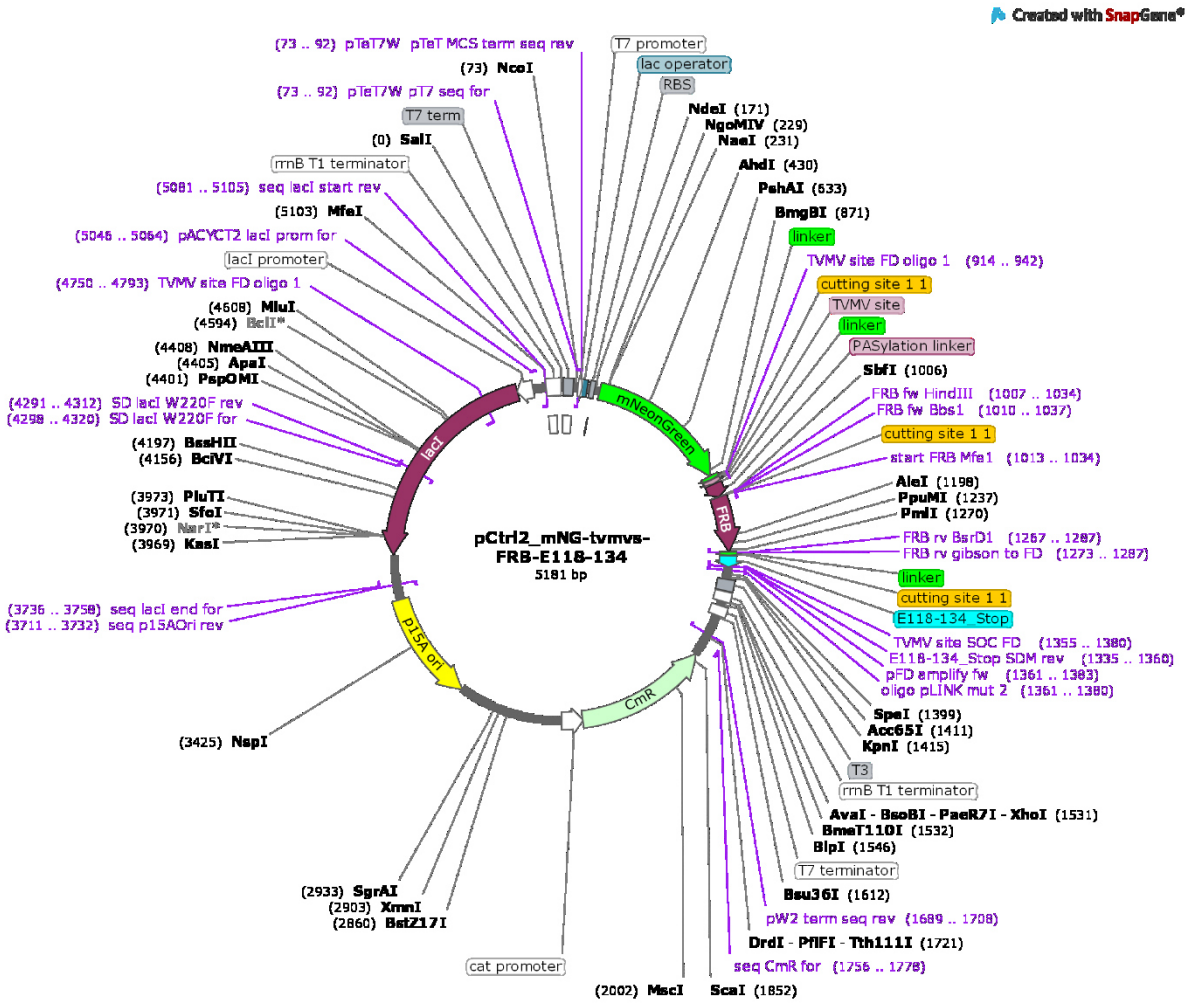

Figure S75 Vector map pCtrl2_mNG-^{TVMV}FRB-E118-134. Figure generated with SnapGene (GSL Biotech LLC).

13.4.18. Figure S15

pCtrl2_mKOkappa

Promoter region:

T7 promoter, *lac operator*, **RBS**, **start codon**

CATGGGCTGCCTAATACGACTCACTATAGG*GGAATTGTGAGCGGATAACAATTCC*CCTCTAGAAA
TAAT**TTTGTTTAACTTTAAGAAGGAGA**TATACAT**ATG**

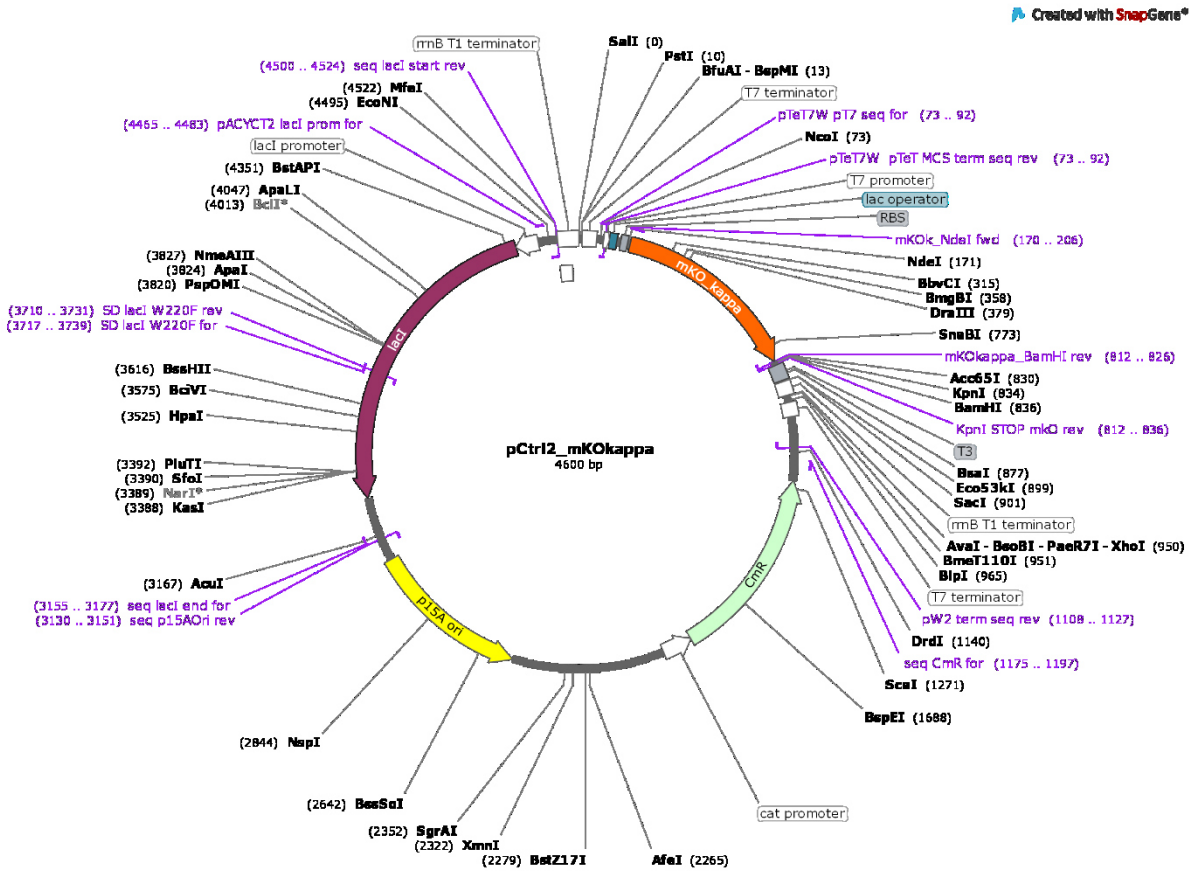

Figure S76 Vector map pCtrl2_mKO$_\kappa$. Figure generated with SnapGene (GSL Biotech LLC).

pCtrl2_T7.100_sRBS_mKO$_{\kappa}$

T7.100 promoter (wild type T7 promoter), *lac operator*, **strong RBS**, **start codon**

CCATGGTAATACGACTCACTATAGG*GGAATTGTGAGCGGATAACAATTCC*ACCGGT**AAAGAGGAGAAAG**GAGCAT**ATG**

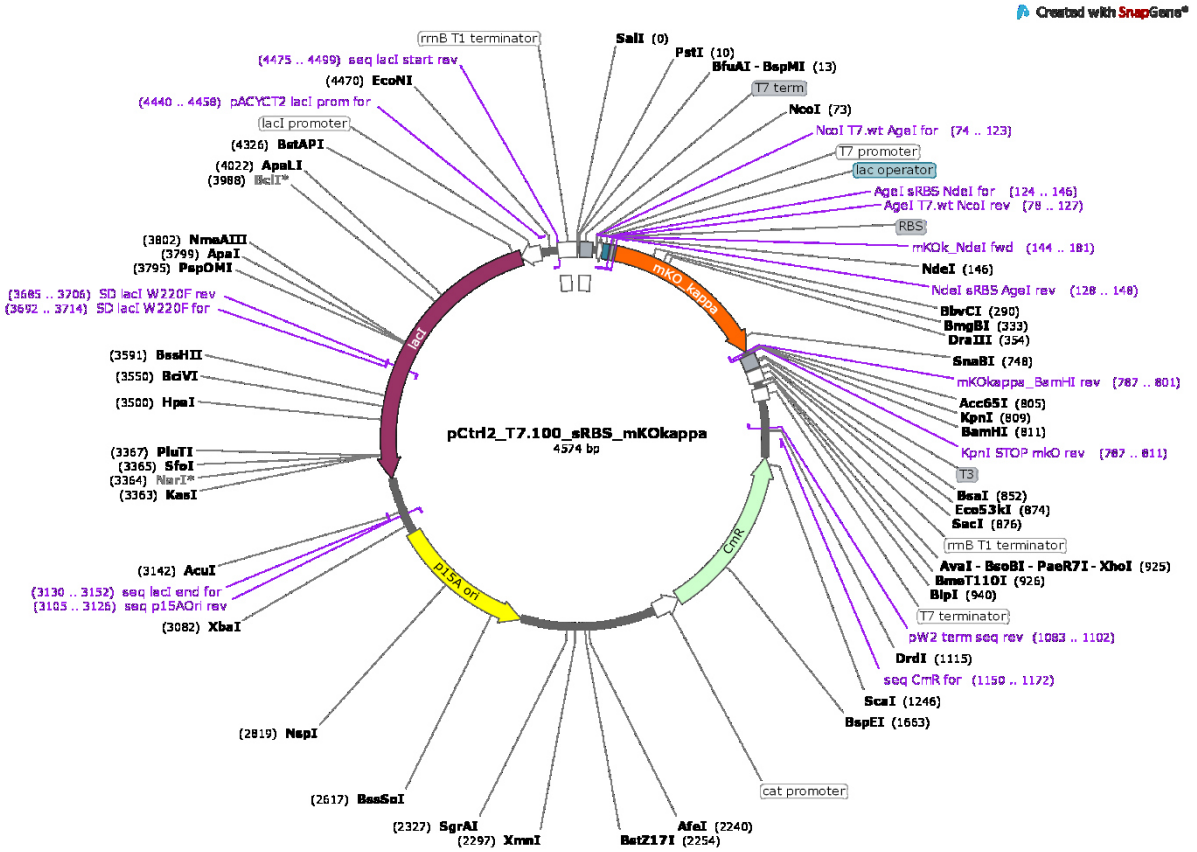

Figure S77 Vector map pCtrl2_T7.100_sRBS_mKO$_{\kappa}$. Figure generated with SnapGene (GSL Biotech LLC).

pCtrl2_T7.03_sRBS_mKOk$_{\kappa}$

Promoter region:

T7.03 promoter, *lac operator*, **strong RBS**, **start codon**

CATGGTAATACGACTCACTACAGG*GGAATTGTGAGCGGATAACAATTCC*ACCGGT**AAAGAGGAG AAAG**GAGCAT**ATG**

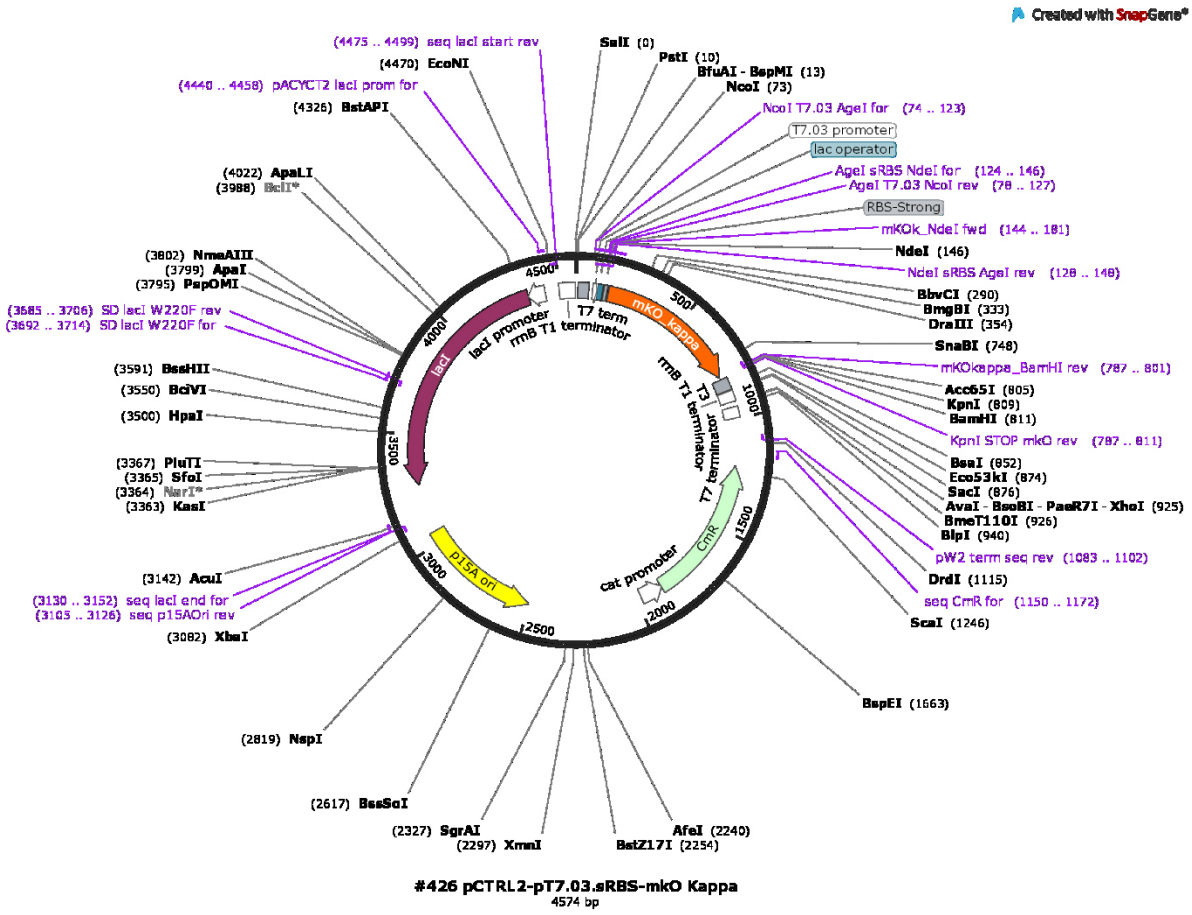

Figure S78 Vector map pCtrl2_T7.100_sRBS_mKO$_{\kappa}$. Figure generated with SnapGene (GSL Biotech LLC).

pCtrl2_T7.03_U9_mKOk$_{\kappa}$

Promoter region:

T7.03 promoter, *lac operator*, **strong RBS**, **start codon**

CCATGGTAATACGACTCACTACAGG*GGAATTGTGAGCGGATAACAATTCC*ACCGGT**GATCCCTCC**
TTACTAGTCTGCAGAAGGAGATATACAT**ATG**

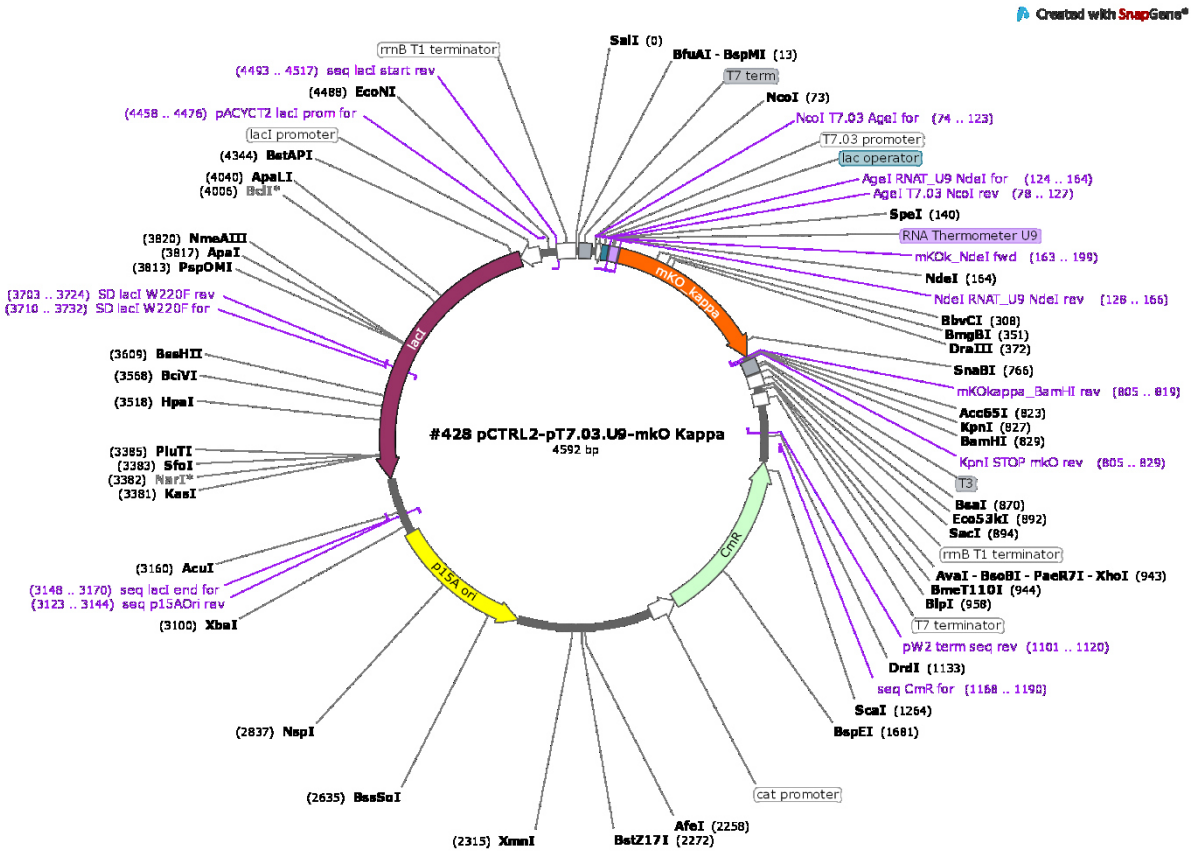

Figure S79 Vector map pCtrl2_T7.100_sRBS_mKO$_{\kappa}$. Figure generated with SnapGene (GSL Biotech LLC).